THE MOTION OF

PARTICLES ENTRAINED IN A PLASMA JET

THE MOTION OF PARTICLES ENTRAINED IN A PLASMA JET

A

THESIS

By

John Arnold Lewis, B.Sc., M.Sc.

Department of Chemical Engineering - McGill University

Under Supervision of Dr. W.H. Gauvin

Submitted to the Faculty of Graduate Studies
and Research of McGill University in partial
fulfillment of the requirements for
the degree of Doctor of Philosophy

McGill University,
Montreal,
Canada.

September 1971

ABSTRACT

Axial and radial profiles of temperature and velocity of an argon plasma jet in open air, were measured by a calorimetric probe, at temperatures up to 11 600°K and velocities up to 410 m/s. The radial profiles were shown to be Gaussian.

Velocities and decelerations of close-sized microspheres (30 - 140μm dia) in the plasma jet were measured by a high-speed streak camera. A maximum particle deceleration of 8 000 g was observed.

Experimental drag coefficients were found to be about 30% greater than standard curve values. This increase was in accord with the computer predictions of the value of the Basset history term in the full equation of motion.

RESUME

Les profils axiaux et radiaux de température et de vitesse ont été mesurés dans un jet de plasma d'argon en plein air au moyen d'une sonde calorimètrique, à des températures allant jusqu'à 11 600°K et jusqu'à des vitesses de 410 m/s. Les profils radiaux étaient Gaussiens.

Les vitesses et décélérations de microsphères de verre entre 30 et 140µm, ont été mesurées au moyen d'une caméra à fente à haute-vitesse. Une décélération maximum de 8 000 g a été observée.

Les coefficients d'entrainement déterminés expérimentallement excédèrent les valeurs de la courbe standard par environ 30%. Cette augmentation est en accord avec les prédictions de la valeur du terme de Basset dans l'équation complète du mouvement, telle que calculée par une programme d'ordinatrice.

ZUSAMMENFASSUNG

Axiale und radiale Profile der Temperatur und Geschwindigkeit eines Argon-Plasmastromes in freier Luft wurden mit einer kalorimetrischen Probe bei Temperaturen bis zu 11 600°K und Strömungsgeschwindigkeiten bis 410 m/s gemessen. Es wurde gezeigt, dass die Profile einer Gauss'schen Verteilung folgen.

Geschwindigkeiten und Geschwindigkeitsabnahmen von Mikrosphären (30 - 140 µm) bekannten Durchmessers (± 10%) wurden im Plasmastrom mit einer Hochgeschwindigkeitsstreifenkamera gemessen. Eine maximale Teilchengeschwindigkeitsabnahme von 8000 g wurde beobachtet.

Die experimentellen Widerstandskoeffizienten waren um 30% höher als die normalen Kurvenwerte. Dieses Resultat war im Einklang mit dem errechneten Wert für die "Basset History" Terme für die Bewegungsgleichung.

"A man would do nothing, if he waited until he could do it so well that no one would find fault with what he had done."

Cardinal Newman

ACKNOWLEDGEMENTS

The author acknowledges the cooperation and assistance of the many people who contributed both directly and indirectly to the work presented in this thesis.

In particular he is indebted to:

Mr. Satyan Katta and Mr. Richard Munz, fellow graduate students, for their assistance in the preparation and execution of the experimental work.

Mr. V. Sollazzo and Mr. A. Garcia, summer students, for their patient assistance with the film analysis.

Dr. Roland Clift for assisting in part of the computer programming and for pointing out the possible significance of the Basset history term.

Drs. J.R. Grace and A.S. Mujumdar for many useful discussion periods.

Dr. S.G. Mason of the Chemistry Department and Pulp and Paper Research Institute of Canada for the use of photographic equipment.

Professor P. LeGoff, Université de Nancy, France, for providing the glass beads used in most of the experiments and for supplying copies of pertinent theses.

Mr. A. Krish and the staff of the Chemical Engineering Workshop for the prompt construction of essential items of equipment.

Noranda Research Centre for library services and additional workshop facilities.

In addition, the author expresses his gratitude to the McConnell Foundation for financial support in the form of a Memorial Fellowship held over a period of four years.

TABLE OF CONTENTS

TABLE OF CONTENTS (cont'd) Page

TABLE OF CONTENTS (cont'd) Page

TABLE OF CONTENTS (cont'd) Page

EXPERIMENTAL SECTION

PART I

TEMPERATURE VELOCITY AND CONCENTRATION

PROFILES IN A FREE ARGON PLASMA JET

TABLE OF CONTENTS (cont'd) Page

PART II

MEASUREMENT OF THE VELOCITY AND DECELERATION OF PARTICLES EMERGING FROM A PLASMA FLAME, BY HIGH-SPEED CINE-STREAK PHOTOGRAPHY

TABLE OF CONTENTS (cont'd)

PART III

THE MOTION OF PARTICLES ENTRAINED IN A PLASMA JET

TABLE OF CONTENTS (cont'd) Page

APPENDICES

LIST OF FIGURES - REVIEW SECTION.

LIST OF FIGURES - PART I

LIST OF FIGURES - PART I (cont'd)

LIST OF FIGURES - PART II

LIST OF FIGURES - PART II (cont'd)

LIST OF FIGURES - PART II (cont'd)

LIST OF FIGURES - PART III

REVIEW SECTION

GENERAL INTRODUCTION

The use of plasma reactors to heat large quantitites of gases to high temperatures may now be considered as being commercially feasible. These devices use the electrical energy of direct-current or radio-frequency discharges (in place of heat released in a combustion reaction) to achieve temperatures of the order of several thousand degrees Kelvin. The removal of the constraint in having to use a combustion product atmosphere allows a broader field of high-temperature reactions to be considered. An example of such a reaction would be the formation of zirconium nitride from the metal in contact with a nitrogen plasma. This reaction only proceeds at a useful rate at a temperature above 2 000°K. Attempting to carry out this reaction in the presence of free or combined oxygen would result in the formation of the dioxide rather than the nitride.

Interest in plasma chemical reactions is now centered in the field of metallurgical operations, where the general approach has been to consider the use of a multi-particle system. The advantage of such an approach would be enhanced heat and mass transfer and reaction rates, due to the favourable surface area-to-volume ratio.

The solution of the overall problem of the transport processes and reaction kinetics of a plasma-particulate system is restricted by the present state of knowledge of the field. As a result of the complex nature of the plasma itself and the non-steady, non-isothermal, limited continuum flowfield around individual particles, any prediction of chemical conversion would be subject to a large degree of uncertainty.

The general aim of this thesis was to compare the actual motion of near-ideal particles in a plasma flame, with predictions based on a

corrected steady-state, isothermal approach to the equation of motion.

In accordance with current practice, this thesis has been written as a number of individual sections, which are complete in themselves. This allows for a compact presentation of each part of the experimental work, in a form which may be subsequently published with only minor modifications. The four main sections of the thesis are:-

(i) A review of pertinent literature in the field of plasmas, particle dynamics and measurement techniques.

(ii) A report on the characterization of an argon plasma jet.

(iii) A report of experimental determination of the velocities and decelerations of particles entrained in a plasma jet.

(iv) A report of the comparison between experimental determinations of drag coefficients and computed non-steady drag coefficients.

PART I - TEMPERATURE

INTRODUCTION

Temperature may be considered as a convenient modulus for the mean energy of a gas system (1.1). This energy is distributed among various degrees of freedom and under normal ambient conditions (760 mm Hg, 300°K), these degrees of freedom are in equilibrium. Of the various techniques for measuring gas temperature, the majority measure the mean energy of one particular degree of freedom. Under ambient conditions therefore, one would expect the same temperature to be given by different experimental techniques. This is not necessarily true when considering plasma temperatures, since the various degrees of freedom have different relaxation times. In cooling of a gas from 10 000°K to 1 000°K, the different degrees of freedom can get "out of step" and it is possible to simultaneously assign to a gas, "temperatures" of 300°K and 10 000°K.

In order to explain this situation, the following sections outline the various definitions of temperature and the main experimental techniques appropriate to each definition. This is followed by a discussion of equilibrium and a comparison of techniques.

DEFINITIONS AND TECHNIQUES

Translation Temperature

At equilibrium, the molecules in a gas have a Maxwell distribution of translation velocities:-

$$(1/n)(dn/dU_t) \propto (U_t^2)\exp[-(1/2)(MU_t^2)/(kT_t)] \quad \ldots\ldots\ldots\ldots\ldots (1.1)$$

where the average kinetic energy of translation may be shown to be:-

$$\overline{E_t} = (1/2)(MU_t^2) = (3/2)kT_t \qquad (1.2)$$

or

$$T_t = \overline{M(U_t)^2}/(3k) \qquad (1.3)$$

Thus the translation (kinetic) temperature is directly proportional to the mean kinetic energy of translation (1.2, 1.3).

From the kinetic theory of gases, it is possible to show that the pressure within a system is directly proportional to the mean kinetic energy of translation of the gas molecules and hence its translation (kinetic) temperature. This is the basis of the standard gas thermometer (1.4).

A second technique of measuring translation temperature is to allow a solid (or liquid) device to come to thermal equilibrium with the gas and to compare a change in some property of the device with the translation temperature of the gas. Typical devices are thermocouples, resistance gauges and mercury-in-glass thermometers (1.1). The assumption that the device temperature and the gas temperature are equal is not always valid. For example, a steady state (but not equilibrium) may be reached in which the rate of convective heat flow into a thermocouple element is balanced by the rate of heat flow out of the element by conduction and radiation (1.5). Such a process could lead to errors of 200°K for nominal temperatures of about 2 000°K.

Rotation-Vibration Temperature

Because they have finite moments of inertia, diatomic and polyatomic molecules may possess significant amounts of rotational and vibrational energy. The distribution of this energy is governed by the Maxwell-Boltzmann law and it is therefore possible to define the rotation-vibration temperature as directly proportional to the mean

rotation-vibration energy. This energy is transferred to the degrees of freedom by the absorption of radiation at discrete frequencies. When the radiation from a source is passed through the gas, the intensity of the beam is either attenuated or amplified, depending on whether the gas is colder or hotter than the source. This effect occurs at the rotation-vibration frequencies and is the principle of the emission absorption method of gas temperature measurement (1.6, 1.7). Difficulties occur with this technique because of averaging over a considerable flame length, while "self-absorption" and changing emissivities cause further uncertainties.

Electron Excitation Temperature

At temperatures in excess of about 6 000°K, molecules are dissociated. The resulting atoms can absorb further radiation but at a frequency different to the rotation-vibration frequency. As this energy is absorbed, electrons jump to higher energy levels. On return to the original energy level, light of a particular frequency is emitted. The intensity of radiation is a function of the concentration of excited atoms. In turn, this concentration is a function of the mean level of excitation energy and hence the electron excitation temperature. As discussed at length by Taurin (1.6), the measurement of intensity of emitted radiation from a gas forms the basis of spectroscopic temperature measurement.

Electron Temperature

Free electrons resulting from ionisation constitute a separate species. The electron temperature is therefore proportional to the mean kinetic energy of translation of the electrons. It is usually estimated

from the variation in the current drawn from a wire as the voltage bias of the wire is changed (Langmuir probes, 1.8, 1.9, 1.10).

Calorimetric Probe

The equilibrium temperature of a gas may be inferred from a determination of the enthalpy of that gas. This principle is applied in calormetric probes by making a heat balance between cooling water passing through the calorimeter and a continuous flow sample of the gas (1.12, 1.13).

Miscellaneous Techniques

Various techniques exist for measuring mean temperatures, such as attenuation of microwaves (1.1), velocity of sound (1.1, 1.14), electron beam excitation (1.15), ablating probes (1.1) and density of radioactive vapour (1.16). Recently, Cabannes et al. (1.17) used separate determinations of gas velocity and impact pressure to infer plasma temperatures from the Bernoulli equation. In addition, comparable results were obtained using a laser interferometric technique.

DISCUSSION

Equilibrium

On a formal basis, it is improper to invoke the concept of temperature, unless all the degrees of freedom of a gas are in mutual equilibrium. In real systems, true equilibrium may be approached, but will never be actually reached. Relaxation of the strict definition is therefore necessary, if the concept of temperature is ever to be applied:

> Where any degree of freedom has its own Maxwell-Boltzmann distribution of energy, one may speak of the "temperature" of that particular degree of freedom (e.g. electron temperature). However, this qualification does not insist on non-equilibrium between degrees of freedom.
>
> Further, where non-equilibrium is concentrated in only one degree of freedom and the amount of energy associated with that non-equilibrium is small, then a real equilibrium may be said to exist. Such is the case with electron temperatures, which may be an order of magnitude higher than other temperatures, but would not change the overall temperature if true equilibrium did occur (1.18).

The concept of "Local Thermal Equilibrium" is important when dealing with plasmas (1.19). The principle suggests that if there is a high concentration of particles in a small volume element, then there will be effectively a local Maxwellian distribution of energy, even though a temperature gradient may exist in the gas.

The effect of electron concentration, gas pressure and ratio of electric field strength has been summarized by Dundas and Thorpe (1.20).

At high electron density ($> 10^{13}/mm^3$) electron and translation temperatures agree, but at lower concentrations the electron temperature can be an order of magnitude higher than the translation temperature. The same effect occurs with decrease of pressure. At high ratios of electric field strength to gas pressure [>1(V/mm)/(mm Hg)] the electron temperature can be nearly two orders of magnitude higher than the translation temperature. Commenting on the energy transfer mechanism in an electric arc and its effect on the equilibrium of temperature of a gas, Hellund (1.21) noted that relaxation times for free electrons were of the order of one microsecond, but for internal excitation were much shorter at about 0.01μs.

Comparison of Techniques

The miscellaneous techniques mentioned earlier, give a mean value across the sampling path. The inability to resolve the steep gradients which can exist in a plasma restricts the applicability of these techniques.

Thermocouples are limited to a useful maximum of about 2 500°K (1.22), and are subject to frequent burn-out due to oxygen contamination.

As pointed out earlier, emission-absorption techniques are subject to errors caused by self-absorption and uncertainties of emissivity. In addition, operation is restricted to the range between 2 000°K and 7 000°K.

Electron temperature measurements are applicable above about 10 000°K. As discussed earlier the electron temperature is not a useful indicator of the average gas temperature.

Excitation temperature measurements require an understanding of spectroscopy. The equipment is large, non-portable and expensive. There is a minimum temperature limit with spectroscopic (excitation) temperature measurement, caused by the low concentration of "emitters". Below this

limit, the light intensity is too low to be accurately measured.

Calorimetric temperature measurement (described in detail in the experimental section of this thesis) is applicable over a wide range from below 1 000°K to 10 000°K. Errors of measurement are caused by heat losses from the calorimeter and disturbances to the gas flow pattern.

CONCLUSIONS

No single method of gas temperature measurement exists which can be used as a simple engineering tool, without corrections of some kind being required or without there being some uncertainty as to the validity of the result.

Below 2 500°K, thermocouple measurement is the more widely used technique, while about 9 000°K, spectroscopic methods are probably the most useful. The range in between (2 500°K - 9 000°K) is the most important when considering heterogeneous reactions of particles in plasmas. It is this range which is most easily covered by a calorimetric probe. This type of device is capable of finite spatial resolution and was for that reason selected for the experimental work of this thesis. The poor reputation of early calorimetric probes was mainly due to limited design experience and improper probe operations (1.22, 1.23).

NOMENCLATURE

$\overline{E_t}$	Average translation energy per molecule	ML^2T^{-2}
k	Boltzmann constant	$ML^2T^{-2}\ deg^{-1}$
M	Mass of molecule	M
n	Number of molecules	-
T_t	Translation temperature	deg
U_t	Translation velocity	LT^{-1}

BIBLIOGRAPHY

1.1 Herzfeld, C.M., ed. "Temperature, Its Measurement in Science and Industry", Reinhold, Vol. 3, Part 2, 3 (1962).

1.2 Moore, W.J., "Physical Chemistry", Longmans-Green 3rd ed., ch. 7 (1961).

1.3 Barrow, S.M. "Physical Chemistry", McGraw Hill, ch. 2 (1966).

1.4 Zemansky, M.W., "Heat and Thermodynamics", McGraw Hill (1957).

1.5 Scadron, M.D., and Warshawsky, I., N.A.C.A. T.N.-2599 (1952).

1.6 Taurin, R.H., "Spectroscopic Temperature Measurement", Elsevier (1966).

1.7 Dieke, G.H., "Physical Measurements in Gas Dynamics and Combustion", Princeton Univ. Press (1964).

1.8 McTaggart, F., "Plasma Chemistry in Electrical Discharges", Elsevier (1967).

1.9 Howatson, A.M., "An Introduction to Gas Discharges" Pergamon (1965).

1.10 Huddlestone, R.H., and Leonard, S.L., "Plasma Dagnostic Techniques", Academic Press (1965).

1.11 Grey, J., and Jacobs, P.F., A.I.A.A.J., 5, 1184 (1967)

1.12 Grey, J., Jacobs, P.F., and Sherman, P., Rev. Sci. Inst. 33, 738 (1962).

1.13 Petrov, M.D., and Sepp, V.A., Teplofizika Vysokikh Temperature 8, 868 (1970).

1.14 Carnevale, E.H., Poss, H.L., and Yos, J.M., Avco Corp. Tech. Rep. RAD-TR-61-13 (1961).

1.15 Muntz, E.P., Univ. of Toronto UTIA Report 71 (1961).

1.16 Ecker, G., A. Phys., 130, 585 (1951).

1.17 Cabannes, F., Chapelle, J., Czerichowski, A., Decroisette, M., et Zamarlick, J., Rev. Int. Htes. Temp. et Refract., 7, 7 (1970).

1.18 Jacobs, P.F., and Grey, J., A.I.A.A. Plasmadynamics Conference 1966, A.I.A.A.-66-192.

1.19 Griem, H.I., "Plasma Spectroscopy", McGraw Hill (1964).

1.20 Dundas, P.H., and Thorpe, M.L., Chemical Engineering, June 14, 124 (1969).

1.21 Hellund, E.J., "The Plasma State", Reinhold (1961).

1.22 Kubanek, G.R., and Gauvin, W.H., Can. J. Chem. Eng. 45, 251 (1967).

1.23 Smith, D.L., and Churchill, S.W., Univ. of Michigan, TR-05607-7-T (1965).

PART II - PLASMAS AND PLASMA DEVICES

INTRODUCTION

Recent reviews of plasma technology were given by Kubanek and Gauvin (2.1), Dundas and Thorpe (2.2) and Ibberson and Thring (2.3). "Plasma Jet Technology" (2.4) is a N.A.S.A. publication which reviews the early work on plasma jets connected with the aerospace industry. "Plasma Technology" is a translation of a Czechoslovak book by Gross, Grycz and Miklossy (2.5) and covers the physics of high pressure plasmas, technical sources of plasmas and technical application of plasmas.

The following sections are a summary of the available information which is pertinent to this thesis. While not being comprehensive, the list of references contain the essential elements of the work on plasmas. Further references may be obtained from the individual bibliographies.

DEFINITION OF PLASMA

The term "plasma", as used in the context of this thesis and by other workers in the field, may be defined as a gas having an appreciable degree of ionisation, usually greater than 0.1% (2.3), a temperature between 2 500°K and 50 000°K, and a pressure of one atmosphere. It has also been used as a shorthand notation for "gas derived from a plasma source, being colder than the temperature limits of a plasma, but still much hotter than ambient".

Description of a Plasma Jet

A plasma jet usually issues from a nozzle at high velocities ($\sim$500 m/s), and high temperature ($\sim$10 000°K) emitting intense radiation in the visible and ultraviolet spectrum, accompanied by considerable noise, if the jet is turbulent. For this reason, it has been called a flame, although there is no chemical combustion as occurs in an oxy-acetylene flame. For a laboratory size unit, the flame is about 75 mm (3 in) in length with a total gas flowrate of about 1×10^{-3} m^3/s($\sim$150 S.C.F.H.).

Under certain conditions, the flame is quiet, laminar and much longer at about 250 mm (10 in).

Plasma Devices

The essential features of a device for producing an (arc) plasma jet are as shown in Fig. 2.1.

a) A cathode consisting of a rod of tungsten about 15 mm in diameter, shaped to a point having a cone half-angle between 30° and 60°. The shaped tip is usually made of tungsten alloyed with thoria or baria to improve the emission of electrons. Water-cooling

FIGURE 2.1

Cross Section of a Typical

Arc Plasma Torch

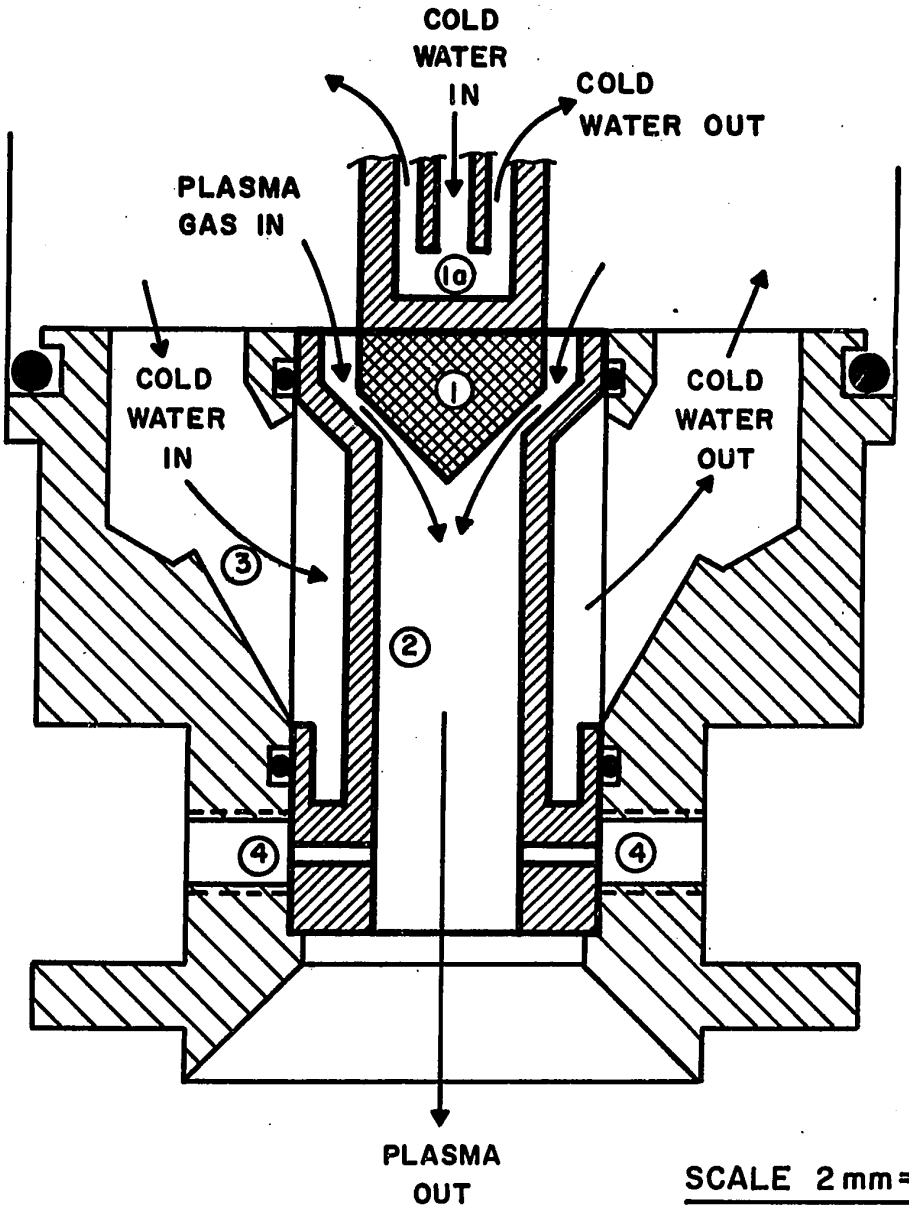

1. THORIATED TUNGSTEN CATHODE.
1a. CATHODE HOLDER.
2. COPPER NOZZLE – ANODE.
3. NOZZLE BODY.
4. PARTICLE INJECTION INLET.

of the rod prevents excessive heating and vaporisation of the tip.

b) A copper anode nozzle concentric with the cathode, with a smooth entrance in which the cathode is centered. The nozzle dimensions are usually about 10 mm-dia. x 30 mm-length. The anode is also water-cooled and usually carries a much greater heat load than the cathode.

c) An insulator section which maintains the cathode and anode at a fixed separation and also excludes the ambient air from upstream of the nozzle.

In operation, an arc is struck between the cathode and anode, while gas (commonly N_2, He, Ar, H_2) is blown through the nozzle. Typical operating conditions would be a voltage between cathode and anode of about 40V and a current around 400A (the voltage depending on the gas used). Of the total 16 Kw (typical) energy input, about 50% is transferred through the cathode and anode to the cooling water, the rest going to raise the temperature of the gas.

Energy Transfer Mechanism

(This section is based on the texts of Somerville (2.6) and Hellund (2.17), and summarises the mechanism by which electrical energy is transferred into thermal energy in the gas.)

In order to start the plasma jet, some means of bridging the gap between cathode and anode is required. This is usually provided by a high frequency, high-voltage discharge generated by a special circuit remote from the torch. The chain of events which occurs is as follows: the high voltage between cathode and anode causes local ionisation of the gas. Electrons near the cathode are accelerated towards the anode by the electric field,

acquiring a sufficient amount of energy to cause ionisation of any atom of gas with which the electrons collide. This ionisation produces a further electron and an ion. The new electron is accelerated toward the anode, repeating the ionisation process. The ion drifts towards the cathode and on impact liberates another electron to start a new chain reaction.

The continual collision of fast moving particles with the generally slow moving atoms and molecules of the gas, raises the random kinetic energy of translation of atoms and molecules, or in other words, increases the gas temperature.

Apart from increasing the random velocity of the gas, part of the electrical energy is used to accelerate the gas in ordered motion through the nozzle. This is caused by the magnetodynamic effect of the electric field on the ionised gas and has been termed a "jet pumping effect" (2.8).

A further fraction of the energy input is lost as radiation to the surroundings. This loss increases rapidly with pressure and according to Hellund (2.7), is the principal effect at pressures greater than 100 Atm ($10^7 n/m^2$).

Plasma Jet Oscillations

When the arc from the cathode to the anode is established, it is effectively a tube of viscous fluid. As a result of the gas flow through the nozzle, there is significant aerodynamic drag on this arc tube. Early workers (2.10) found it "hard to conceive of drag being imposed upon the light ethereal arc column". However, Abramovich (2.11) refers to the analogous situation of the deflection of jets in cross winds.

As a result of the drag on the arc tube, the anode arc root is blown downstream, lengthening the arc and increasing the voltage drop along it. When the arc has been stretched to a maximum length, the arc root reattaches itself upstream and the old arc root is extinguished. This cyclic behaviour has been observed by Eckert and Pfender (2.12) using a plane anode. The effect on spectroscopic temperature fluctuations was shown by Adcock (2.13), who suggested that the fluctuation of the heavy particle temperature was minimal. The effect on the cathode-anode voltage drop has been measured by a number of workers including Lemoine (2.14), Pfender and Cremers (2.15) and Wheaton and Dean (2.10).

Miscellaneous Applications of Plasma Torches

Apart from applications as high temperature reactors for heterogeneous-particulate systems, plasmas have an established role in metallurgical operations in the following fields (2.16);

Ultrafine powder production ($< 1\mu m$);

Spheroidisation (50-150μm).

Flame spraying;

Spray forming on a prepared mandrel;

Welding and cutting;

Melting furnace.

Modified Plasma Torches

Where solid particles are injected into a flame, it is difficult to take advantage of the hot central core of the jet. Powders are usually injected into the flame at the nozzle exit and are blown downstream without penetrating the hot core. To get around this difficulty, the plasma devices of the hollow cathode-rotating wall type have been used. A

typical design is that of Whyman (2.8) and Bryant, Cox and Whyman (2.9). Particles were dropped down the center of the cathode and entrained in the core, due to the magnetodynamic pumping effects mentioned earlier. The flame was considerably expanded by the effect of the wall rotating at about 400 rpm and also by the effect of raising the cathode away from the anode after the arc had been struck.

Radio Frequency Generated Plasmas

As an alternative to the use of D.C. arcs, plasmas may be generated by the use of a high-frequency discharge ($\sim$4 MHz) in a suitably designed coil, with the plasma gas confined to flow in a quartz tube through the coil. A typical laboratory unit would have a 50kW input capacity, using a four or five turn coil having a diameter of about 50 mm and a pitch of 10 mm. R.F. plasmas, as these devices are commonly called, have the advantages of product purity (no electrode contamination), lower operating costs (partially offset by higher capital cost) and practically continuous running.

R.F. plasmas were originally developed by Reed (2.17) and are now available as industrially sized units with capacities of several megawatts. Dundas and Thorpe (2.18) described such a unit used for the production of titanium dioxide pigment.

BIBLIOGRAPHY

2.1 Kubanek, G.R., and Gauvin, W.H., Can. J. Chem. Eng. 45, 251 (1967).

2.2 Dundas, P.H., and Thorpe, M.L., Chem. Eng. 79, 123 (1969).

2.3 Ibberson, V.J., and Thring, M.W., Ind. Eng. Chem. 61, 49 (1969).

2.4 Dennis, P.R., Ed. "Plasma Jet Technology", N.A.S.A. SP-5033 (1965).

2.5 Gross, B., Grycz, B., and Miklossy, K. "Plasma Technology", Iliffe (1969).

2.6 Somerville, J.M., "The Electric Arc", Methuen (1969).

2.7 Hellund, E.J., "The Plasma State", Reinhold (1961).

2.8 Whyman, D., J. Sci. Inst. 44, 525 (1967).

2.9 Bryant, J.W., Cox, J.M., and Whyman, D., J. Sci. Inst. , Ser. 2, 2, 779 (1969).

2.10 Wheaton, J.R., and Dean, R.C., Research Report, "On Anode Gas-Sheath Electrical Breakdown", Dartmouth College, Hanover, New Hampshire (1961).

2.11 Abramovich, G.N., "The Theory of Turbulent Jets", M.I.T. Press (1963).

2.12 Eckert, E.R.G., and Pfender, E. Advances in Heat Transfer, Vol. 4, Academic Press (1967).

2.13 Adcock, B.D., A.I.A.A.J. 4, 2249 (1966).

2.14 Lemoine, A., Docteur Ingenieur Thesis, Université de Nancy, France (1969).

2.15 Pfender, E., and Cremers, C.J., A.I.A.A.J. 3, 1345 (1965).

2.16 Moss, A.R., and Young, W.J., Powder Metallurgy, 7, 261 (1964).

2.17 Reed, T.B., J. Appl. Phys. 32, 5 (1961).

2.18 Dundas, P.H., and Thorpe, M.L., Chem. Eng. Prog. 66, 66 (1970).

PART III - CHEMICAL REACTIONS IN PLASMAS

Chemical reactions carried out in plasma devices may be classified into homogeneous or heterogeneous, condensed phase or vapour phase, with phase change of the products or without phase change.

Studies of vapour phase homogeneous reactions without phase change have been mainly confined to the production of acetylene from various feed-stocks. The high cost of electricity (in kilowatt hours per pound of product) has restricted the commercial viability of plasma processes in this area.

Heterogeneous systems involving the use of metal ores are, however, in a more favourable position. Because of the higher molecular weights, the theoretical power requirements per unit mass (as opposed to per mole) are lower than in homogeneous systems. In practice, this advantage would be offset by the relative efficiencies of homogeneous and heterogeneous systems.

Table 3.1 shows a summary of the work on heterogeneous reactions over the past decade.

The majority of workers mentioned in Table 3.1 used the so-called "black-box" approach to the problem of effecting chemical reactions in plasma devices. In general, no realistic effort was made to understand the details and complexity of the transport processes or the high-temperature reaction kinetics. Attention was focussed on the difference between the feed and product, with a poor understanding of the intermediate stages in the conversion. Borgianni *et al.* (3.10) attempted to solve the theoretical problem but were not successful in their experiments aimed

at achieving useful conversions of material.

According to the Tafa division of Humphreys Corporation, the size of the plasma device is of great importance. In scaling up from 30kW to 1MW, the ratio of power costs was reduced by more than one order of magnitude. It is claimed by this company that their process for the dissociation of zircon sand is now commercially viable. In addition, they are believed to be carrying out experiments on large-scale production of titanium carbide and other similar materials.

CONCLUSIONS

Plasma chemical reactions are beginning to become commercially interesting. Better understanding of the transport processes should lead to a more fruitful application of these high-temperature devices.

TABLE 3.1

Summary of Heterogeneous Reactions

in Plasmas

Summary of Heterogeneous Chemical Reactions in Plasmas

	Author	Date	D.C. R.F.	Feed	Product	Efficiency %	Commercial viable process	Comments
3.1	Warren & Shimizu	1964	R.F.		Metal Nitrides		No	
	" " "	1964	R.F.	Al_2O_3	Al		No	Electricity costs 5 times Bayer process
	" " "	1964	R.F.	Manganese ores			No	Extinction of flame
3.2	Brown	1967	D.C.	ZrO_2	Zr		No	Minor weight change
3.3	Huska & Clump	1967	R.F.	MoS_2	Mo	70	No	
3.4	Jones	1967		Iron ore	Steel			Cited by Freeman
3.5	Rains	1968	R.F.	Al_2O_3	Al	46	No	CO, CH_4 quenching
3.6	Stokes	1969	D.C.	Ta_2O_5	Ta	50	No	
				WO_3	W	90	No	
				Iron oxide	Fe	100	No	
3.7	Gilles & Clump	1970	D.C.	Iron ore	Fe	64	No	Hydrogen plasma
3.8	Matsumoto & Shirato	1970	D.C.	$ZrSiO_4$	ZrN	50	No	Zirconium silicate pellet formed anode

.... continued

TABLE 3.1 (cont'd)

	Author	Date	F.C. R.F.	Feed	Product	Efficiency %	Commercial viable process	Comments
3.9	Charles et al.	1970	R.F.	Mixed refractory oxides				
				$MnSiO_3$	MnO	30	No	
				FeS	Fe_2O_3	80	No	
				MoS_2	Mo	70	No	
3.10	Borgianni et al.	1969	R.F.	Al_2O_3 CuO NiO TiO_2			No	Attempt at realistic analysis of transport processes
3.11	Dundas & Thorpe	1970	R.F.	$TiCl_4$ (vapour)	TiO_2	High	Yes	Review of industrial processes
3.12	TAFA Div. Humphreys Corp.	1970	R.F.	$ZrSiO_4$	ZrO_2 SiO_2	High	Yes	1 MW capacity
		1971	R.F.	$TiCl_4$	TiC			

BIBLOGRAPHY

3.1 Warren, I.H., and Shimizu, H., Canadian Chemical Engineering Conference, Hamilton, Ontario (1964).

3.2 Brown, R.A.S., C.I.M.M. Conference of Metallurgists, Kingston, Ontario (1967).

3.3. Huska, P.A., and Clump, C.W., Ind. Eng. Chem. Proc. Res. and Dev. 6, 238 (1967).

3.4 Freeman, M.P., Advances in High Temperature Chemistry, Vol. II, pp. 151-207 (1969).

3.5 Rains, R.K., Ph.D. Thesis, Univ. of Michigan (1968).

3.6 Stokes, C.S., Advances in Chemistry Series, No. 80, pp. 390-405 (1969).

3.7 Gilles, H.L., and Clump, C.W., Ind. Eng. Chem. Proc. Res. and Dev. 9, 194 (1970).

3.8 Matsumoto, O., and Shirato, Y., Denki Kagaku 381, 168 (1970),(in English).

3.9 Charles, J.A., Davies, C.J., Jervis, R.M., and Thursfield, G., Trans. Inst. Min. and Met. (England) 79, C54 (1970).

3.10 Borgianni, C., Capitelli, M., Cramarossa, F., Triolo, L. and Molinari, E., Combustion and Flame, 13, 181 (1969).

3.11 Dundas, P.H., and Thorpe, M.L., Chem. Eng. Prog. 66, 66 (1970).

3.12 Humphreys Corporation (Tafa). Direct communication (19. VII. 71).

PART IV - PARTICLE DYNAMICS

INTRODUCTION

For the sake of clarity, this section begins with a discussion of Newton's second law and a definition of drag coefficient, followed by a review of the individual factors affecting the magnitude of the drag coefficient. The material is based in part on the recent review of Clift and Gauvin (4.1), Crowe *et al.* (4.11) and Zarin (4.2). It is restricted to the regimes of interest applicable to this thesis (i.e. $Re < 100$, $M < 0.2$).

NEWTON'S SECOND LAW

Newton's second law as stated by Streeter (4.3) is:-

> "The resultant force acting on a control volume element is equal to the time rate of increase of linear momentum within the control volume, plus the net efflux of linear momentum from the control volume."

This may be written in vector notation:-

$$\sum \underline{F} = \partial/\partial t \int_{cv} \rho \underline{V} dv + \int_{cs} \rho \underline{V}\, \underline{V} \cdot \underline{dA} \qquad \ldots\ldots\ldots\ldots\ldots\ldots\ldots\ldots \quad (4.1)$$

For a spherical particle of constant mass and shape, this reduces to the familiar

$$\sum F_p = m_p (dV_p/dt) \qquad \ldots\ldots\ldots\ldots\ldots\ldots\ldots\ldots \quad (4.2)$$

However, where the mass of the particle is changing, the second term of equation (4.1) is required. A simple example follows. For a rocket engine in a gravity-free field, but subject to the aerodynamic drag,

the equation of motion (again given by Streeter) is

$$-F_D = m_p(dV_p/dt) - \dot{m}_p V_R \quad \ldots\ldots\ldots\ldots\ldots\ldots\ldots\ldots (4.3)$$

where F_D is the drag on the rocket in the direction opposing the motion and V_R is the velocity of the gas expelled from the engine and measured relative to it.

It is noted that the acceleration term is measured from fixed coordinates and is an absolute acceleration. In most cases of particle dynamics, the gas acceleration is zero and therefore the particle absolute acceleration measured from a fixed frame of reference is equal to the relative acceleration measured from a frame of reference translating with gas. In this study, it is necessary to retain the distinction because the gas itself has a very significant deceleration.

DRAG FORCE AND DRAG COEFFICIENT

The drag force on a particle may be defined as "that force on a particle due to the flow of fluid around it and is the sum of the directed pressure and skin friction effects". At this stage, no distinction is made as to whether the definition is for steady state or one instant in time.

The drag force is related to the non-dimensional drag coefficient by the defining equation:-

$$F_D = -(1/2)(C_D A \rho_g)|V_p - V_g|(V_p - V_g) \quad \ldots\ldots\ldots\ldots\ldots (4.4)$$

For a spherical particle and neglecting gravity, the equation reduces to

$$dV_p/dt = -(3/4)(\rho_g/\rho_p)(C_D/D_p)|V_p - V_g|(V_p - V_g) \quad \ldots\ldots (4.4a)$$

or

$$C_D = -(4/3)(\rho_p/\rho_g)(D_p)(dV_p/dt)/\left[|V_p - V_g|(V_p - V_g)\right] \quad \ldots\ldots\ldots\ldots \quad (4.4b)$$

FACTORS AFFECTING THE DRAG COEFFICIENT

The following sections discuss the effects of a number of individual factors in isolation on the drag coefficient:-

(i) Reynolds Number and the Standard Curve

It is recalled that the Reynolds number is a measure of the ratio of inertial to viscous effects for the flow around a particle. At low Reynolds number ($Re < 0.1$) the viscous effects predominate and the Stokesian solution of the equation of motion may be used, with the well-known result:-

$$C_D = 24/Re \quad \ldots\ldots\ldots\ldots\ldots\ldots\ldots\ldots\ldots\ldots\ldots\ldots \quad (4.5)$$

In the Stokesian regime, two thirds of the drag is due to skin friction, and one third is due to the pressure effect (form drag). The flow around the particle is reasonably symmetrical and its effect pervades the whole flow field.

As the Reynolds number increases, the inertial effects become more important (as shown in Fig. 4.1, from ref. (4.37)) and the flow pattern fore and aft shows a definite asymmetry. The linearised Navier-Stokes equation first used by Oseen resulted in the solution:-

$$C_D = (24/Re)[1 + (3/16)(Re) - (19/1280)(Re)^2] \quad \ldots\ldots\ldots\ldots\ldots \quad (4.6)$$

According to Zarin (4.2), this agrees with experimental results up to a Reynolds Number of 0.90.

The numerical and experimental work between the Oseen range and

FIGURE 4.1

Variation of Ratio of Skin-Friction to Form-Drag for Spheres, as a Function of Reynolds Number (taken from LeClair et al. (4.37))

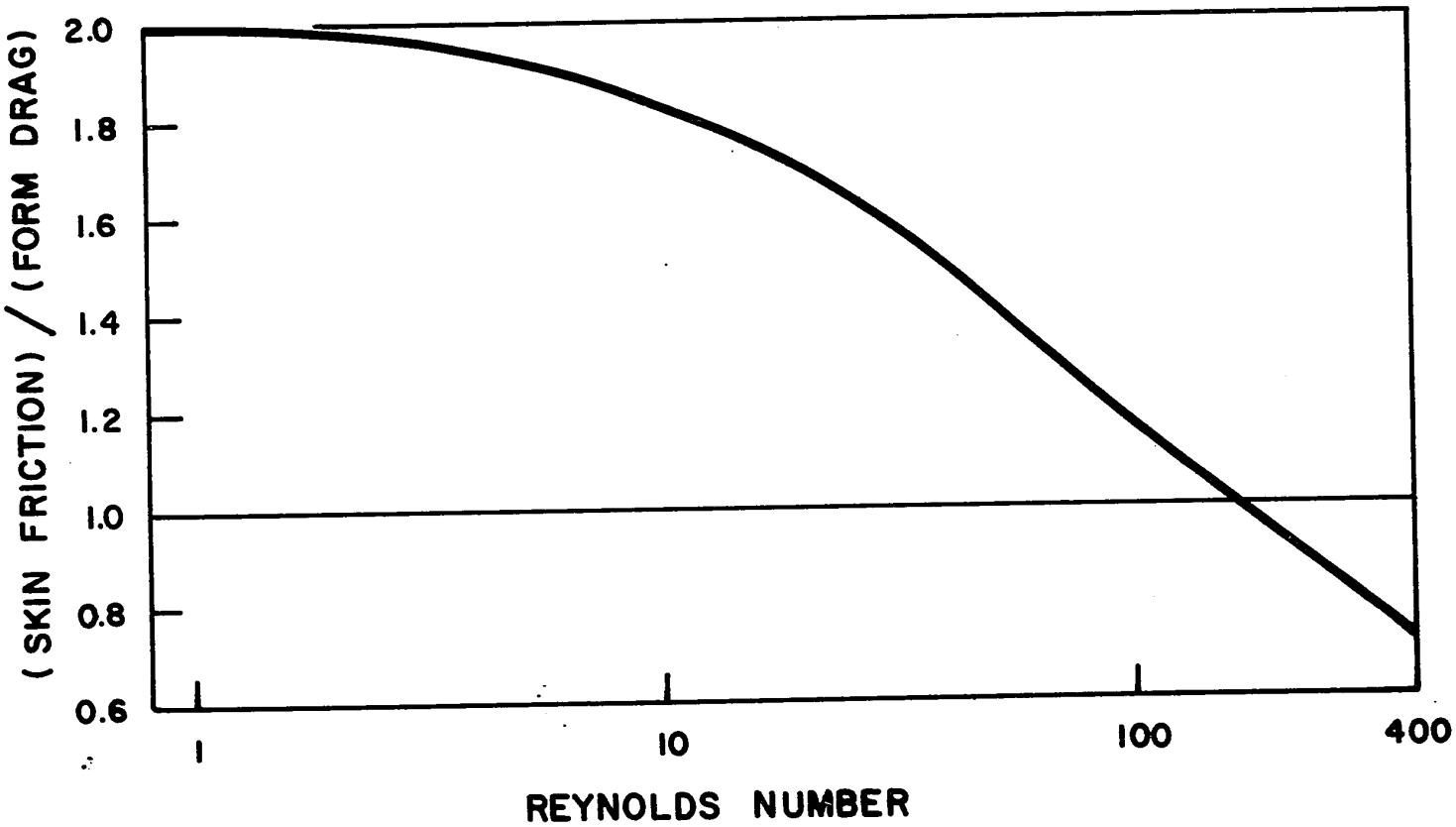
(SKIN FRICTION) / (FORM DRAG)
2.0
1.8
1.6
1.4
1.2
1.0
0.8
0.6
1
10
100
400
REYNOLDS NUMBER

a Reynolds number of about 500 is summarised by Pruppacher, LeClair and Hamielec (4.4) and is further condensed here. As the Reynolds number increases beyond the Oseen limit, the fore-aft asymmetry increases until a Reynolds number of about 20 is reached. At this point, a small wake behind the sphere begins to form and grows with increasing Reynolds number. At Re$\sim$30, the length of the vortex is about 0.2 sphere diameter. At a Reynolds number of about 400, the vortex behind the sphere begins to shed periodically,

These changes in flow pattern are reflected in the experimental C_D values of Beard and Pruppacher (4.5):-

$$0.2 \leqslant Re \leqslant 2, \quad C_D = (24/Re)[1 + 0.1(Re)^{0.99}] \quad \ldots\ldots \quad (4.7a)$$

$$2 \leqslant Re \leqslant 21, \quad C_D = (24/Re)[1 + 0.11(Re)^{0.81}] \quad \ldots\ldots \quad (4.7b)$$

$$21 \leqslant Re \leqslant 200, \quad C_D = (24/Re)[1 + 0.189(Re)^{0.632}] \quad \ldots\ldots\ldots \quad (4.7c)$$

where it is noted that the break between the second and third correlations corresponds to the onset of flow separation. In view of the experimental techniques used, it is considered that these experimental results are probably the most reliable data available.

A useful engineering approximation of the Beard and Pruppacher data is:-

Reynolds Number	Increase in Drag Coefficient above Stokesian Value (%)
0.1	1
1	10
10	100

(Further effects of an increase in Reynolds number are beyond the scope of this thesis and are not considered here. Reference is made to the reviews of Torobin and Gauvin (4.12a, 4.12b) for a description of the effects of laminar-turbulent boundary layer transition.)

(ii) The Effect of Turbulence

This thesis is concerned with a regime of low Reynolds number and high ratio of Eulerian macroscale of turbulence to particle diameter. This section of the review is therefore restricted to the above field as far as possible.

For the case of flow in the Stokesian regime, Shirazi, Chao and Jones (4.6) used a Fourier transform method to predict the particle Lagrangian Energy Spectral Distribution Function from the Eulerian statistics of the fluid. The conventional Stokesian drag coefficient was used except that the Basset history term was also included. (This term will be discussed under the effects of acceleration.) Earlier analyses of a similar type were carried out by Lumley (4.7) and by Tchen (4.8). A somewhat over-simplified conclusion which can be derived from these works is that a small particle in a turbulence flow field, does not "see" the eddies, but a fluctuating free-stream velocity. The results of Soo et al. (4.9) show that for glass beads ($D_p \sim 100\mu m$) entrained in a gas stream, the fluctuation of particle velocity can be greater than that of the gas.

In the upper end of the Reynolds number regime, there is a lack of relevant and consistent experimental data. For a Reynolds number range $50 < Re < 700$ Uhlherr and Sinclair (4.10) measured the effect of the relative free-stream turbulence on the particle drag coefficient in a solid liquid flow system. The scale of turbulence was not measured

and therefore a comparison with the results of Zarin (4.2) must be treated with caution. The latter worked with magnetically-supported spheres which remained in a fixed location while air was blown past them. (The ratio of scale of turbulence to sphere diameter was about 3). For Zarin (4.2) and for Uhlherr and Sinclair (4.10), the general conclusion was that an increase of relative turbulence intensity increased the drag on a particle, with Zarin showing a lesser increase of the two works. However, it is noted that for low intensities of turbulence ($I_R \sim 0.03$) Uhlherr and Sinclair (4.10) found a decrease in the drag coefficient, which was attributed to a decrease in the size of the wake and therefore a decrease in the form drag. The increase in the drag coefficient at higher turbulence intensities was believed to be caused by the higher front stagnation shear stress.

While Zarin did not observe drag coefficients below the standard curve, extrapolation of his results below Re = 200 would indicate that such a decrease is possible for $50 < Re < 100$.

For the range $10 < Re < 50$, Uhlherr and Sinclair (4.10) carried out flow visualisation experiments and found that an increase of turbulence intensity appeared to delay the onset of the recirculating wake until a higher (30-50) Reynolds number. The drag coefficient was found also to increase with increase of relative turbulence intensity.

(iii) Relative Acceleration

This section is concerned with an examination of the differences between steady-state and transient determinations of drag coefficients.

At steady state, the flow-field around a particle is by definition independent of time. This situation occurred in the experiments performed

by Zarin (4.2) and by Beard and Pruppacher (4.5). In both cases, the particle-gas relative velocity was constant and the drag force was determined either magnetically (Zarin (4.2)) or from the weight of the particle (Beard and Pruppacher (4.5)).

In contrast, free-flight experiments determine the drag force by equating it to the product of the mass of the particle by its absolute acceleration (e.g. Crowe et al. (4.11), Torobin and Gauvin (4.12f)). In general, the gas velocity is nearly constant but the relative velocity between particle and gas will be continuously changing. The flow field around the particle must therefore attempt to adjust continuously to the expected steady state value. However, if the relative acceleration is high, then there will be a considerable lag between the actual instantaneous flow field around the particle and the equivalent steady state flow field. (In the language of Control Theory, the output from a first order differential system lags behind the ramp imput to that system by an amount proportional to the time constant of that system.)

The Acceleration Modulus is a useful non-dimensional group when comparing relative accelerations in different systems:

$$N_{AM} = \dot{V}_R/(V_R^2/D_p) \qquad \ldots\ldots\ldots\ldots\ldots\ldots\ldots\ldots\ldots\ldots \quad (4.8a)$$

A value of N_{AM} above unity would be considered high, a value much less than unity would be considered low. The acceleration modulus may be interpreted as the ratio of the relative acceleration to the convective acceleration, or alternatively as the ratio of a transit time to a scaled relative acceleration:-

$$N_{AM} = (D_p/V_R)/(V_R/\dot{V}_R) \qquad \ldots\ldots\ldots\ldots\ldots\ldots\ldots\ldots\ldots\ldots \quad (4.8b)$$

The effect of the lag in the configuration of the flow field is expressed in the equation of motion of the particle by the Basset history term (e.g. Hinze (4.13), Odar (4.14), Rudinger (4.15)):-

$$F_H = (3/2)(D_p)^2(\pi\rho_g\mu_g)^{1/2}\int_o^t \left[(dV_p/dt' - dV_g/dt')(t - t')^{-1/2}\right] dt' \quad \ldots\ldots (4.9)$$

This is a convolution integral which sums the history of the relative motion between particle and gas, but gives most weight to later events and a minimal weight to the earlier events.

According to Odar (4.14), the coefficient (3/2) is a function of the acceleration modulus, dropping by about 50% as $1/N_{AM}$ increases from zero to unity. In view of the differences in flow pattern between the Stokesian ($Re < 0.1$) and steady vortex ($Re < 30$) regimes, it is suggested that there may be a variation of coefficient with Reynolds number. According to Rimon and Cheng (4.16), the time to reach a steady-state flow pattern is (1.5 to 5)D_p/V_R seconds, increasing only slowly with Reynolds number. They suggested the relaxation time for a one mm particle having a relative velocity of 3 m/s would be about 1 ms. The effective value of the coefficient could perhaps be estimated from an extension of the work of LeClair and Hamielec (4.17) who calculated the drag on an accelerating sphere by solving for the whole flow field.

Apart from the effect of the history of the motion on the drag coefficient of a particle, the "added mass" must also be considered. A full derivation of the equation of motion for Stokesian flow includes the term:-

$$F_{AM} = 1/2(\pi D_p^3 \rho_g/6)(dV_p/dt - dV_g/dt) \quad \ldots\ldots\ldots\ldots\ldots\ldots \quad (4.10)$$

If the gas itself were not accelerating, this term would effectively increase the mass of the particle by an amount equal to one half of the amount of fluid displaced. Again, Odar (4.14) suggests that the coefficient is a function of the acceleration modulus, decreasing from a value of 1.05 at low N_{AM} to 0.5 at high N_{AM}. It was mentioned earlier that the size of a vortex behind a sphere was a strong function of Reynolds number. It is therefore suggested that this will have some effect on the added mass coefficient. An interesting interaction of the concepts of history and added mass is given by the results of LeClair and Hamielec (4.17). They calculated that the vortex behind a sphere could be suppressed by particle acceleration up to a Reynolds number of about 140.

Very little experimental data are available in the Reynolds number regime of interest. The work of Ingebo (4.36) ($1 < Re < 400$) has been criticized in the past. He obtained a drag coefficient-Reynolds number correlation which was independent of mass transfer or acceleration. His experimental technique appears to have relied on taking the difference in the mean velocity of groups of particles at different locations. No discussion was made as to the validity of this approach. His results were summarised by the correlation:-

$$C_D = 27/(Re)^{0.84} \quad \ldots\ldots\ldots\ldots\ldots\ldots\ldots\ldots\ldots\ldots \quad (4.11)$$

Ingebo's data points fall below the standard curve. The reduction in the drag coefficient has been attributed to both turbulence and acceleration (Crowe et al. (4.11) and Clift and Gauvin (4.1)). As

discussed later in the experimental section, the history and added mass effects would also be expected to give a reduction in the drag coefficient, but not necessarily of the magnitude reported by Ingebo (4.36).

(iv) Shape and Orientation

According to Marchildon et al. (4.18), the motion of particles below Re = 100 is devoid of secondary motion, as might be expected from the steadiness of the wake formation. In this regime, it was noted that irregularly shaped particles oriented themselves with the largest surface area normal to the direction of flow.

In Stokesian flow, no preferred orientation was noticed. According to a reference given in O'Brien (4.19), the Stokesian drag on a deformed body is bounded by the limits of the drag on the two spheres which would just enclose the body, or be enclosed by it. As summarised by Munz (4.20), a common approach to estimating drag coefficients for irregular particles has been to use a geometric mean diameter and a correction factor appropriate to the shape of the particle.

(v) Particle Rotation

Nurekenov (4.21) reported rotation rates of about 10^4 rad/s (2 000 rev/sec) for 100μm coal dust particles in the intense shear field of a cyclone. It may be supposed that the shear field in jets is of the same order of magnitude and that similar rotation rates would be possible. In the case of a particle entrained in a cyclone or in a jet, the combined rotation and translation results in a tumbling motion rather than a screw motion.

As summarised by Selberg and Nicholls (4.22) the effect of

rotation becomes only of importance at high Reynolds numbers ($\sim 8 \times 10^4$) where the drag coefficient is reduced from 0.52 to 0.48 (8%) for a ratio of peripheral velocity to relative translation velocity increasing from zero to unity. According to Luthander (4.23), below the critical Reynolds number, a velocity ratio less than 2 has very little effect on C_D.

(vi) Effect of Mass Transfer

A spherical particle at rest evaporating uniformly in empty space would have no thrust exerted on it. The same result would apply if it were in a stagnant fluid. If, however, the vapour evolution around the particle were not symmetrical, then there would be a net thrust on the particle in a direction opposite to the direction of maximum evaporation. In other words there would be a net rocket thrust effect on the particle.

Since mass transfer in the case of a moving particle is usually highest at the front stagnation point, then any rocket thrust effect would reinforce the drag on the particle. According to Eisenklam et al. (4.24) this effect was a contributory reason for the reduction in the drag coefficient of 100μm droplets burning in air. It was not explicitly stated that the highest vapour evolution rate was at the rear stagnation point. If this were not so, then there would be some inconsistency in their conclusion.

Hamielec et al. (4.25) carried out numerical computations on the effect of vapour evolution from spheres in the range $1 < Re < 100$. Their results are summarised in Fig. (4.2) and Fig. (4.3). For a given

FIGURE 4.2

Effect of Evaporation on Skin Friction and Form Drag

(Re = 1, taken from Hamielec *et al.* (4.25))

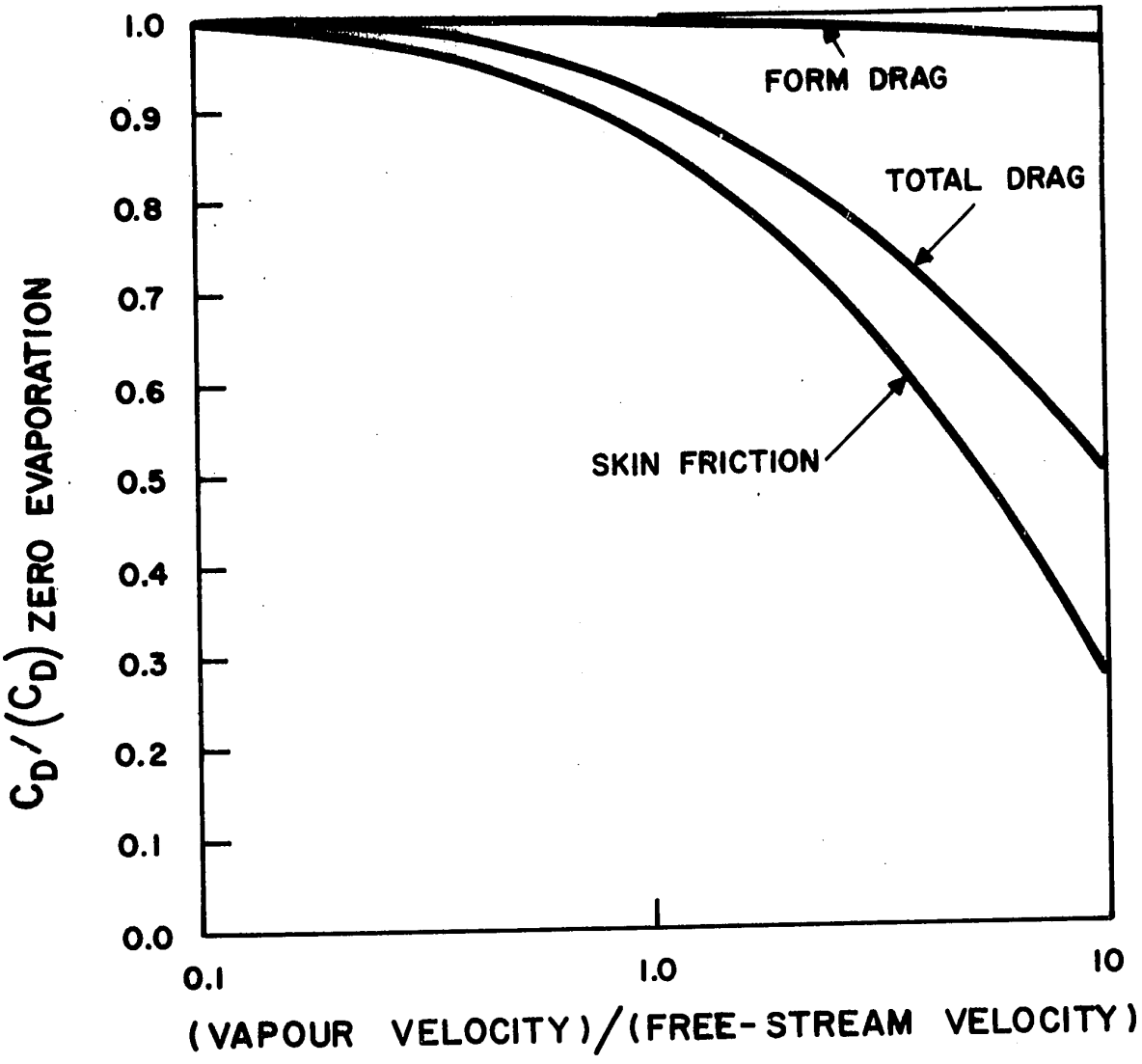
1.0
0.9
0.8
0.7
0.6
0.5
0.4
0.3
0.2
0.1
0.0
FORM DRAG
TOTAL DRAG
SKIN FRICTION
$C_D'/(C_D)$ ZERO EVAPORATION
0.1
1.0
10
(VAPOUR VELOCITY)/(FREE-STREAM VELOCITY)

FIGURE 4.3

Effect of Reynolds Number on Drag at Constant Ratio of Vapour Velocity to Free-Stream Velocity (taken from Hamielec *et al.* (4.25))

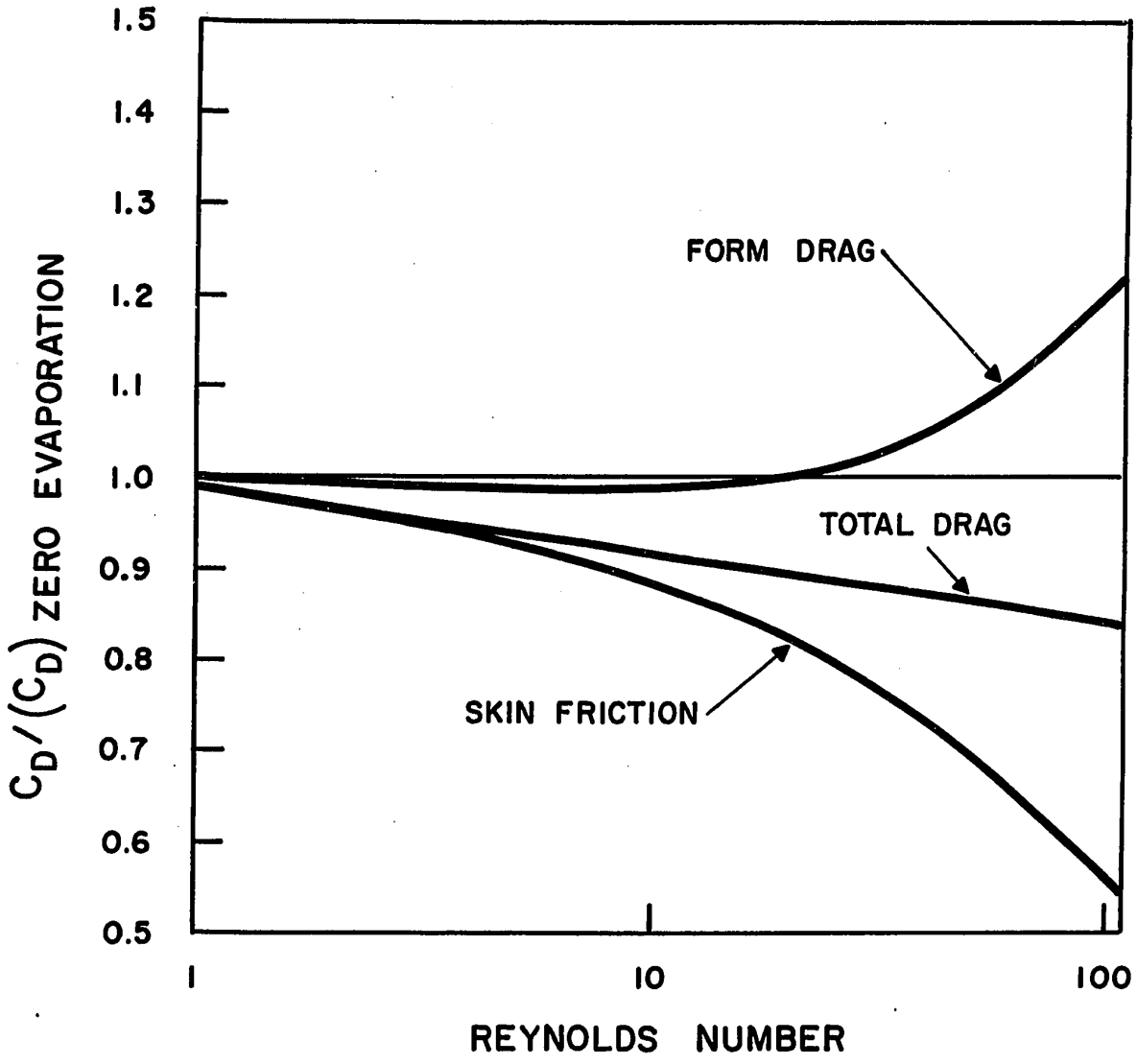
1.5
1.4
1.3
1.2
1.1
1.0
0.9
0.8
0.7
0.6
0.5
$C_D'/(C_D)$ ZERO EVAPORATION
FORM DRAG
TOTAL DRAG
SKIN FRICTION
1
10
100
REYNOLDS NUMBER

Reynolds number (Re = 1), the skin friction may be reduced by a factor of 4, with a slight decrease in the pressure drag, giving a net drag decrease of about 50%. This is consistent with a decrease of local velocity gradients and an increase in pressure at the rear of the sphere.

At higher Reynolds numbers (Re = 40), the skin friction is still reduced but the form drag is increased slightly.

(vii) Effect of Heat Transfer and Temperature Gradients

Heat transfer between particles and gas can affect the drag coefficients in a number of different ways. In the case of extreme non-isothermal conditions, the first problem is the question of the temperature at which to evaluate the fluid properties. In heat transfer to and from cylinders with modest temperature ratios ($\sim$1.3), it has been generally adequate to use a "mean film temperature". This is defined as the arithmetic mean of the particle and free stream temperatures, and has been discussed by Kubanek (4.26), Ahmed (4.28) and Douglas and Churchill (4.27). The advent of plasma torches allowed temperature ratios of the order of 4 (4.26) and the convenient approach of Douglas and Churchill was then found to be limited in applicability. In the range $4 < Re < 40$, a Nusselt number correction factor was determined by Ahmed (4.28) for heat transfer from a plasma flame to a cooled film anemometer.

$$Nu = Nu_{av}(\nu_{av}/\nu_{\infty})^{0.15} \quad \ldots\ldots\ldots\ldots\ldots\ldots\ldots\ldots\ldots\ldots \quad (4.12)$$

The kinematic viscosity ratio was found to represent the data more closely than a temperature ratio.

Babii and Ivanova (4.29) measured the drag coefficient of coal

and coke particles (100μm to 1000μm in diameter) in the range $1 < Re < 1000$. They found it was possible to correlate their data using the gas temperature and a correcting factor $(T_p/T_g)^{1.7}$, although they preferred a correlation based on using different temperatures for the density in equation 4 and the kinematic viscosity of the Reynolds number.

Basov and Popov (4.30) measured drag coefficients at varying particle temperatures in the range $4000 < Re < 12000$ based on the gas temperature and concluded that in this range, the surface temperature was not an important factor.

In a numerical solution of the problem in the Stokesian regime, Kassoy et al. (4.31) derived an approximately linear correction to the drag coefficient. Based on the free stream gas temperature, the correction may be simplified to:-

$$C_D = (C_D)_{iso}[1 + 0.55(T_p - T_\infty)/T_\infty] \quad \ldots\ldots\ldots\ldots\ldots\ldots (4.13)$$

This was applicable to a hot sphere in a cold gas, but the slight curvature of their plot would only be expected to reduce the correction a small amount for the reverse case. It will be shown in the experimental part of this thesis that the Kassoy et al. (4.31) drag correction is reasonably consistent with using a mean film temperature and Ahmed-type correction.

Lemoine and Le Goff (4.32) in work similar to the present thesis project, used a correction factor which was independent of temperature. While obviously inadequate for general purposes, this correction factor was presumably justified for their restricted range of operation.

In the above references, no mention was made of possible major

changes in the flow pattern around the sphere. According to Schlichting (4.33), a heated surface could cause premature transition of the boundary layer with its consequent effects on drag coefficient. This is, however, outside the range of this thesis ($Re < 100$).

At the much lower Reynolds numbers in the Stokesian regime, it has been found by Hamielec and Woo (4.34) that natural convection effects play a dominant role in changing the drag coefficient. A hot particle falling freely at terminal velocity in a cold gas would have a near-normal drag coefficient, associated with a reasonably unchanged flowfield. However, if the particle were colder than the gas, the flow around the particle would be reversed as seen schematically in Fig. (4.4) with a drastic reduction in the drag coefficient. For very low Reynolds numbers, the drag coefficient would be negative, implying complete domination of the downward convection current. The criterion to determine whether natural convection is important is Gr/Re^2. For values less than unity, natural convection is of minor importance.

(viii) Compressibility and Non-Continuum Flow

While the free-stream relative velocity near the front stagnation point of a sphere may be less than Mach 1, the acceleration of the flow around the sphere may be sufficient to raise the Mach number close to unity and cause deviations in the flow field by the generation of a shock wave. It is obvious that low free-stream Mach numbers would not suffer this effect, since the equatorial Mach number would still be low. Zarin (4.2) refers to the data of Hoerner (4.35) in which the drag coefficient for the range $10^4 < Re < 10^5$ is doubled as the Mach number

FIGURE 4.4

Effect of Opposing Flow for a Cold Particle

in a Hot Low Velocity Gas

(taken from Hamielec and Woo (4.34))

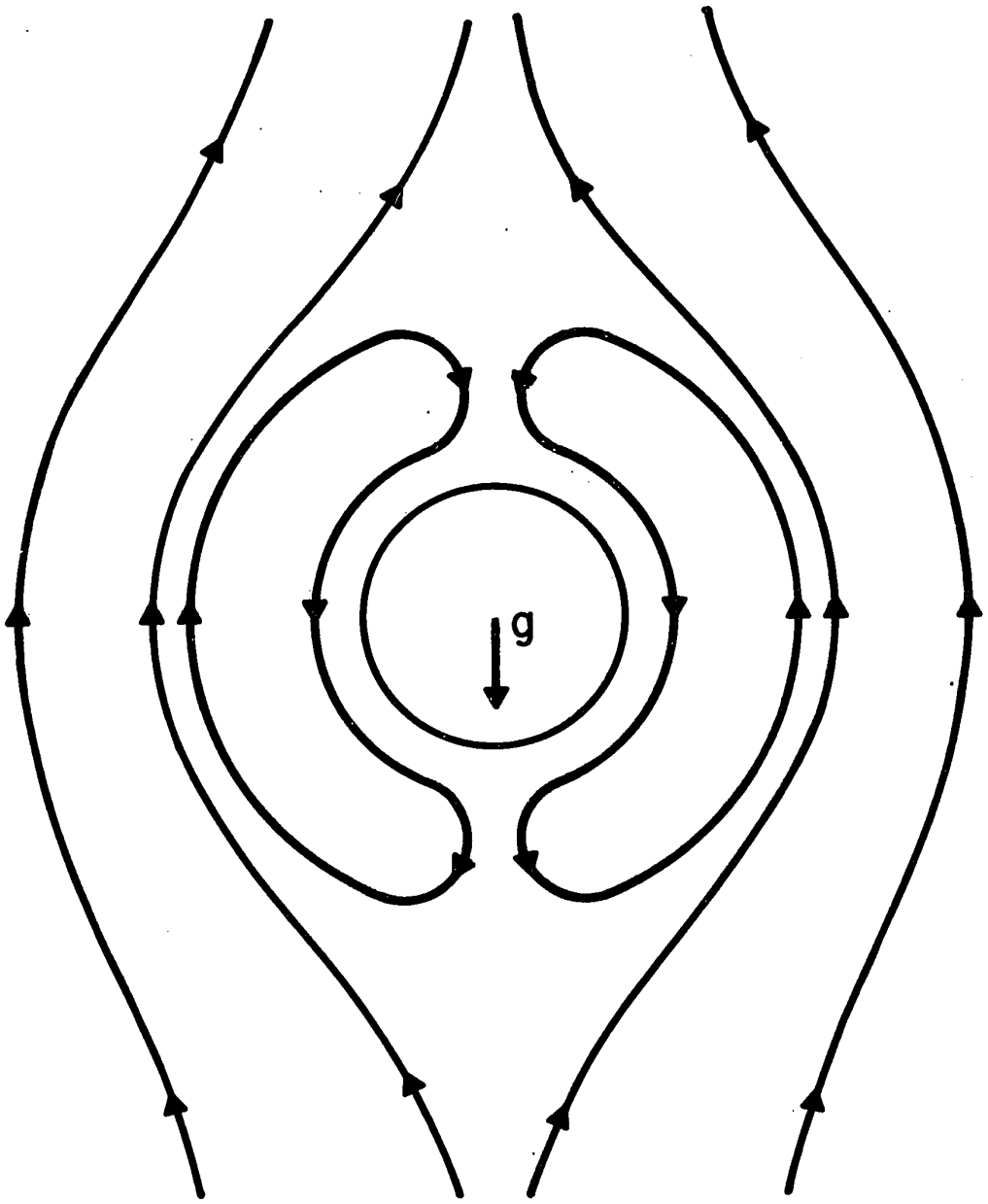
g

increases from 0.1 to 1.

Apart from the effect on compressibility, the Mach number is a factor in determining whether or not continuum flow may be said to exist. The Knudsen number is a measure of this quantity and is defined

$$Kn = M/Re \qquad (Re < 1) \qquad \ldots\ldots\ldots\ldots\ldots\ldots \quad (4.14)$$

or

$$Kn = M/(Re)^{1/2} \qquad (Re < 1) \qquad \ldots\ldots\ldots\ldots\ldots\ldots \quad (4.15)$$

Four regimes of Knudsen number are generally recognised (Zarin (4.2)):-

Continuum	$Kn < 0.01$
Slip	$0.01 < Kn < 0.1$
Transition	$0.1 < Kn < 3.0$
Free Molecular	$3.0 < Kn$

Part of the experimental work of Zarin (4.2) was in the slip flow regime ($Kn < 0.06$).

It was found that at Re = 100, the drag coefficients laid above the standard curve by about 3 per cent, increasing to 8 per cent at Re = 4000. Considering that the Beard and Pruppacher results (4.5) also show deviations of this magnitude, it may be concluded that minor incursion into the slip flow regime does not have any significant effect on the drag coefficient.

DISCUSSION

In the above review, the various effects were considered in isolation. In reality, these effects occur simultaneously and should not be considered as additive, since they may give rise to complex interrelationships.

CONCLUSIONS

The effect of Reynolds number is well established in the regime of interest.

The effect of turbulence has not been adequately investigated, particularly with reference to the ratio of scale of turbulence to particle size.

Relative acceleration is beginning to be more clearly understood through the Basset history term, but no general comment can be made on whether an increase in drag coefficient would be expected.

Mass transfer away from a particle should reduce the drag coefficient below the expected value.

Heat transfer from a particle to the free-stream would be expected to increase the drag coefficient above the isothermal value. More experimental and computational work is required in this area.

NOMENCLATURE

A	Particle projected area	L^2
C_D	Drag coefficient	-
$C_{D(iso)}$	Isothermal drag coefficient	-
D_p	Particle diameter	L
$\underline{F}$	Force	$M\ L\ T^{-2}$
F_{AM}	Force due to added mass	$M\ L\ T^{-2}$
F_D	Drag force	$M\ L\ T^{-2}$
F_H	Force due to history effect	$M\ L\ T^{-2}$
F_p	Force on particle	$M\ L\ T^{-2}$
Gr	Grashof number ($= D_p^3.\beta.g.\Delta T/\nu^2$)	-
Kn	Knudsen number	-
M	Mach number	-
m_p	Particle mass	M
$\dot{m}_p$	Particle mass evaporation rate	$M\ T^{-1}$
N_{AM}	Acceleration modulus (number)	-
Nu	Nusselt number	-
Nu_{av}	Nusselt number evaluated at average film temperature	-
R_p	Particle radius	L
Re	Reynolds number	-
t	Time	T
t'	Convolution time	T
T_p	Particle temperature	^oK

T_g	Gas temperature	$^{\circ}K$
v	Volume element	L^3
V_g	Gas velocity	$L\ T^{-1}$
V_p	Particle velocity	$L\ T^{-1}$
V_R	Relative velocity ($V_p - V_g$)	$L\ T^{-1}$
μ	Viscosity	$M\ L^{-1}\ T^{-1}$
ν_∞	Kinematic viscosity at free stream temperature	$L^2\ T^{-1}$
ν_{av}	Kinematic viscosity at mean film temperature	$L^2\ T^{-1}$

BIBLIOGRAPHY

4.1 Clift, R., and Gauvin, W.H., Can. J. Chem. Eng. (in press).

4.2 Zarin, N., NASA CR-1585 (1970).

4.3 Streeter, V.L., "Fluid Mechanics", fifth edition, McGraw Hill (1971).

4.4 Pruppacher, H.R., LeClair, B.P., and Hamielec, A.E., J. Fluid Mech. 44, 781 (1970).

4.5 Beard, K.V., and Pruppacher, H.R., J. of the Atmospheric Sciences 26, 1066 (1969).

4.6 Shirazi, M.A., Chao, B.T., and Jones, B.G., "On the Motion of Small Particles in a Turbulent Fluid Field", Nuclear Engineering Laboratories Report, University of Illinois at Urbana, Illinois.

4.7 Lumley, J.L., Ph.D. Thesis, The John Hopkins University (1957).

4.8 Tchen, C.M., Ph.D. Thesis, Delft (1947).

4.9 Soo, S.L., Ihrig, H.K., El Kouh, A.F., Trans A.S.M.E., J. Basic Eng. 609 (1960).

4.10 Uhlherr, P.H.T., and Sinclair, C.G., Proceedings Chemeca 1970, 1, 13 (1970), (Butterworths of Australia).

4.11 Crowe, C.T., Babcock, W.R., and Willoughby, P.G. "Drag Coefficient Data for Particles in Low Mach Number Rarefied and Near-Rarefied Flow Regimes Obtained with a Microballistic Range". International Symposium on Two Phase Systems, Haifa, Israel (August 1971).

4.12 Torobin, L.B., and Gauvin, W.H., a) Can. J. Chem. Eng. 37, 129 (1959)
b) " " " " 37, 167 (1959)
c) " " " " 38, 142 (1960)
d) " " " " 38, 142 (1960)
e) " " " " 39, 113 (1961)

4.12 Torobin, L.B., and Gauvin, W.H., f) A.I.Ch.E.J. 7, 615 (1961).

4.13 Hinze, J.O., "Turbulence", McGraw Hill (1959).

4.14 a) Odar, F., and Hamilton, W.S., J. Fluid Mech. 18, 302 (1964).

b) Odar, F., J. Fluid Mech. 25, 591 (1966).

c) Odar, F., U.S. Army Cold Regions Research and Engineering Laboratory (CRREL) R.R., 190 (July 1966).

4.15 Rudinger, G., Ch. 3, "Relaxation in Gas Plarticle Flows" (Vol. 1) ed. P.W. Wegener, M. Dekker (1969).

4.16 Rimon, Y., and Cheng, S.I., Physics of Fluids 12, 949 (1969).

4.17 LeClair, B.P., and Hamielec, A.E., Fluid Dynamics Symposium, McMaster Univ., Hamilton (Aug. 1970).

4.18 Marchildon, E.K., Clamen, A., and Gauvin, W.H., Can. J. Chem. Eng. 42, 178 (1964).

4.19 O'Brien, V., A.I.Ch.E.J. 14, 870 (1968).

4.20 Munz, R.J., Ph.D. Project Proposal, Dept. Chemical Engineering, McGill University (June 1971).

4.21 Nurekenov, E., Problemy Teploenergetiki I Prikladnoi Teplofizika VYP-1, 270 (1964).

4.22 Selberg, B.P., and Nicholls, J.A., A.I.A.A. J. 6, 401 (1968).

4.23 Luthander, S., and Rydberg, A., Zeit. F. Physik 36, 552 (1935).

4.24 Eisenklam, P.A., Arunachalam, S.A., and Weston, J.A., 11th International Symposium on Combustion 715 (1967).

4.25 Hamielec, A.E., Hoffman, T.W., and Ross, L.L., A.I.Ch.E.J. 13, 212 (1967).

4.26 Kubanek, G.R., Ph.D. Thesis, McGill University, Montreal (1966).

4.27 Douglas, W.J.M., and Churchill, S.W., Chem. Eng. Prog. Symp., Ser. 52, no. 18, 23 (1956).

4.28 Ahmed, A.M., Mechanical Engineering Research Laboratories T.N. 67-5, McGill University, Montreal (1967).

4.29 Babii, V.I., and Ivanova, I.P., (Solid-Propellant Combustion; 2nd All Union Conference, Novosibirsk, USSR, Nov. 1963; Proceedings) Tech. Inf. Service, A.I.A.A., microfiche A70-28582.

4.30 Basov, V.N., and Popov, V.A., Izv. Akad. Nauk. SSSR, Otd. Tekh. Nauk. 8, 12 (1958) (in English NASA TT F-10,033).

4.31 Kassoy, D.R., Adamson, T.C., Messiter, A.F., Physics of Fluids 9, 671 (1966).

4.32 Lemoine, A., and Le Goff, P., Chimie et Industrie 102, 1304 (1969), also Lemoine, A., Doc. Ing. Thesis, Univ. of Nancy (1969).

4.33 Schlichting, H., "Boundary Layer Theory", McGraw Hill (1960).

4.34 Hamielec, A.E., and Woo, S.W., in preparation, Department of Chemical Engineering, McMaster Univ., Hamilton, Canada (1971).

4.35 Hoerner, S.F., "Fluid Dynamic Drag", pub. by author (1958).

4.36 Ingebo, R.D., N.A.C.A. TN 3762 (Dec. 1956).

4.37 LeClair, B.P., Hamielec, A.E., and Pruppacher, H.R., J. of The Atmospheric Sciences 27, 308 (1970).

PART V - MEASUREMENT TECHNIQUES

The extreme conditions occurring in a plasma-particulate system result in considerable demands on the limited capability of measurement techniques:

(a) The gas temperature is sufficient to destroy any unprotected probe placed in the hot zone;

(b) Particle diameters border on the resolution dimensions of optical systems;

(c) Particle velocities are beyond the range of conventional equipment.

The need to take measurements in a plasma-particulate system necessitated a broad review of experimental techniques. A summary of this review is given below.

(N.B. Because of its importance in this work, gas temperature was considered in the first section of this thesis.)

PARTICLE VELOCITY

The selection of a particular technique for the measurement of particle velocities depends on the particle size, its velocity and the field of view to be covered. Fig. (5.1) presents a classification of some of the more useful methods which are described in the following sections, together with a brief account of applications.

PHOTOGRAPHIC METHODS

Still Photography

Regular 35 mm cameras have been used in two different ways to measure particle velocity. These involve the use of single-flash and multiple-flash illumination.

Using single-flash, the length of the streak and the duration of the flash give the image velocity. The magnification then gives the particle velocity by simple ratio. It should be noted that focal plane shutters used in high quality cameras can give considerable elongation of the streak, if the object is moving in a direction opposite to that of the shutter. This problem is avoided by the use of multiple flash, where the distance between streak centres is used.

Single flash was used by Desai *et al.* (5.1) to measure the velocity of 40-80μm Boron Nitride particles in a low-velocity R.F. plasma. The measured particle velocities were in the range 4-10 m/s.

Multiple flash was used by Painter (4.2) for 150μm polystyrene beads in water, with velocities around 4 m/s.

Ciné-Photography

The word "Ciné" is used in the context of this thesis to imply

FIGURE 5.1

Classification of Particle Velocity

Measurement Techniques

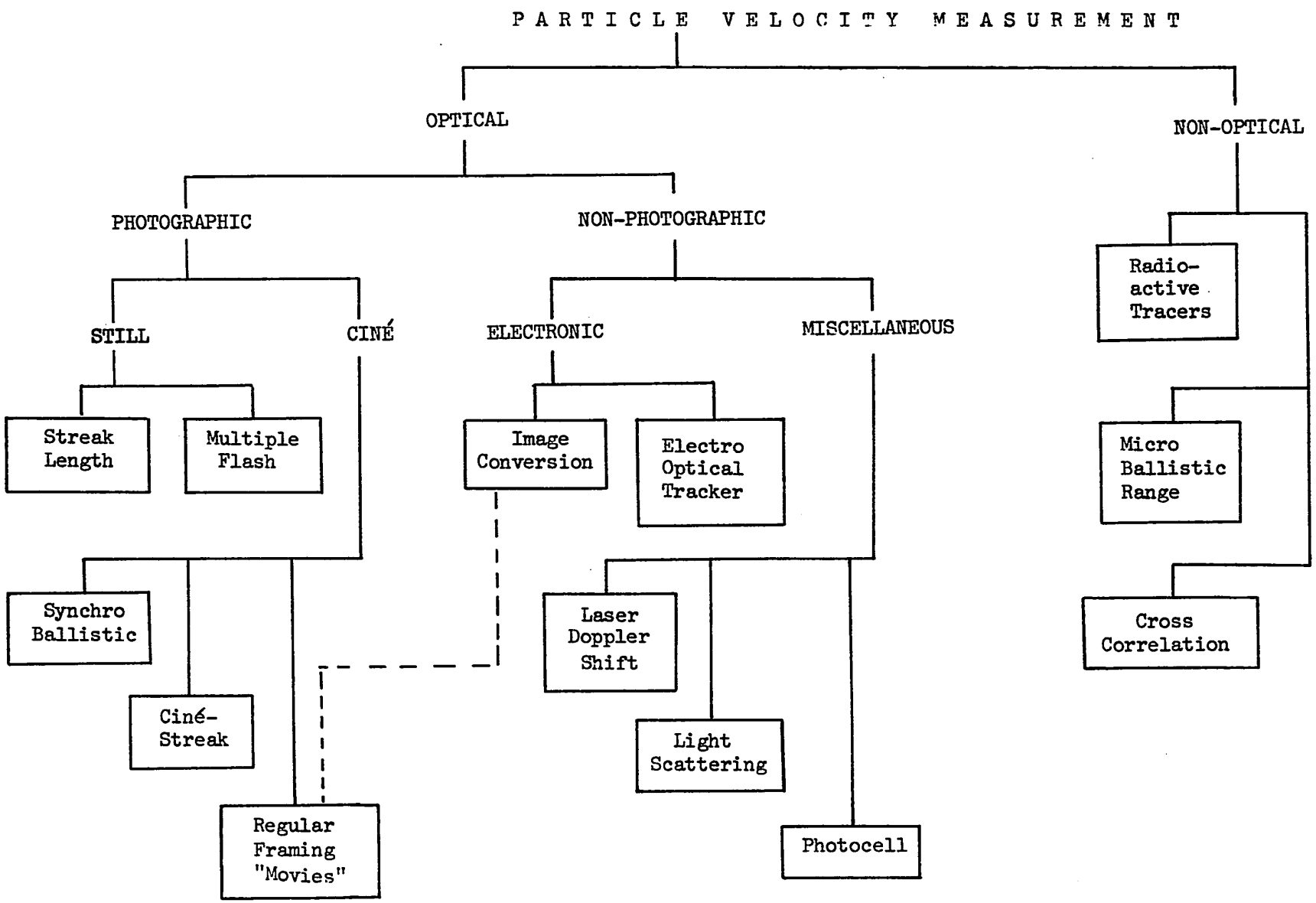
PARTICLE VELOCITY MEASUREMENT
OPTICAL
NON-OPTICAL
PHOTOGRAPHIC
NON-PHOTOGRAPHIC
STILL
CINÉ
ELECTRONIC
MISCELLANEOUS
Radio-active Tracers
Streak Length
Multiple Flash
Image Conversion
Electro Optical Tracker
Micro Ballistic Range
Synchro Ballistic
Laser Doppler Shift
Cross Correlation
Ciné-Streak
Light Scattering
Regular Framing "Movies"
Photocell

motion of the film relative to fixed coordinates. It includes situations where rotating mirrors reflect images on to a stationary film.

(i) Regular Framing "Movies"

Regular framing "movies" are a simple series of still photographs taken at a constant time interval (usually 24 frames per second). High speed cameras using rotating prisms can operate at 10^4 frames/s, while rotating mirror cameras can operate at 10^6 frames/s. Particle velocities are determined from the distance travelled between frames and the framing rate.

Wang (4.3) using a "Hycam" unit operating at 4 000 frames/s and covering a field of view of about 130 mm, was able to measure the velocity of 2-6 mm particles moving at 4-15 m/s in air.

Moore et al. (4.4) using a "Fastax" unit at 2 000 frames/s, determined velocities around 50 m/s for 6-13μm particles of flame-sprayed alumina.

Also using a "Fastax" camera, Manning and Gauvin (5.5) studied the motion of droplets in a spray drier and obtained velocities in the range 5-25 m/s for diameters in the range 15-30μm.

(ii) Ciné-Streak

In ciné-streak recording, the film is transported horizontally through the camera at constant velocity. (This is in contrast to "movies", where the film is effectively stopped while each frame is exposed.) The particle being photographed moves vertically downwards across the field of view of the lens. The point image of this particle therefore moves vertically upwards across the film. Relative to the film, the image has its own velocity plus the negative of the film velocity. The resultant

streak is therefore the vectorial sum of the two components. By determining the angles of the streak relative to the direction of motion of the film, the film velocity and the object-image magnification, the particle velocity may be calculated.

$$V_p = [V_f \tan(\theta)]/M_{of} \quad \ldots\ldots\ldots\ldots \quad (5.1)$$

It should be noted that no pictures or frames are produced as is the case in regular "movies".

One of the advantages of ciné-streak is that the position of the object is determined continuously in the time dimension and in one spatial dimension. In addition, the film translation velocity can be an order of magnitude less than the equivalent framing rate for "movies".

The technique was used by Moore et al. (5.5) and by Lemoine et al. (5.6). The latter determined velocities of the order of 100 m/s for 50μm alumina and carbon particles in an argon plasma jet.

(iii) Synchro-Ballistic

The synchro-ballistic technique is an adaptation of ciné-streak.

The particle image is arranged to move in the same direction as the film and at the same velocity. With this condition, the image is synchronised with the film and a clear image is produced. When the velocities are not matched, the recorded image on the film may be stretched out or reduced in size.

The technique has been applied by Mettenburg (5.7) to the measurement of the bullet velocities. Using an object-film distance of 20 m, velocities of about 2 000 m/s were successfully detected.

Effectively the same technique was used by Ingebo (5.8) who

detected velocities of 30 m/s for particles in the size range 20-120μm. In this equipment, the film was stationary, but a rotating mirror allowed synchronisation of the image on the film.

A broad review of Military Applications of photographic techniques was made by Hyzer (5.9).

ELECTRONIC METHODS

Image Converter Cameras

The image converter camera employs a photo-cathode and anode to give enhanced image intensity. In simple terms, the system is similar to a television camera and display tube in one unit. By use of electronic shuttering and image deflection, exposure times of about 10 ns (i.e. 10^{-8} seconds) are possible. A typical commercially available unit is described in reference (5.10).

Electro-Optical Tracker

The electro-optical tracker also employs a photo-cathode and anode. Using an electron multiplier-detector, the position of the electron image is held constant by varying the voltage to the electron deflection plates. This voltage represents in analog form the position of an object at a given instant. The first and second derivatives may therefore be taken electronically to give the velocity and acceleration. The instrument is described in reference (5.11). Somerscales (5.12) describes an application of the device, where 3-7 mm particles were tracked in water at about 40 mm/s.

MISCELLANEOUS OPTICAL METHODS

Laser Doppler Shift

When light is reflected from an object which is moving towards an

observer, the reflected signal is returned at a higher frequency than the transmitted signal, the change of frequency being proportional to the particle velocity.

$$\Delta\nu = (1/2\pi)\overline{K}\cdot V_p \qquad (5.2)$$

Using a laser beam (which has a narrow frequency band width), changes in frequency as low as 10 Hz may be detected.

The technique has been reviewed by Angus et al. (5.13) and by Fridman, et al. (5.14). James et al. (5.15) reported velocities of about 1 300 m/s for 20μm aluminum particles emerging from a rocket engine.

Light Scattering

The reduction in intensity of a beam of light passing through a cloud of particles is given by the following expression:-

$$I/I_o = \exp(-\rho_n/k) \qquad (5.3)$$

For a constant feedrate, a particle number continuity equation may be written:-

$$(dN/dt) = A(V_p)_1(\rho_n)_1 = A(V_p)_2(\rho_n)_2 \qquad (5.4)$$

$$(V_p)_1/(V_p)_2 = (\rho_n)_1/(\rho_n)_2 \qquad (5.5)$$

By combining equations (5.3) and (5.5), the mean particle velocity may be calculated.

This technique has been used by Buckley (5.16) and Rudinger (5.17). The latter determined velocities in the range 10-40 m/s for glass beads 30-90μm diameter.

Laderman et al. (5.18) measured the delay time between signals

from a pair of photocells. The inhomogeneity in the flow resulted in similar noise patterns which could be compared on an oscilloscope. Velocities of about 2 000 m/s were reported for 1-4μm particles.

Photocells

Marchildon (5.19a) and Clamen and Gauvin (5.19b) in this laboratory used a set of nine photocells spaced at intervals of 0.6 m to record the flight of single particles in the size range 2-25 mm. Maximum velocities of around 200 m/s were reported.

The method is limited by the finite response time of the detectors used. Devices cooled to cryogenic temperatures and having time constants of about 100 ns are available for special purposes (5.20).

NON-OPTICAL TECHNIQUES

Radio-Active Tracers

Prior to the work of Clamen and Gauvin, Torobin and Gauvin (5.21) used radio active particles detected by Geiger scintillation counters. Particle velocities and diameters were in about the same range as used by Clamen.

Micro-Ballistic Range

Crowe et al. (5.22) developed a novel device which was not restricted by problems of optical resolution. Charged particles moving at about 500 m/s were aimed at a line of Faraday cages. Each cage (consisting of a short tube) was charged in turn by the passage of the particle. The voltage from each cage was displayed on an oscilloscope and the transit time measured. Knowing the separation of cages, the particle velocity was easily calculated.

Cross-Correlation

The cross-correlation function of two signals x(t) and y(t) is given by

$$\theta(\tau) = \lim_{t \to \infty} (1/t) \int_0^t \left[x(t-\tau) y(t) \right] dt \qquad \ldots\ldots\ldots\ldots\ldots\ldots\ldots\ldots\ldots\ldots (5.6)$$

where τ is the delay time between signals. When τ is equal to the transit time between signal stations, $\theta(\tau)$ has a maximum value. Correlating the signals from two pressure transducers separated by a distance of 0.6 m, Beck et al. (5.23) were able to measure the mean velocity of particles in the pipe flow.

TABLE 5.2

Particle Velocity Techniques Arranged According to a Time-Scale

Time (seconds)	Technique
10^{-3}	Photocells Cross-Correlation Electro-Optical Tracker Still-Photography (single flash)
10^{-4}	Still Photography (multiple flash) High-Speed framing movies Laser Doppler Shift Light Scattering
10^{-5}	Ciné-Streak Synchro-Ballistic Micro-Ballistic Range
10^{-7}	Image Converter Camera

CONCLUSIONS

A provisional selection of techniques may be made according to the time scale shown in Table (5.2), where each technique is successively faster than the preceding technique.

Where it is unimportant to follow individual particles, the averaging techniques (laser-doppler shift, light-scattering and cross-correlation) have an obvious advantage.

PARTICLE TEMPERATURE

In the study of particulate systems, the particle temperature is of prime importance when considering reaction kinetics, but is of lesser importance with regard to particle residence times. The reason for this is that an error in particle temperature would be reflected in a reduced error in the equation of motion, by virtue of the use of the average temperature between particle and free stream. Further, an error in this reference temperature would result in a still smaller error in the particle acceleration.

The following sections briefly discuss the methods that have been used for the measurement of particle and droplet temperatures.

Thermocouples

Manning and Gauvin (5.5) used thermocouples to measure the temperature of droplets in a study of spray-drying. The method relied on the fact that the thermocouple tip was being continually wetted by the dense stream of droplets.

The technique would not be applicable to low number-density streams or to solid particles.

Pyrometers

Themelis and Gauvin (5.24) developed a two-wavelength pyrometer to measure the temperature of iron oxide particles in the size range 5-100μm dia. The device used a dual-filter disc rotating at 8 000 rpm and was calibrated against a black body surface having a diameter of about 20 mm. Because the pyrometer took the ratio of two readings at two different wavelengths it was insensitive to particle emissivity changes. Further the target area covered

a large number of particles and therefore took the average of their temperatures. Because of this averaging process and the steady state nature of the system, it was immaterial whether or not the two filters were exposed to some heterogeneity in particle temperature.

In applying the method to low number density streams, the combined radiation from groups of particles could have a considerable time fluctuation. In addition, the fraction of the target area covered by the few particles in view would be very small resulting in a total amount of radiation below the linear threshold of the detector. According to a bulletin issued by a manufacturer of pyrometers (5.25), glass temperature measurement (which is of concern in this thesis) is complicated by the high transmission of radiation in certain wavebands.

Detectors having microsecond response time are available (5.20), but operate at cryogenic temperatures. The added complication of refrigeration requirements would be unlikely to lead to a convenient size of instrument.

Photographic Pyrometry

The intensity of radiation from a surface is a function of its temperature and of its emissivity. The density of a photographic image is a function of the intensity of the incident radiation. Therefore, measuring the density of an image of a self-illuminated object, enables the surface temperature of that object to be estimated. Exton (5.26) used this technique to measure the surface temperature of an ablating test model (1 250°K-3 800°K) in the exhaust of a rocket engine and was able to detect the point of flow separation.

The technique has also been used by Pollack and Hickel (5.27) with infra-red film to measure the temperature of rotating turbine blades (800°K-1 600°K).

At the time of writing, this technique has not been used for small particles. Problems would be caused by threshold resolution and the effect of image streak velocity.

Calorimeters

Lemoine (5.28) used small calorimeters to estimate the temperature of particles emerging from plasma flames. Several different designs were tried, the most successful being based on the melting of an insulated block of ice. Corrections were applied for the effect of heat transfer without particles. In view of the obvious experimental difficulties, the scatter in the data was not unreasonable.

CONCLUSIONS

The measurement of the temperature of particles in flight presents considerable experimental difficulties, which have yet to be completely overcome. Except for slow-moving dense particulate systems (5.24), a satisfactory method does not appear to exist for estimating such temperatures. Development of a suitable device would be a considerable contribution to the study of particulate systems.

GAS VELOCITY

Trokhan (5.29) made a comprehensive review of experimental techniques for the measurement of gas velocity, classifying them into three groups:-

(a) Kinematic techniques based on the time of flight of tracer particles;

(b) Dynamic techniques based on the interactions between the flow and an inserted probe (i.e. Pitot-tubes and hot-wire anemometry);

(c) Physical methods based on the quantitative assessment of phenomena occurring in the gas and which are a function of the gas velocity.

The following sections review methods which have been (or are potentially) useful in the measurement of plasma jet velocity.

Gas Tracers

Chen (5.30) focussed a Q-switched giant-pulse ruby-laser beam into a plasma jet and followed the motion of the intense plasma "drop" downstream by means of a streak-drum camera. The background radiation was found to be unimportant and distortion due to the finite size of the drop was calculated as being negligible.

Using a pair of photomultiplier tubes separated by a known distance, Cabannes *et al.* (5.31) measured the time of flight of naturally-occurring and spark-induced light-intensity fluctuations. The signals were fed to a dual beam oscilloscope and the transit time ($\sim$40μs) could be read directly. Measured velocities were about 500 m/s.

Particle Tracers

Gas velocities in plasma jets have been measured by determining the velocity of boron nitride tracer particles. Dennis (5.32) refers to the work of the Plasmadyne Corporation who used 5μm-particles with external illumination. The method was also used by Desai et al. (5.1) in an R.F. plasma. The diameter of the particles used was in the range 40-80μm. This is in the same range as the present work, where large differences between gas velocity and particle velocity were shown to exist.

The question of relaxation times and distances has been considered by Cady (5.33). For a sphere in isothermal Stokesian motion, the relaxation time (ignoring history, see section on particle dynamics) is given by:-

$$\tau_r = (4/9)(D_p)^2(\rho_p/\mu_g) \quad \ldots\ldots\ldots\ldots\ldots\ldots\ldots\ldots\ldots\ldots (5.7)$$

and the relaxation distance

$$L_r \simeq (\overline{V}_p)(\tau_r) \quad \ldots\ldots\ldots\ldots\ldots\ldots\ldots\ldots\ldots\ldots\ldots\ldots (5.8)$$

Using the data of Desai et al. (5.1), the approximate relaxation distance was found to be in excess of the dimensions of their plasma system. The interpretation of their results is therefore open to question.

Laser Anemometry

Laser anemometry (5.12) is a special case of the use of tracer particles. The principle of the method was described earlier. Since the diameter of such particles may be less than one micron, the difficulty of velocity relaxation is minimised.

Cross-Correlation

Cross correlation has also been applied to gas velocity measurement.

Abeysekera and Beck (5.34) correlated synthetic temperature pulses in pipe flow and achieved an accuracy better than 8%. Cross-correlation electron density measurements were used by Johnston et al. (5.35) to measure velocities in a low-density plasma jet and also by Heckman et al. to measure velocities in the wake of a sphere in a rarefied atmosphere.

Sequential Spark

The sequential spark technique involves a high voltage (~100kV) between two electrodes. An initial spark creates a path of least resistance through the gas. This path is blown downstream by the gas and subsequent discharges follow this path. By photographing the traces in two dimensions, the incremental distance and time (and hence velocity) may be determined. This technique was used by Heckman et al. (5.36). It was suggested that the conductivity of a plasma would cause an indistinct spark, making the technique impractical for the present application.

Hot-Wire and Cooled Probe Anemometry

Hot wire anemometry is based on the principle that the heat transfer coefficient between wire and free stream is a function of the relative velocity between them. In general, the wire is heated to above ambient conditions by an electrical current passed along the wire. The maximum temperature which can be used is therefore the burn-out temperature of the wire.

By reversing the direction of heat flux from the gas to the wire, this limitation would be removed.

This technique has been successfully applied in the cooled film anemometer, as described by Fingerson (5.37). In order to reverse the direction of heat flow, high pressure water is passed through the centre of

the "wire" which is actually a thin glass tube coated with metal (which acts as the heating element). The technique is discussed further under the section on Turbulence, but it is noted here that even for mean velocity, the device still requires calibration.

Pitot Tubes

The Pitot tube is probably the most universally applied device for the measurement of gas velocity. In isothermal incompressible, inviscid flow,the stagnation pressure is given by Bernoulli's equation:-

$$\Delta P = (\rho_g)(V_g)^2/2 \quad \ldots\ldots\ldots\ldots\ldots\ldots\ldots\ldots\ldots\ldots\ldots\ldots\ldots\ldots\ldots\ldots (5.9)$$

The Pitot tube is subject to a number of factors which are discussed below:-

(i) Viscosity Effects

The impact pressure is increased at low Reynolds number due to the effects of viscosity which pervade the whole flow field. According to Folsom (5.38), the increase would be about 100% at Re = 5, but negligible for Re > 300.

(ii) Turbulence

Both impact and static pressures are affected by turbulence, although there is some suggestion that the magnitude and sign is a function of the scale of turbulence (5.39).

(iii) Knudsen Number

At high Knudsen number ($K_n \gg 0.01$) the impact pressure increases above the Bernoulli value (5.40). Arney (5.41) suggested that temperature differences could have some importance in non-continuum flow.

(iv) Shear Flow

In shear flow, the approach velocity changes from one side of the probe to the other. The aerodynamic centre of the probe may be displaced towards the region of higher velocity. According to Daily and Hardison (5.42), this can be as much as 0.2 probe diameter.

(v) Temperature Boundary Layer

Smith and Churchill (5.43) suggested the use of a mean film temperature to correct for the effect of changing gas density across the boundary layer. In the same laboratory, Carleton (5.44) carried out a semi-theoretical analysis for the stagnation pressure at the tip of a cold hemispherical probe:

$$\Delta P = (\rho_g V_g^2)/2 + (\rho_g V_g^4)/(8\gamma\rho_g) + (4\bar{\mu}V_g)/[D_p(1 + 0.55/Re)] \quad \ldots\ldots\ldots (5.10)$$

The first term on the right-hand side represented the conventional Bernoulli effect, the second term accounted for compressibility, while the third term was a function of the temperature gradient. The first two terms were evaluated at the free-stream temperature and the third term at the temperature corresponding to the mean enthalpy of the gas. According to Carleton's analysis (5.44), the temperature correction was due to viscous effects and not density changes. Maximum corrections of 3% for compressibility and 14% for the viscosity term were obtained by Carleton. Since the viscosity correction is inversely proportional to probe diameter, the effect on the much larger probes used in the present work would be reduced to less than 5%. It is interesting to compare the work of Cabannes *et al.* (5.31) and Carleton. Cabannes measured a velocity and an impact pressure, inferring a gas temperature, while Carleton measured a spectroscopic temperature and an impact pressure

and inferred a velocity. It would be desirable to test the mutual agreement resulting from simultaneous determinations of all three variables.

(vi) Static Pressure

The importance of static pressure measurement has been discussed by Folsom (5.38), Schulze and Rayle (5.46). Improper location of static pressure toppings and tap holes which are too large can lead to errors of several percent.

CONCLUSIONS

The selection of a particular technique among the many available depends on the job in hand and the accuracy required. The Pitot tube is a tried and tested device and is reasonably well understood. The laser anemometer appears to be a promising technique with a wide potential application.

TURBULENCE

The importance of turbulence has been discussed in the section on particle dynamics. In summary, the main influence is at high Reynolds number ($Re > 10^3$) and where the macroscale scale of turbulence is comparable to the dimension of the object in the turbulence field. In this regime, it strongly affects the heat-transfer. This has recently been investigated in detail by Mujumdar (5.47) for cylinders, and by Galloway and Sage for spheres (5.48).

At low Reynolds number ($Re < 100$) the effect of turbulence on momentum transfer is minor, the main result being a dispersion of particles in the flow field.

Apart from direct effects on particle motion, turbulence has an indirect effect in that it influences axial and radial profiles of the temperature and velocity of the jet, as well as the concentration of the entrained gas surrounding the jet.

The following sections review potentially useful techniques for the measurement of turbulence parameters in a plasma jet.

Pitot Tube

In most cases of Pitot tube operation, the impact pressure fluctuates about a mean value. A qualitative assessment of turbulence may therefore be made as to whether the flow is turbulent or quiescent. The extraction of quantitative data is subject to errors caused by resonance in the Pitot cavity and the time constant of the pressure transducer. Keeping the volume inside the cavity to a minimum and using a suitable capcitance transducer, some useful quantitative data may be extracted.

Broer and deHaan (5.49) compared the turbulence intensity behind a number of wire-mesh grids using both hot-wire anemometry and Pitot tubes. The agreement was described as "surprisingly good".

While the above general method is subject to criticism, it should be noted that calorimetric probes (review section 1) can be operated as cooled Pitot tubes, merely by closing off the gas sample passage.

Hot-Wire and Cooled Film Anemometers

With hot-wire, or cooled-film anemometers, the major problem is to uncouple the simultaneous temperature and velocity fluctuations which have comparable effects on the electrical output signal. This may be overcome by operating two probes simultaneously at two different outputs and combining the two signals (5.50).

However, the method has an upper gas temperature limit of about 2 000°K, which is below the useful operating range of plasma jets.

Assuming a model for the change in turbulence intensity along the axis of a non-isothermal jet, it would be possible to measure turbulence intensities in the cold region of the jet with a hot wire anemometer and then extrapolate back to the region of interest. Due allowance would still have to be made for the simultaneous temperature fluctuations.

Tracer Diffusion

Soo *et al.* (5.51) estimated the intensity of turbulence and the Lagrangian integral scale in pipe flow, by measuring the diffusion of a gas tracer from a point source. Baltas and Gauvin (5.52) applied the same method in the expanding jet of a spray drier, correcting for the changing gas velocity. Application of the technique to plasma jets would probably require

the incorporation of a model of decaying turbulence, as for example developed by Shkarofsky (5.53).

Correlation Decay

Johnston et al. (5.54) estimated turbulence intensities from the decay in the correlation of signals from pairs of Langrangian probes in a plasma jet. The estimated intensity of turbulence was 24% for a static pressure of 25 mm Hg. A simplified analysis was used which did not appear to take into account the affect of decaying turbulence.

Laser Anemometry

Fridman et al. (5.55) developed a system to estimate turbulence intensity using three converging laser beams. The technique involved measured the r.m.s. deviation in the Doppler shift frequency which was proportional to the average velocity fluctuation. The method does not yet appear to have been applied to turbulence in plasma jets.

CONCLUSIONS

Pitot tubes would probably be the simplest and quickest (but also the least accurate) method of measuring turbulence intensity.

Cooled film anemometers are not capable of operating in the regions of a plasma jet close to the nozzle exit.

Tracer diffusion and cross-correlation techniques would be subject to errors caused by decaying turbulence.

Laser anemometry is still in the developing stage, but has a promising future as a general method of measuring turbulence.

NOMENCLATURE

A	Flow area	L^2
D_p	Particle diameter	T
I	Light intensity after passing through cloud of particles	-
I_o	Light intensity before passing through cloud of particles	-
$\overline{K}$	Doppler shift proportionality vector	L^{-1}
k	Constant depending on particle size and path length	L^{-3}
L_R	Relaxation distance	L
M_{of}	Object film magnification	-
N	Number of particles	-
P_g	Gas pressure	$ML^{-1}T^{-2}$
ΔP	Impact pressure rise	$ML^{-1}T^{-2}$
Re	Reynolds number	-
t	Time	T
V_f	Film velocity	LT^{-1}
V_g	Gas velocity	LT^{-1}
V_I	Image velocity	LT^{-1}
V_p	Particle velocity	LT^{-1}
$(V_p)_1$	Particle velocity at position 1	LT^{-1}
$(V_p)_2$	Particle velocity at position 2	LT^{-1}
x	Upstream signal	-

NOMENCLATURE (cont'd)

y	Downstream signal	-
γ	Ratio of specific heats	-
θ	Streak angle	-
$\theta(\tau)$	Correlation function	-
μ_g	Gas viscosity	$ML^{-1}T^{-1}$
$\overline{\mu}$	Average gas viscosity across "thermal boundary layer"	$ML^{-1}T^{-1}$
ν	Frequency	T^{-1}
ρ_g	Gas density	ML^{-1}
ρ_n	Particle number density	L^{-3}
$(\rho_n)_1$	Particle number density position 1	L^{-3}
$(\rho_n)_2$	Particle number density position 2	L^{-3}
ρ_p	Particle density	ML^{-3}
τ_r	Relaxation distance	T

BIBLIOGRAPHY

5.1 Desai, S.V., Daniel, E.S., and Corcoran, W.H., Rev. Sci. Inst. 39, 612 (1968).

5.2 Painter, D.J., Ph.D. Thesis (1969), Univ. of Christchurch, New Zealand.

5.3 Wang, C.C., M.Eng. Thesis (1969), McGill Univ., Montreal.

5.4 Moore, D.G., Hayes, W.D., and Crigler, A.W. (Wright Air Development Center) WADC Technical Report 59-658 (1959).

5.5 Manning, W.P., and Gauvin, W.H., A.I.CH.E.J. 6, 184 (1960).

5.6 Lemoine, A., Stachoviak, F., Cheylan, J., Pauvergne, J.P., et Le Goff, P., Rev. Gen. Thermique 85, 33 (1969).

5.7 Mettenburg, C.W., N.O.T.S., T.N. 3063-39 (1957).

5.8 Ingebo, R.D., N.A.C.A., T.N.-3762 (1956).

5.9 Hyzer, W.G., "Photographic Instrumentation, **Science and Engineering**", (1965) (U.S. Govt. Printing Office).

5.10 T.R.W. Instruments bulletin "Characteristics of the T.R.W. image converter cameras".

5.11 Starer, R.L., Reprint from Instrument and Control Systems (February, 1967).

5.12 Somerscales, E.F.C., Physics of Fluids 13, 1866 (1970).

5.13 Angus, J.C., Morrow, D.L., Dunning, J.W., and French, M.J. Ind. Eng. Chem. 61, 8 (1969).

5.14 Fridman, J.D., Huffaker, R.M., and Kinnard, R.F. Reprint from Laser Focus (November 1968).

5.15 James, R.N., Babcock, W.R., and Seifert, H.S., A.I.A.A.J. 6, 160 (1960).

5.16 Buckley, F.T., A.I.A.A.J. 8, 1153 (1970).

5.17 Rudinger, G., U.S. Office of Navel Research, Project Squid. Technical Report CAL-97-PU; also as A.S.M.E. paper 69-WA/FE-22.

5.18 Laderman, A.J., Lewis, C.H., and Bryon, S.R., A.I.A.A.J. 7, 556 (1969).

5.19a Marchildon, E.K., Ph.D. Thesis (1969), McGill Univ., Montreal.

5.19b Clamen, A., and Gauvin, W.H., Can. J. Chem. Eng. 46, 73 (1968).

5.20 Mullard technical bulletin, Infrared Detectors (1969).

5.21 Torobin, L.B., and Gauvin, W.H., A.I.Ch.E.J. 7, 406 (1961).

5.22 Crowe, C.T., Babcock, W.R., and Willoughty, P.G., International Symposium on Two Phase Systems, Haifa, Israel (1971).

5.23 Beck, M.S., Drave, J., Plaskowski, A., and Wainwright, N., Powder Technology 2, 269 (1968/69).

5.24 Themelis, N.J., and Gauvin, W.H., Can. J. Chem. Eng. 40, 157 (1962).

5.25 Ircon Inc., Chicago, Illinois, Bulletin 7 001.

5.26 Exton, R.J., A.I.A.A.J., 7, 2262 (1969).

5.27 Pollack, F.G., and Hickel, R.O., N.A.S.A., T.N. D-5179 (1969).

5.28 Lemoine, A., Docteur Ingenieur Thesis (1969) Univ. of Nancy, France.

5.29 Trokhan, A.M., Measurement Techniques (Izmeritel'Naya Tekhnika) 8, 5 (1968); (translated from the Russian).

5.30 Chen, C.J., J. App. Phys. 37, 3092 (1966).

5.31 Cabannes, F., Chapelle, J., Czernichowski, A., Decroisette, M., and Zamarlick, J., Rev. Int. Hautes. Temp. et Refract., 7, 7 (1970).

5.32 Dennis, P.R. (ed) N.A.S.A., SP 5033, 146 (1965).

5.33 Cady, C.M., "Physical Measurements in Gas Dynamics and Combustion", ed. R.W. Ladenburg, Princeton U.P. (1954).

5.34 Abeysekera, S.A., and Beck, M.S., "Cross Correlation Applied to Pulsating Flow Measurement", School of Engineering of Bradford (England) (1968).

5.35 Johnston, T.W., Richard, C., Ghosh, A.K., Carswell, A.I., and Graf, K. Symposium on Turbulence of Fluids and Plasmas, Polytechnic Institute of Brooklyn, p. 65 (1968).

5.36 Heckman, D., Tardif, L., Lahaye, C., Symposium on Turbulence of Fluids and Plasmas, Polytechnic Institute of Brooklyn, p. 441 (1968).

5.37 Fingerson, L.M., Ph.D. Thesis (1961), Univ. of Minnesota; also Ahmed, A.H., Mechanical Engineering Research Laboratories, McGill University, Montreal, T.N.-67-5 (1967).

5.38 Folsom, R.G., Review of the Pitot Tube, Trans. A.S.M.E., October 1956, 1447-1460.

5.39 Toomre, A., Aeronautical Research Council (U.K.), A.R.C. 22,010.

5.40 Chambré, P.L., and Schaaf, S.A., "Physical Measurements in Gas Dynamics and Combustion", Ed. R.W. Ladenburg, Princeton U.P. 1954, p. 111.

5.41 Arney, G.D., and Bailey, A.B., A.I.A.A.J. 1, 2863 (1963).

5.42 Daily, J.W., and Hardison, R.L., Hydrodynamics Laboratory, Report 67, Department of Civil Engineering, M.I.T., (1964).

5.43 Smith, D.L., and Churchill, S.W., University of Michigan, Report 05607-1-T.

5.44 Carleton, F.E., Ph.D. Thesis, Univ. of Michigan (1970).

5.45 Schulze, W.M., Ashby, G.R., and Erwin, J.R., N.A.C.A. T.N. 2830.

5.46 Rayle, R.E., M.Eng. Thesis, M.I.T. (1949).

5.47 Mujumdar, A.S., Ph.D. Thesis, McGill Univ., Montreal (1971).

5.4 Galloway, T.R., and Sage, B.H., A.I.Ch.E.J. (in press).

5.49 Broer, L.J.F. and DeHaan, R.E., A.A.M.P., 11b, 162 (1968).

5.50 Ellington, D., Park, K.R., and Desjardins, P.,"Hypersonic Wake Studies Using Cooled Film Anemometer Techniques", Defence Research Establishment, Valcartier, Quebec (1971)

5.51 Soo, S.L., Ihrig, H.K., and El Kouh, A.F., Trans. A.S.M.E. J. Basic Eng. 609 (1960).

5.52 Baltas, L., and Gauvin, W.H., A.I.Ch.E.J. 15, 772 (1969).

5.53 Shkarofsky, I., Symposium of Turbulence in Fluids and Plasmas, Polytechnic Institute of Brooklyn (1968).

5.54 Johnston, T.W., Richard, C., Ghosh, A.K., Carswell, A.I., and Graf, K., Symposium of Turbulence in Fluids and Plasmas, Polytechnique Institute of Brooklyn (1968).

5.55 Fridman, J.D., Huffaker, R.M., and Kinnard, R.F., Laser Focus, Nov. (1968).

PART VI - JETS

INTRODUCTION

This section is a summary of the work on jets which is applicable to the present thesis. Forstall and Shapiro (6.1) provided a comprehensive review on jets prior to 1950, while more recent reviews have been given by Libbey (6.2), Ferri et al. (6.3) and Ferri (6.4). Abramovich (6.5) and Birkhoff and Zarantonello (6.6) are two standard texts on jets.

In the context of this thesis, reference to isothermal jets includes systems where temperature differences exist, but the temperature ratio between centre-line and free-stream is small [$\sim$1.3, ref. 6.7] compared to the ratio in plasma systems. This implies only a minor change in density or velocity due to gas cooling.

AXIAL PROFILES

In most jets, the region close to the nozzle (the "core region") shows constant values of concentration, temperature and velocity, along the centre-line. Beyond this region, the three variables decay rapidly with distance. In near isothermal systems, the decay shows an inverse relationship with distance from the effective or virtual origin of the jet (6.5).

$$\Delta C_m = k_1/X \quad \ldots\ldots\ldots\ldots\ldots\ldots\ldots\ldots\ldots\ldots\ldots\ldots \quad (6.1a)$$

$$\Delta T_m = k_2/X \quad \ldots\ldots\ldots\ldots\ldots\ldots\ldots\ldots\ldots\ldots\ldots\ldots \quad (6.1b)$$

$$U_m = k_3/X \quad \ldots\ldots\ldots\ldots\ldots\ldots\ldots\ldots\ldots\ldots\ldots\ldots \quad (6.1c)$$

where k_1, k_2, k_3 are constants and X is the distance from the origin

of the jet, which may be several diameters downstream from the nozzle exit.

In turbulent plasma jets, the ten-fold decrease in temperature of the jet causes a corresponding decrease in the specific volume of the gas. Lemoine (6.8) obtained an inverse square decay for the centre line gas velocity in an argon plasma jet.

$$U_m = 650 \text{ m/s} \qquad (Z < 1.5 \text{ cm})$$
$$U_m = 650[2.5/(Z + 1)]^2 \text{ m/s} \qquad (Z > 1.5 \text{ cm}) \qquad \ldots\ (6.2)$$

This is in general agreement with Grey and Jacobs (6.9) who observed that a heated jet decays much more rapidly than an isothermal jet. O'Conner et al. (6.10) noted that centre-line values of concentration decayed more rapidly than enthalpy, which decayed more rapidly than velocity.

RADIAL PROFILES

According to Warren (6.11), the radial profiles in the core region of a jet are approximated by the following expressions:-

$$U_r = (U_m)\exp[-\lambda(r^2 - r_i^2)/(r_{1/2}^2 - r_i^2)] \qquad r > r_i \quad \ldots\ (6.3a)$$

$$U_r = U_m \qquad r < r_i \quad \ldots\ (6.3b)$$

Beyond the core region of a near-isothermal jet, it is well established (6.5, 6.6), that radial profiles may be represented by a Gaussian curve:-

$$U_r = U_m \exp[-\lambda(r/r_{1/2})^2] \qquad \ldots\ (6.4)$$

Further, it is well-established that the half-radius increases

linearly with distance from the jet origin. For this reason, the jet has been described as conical in shape.

For non-isothermal jets, O'Connor et al. (6.10) showed that radial property variations could be well represented by Gaussian curves. Their results indicated that the half-radii did not increase linearly with distance. The curvature of their results however was in the opposite direction to that of Grey and Jacobs (6.9). Carleton (6.13) obtained a number of profiles close to an argon plasma jet. In spite of the experimental difficulties his results were again a close fit to a Gaussian distribution.

GENERAL EFFECTS

(i) Turbulence

The evolution of vortices in a round jet was studied by Becker and Massaro (6.14). The regular periodicity of vortex shedding was demonstrated by repretitive stoboscopic-illumination of an oil condensation smoke. They came to the tentative conclusion that the Strouhal number had a constant value of about 0.5. It was suggested that the vortex pattern for a sharp-edged orifice would be different to that for a square-edged orifice.

Grey and Jacobs (6.9) suggested that the turbulence in their plasma jet was generated in the nozzle and was not controlled by flow parameter variations.

In a study of isothermal jets, Davies (6.15) noted a variation of the convective velocity of eddies as a function of the centre-band frequency of his signal filter system. A maximum difference of twenty percent above and below the mean velocity was noticed for the highest

and lowest measured frequencies.

(ii) Orifice Shape

The round jet is the most common shape that has been considered. Sforza et al. (6.16) studied the effect of various shaped orifices including triangles and slots of various length/width ratios. It was concluded that beyond the core region of jets issuing from equilateral-triangle orifices (and for other regular polygons) the axial profiles would follow the pattern for round jets. This would probably have a general usefulness, in that other small irregularities would only influence the system in the core region.

(iii) Jets in Crosswinds

Shandorov (6.17), cited by Abramovich (6.5) correlated the deflection of a jet in a crosswind in terms of a horizontal penetration (y) and a vertical penetration (x) as a function of the dynamic pressures of the crossflow and of the jet ($\rho_1 U_1^2/2, \rho_2 U_2^2/2$).

$$(x/d) = [(\rho_2 U_2^2/2)/(\rho_1 U_1^2/2)](y/d)^{2.55} + [1 + (\rho_2 U_2^2/2)/(\rho_1 U_1^2/2](y/d)\cot(\alpha) \quad \ldots\ldots\ldots\ldots\ldots\ldots \quad (6.5)$$

Patrick (6.18) obtained the following correlation for a jet perpendicular to a cross stream.

$$(y/d) = (U_2/U_1)^{0.687}(x/d)^{0.36} \quad \ldots\ldots\ldots\ldots\ldots\ldots\ldots\ldots \quad (6.6)$$

For an isothermal system, the two equations would reduce to:

$$(x/d) = (y/d)^{2.55}(U_1/U_2)^{2.0} \quad \text{(Shandorov)} \quad \ldots\ldots\ldots\ldots \quad (6.7)$$

$$(x/d) = (y/d)^{2.79}(U_1/U_2)^{1.9} \quad \text{(Patrick)} \quad \ldots\ldots\ldots\ldots \quad (6.8)$$

The two equations therefore show a remarkable agreement.

The problem of the deflection of non-isothermal jets has only been investigated for low temperature ratios. No work has been discovered for the deflection of small jets within a large jet.

CONCLUSION

The degree of understanding of the variation of jet parameters in an arc-plasma system is severely limited by the difficulties of applying experimental techniques. The complexity of the arc discharge plasma jet could possibly explain lack of agreement between authors.

Plasma jets show Gaussian radial distributions of properties and an approximately inverse square axial decay, with concentration decaying faster than temperature and temperature decaying faster than velocity.

NOMENCLATURE

ΔC_m	Excess axial concentration above ambient	ML^{-3}
d	Jet orifice diameter	L
k_1, k_2, k_3	Constants in equation (1)	-
r	Radius	L
$r_{1/2}$	Radius at which property has half the centre-line value	L
r_i	Radius of edge of jet core	L
ΔT_m	Excess axial temperature above ambient	θ
U_m	Axial velocity of gas	LT^{-1}
U_r	Velocity of gas in axial direction at a displacement 'r'	LT^{-1}
U_1	Velocity of crossflow stream	LT^{-1}
U_2	Initial jet velocity	LT^{-1}
x	Vertical penetration of a horizontal jet in a vertical crosswind	L
X	Distance from virtual origin of jet	L
y	Horizontal penetration of a horizontal jet in a vertical crosswind	L
Z	Distance from nozzle exit	L
α	Angle between the direction of crossflow and the axis of jet	-
λ	Constant (= ln 2)	-
ρ_1	Density of crossflow stream	ML^{-3}
ρ_2	Initial density of jet	ML^{-3}

BIBLIOGRAPHY

6.1 Forstall, W., and Shapiro, A.H., Trans. A.S.M.E., J. App. Mech. 17, 399 (1950).

6.2 Libby, P.A., J. Am. Rocket Soc. 32, 388 (1962) (cited in 11).

6.3 Ferri, A., Libby, P.A., and Zakkay, V., Polytech. Inst. Aerospace Lab. Report 713 (1962) (cited in 11).

6.4 Ferri, A. J. Roy. Aero. Soc. 68, 575 (1964).

6.5 Abramovich, G.N., "The Theory of Turbulent Jets", M.I.T. Press (1963).

6.6. Birkhoff, G., and Zarantonello, E.H., "Jets, Wakes and Cavities", Academic Press (1957).

6.7 Corrsin, S., and Uberoi, M.S., N.A.C.A. Report 998 (1950).

6.8 Lemoine, A., Docteur Ingenieur Thesis, Univ. of Nancy, France (1969).

6.9 Grey, J., and Jacobs, P.F., A.I.A.A.J., 2, 433 (1964).

6.10 O'Connor, T.J., Comfort, E.H., and Cass, L.A., A.I.A.A.J. 4, 2026 (1966).

6.11 Warren, W.R., Princeton Univ., Dept. Aero. Eng. Report 381 (1957) (cited in 11).

6.12 Donaldson, C.D., and Gray, K.E., A.I.A.A.J. 4, 2017 (1966).

6.13 Carleton, F.E., Ph.D. Thesis, Univ. of Michigan (1970).

6.14 Becker, H.A., and Massaro, T.A., J. Fluid. Mech. 31, 435 (1968).

6.15 Davies, P.O.A.L., A.I.A.A.J. 4, 1971 (1966).

6.16 Sforza, P.M., Steiger, M.H., and Trentecoste, N., A.I.A.A.J. 4, 800 (1966).

6.17 Shandorov, G.S., Zh. Tekhn. Fiz. 37, 1 (1957) (cited in (5)).

6.18 Patrick, M.A., Univ. of Sheffield, England, Fuel Socy. J., 16, 46 (1966).

EXPERIMENTAL SECTION

PART I

TEMPERATURE, VELOCITY AND CONCENTRATION PROFILES IN A FREE ARGON PLASMA JET

INTRODUCTION

In order to model the motion of particles in a plasma jet, it was necessary to determine the axial and radial profiles of temperature and velocity of the argon plasma gas, as well as the concentration of entrained air. A calorimetric probe was selected as the most suitable instrument for these measurements for the following reasons:

(i) Thermocouples (1) were not useful above a temperature of 2 500°K, while spectroscopic temperature measurements are inaccurate below 9 000°K.

(ii) Calorimetric techniques could be applied over a wide temperature range, with a reasonable degree of spatial resolution.

(iii) The probe could be used as a Pitot tube for the measurement of gas velocity and as a gas sampling probe, without any modification or extra equipment being required.

The calorimetric probe was mainly developed by Grey and co-workers (2, 3, 4). Other users of such devices have included Smith and Churchill (5), Petrov and Sepp (6) and Cheylan (7). A recent design improvement by Grey (in the form of a water-cooled insulating jacket around the calorimeter) enabled lower gas temperatures to be measured. Prior to this development, the calorimetric methods were considered to be inaccurate due to heat transfer to the calorimeter from gas flowing over the outside surface of the probe (5).

EXPERIMENTAL

EQUIPMENT

(i) Plasma Torch

The plasma torch used in the experiments is shown in Figs. 1, 2, 3. The essential components of the torch were the cathode and anode (Fig. 3). The cathode consisted of a thoriated tungsten rod 12 mm (0.5 in) diameter, with a 45-degree half-angle cone point. The copper anode was made in the form of a nozzle, having an inside diameter of about 10 mm (7/16 in) and a length of 50 mm (2 in). Both cathode and anode were water-cooled to prevent material erosion. Provision was made for injection of secondary streams into the jet via two side nozzles connected to the bottom end of the anode nozzle. In later experiments (reported in Part II of this thesis) these injection nozzles were used to introduce particles into the plasma flame. Power to the torch was supplied from a 40kW rectifier.

In operation, an arc was struck between the cathode and anode, while gas was passed through the nozzle. The acceleration of free electrons in the arc increased their kinetic energy and hence temperature. This energy was transferred to ions and atoms by normal collision processes.

(ii) Calorimetric Probe

The principle of operation of a calorimetric probe is an enthalpy balance between a continuous sample of the hot gas and the calorimeter cooling water. In its simplest form, the heat balance may be stated:

$$\dot{M}_g \Delta h_g = \dot{M}_w \Delta h_w \quad \ldots\ldots\ldots\ldots\ldots\ldots\ldots\ldots\ldots\ldots\ldots\ldots \quad (1)$$

FIGURE 1

Cross Section of

Plasma Torch

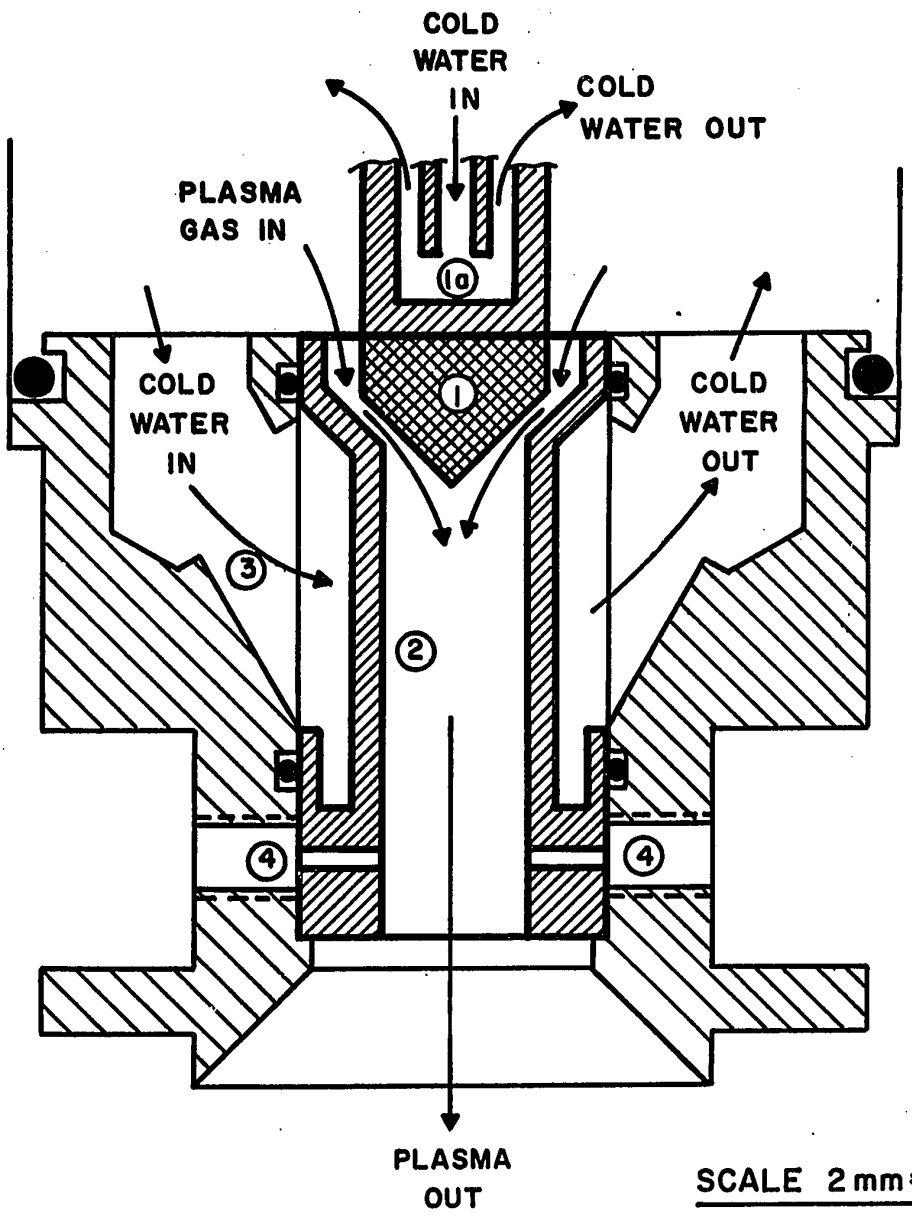

1. THORIATED TUNGSTEN CATHODE.
1a. CATHODE HOLDER.
2. COPPER NOZZLE – ANODE.
3. NOZZLE BODY.
4. PARTICLE INJECTION INLET.

FIGURE 2

Photograph of Plasma Torch

Anode and Cathode

FIGURE 3

Photograph of

Complete Plasma Torch

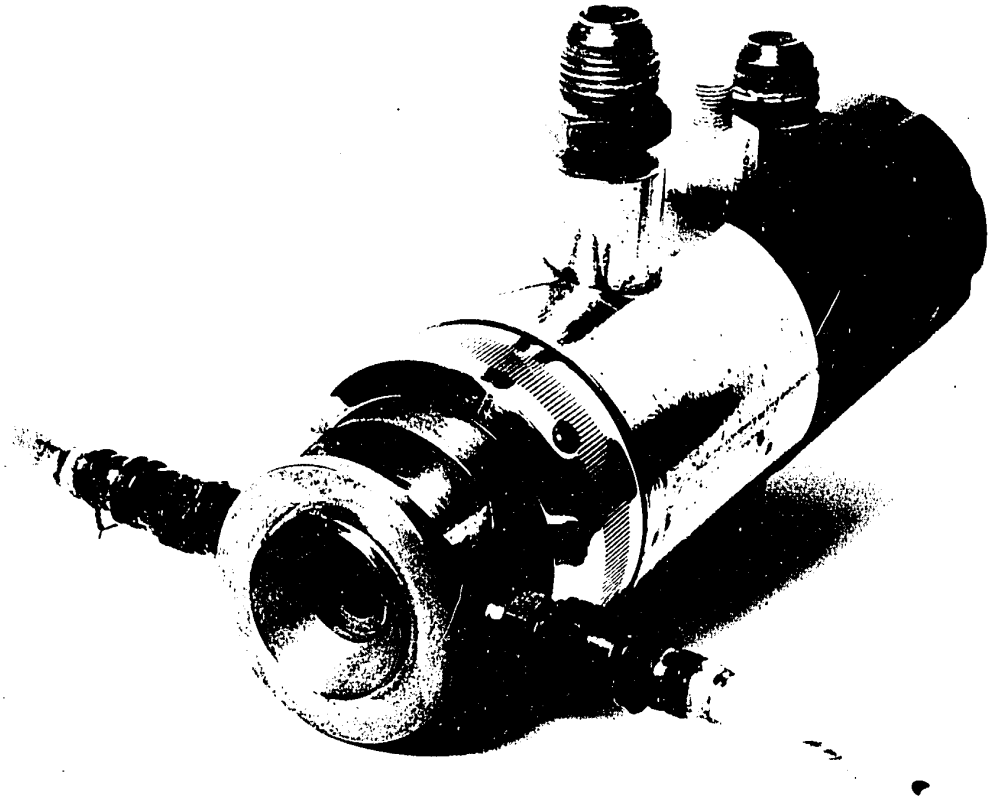

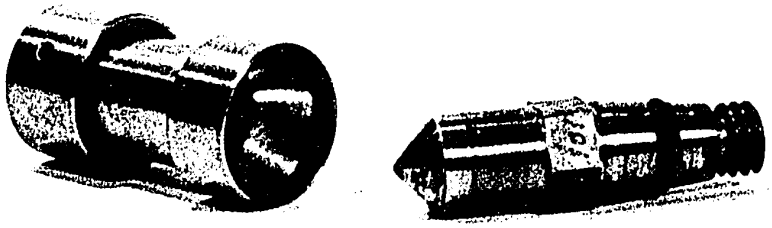

The working section of the probe consisted of an assembly of six tubes, as shown in Fig. 4, having an overall diameter of 8 mm and a length of 150 mm. The inner three tubes formed the calorimeter, with thermocouples placed at the appropriate inlet and outlet positions. The outer three tubes formed the insulating jacket around the calorimeter. Fig. 5 shows a detail-view of the probe tip, while Fig. 6 shows the complete unit. The jacket and calorimeter were mounted on a strut (40 mm diameter, 450 mm length) cooled by recirculating water. The jacket and calorimeter were fed from a high-pressure (5×10^6 N/m^2, 800 psi) water supply as shown in Fig. 7. The high pressure was generated by using a bank of water bottles pressurised directly with nitrogen. A detailed engineering description of the water supply is given in reference (8).

The gas flowrate was estimated from the pressure upstream of a critical orifice. As shown in Fig. 8, the calibration graph was remarkably linear.

PRELIMINARY EXPERIMENTS

Torch Oscillations

One of the features of d.c. plasma torch operation is the periodic fluctuation ($\sim$10 kHz) in the voltage between cathode and anode. According to Eckert and Pfender (9) this fluctuation is due to the arc being blown down the nozzle by the flow of gas. As the arc length is increased, its resistance and hence voltage drop increases in proportion.

In order to investigate this phenomenon, a study was made using a slightly smaller nozzle and nitrogen as the working gas. (The change of torch and gas were due to temporary problems of spare parts and equipment scheduling.)

FIGURE 4

Cross Section of

Calorimetric Probe

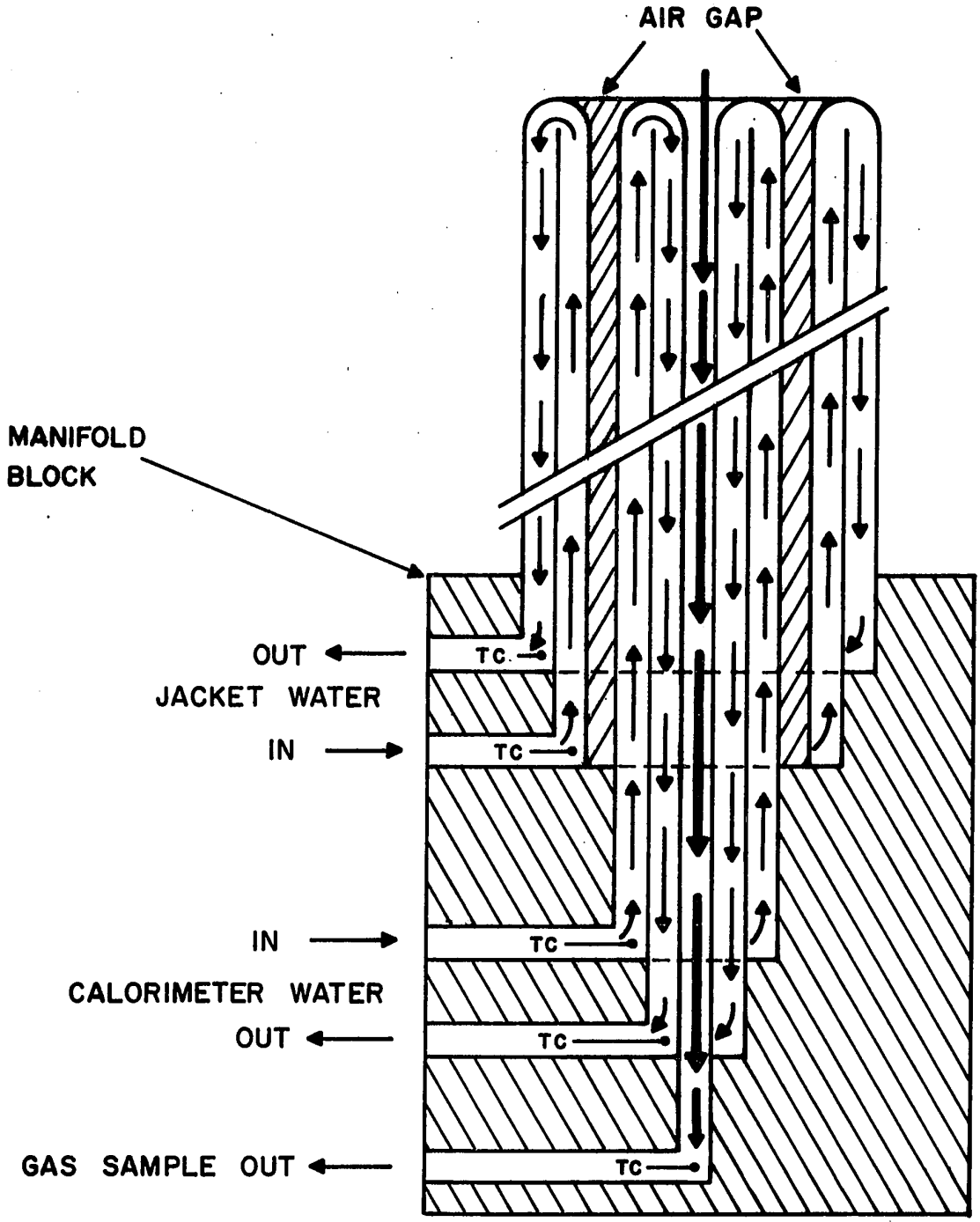
AIR GAP
MANIFOLD
BLOCK
OUT
JACKET WATER
IN
IN
CALORIMETER WATER
OUT
GAS SAMPLE OUT
TC
TC
TC
TC
TC

FIGURE 5

Detail of

Calorimetric Probe tip

FIGURE 6

Overall View of

Calorimetric Probe

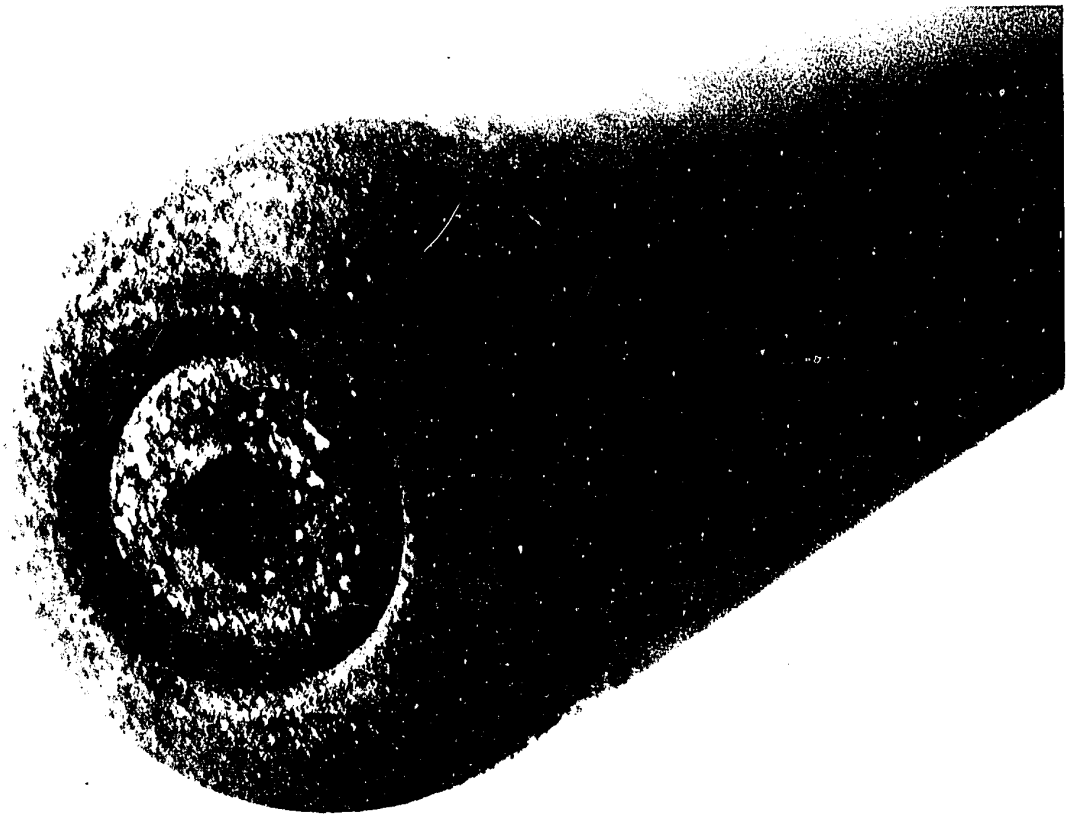

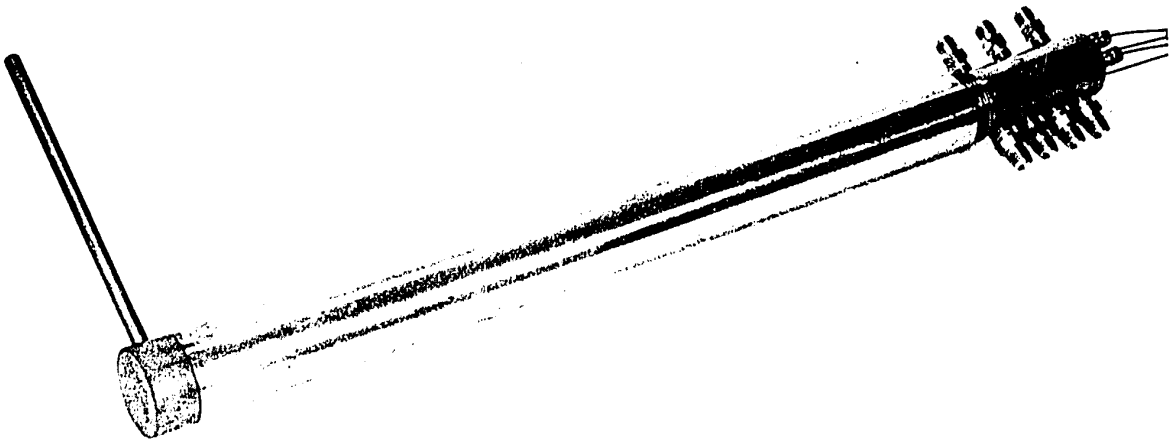

FIGURE 7

High Pressure Water Supply

for Calorimetric Probe

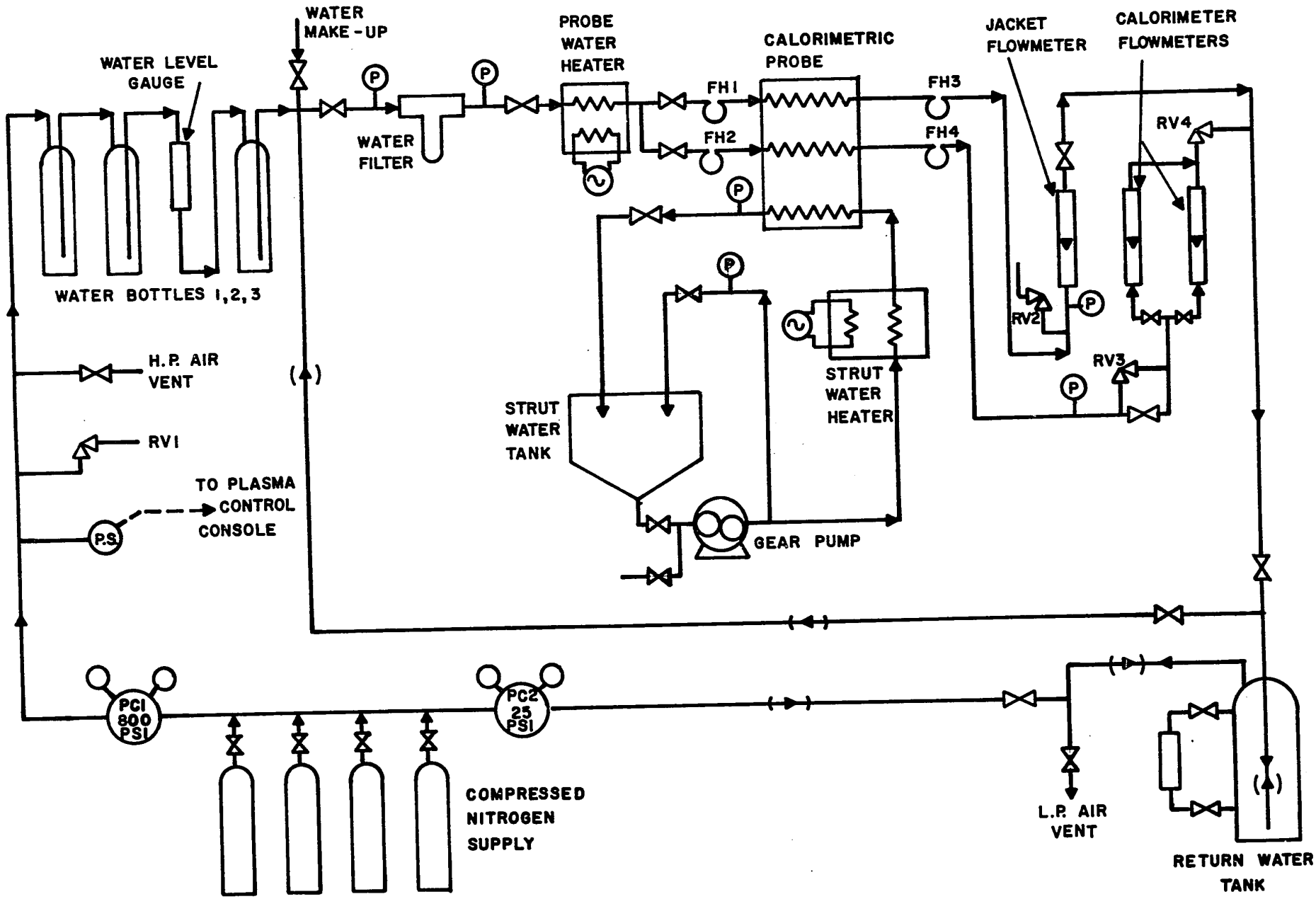
WATER MAKE-UP
WATER LEVEL GAUGE
PROBE WATER HEATER
CALORIMETRIC PROBE
JACKET FLOWMETER
CALORIMETER FLOWMETERS
FH1
FH2
FH3
FH4
WATER FILTER
RV4
WATER BOTTLES 1,2,3
RV2
RV3
H.P. AIR VENT
STRUT WATER HEATER
STRUT WATER TANK
RV1
TO PLASMA CONTROL CONSOLE
P.S.
GEAR PUMP
PC1 800 PSI
PC2 25 PSI
COMPRESSED NITROGEN SUPPLY
L.P. AIR VENT
RETURN WATER TANK

FIGURE 8

Critical Orifice

Flowrate Calibration Graph

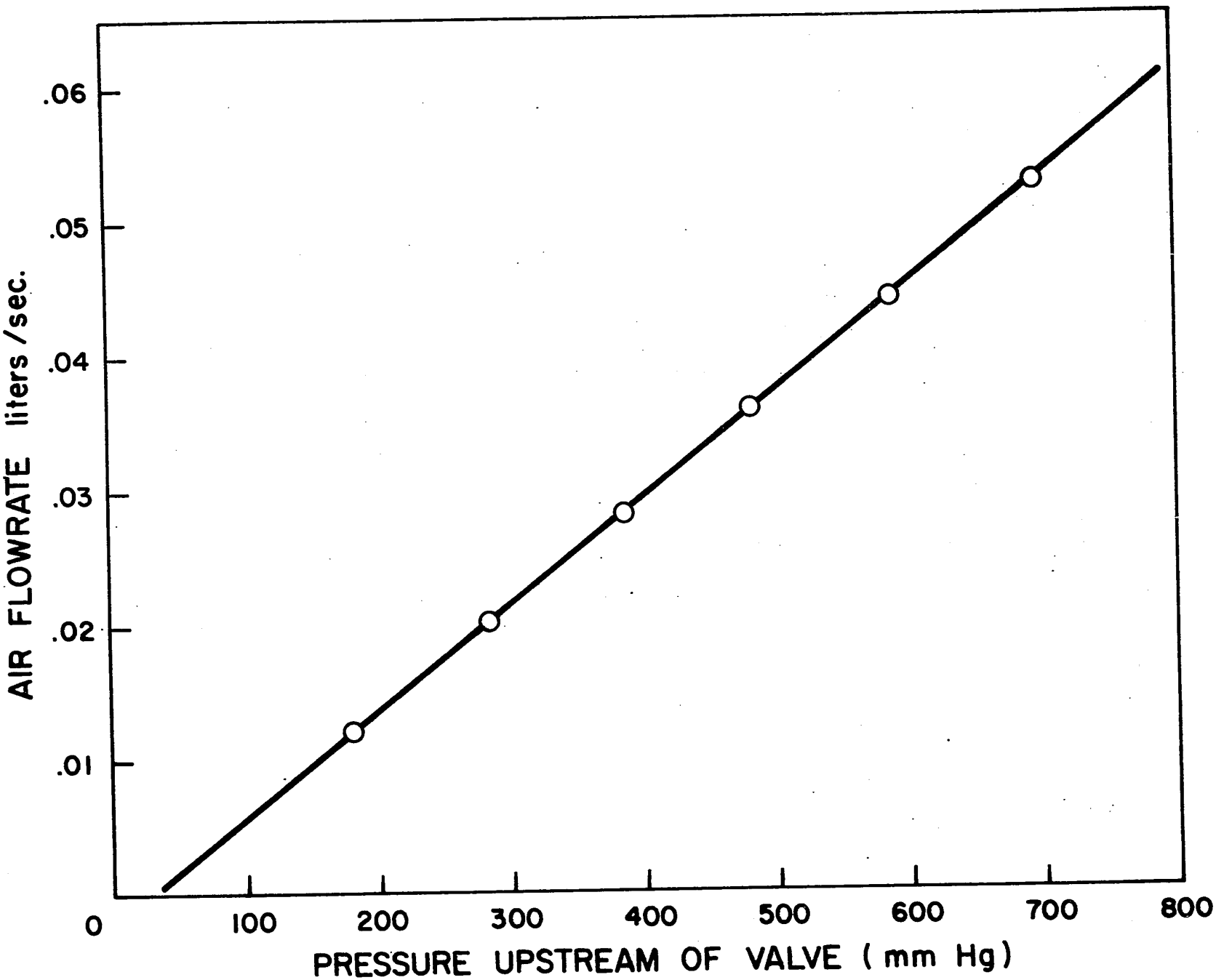
.06
.05
.04
.03
.02
.01
AIR FLOWRATE liters /sec.
0
100
200
300
400
500
600
700
800
PRESSURE UPSTREAM OF VALVE (mm Hg)

The cathode-anode voltage was monitored with an oscilloscope. At a particular operating condition, a 10 kHz saw-tooth waveform was observed. The voltage was seen to rise slowly from a minimum of $\sim$ 40V to a maximum of about 60V corresponding to the stretching of the arc, followed by a sharp drop back to 40V as the arc root reattached itself close to the cathode tip.

Using a pulse counter the frequency of the discharge was determined for a variety of gas flowrates and nominal power inputs. The results are shown in Fig. 9, where it is seen that the frequency varied between 5 Khz and 15 kHz, increasing with power input and gas flowrate. These two factors should both increase the velocity of the gas in the nozzle. An approximate calculation was therefore made, on the assumption that the arc root travelled the whole length of the anode, at the mean gas velocity:

$$V_g = (50)(10^{-3})/(10^{-4}) = 500 \text{ m/s} \quad \ldots\ldots\ldots\ldots\ldots\ldots\ldots\ldots \quad (2)$$

The gas nozzle velocity so determined is in good agreement with typically expected values of the jet velocity near the nozzle exit.

Probe Calibration

In order to check the operation of the calorimetric probe, the temperature and velocity of the plasma jet were estimated at a point 200 mm below the nozzle exit, using a bare-junction thermocouple and a set of three different Pitot tubes. These three tubes were:

(i) The calorimetric probe itself.

(ii) A 3 mm o.d. by 10 mm length tube mounted on a water-cooled support.

(iii) A 3 mm o.d. by 100 mm length uncooled tube on an uncooled copper support.

FIGURE 9

Frequency of Oscillation of

Plasma Torch

As a Function of

Power Input and Gas Flowrate

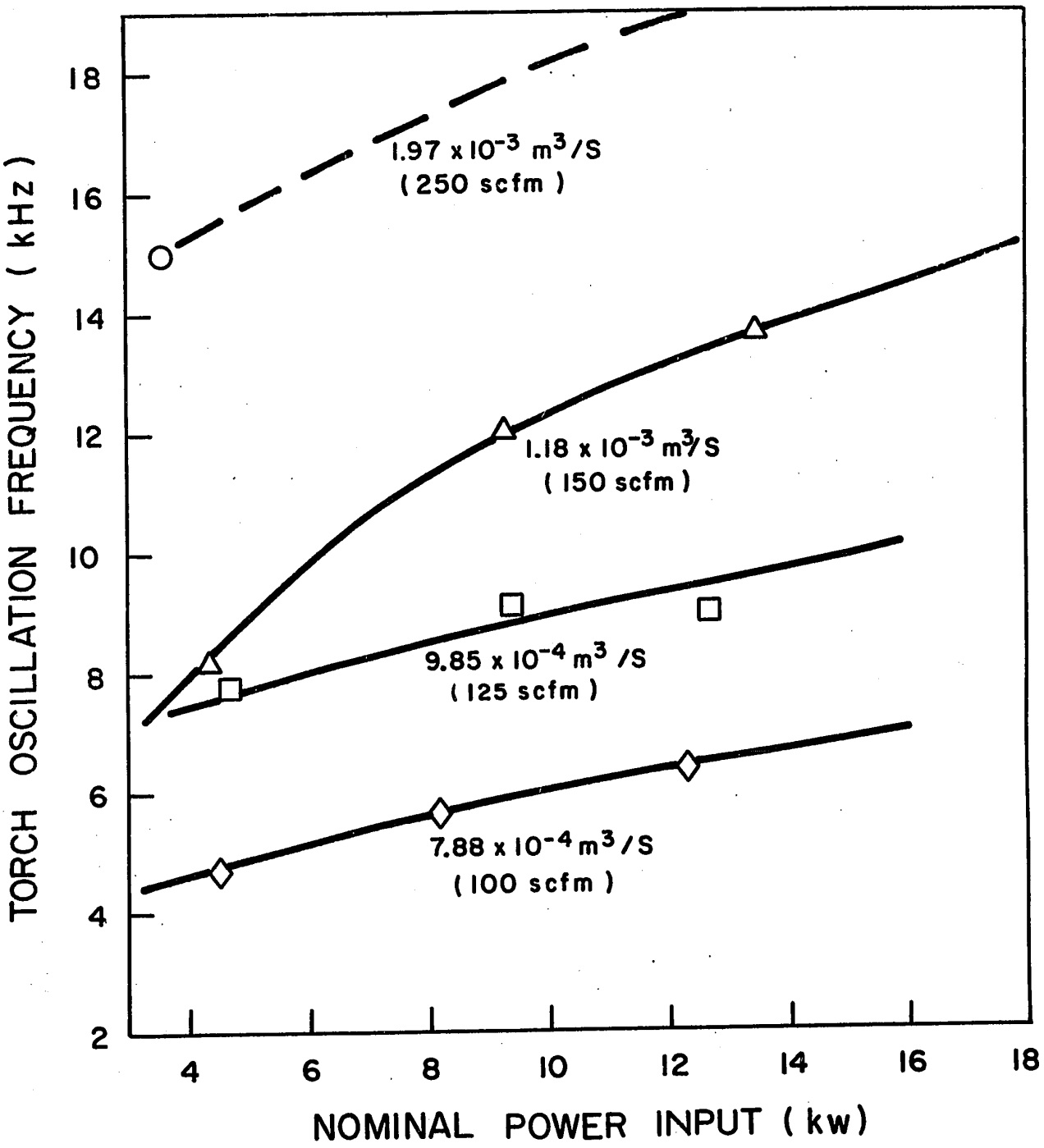
TORCH OSCILLATION FREQUENCY (kHz)
NOMINAL POWER INPUT (kw)
1.97 x 10-3 m3/S
(250 scfm)
1.18 x 10-3 m3/S
(150 scfm)
9.85 x 10-4 m3 /S
(125 scfm)
7.88 x 10-4 m3 /S
(100 scfm)
2
4
6
8
10
12
14
16
18

In each case, the mean impact pressure was 105 mm of horizontal displacement on a methyl alcohol manometer with a slope of 1/5. Therefore, no difference was observed as a result of changes in probe geometry and temperature.

The concentration of entrained air was determined by gas chromatography, using plasma feed gas as the carrier. By this means, calibration of the chromatograph and detection of air were simplified.

As a result of radiation and conduction heat transfer away from the thermocouple bead, there was a significant difference between the gas temperature and the temperature of the thermocouple itself. Using the method of Scadron and Warshawsky (10), corrections were applied to the thermocouple-Pitot-tube data to obtain the gas temperature and velocity. These corrections were:

Radiation

$$\Delta T_r = \left[\sigma \varepsilon_{tc} D_{tc} T_{tc}^4 \left[1 - (T_d/T_{tc})^4\right]\right] \cdots \Big/ \left[Nu_b k_b \left[1 + (4\sigma \varepsilon_{tc} D_{tc} T_{tc}^4)/(Nu_b k_b T_b)\right]\right] \quad \ldots\ldots\ldots\ldots\ldots (3)$$

Conduction

$$\Delta T_c = (T_{tc} - T_{sh}) \left[\psi/(1 - \psi)\right] \quad \ldots\ldots\ldots\ldots\ldots\ldots\ldots\ldots (4)$$

where $$\psi = \operatorname{sech}(L_{tc}/2) \quad \ldots\ldots\ldots\ldots\ldots\ldots\ldots\ldots\ldots\ldots (5)$$

$$\eta = \left[4(Nu)_b k_b/(d_{tc}^2 k_{tc})\right]^{0.5} \quad \ldots\ldots\ldots\ldots\ldots\ldots\ldots\ldots (6)$$

and $$(Nu)_b = 0.32 + 0.478\,(Re)_b^{0.5}(Pr)_b^{0.33} \quad \ldots\ldots\ldots\ldots\ldots\ldots (7)$$

The thermocouple emissivity was taken from the average value given in reference (11).

The estimated thermocouple temperature was (1520 ± 60)°K, the uncertainty being mainly due to the question of thermocouple emissivity. The equivalent calorimetric temperature was (1 500 ± 80)°K. Appendix A shows a sample calculation of a calorimetric temperature from the basic experimental data.

The effects of interaction between the calorimeter, strut and jacket, together with the heat generation in the water due to the large pressure drop (ΔT = 3°R/1 000 psi), prevented the application of a simple enthalpy balance and necessitated a number of corrections.

The effects of heat generation and calorimeter-strut interaction were demonstrated in a preliminary experiment in which the probe was operated in cold air. Fig. 10 shows the temperature rise of the calorimeter water (in terms of the thermocouple output) as a function of the mean temperature between the calorimeter and jacket, with the calorimeter water flowrate as a second parameter. Fig. 10 was used to estimate the first correction to the calorimeter output under formal operating conditions.

Conduction heat transfer between calorimeter and jacket required a second correction (Fig. 11). This correction was assumed to be inversely proportional to the calorimeter water flowrate.

In contrast to simple stagnation flow, where the gas velocity is zero at only one point, the use of a calorimetric probe, where gas is sampled through the central opening, results in the formation of a stagnation ring. If the gas sample rate were "balanced", then the stagnation ring would by definition be located directly over the air gap between the inner and outer jackets of the probe (Fig. 12).

FIGURE 10

Calorimeter Thermocouple Output
as a Function of
(i) Mean Temperature Difference
Between Strut and Calorimeter
and
(ii) Calorimeter Water Flowrate
(Probe Operating in Cold Air)

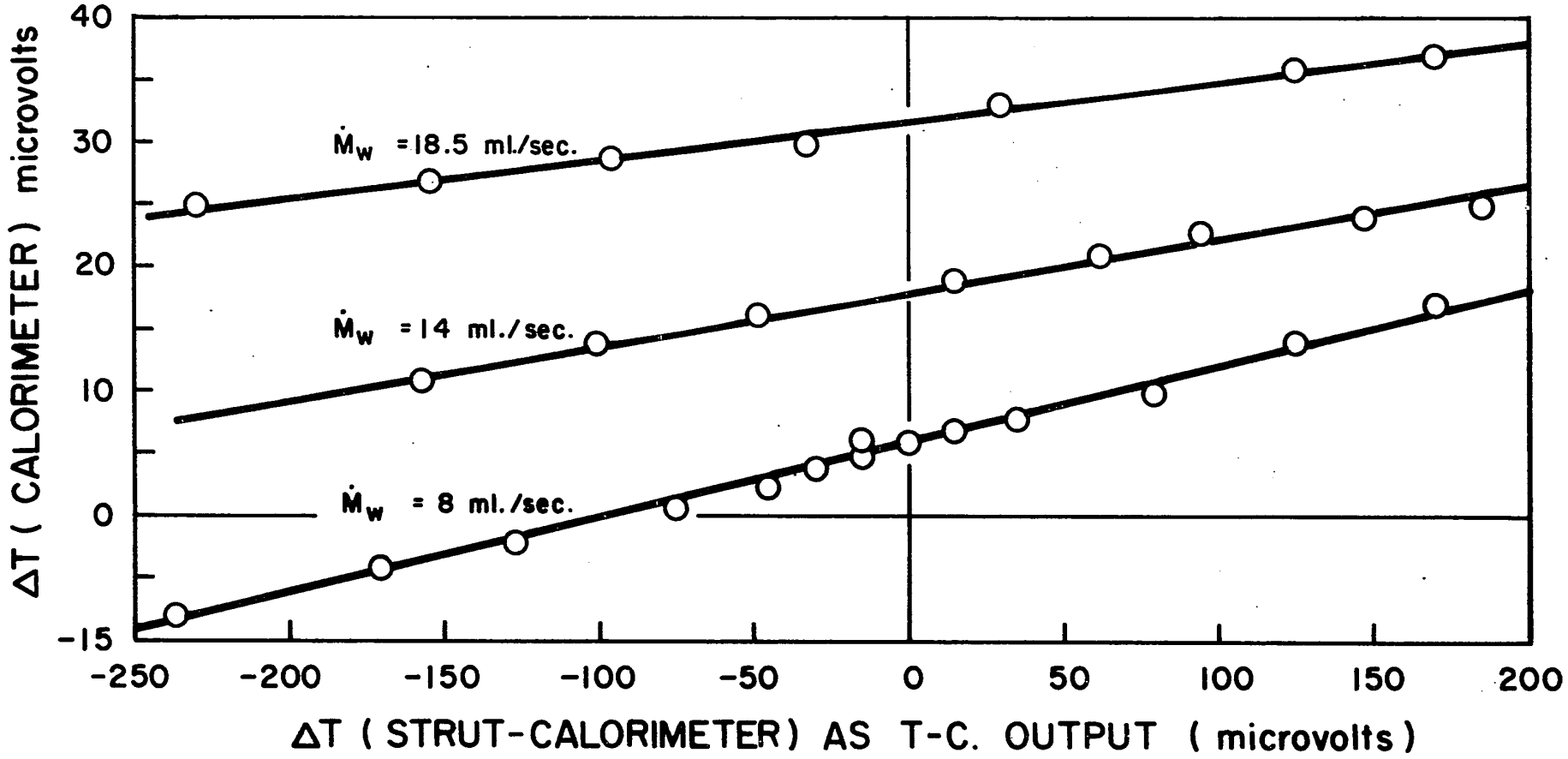
40
30
20
10
0
-15
ΔT (CALORIMETER) microvolts
$\dot{M}_w$ =18.5 ml./sec.
$\dot{M}_w$ =14 ml./sec.
$\dot{M}_w$ = 8 ml./sec.
-250
-200
-150
-100
-50
0
50
100
150
200
ΔT (STRUT-CALORIMETER) AS T-C. OUTPUT (microvolts)

FIGURE 11

Calorimeter Thermocouple Output

as a Function of

Mean Temperature Difference

Between Jacket and Calorimeter

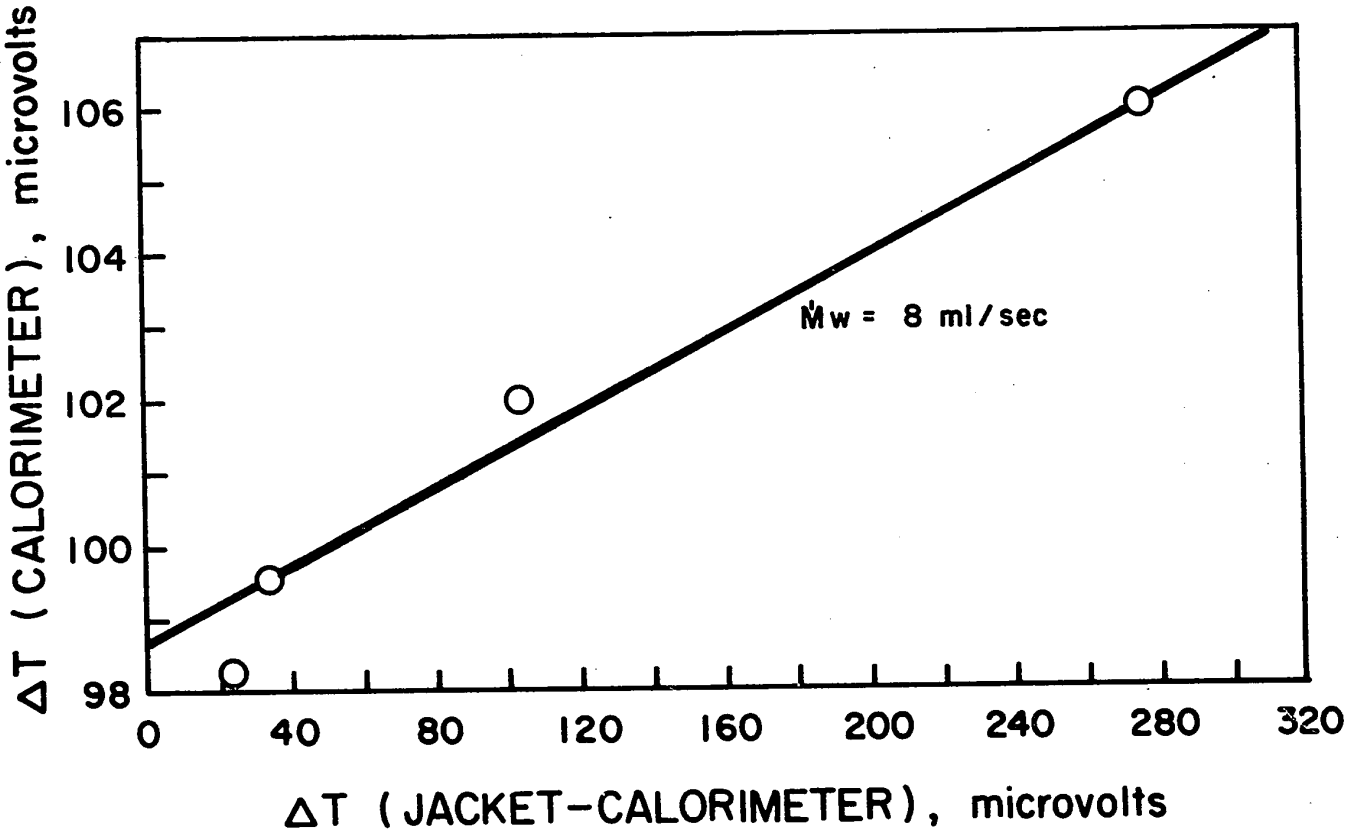
ΔT (CALORIMETER), microvolts
106
104
102
100
98
0
40
80
120
160
200
240
280
320
ΔT (JACKET-CALORIMETER), microvolts
Ṁw = 8 ml/sec

FIGURE 12

Flow Pattern of Gas

over

Calorimetric Probe Tip

LOW
SAMPLING
RATE

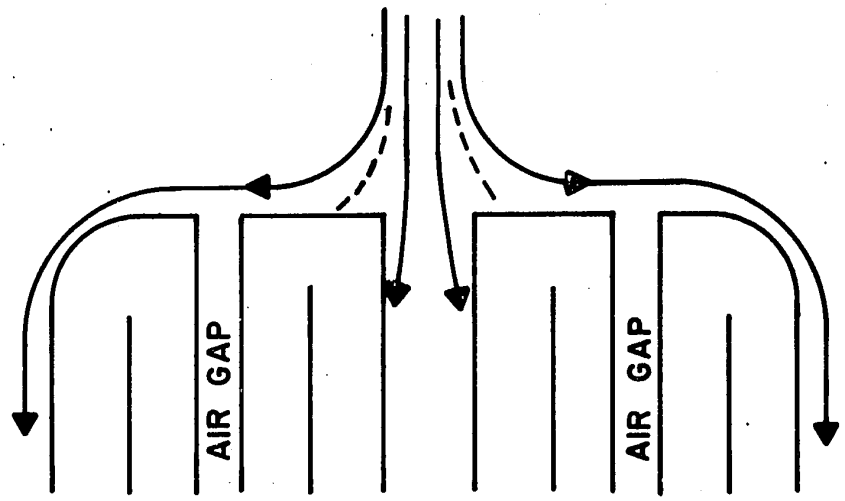

BALANCED
SAMPLING
RATE

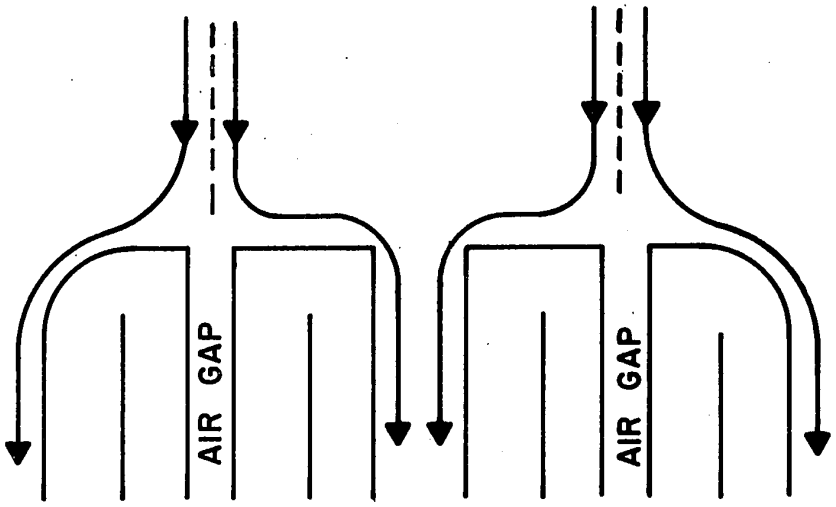

HIGH
SAMPLING
RATE

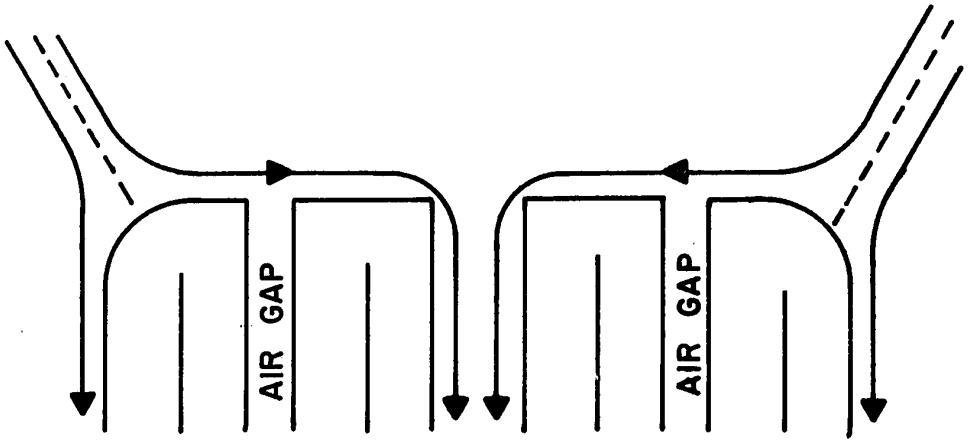

Due to design constraints, it was not possible to operate under this condition, resulting in heat being transferred to the calorimeter, by gas which passed over the jacket.

The asymtotic value of the calorimeter temperature was therefore estimated by varying the gas sample rate over a wide range of values, with the results as shown in Fig. 13.

FORMAL EXPERIMENTS

In the formal experiments, the torch was mounted vertically in open air, with the nozzle pointing downwards. The torch was operated at one set condition throughout the experiments:

Argon Plasma Gas Flowrate	2.7×10^{-6} m^3/s (35 SCFH)
Arc Voltage	30V
Arc Current	650A

In addition 6.3×10^{-7} m^3/s, (8 SCFH) argon was added to the main gas flow via the particle injection nozzles. This flowrate corresponded to that used when injecting particles into the flame (Part II of the experimental section of this thesis).

Axial profiles of temperature, velocity and concentration were determined by use of the calorimetric probe at distances between 25 mm (one inch) and 200 mm (8 inch) from the nozzle exit. No measurements were taken closer to the nozzle exit, since the probe tip was already in the luninous core of the jet; further decrease in the nozzle probe distance would have caused significant distortion of the jet flowfield.

As a result of the repeated mechanical and thermal cycling in

FIGURE 13

Calorimetric Gas Temperature

as a function of

Gas Sampling Rate

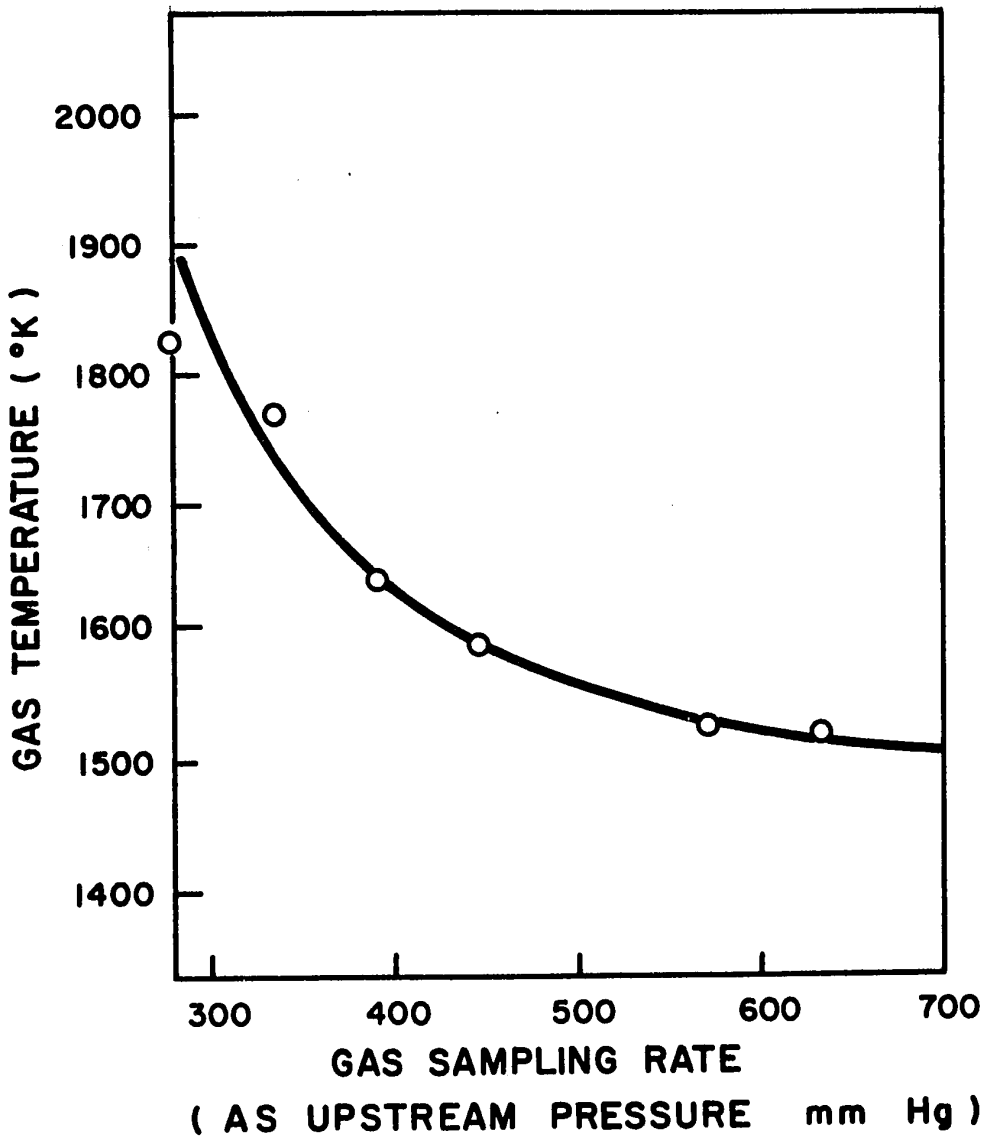
2000
1900
1800
1700
1600
1500
1400
GAS TEMPERATURE (°K)
300
400
500
600
700
GAS SAMPLING RATE
(AS UPSTREAM PRESSURE mm Hg)

the above experiment, the probe developed a small leak in the calorimeter section. A major repair of the probe was therefore necessary, which precluded any further work with the probe at that time. Radial profiles of temperature and velocity were obtained at a distance of 178 mm from the nozzle exit, using a bare junction thermocouple and impact pressure measurements (corrected as before). The position chosen corresponded to the plane of observation of later particle velocity studies (Part II).

RESULTS

The axial profiles of temperature, velocity and concentration are shown in Fig. 14. These results are plotted in non-dimensional form, i.e. they are normalized in terms of their maximum values at 25 mm from the nozzle exit. It is noted that the temperature and velocity profiles are remarkably similar and that 90% of the jet decay (temperature, velocity, concentration) occurred within a distance of ten nozzle diameters.

Fig. 15. shows the variation of the nominal gas enthalpy as the gas sampling rate was varied over the range of operation. The existence of the plateaux at the highest gas sampling rate should be noted. Figs. 16 and 17 show the east-west radial profiles of temperature and velocity at 178 mm from the torch nozzle exit. The half radii data are summarised:

	North-South mm	East-West mm
T	26.7	24.4
V	18.1	16.3

The near Gaussian distribution in Fig. 16 and 17 are clearly seen. The deviations from the Gaussian curve at the velocity edge of the jet are due simply to the measurement errors.

FIGURE 14

Normalized Axial Profiles of

Temperature

Velocity

Concentration (of Argon in Air)

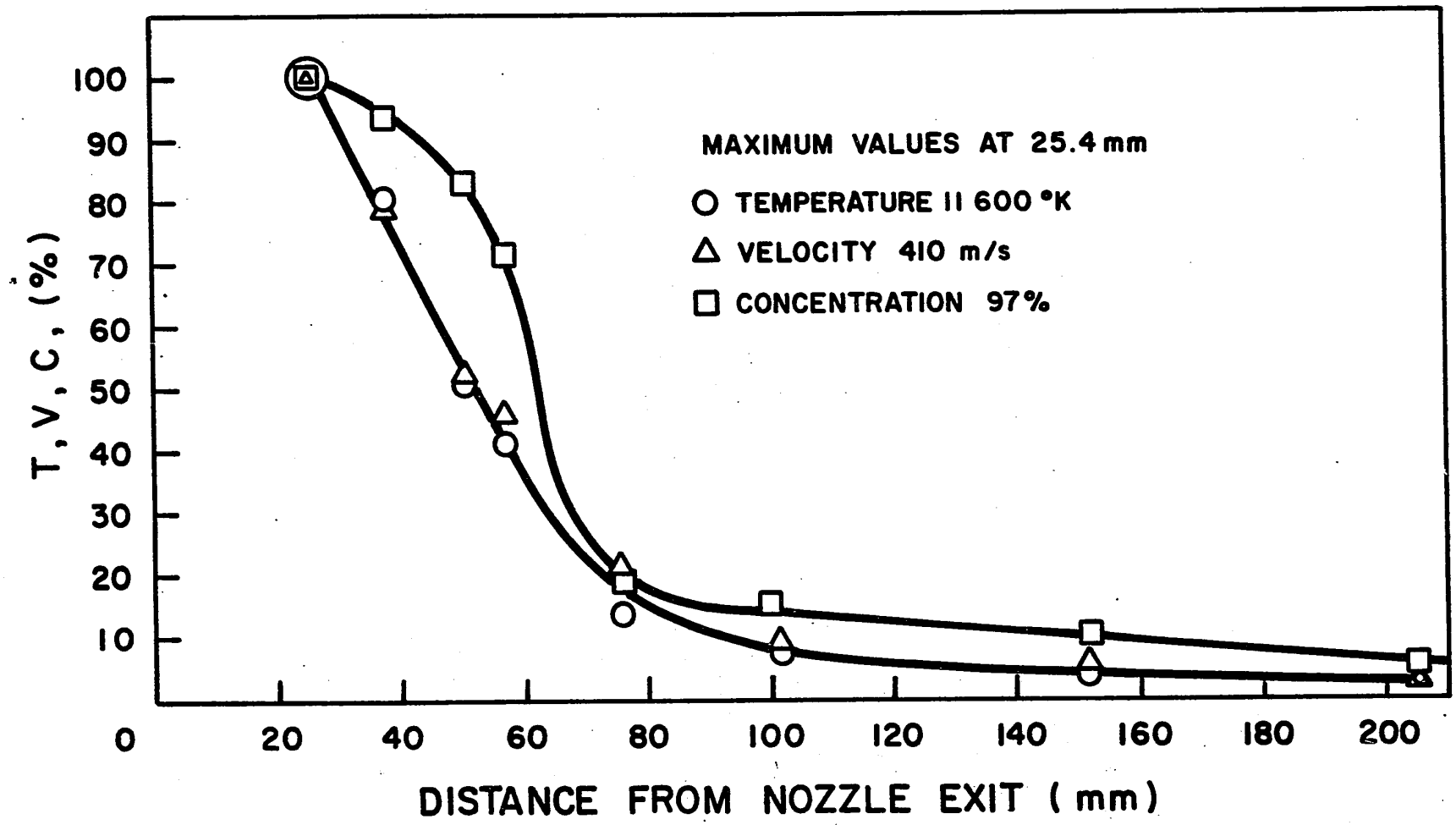
MAXIMUM VALUES AT 25.4 mm
TEMPERATURE 11 600 °K
VELOCITY 410 m/s
CONCENTRATION 97%
T, V, C, (%)
100
90
80
70
60
50
40
30
20
10
0
20
40
60
80
100
120
140
160
180
200
DISTANCE FROM NOZZLE EXIT (mm)

FIGURE 15

Nominal Gas Enthalpy Change

as a Function of

Gas Sampling Rate

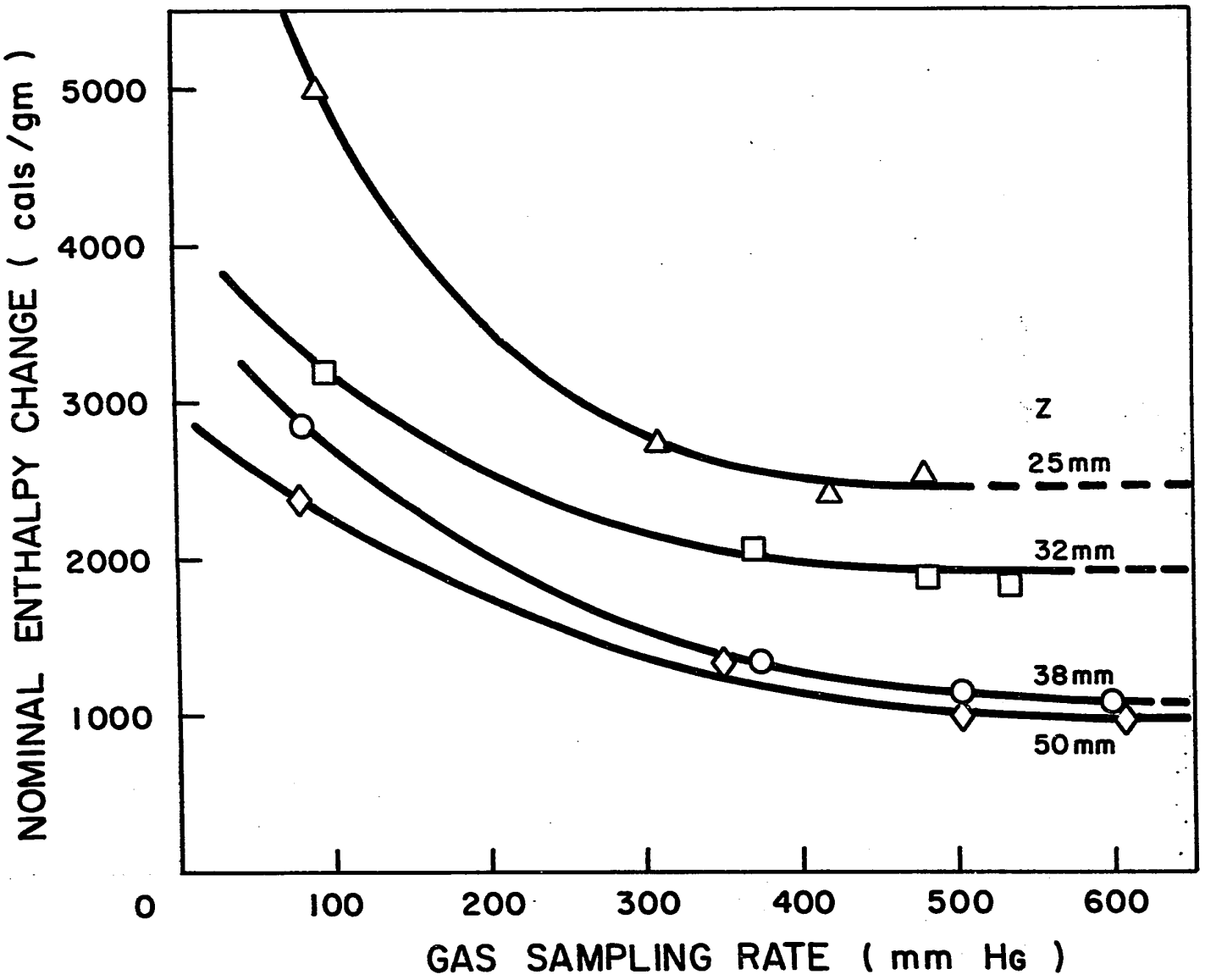
NOMINAL ENTHALPY CHANGE (cals /gm)
5000
4000
3000
2000
1000
0
100
200
300
400
500
600
GAS SAMPLING RATE (mm Hg)
Z
25mm
32mm
38mm
50mm

FIGURE 16

Radial Profile of Temperature

at 178 mm from Torch Nozzle Exit

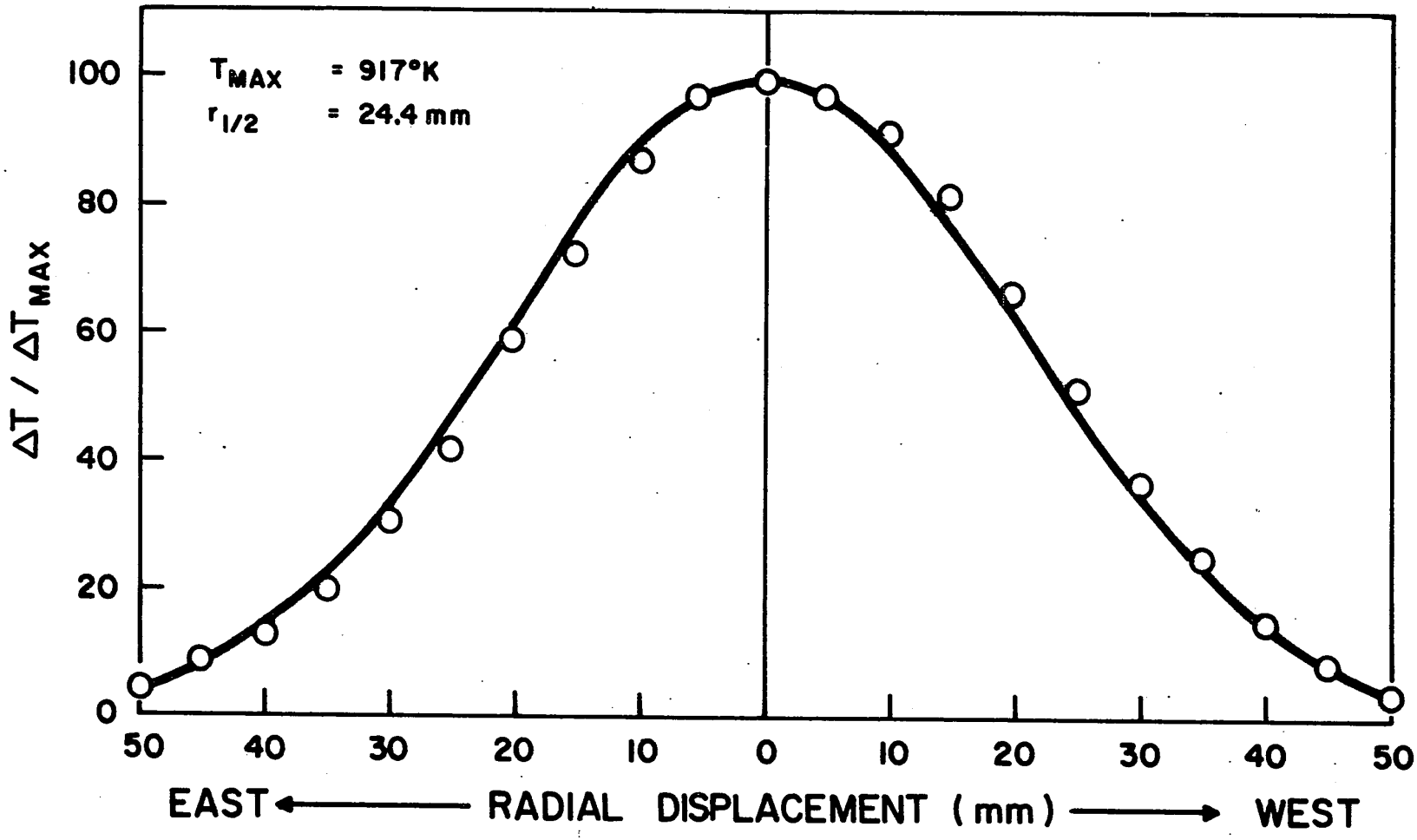
T_{MAX} = 917°K
$r_{1/2}$ = 24.4 mm
100
80
60
40
20
0
$\Delta T / \Delta T_{MAX}$
50
40
30
20
10
0
10
20
30
40
50
EAST
RADIAL DISPLACEMENT (mm)
WEST

FIGURE 17

Radial Profile of Velocity

at 178 mm from Nozzle Exit

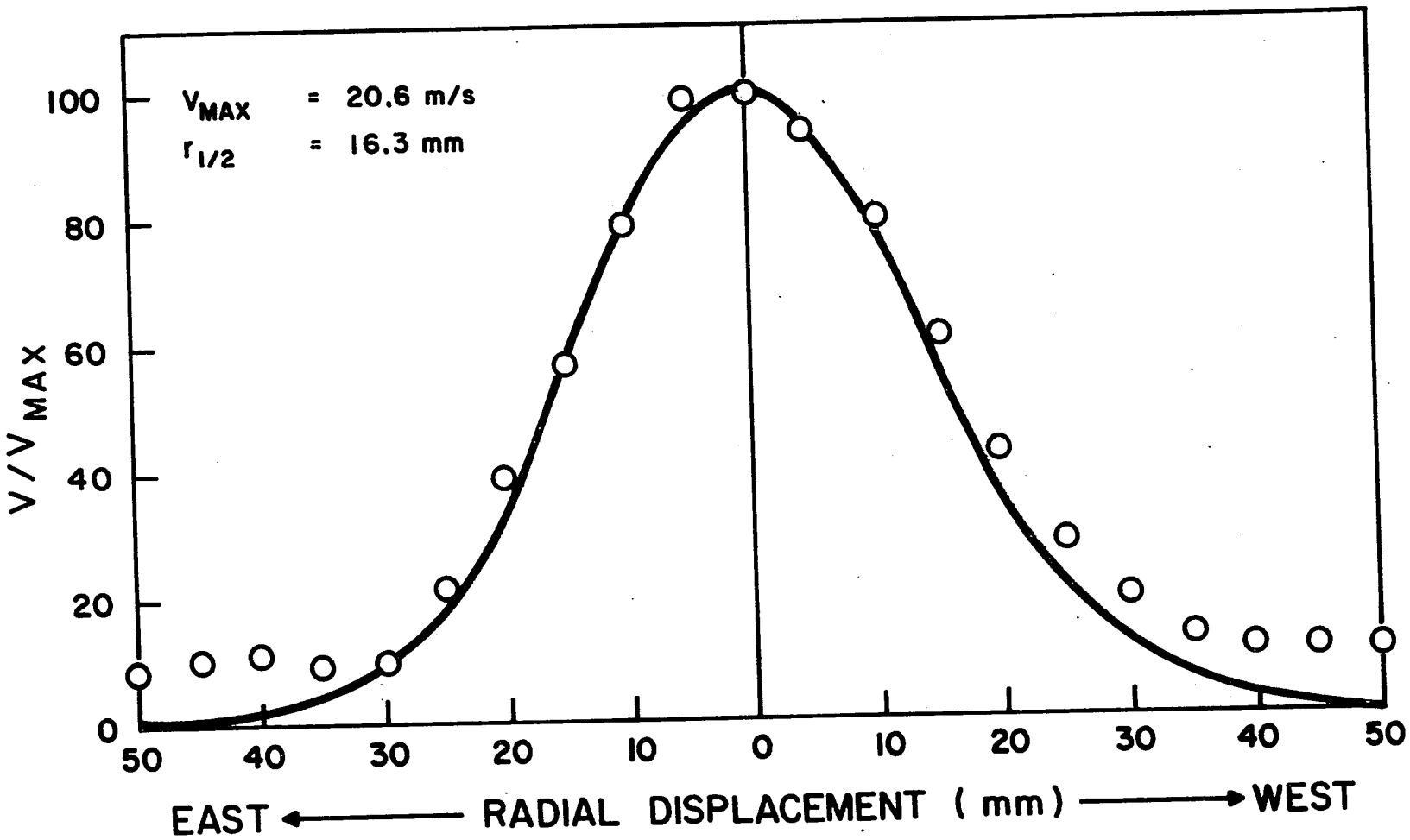
V_{MAX} = 20.6 m/s
$r_{1/2}$ = 16.3 mm
100
80
60
40
20
0
V / V_{MAX}
50
40
30
20
10
0
10
20
30
40
50
EAST ← RADIAL DISPLACEMENT (mm) → WEST

According to O'Connor *et al.* (12), the square of the ratio of the velocity half radius to the temperature half radius should be equal to the turbulent Prandtl number. In this case:

$$Pr_t = \left[(0.71 + 0.64)/2\right]^2 \Big/ \left[(1.05 + 0.96)/2\right]^2$$

$$= \underline{0.45}$$

DISCUSSION OF RESULTS

Temperature

The rôle of radiation in temperature measurements was considered both from the point of view of the effect of the flame on the calorimeter and also of the converse effect. Using a thermopile, Cremers and Pfender (13) carried out measurements of radiation intensity for a plasma torch having a nozzle diameter slightly smaller than that used in the present work. The equivalent heat flow to the calorimeter, due to radiation, would have been less than 0.1 percent of the heat given to the calorimeter by the gas flowing through the sample tube. It was therefore considered that not only would radiation have had a negligible effect on the calorimetric temperature measurements, but also from the point of view of radiation balance, the cold surface of the calorimeter would not have disturbed the temperature of the flame upstream of the probe. This suggestion was reinforced by comparing the spectroscopic temperature of Cremers and Pfender (13) with the maximum calorimetric temperature of the present work.

Extrapolating both sets of results to a common synthetic point in space and operating conditions, the spectroscopic temperature was estimated at 12 000°K, while the calorimetric temperature was estimated at 12 300°K. Since the uncertainty in the data of Cremers and Pfender was about ± 1 000°K,

the calorimetric temperature was considered to be of at least comparable accuracy.

Velocity

The half radius of the undisturbed jet near the nozzle exit would have been comparable to the size of the calorimetric probe. The possibility therefore existed for distortion of the flowfield when making impact pressure measurements very close to the nozzle exit. While the probe diameter was therefore larger than desirable, it is noted that initial trials with a smaller probe were unsuccessful due to the inability of the smaller and weaker probe to withstand the aggressive environment of the plasma flame.

The gas velocity results must therefore be treated with a degree of reservation, until such time as they can be compared with data obtained by non-contact methods such as Laser anemometry (14).

No correction was applied for the effects of the difference in temperature between free-stream and probe surface. According to Carleton (15), a correction is required for the effects of low Reynolds number flow, where Re is based on the mean film temperature. In his work, the measured impact pressure was reported as being a maximum of 13% above the true value, but in his analysis, this correction was inversely proportional to probe diameter. For the present work, this would result in a correction of 5% in the impact pressure or 2% in the gas velocity. This was considered to be a trivial correction and was therefore ignored.

Composition

The composition of the gas as given by the chromatograph was that for a mixture at 300°K. The actual composition of the gas at the elevated

temperatures of the plasma jet, could have included nitrogen-oxygen, nitrogen-argon and oxygen-argon species. Consideration of the chemical reaction of the gases is beyond the scope of this thesis. It would be complicated by non-equilibrium effects due to the rapid cooling of the gas.

In view of the similarity in the properties of argon, nitrogen and oxygen over a wide range of temperatures (tabulated in Appendix D), it would seem reasonable to apply the composition data from the low temperature chromatographic analyses to the calculation of Reynolds and Nusselt numbers at high temperature.

CONCLUSIONS

The temperatures obtained by use of calorimetric probe agreed with both thermocouple and spectroscopic data.

The results of velocity and concentration were subject to a degree of reservation and should ideally be compared with data obtained by other techniques.

The measured maximum temperature and velocity were 11 600°K and 410 m/s. Ninety percent decay of the jet parameters (T, V, Conc.) occurred within a distance of ten diameters from the nozzle exit.

The radial distributions of temperature and velocity were Gaussian, with a ratio of velocity half radius to temperature half radius of 0.68.

NOMENCLATURE

D_{tc}	Diameter of thermocouple wire
Δh_g	Enthalpy change of gas
Δh_w	Enthalpy change of cooling water
k_B	Bulk conductivity of gas
L_{tc}	Length of exposed thermocouple wire
$\dot{M}_g$	Gas mass flowrate
$\dot{M}_w$	Water mass flowrate
Nu_B	Nusselt number evaluated at bulk gas temperature
Pr_B	Prandtl number evaluated at bulk gas temperature
* Re_B	Reynolds number evaluated at bulk gas temperature
T_B	Bulk gas temperature
T_D	Temperature of enclosing duct
T_{sh}	Temperature of thermocouple sheath
T_{tc}	Temperature of thermocouple junction
ΔT_c	Conduction temperature correction
ΔT_R	Radiation temperature correction
ε_{tc}	Emissivity of thermocouple junction
η	Defined in equation (6)
σ	Stefan-Boltzmann constant
ψ	Defined in equation (5)
* Pr_t	Turbulent Prandtl number

BIBLIOGRAPHY

1. Kubanek, G.R., and Gauvin, W.H., Can. J. Chem. Eng. 45, 251 (1967).
2. Grey, J., Jacobs, P.F., and Sherman, M.P., Rev. Sci. Inst. 33, 738 (1962).
3. Grey, J., I.S.A. Trans. 4, 102 (1965).
4. Incropera, I., and Leppert, G., I.S.A. Trans. 6, 35 (1967).
5. Smith, D.L., and Churchill, S.W., Univ. of Michigan 05607-1-T (1965).
6. Petrov, M.D., and Sepp. V.A., Teplofizika Vysokikh Temperatur 8, 868 (1970).
7. Cheylan, J., Doc. Ing. Thesis, Univ. Nancy, France (1970).
8. Lewis, J.A., Progress Report, "Calibration of Greyrad Calorimetric Probe", McGill Univ., Montreal, (Jan. 1971).
9. Eckert, E.R.G., and Pfender, E., Advances in Heat Transfer, Vol. 4, Academic Press (1967).
10. Scadron, M.D., and Warshawsky, I., N.A.C.A. TN-2599 (1952).
11. Fishenden, M., Int. J. Heat and Mass Trans. 5, 67 (1962).
12. O'Connor, T.J., Comfort, E.H., and Cass, L.A., A.I.A.A.J. 4, 2026 (1966).
13. Cremers, C.J., and Pfender, E., ARL-64-191 (1964).
14. Angus, J.C., Morrow, D.L., Dunning, J.W., and French, M.J., Ind. Eng. Chem. 61, 8 (1969).
15. Carleton, F.E., Ph.D. thesis, Univ. Michigan (1970).

PART II

Measurement of the Velocity and Deceleration of Particles Emerging from a Plasma Flame By High-Speed Ciné-Streak Photography

INTRODUCTION

Over the past fifteen years, there has been a considerable amount of development work on plasma devices based on direct-current-arc and radio-frequency electrical discharges. The point has now been reached where it is possible to heat commercial quantitites of various gases to temperatures in excess of 10 000°K (18 000°F), at a pressure of one atmosphere.

Plasma devices have been used to carry out a variety of high-temperature chemical reactions, including the manufacture of acetylene (1), titanium dioxide (2), zirconium (3) and high purity silica (3)

The design of chemical reactors requires a knowledge of the residence time of particles during their passage through the flame. This is one of the major factors which control the degree of conversion of the feed material. However, large temperature and velocity gradients would cause a degree of uncertainty in any prediction of particle motion through a plasma reactor. In order to assess the reliability of such predictions, it was considered desirable to make a comparison with data from a real system.

Lemoine and LeGoff (4) recently determined the velocity of a variety of different particles within a plasma flame, by the use of ciné-streak photography. However, the particle shape was not regular, the size distribution was wider than regular sieve dimensions and also the particles had been coated with barium nitrate to improve their luminosity. Evaporation of this material could have reduced the drag on the particles (5), and therefore there would be some uncertainty in the interpretation of their data. In addition, no estimation of particle acceleration or

deceleration was made, presumably because of indistinct recording of streaks.

A program of experiments was therefore carried out in which near-ideal particles were injected into a 40kw DC arc-plasma. Using a high-speed camera in streak mode, the velocity and deceleration of these particles were measured as they emerged from the visible part of the flame.

EXPERIMENTAL EQUIPMENT

D.C. Plasma Torch

The basic components of the torch are shown in Figs. 1 and 3 and the complete unit in Fig. 2. The cathode consisted of a thoriated tungsten rod 12 mm (0.5 in) in diameter with a 45 degree half angle cone point. The anode was made from copper, in the form of a nozzle, with an inside diameter of about 10 mm (7/16 in) and a length of about 50 mm (2 in). The torch was mounted vertically downwards in open air, with no confining walls below the nozzle exit.

In operation, an arc was struck between the cathode and anode, with argon gas blown through the nozzle. Fixed operating conditions of 650A, 30V and a gas flowrate of 3×10^{-4} m^3/s (35 SCFH) were used throughout the experiments. On the 18kW power input, about half was carried away in the cooling water to the cathode and anode, with the remainder going to heat the gas. Ear muffs and face shields were used during operation of the torch, since the jet noise and intense radiation of the flame presented a considerable hazard to operators.

Axial profiles of gas temperature, velocity and concentration (argon in air) are shown in Fig. 4.

Feed Material

Because of their superior sphericity, their inertness and non-volatility, glass beads were selected as the most suitable material for this study. Commercially available material was treated at the University of Nancy, France, to remove non-spherical particles. At the same time, separation into close-size fractions was carried out. It was estimated that less than five percent of the material was non-spherical, the majority

FIGURE 1

Cross Section of Plasma Torch

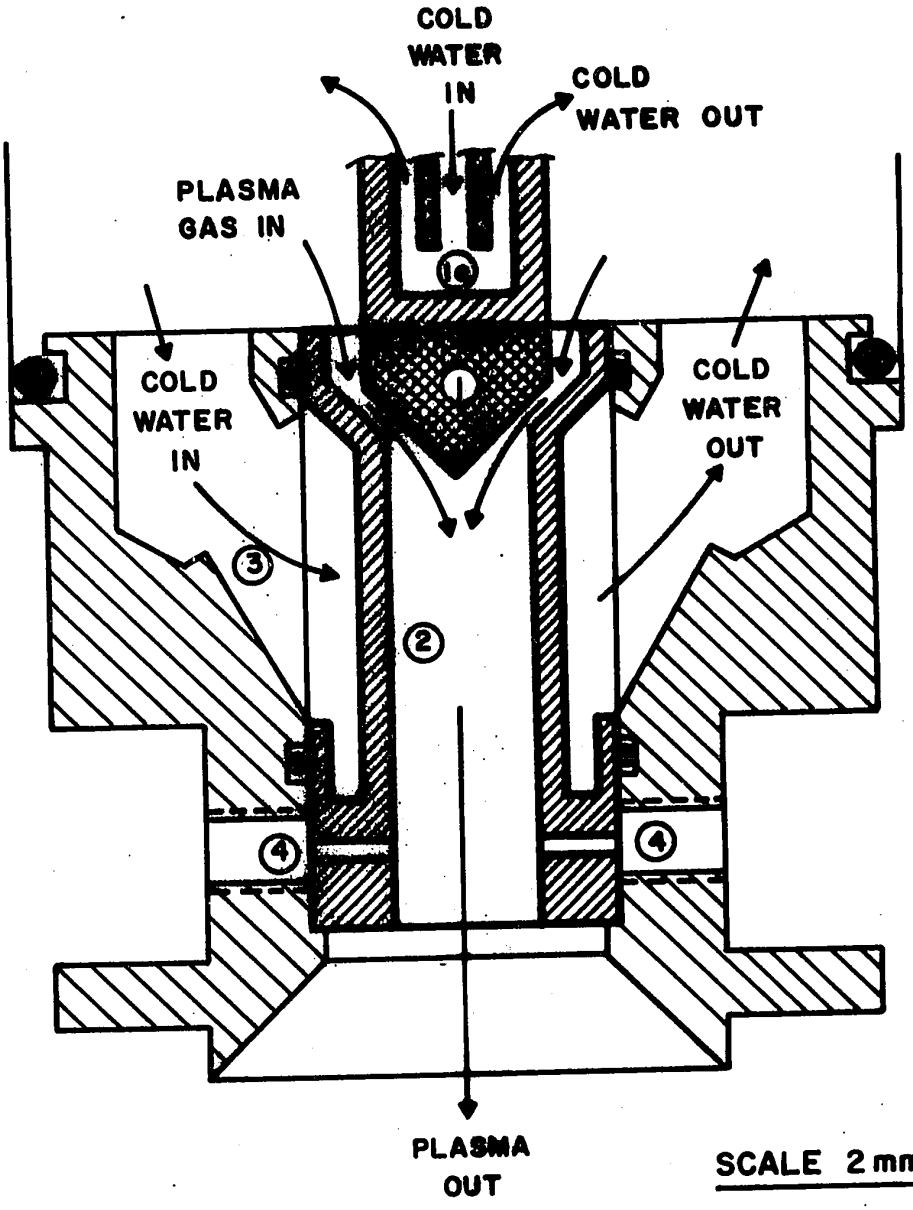

SCALE 2 mm = 1 mm

1. THORIATED TUNGSTEN CATHODE.
1a. CATHODE HOLDER.
2. COPPER NOZZLE – ANODE.
3. NOZZLE BODY.
4. PARTICLE INJECTION INLET.

FIGURE 2

Photograph of Complete Torch

FIGURE 3

Photograph of Torch Components

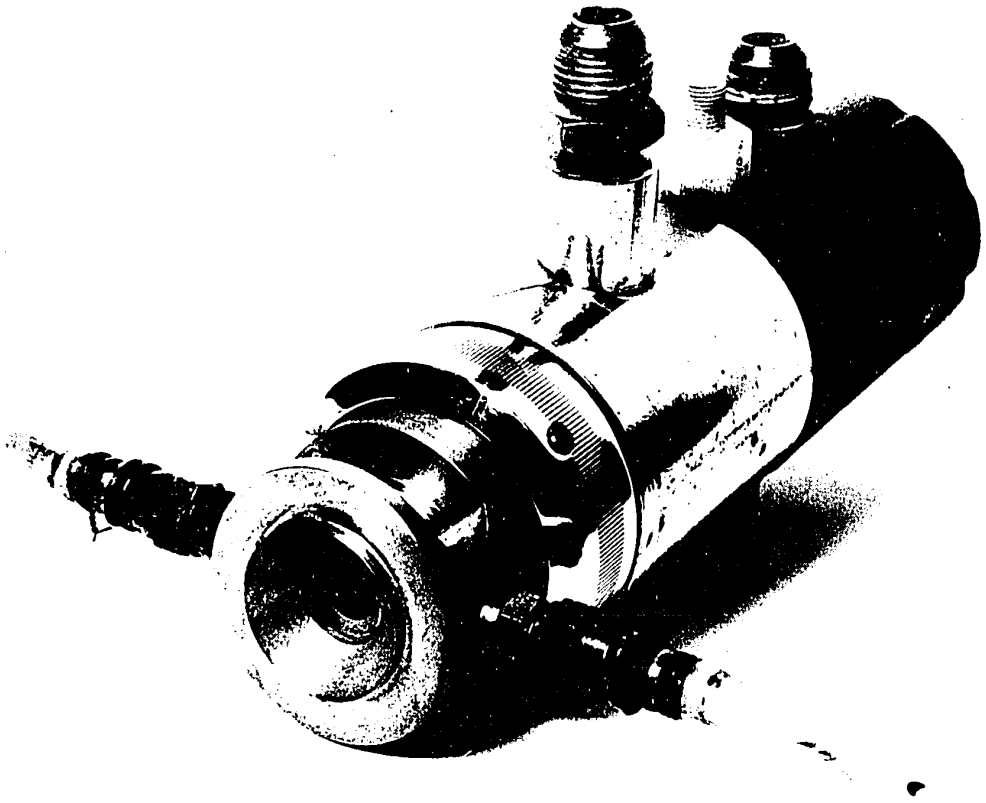

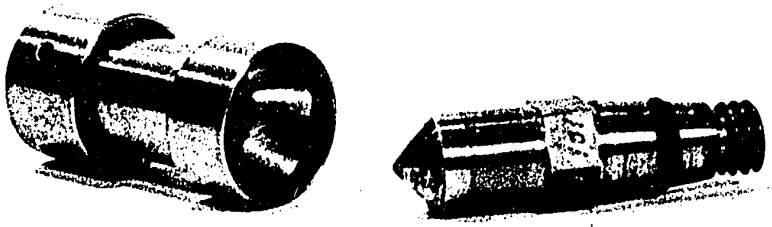

FIGURE 4

Normalized Axial Profiles

of

Temperature,

Velocity,

Concentration of Argon in Air

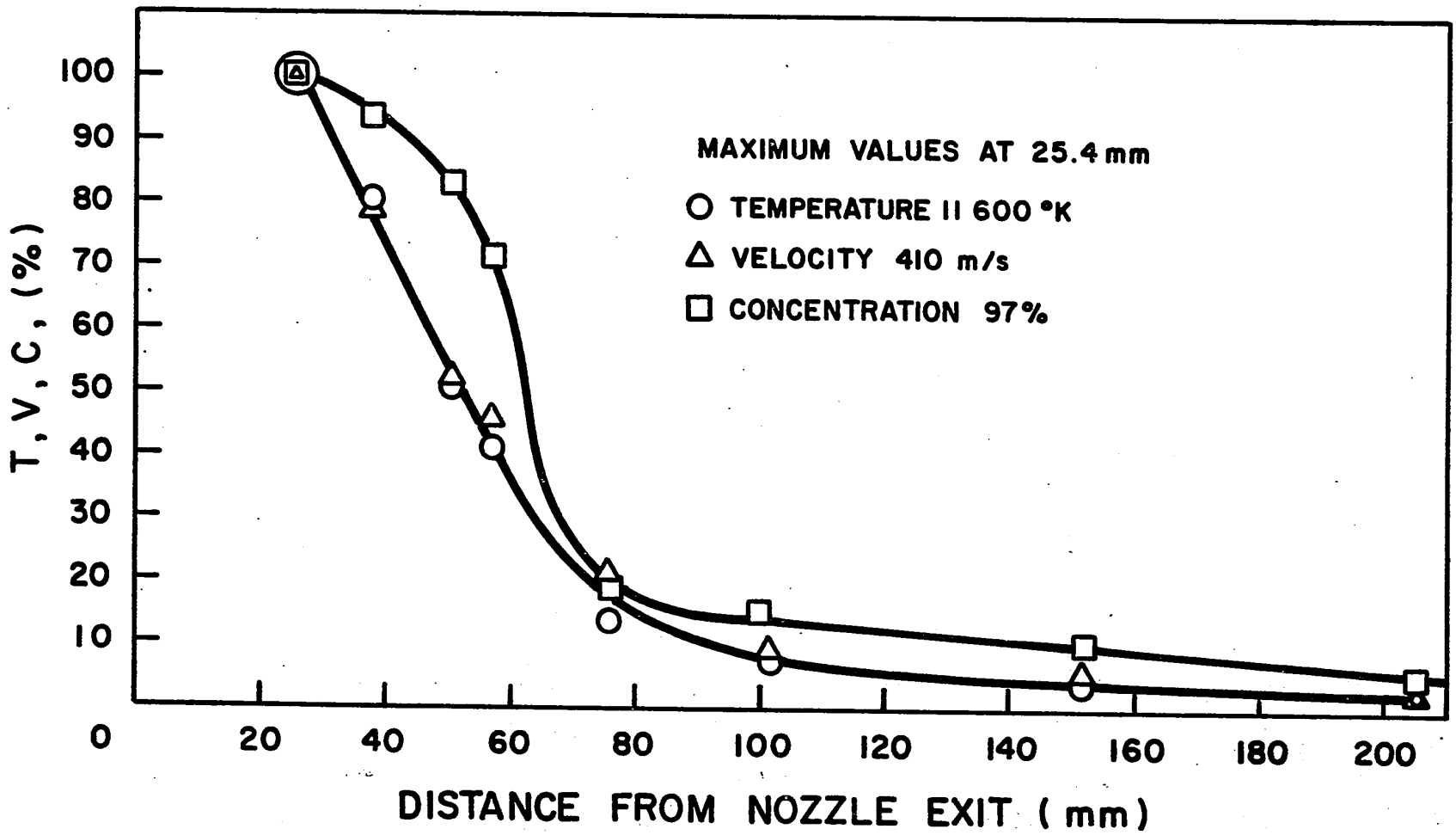
MAXIMUM VALUES AT 25.4 mm
TEMPERATURE 11 600 °K
VELOCITY 410 m/s
CONCENTRATION 97%
T, V, C, (%)
100
90
80
70
60
50
40
30
20
10
0
20
40
60
80
100
120
140
160
180
200
DISTANCE FROM NOZZLE EXIT (mm)

of defects consisting of small spheres stuck to the larger particles.

Typical scanning electron micrographs of the feed and product are shown in Figs. 5 and 6.

Particle Feeder

In order to achieve an even flowrate of particles through the plasma torch, several devices were considered. The following design (Fig. 7) is a copy of a particle feeder developed at the University of Nancy, France (4).

The particles were held in a vertical tube closed at its bottom end and terminating at the top with a standard Tee tube fitting mounted sideways. The carrier gas was introduced from a second tube which was pushed into the reservoir tube by a continuously variable drive mechanism. Sealing was carried out by means of Teflon ferrules which could be compressed without causing excessive friction.

The entrained particles were carried out through the side-arm of the Tee to a second Tee which split the flow evenly, feeding each half to its injection nozzle and hence into the plasma flame.

The flowrate of 44-53μm glass beads is shown in Fig. 8.

It should be noted that the major factor controlling the feedrate was the motor speed, the gas flowrate being relatively unimportant.

Ciné-Streak Camera*

The camera used in this work was a regular high-speed 16 mm movie camera with the additional capability of streak operation.

---

* (In this paper, the term "ciné-streak" is used in preference to just "streak" to avoid any confusion with still camera work using single exposures.)

FIGURE 5

Glass Beads before passing through Torch

FIGURE 6

Glass Beads after passing through Torch

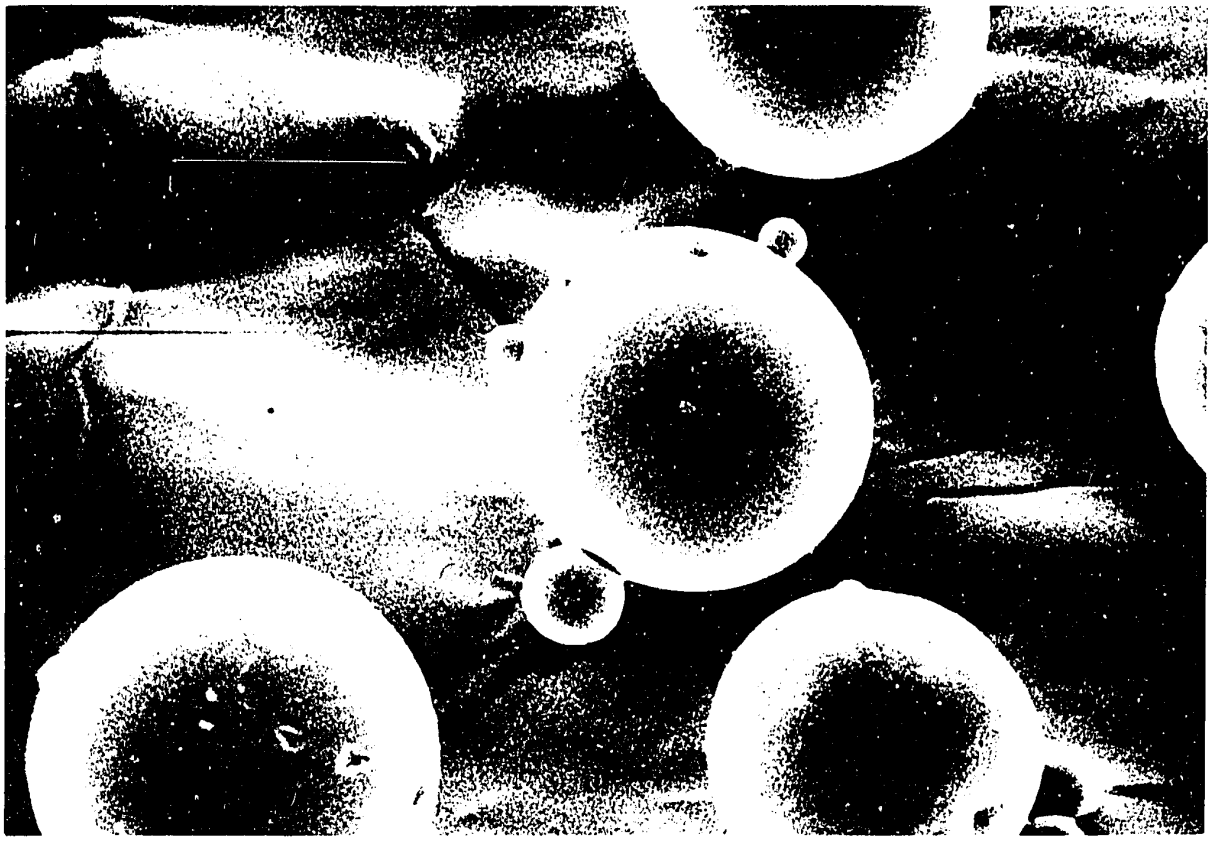

FIGURE 7

Low Mass Rate Particle Feeder

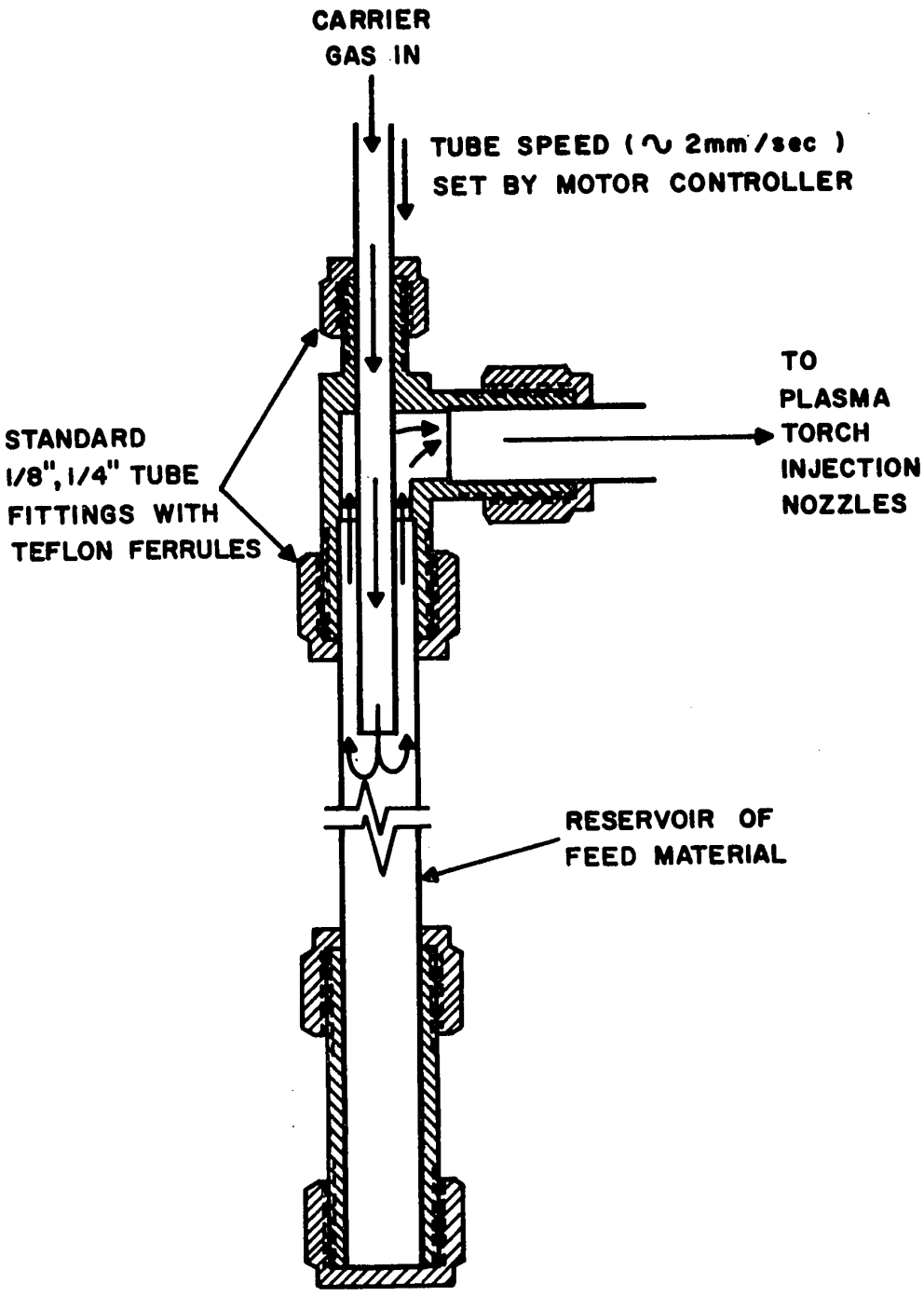
CARRIER
GAS IN
TUBE SPEED (∿ 2mm/sec)
SET BY MOTOR CONTROLLER
TO
PLASMA
TORCH
INJECTION
NOZZLES
STANDARD
1/8", 1/4" TUBE
FITTINGS WITH
TEFLON FERRULES
RESERVOIR OF
FEED MATERIAL

FIGURE 8

Calibration Graph

of

Particle Feeder

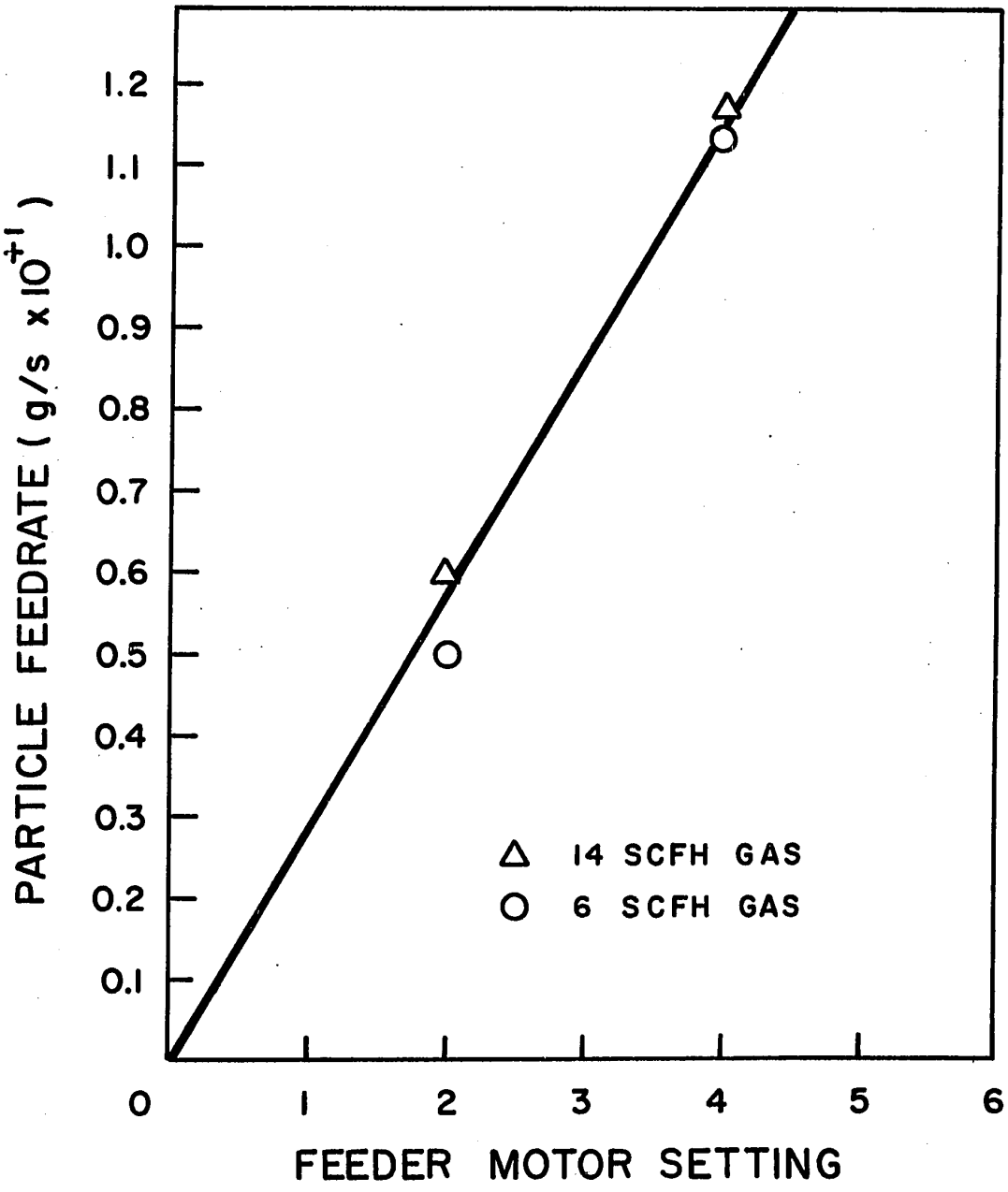
PARTICLE FEEDRATE (g/s x 10+1)
1.2
1.1
1.0
0.9
0.8
0.7
0.6
0.5
0.4
0.3
0.2
0.1
0
1
2
3
4
5
6
FEEDER MOTOR SETTING
14 SCFH GAS
6 SCFH GAS

A D.C. motor and speed control system were used to drive the film through the gate at (ideally) a constant linear velocity. The actual velocity was determined from the distance between timing marks exposed on the edge of the film by a small light-source. The neon bulb of this device was powered by a pulse generator operating at a frequency of 1052 $\pm$ 1 Hz. Calibration of this timing light generator showed a drift of only two percent in two years and was therefore considered to have a reasonably stable operation. Fig. 9 shows the results of several film velocity determinations. It is noted that at a demand velocity of about 16 m/s (50 ft/s), there was a typical overshoot in the actual film velocity, with the steady state value being reached after half the film had been exposed.

The optics of the streak system are shown in Figs. 10, 11 and 12. A 35 mm format lens was used to minimize distortion of the film edges. The focal length and aperture were 55 mm and f:2, respectively. A right-angled prism incorporated in the lower half of the film gate was used to deflect the images onto the film above as shown in Fig. 10. A slit mask was located just below the gate, with the length of the slit at right-angles to the direction of motion of the film. Because of the slit dimensions (0.5 mm x 10 mm), only those images moving parallel to the slit were recorded on the film.

FIGURE 9

Camera Film Speed Calibration

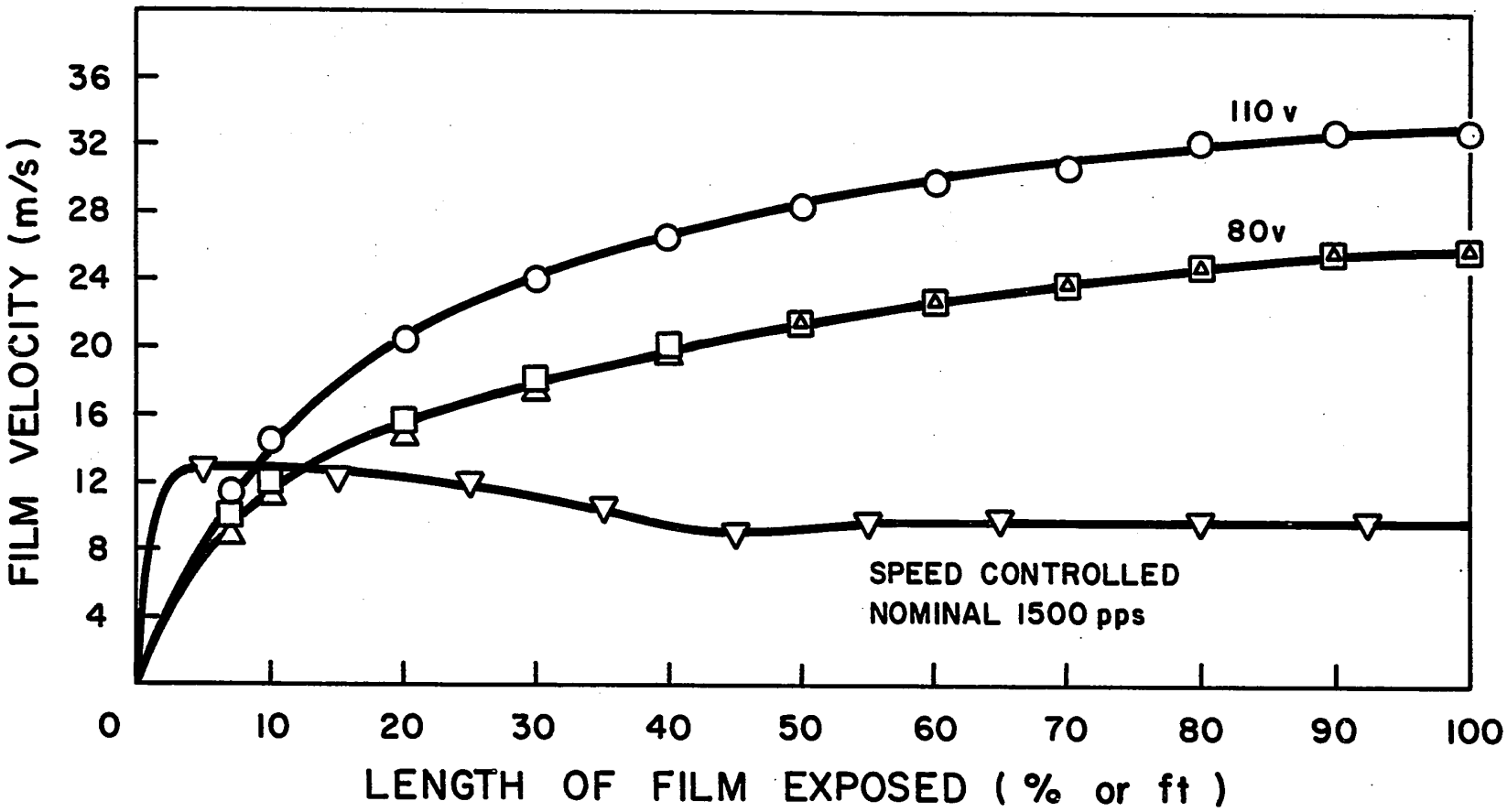
FILM VELOCITY (m/s)
36
32
28
24
20
16
12
8
4
0
10
20
30
40
50
60
70
80
90
100
LENGTH OF FILM EXPOSED (% or ft)
110 v
80v
SPEED CONTROLLED
NOMINAL 1500 pps

FIGURE 10

Ciné-Streak Camera, Optics Schematic

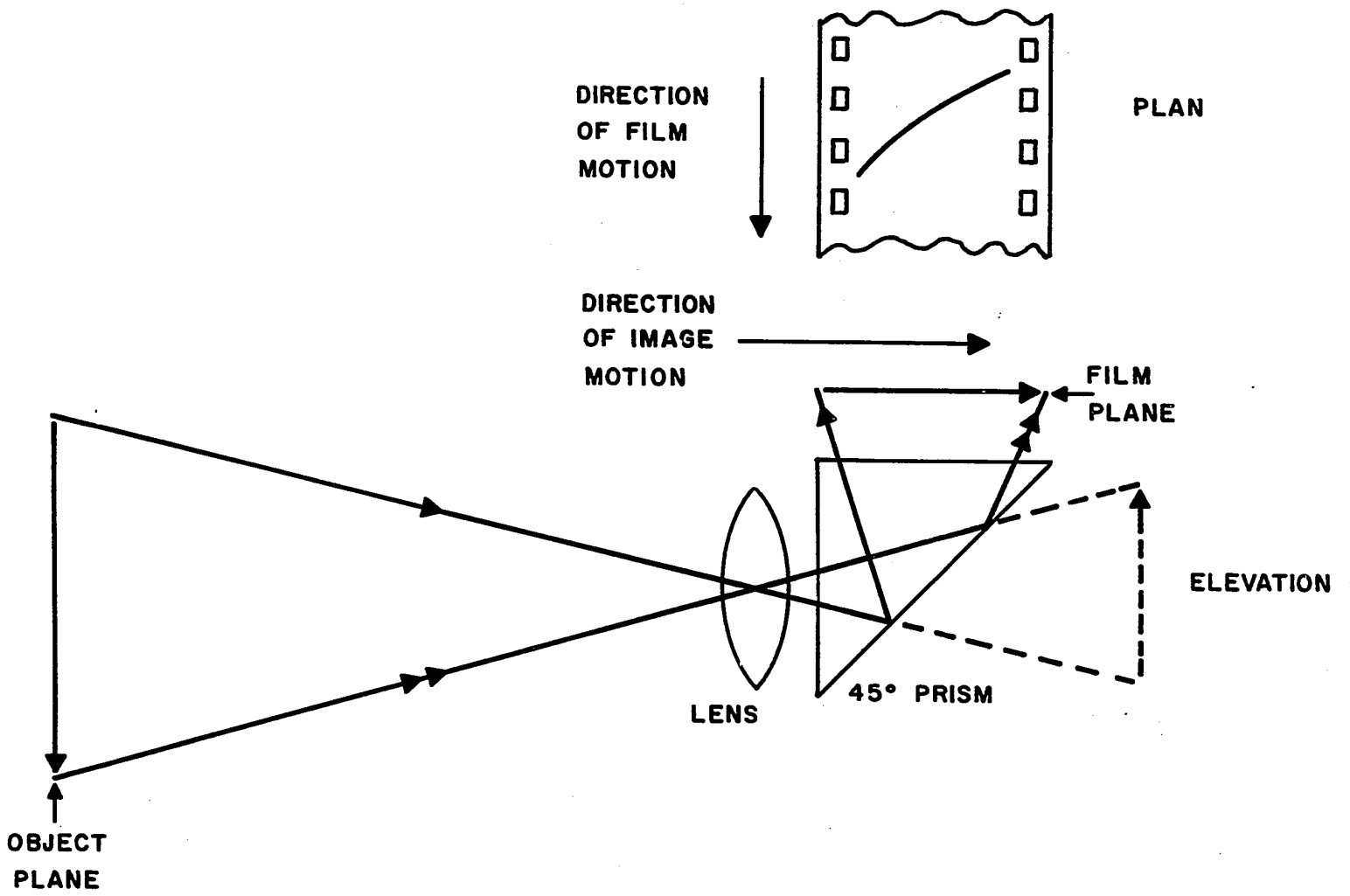
DIRECTION
OF FILM
MOTION
PLAN
DIRECTION
OF IMAGE
MOTION
FILM
PLANE
ELEVATION
LENS
45° PRISM
OBJECT
PLANE

FIGURE 11

Photograph of Main Optical Components

for Streak Photography

FIGURE 12

Photograph of High Speed Camera

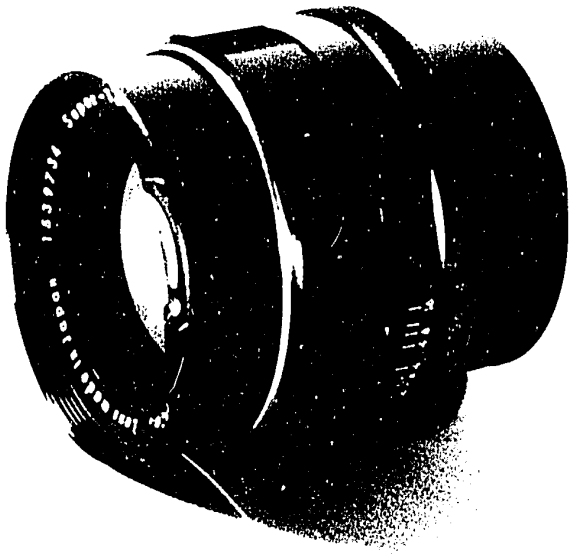

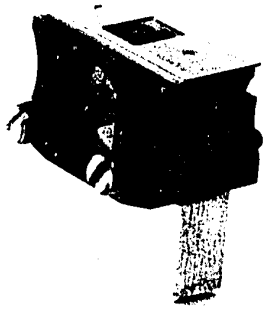

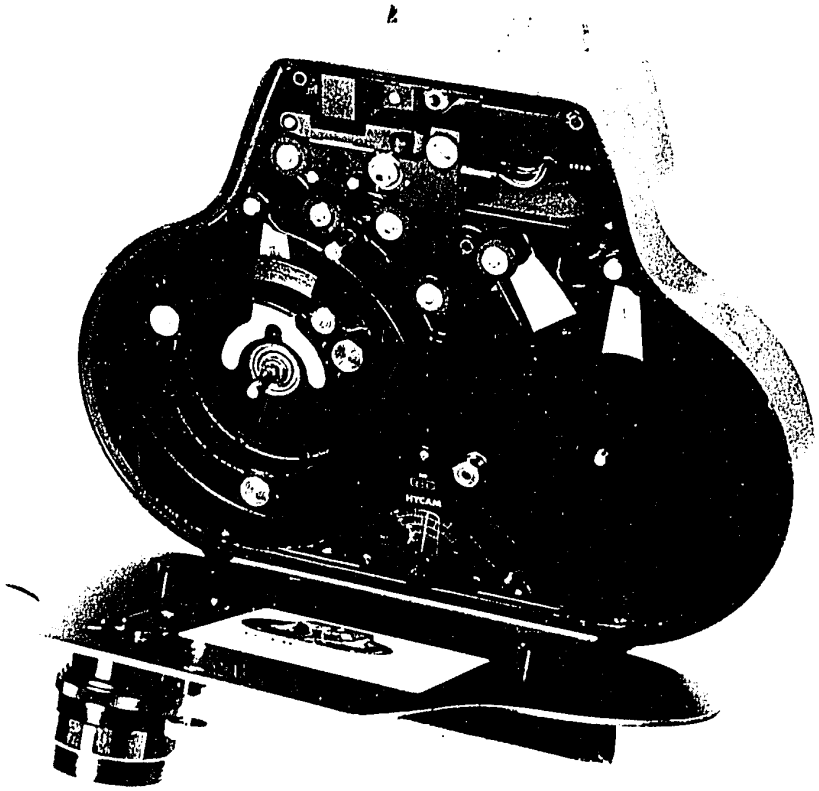

Analysis of Particle Velocity and Acceleration Measurement by Cine-Streak Photographs

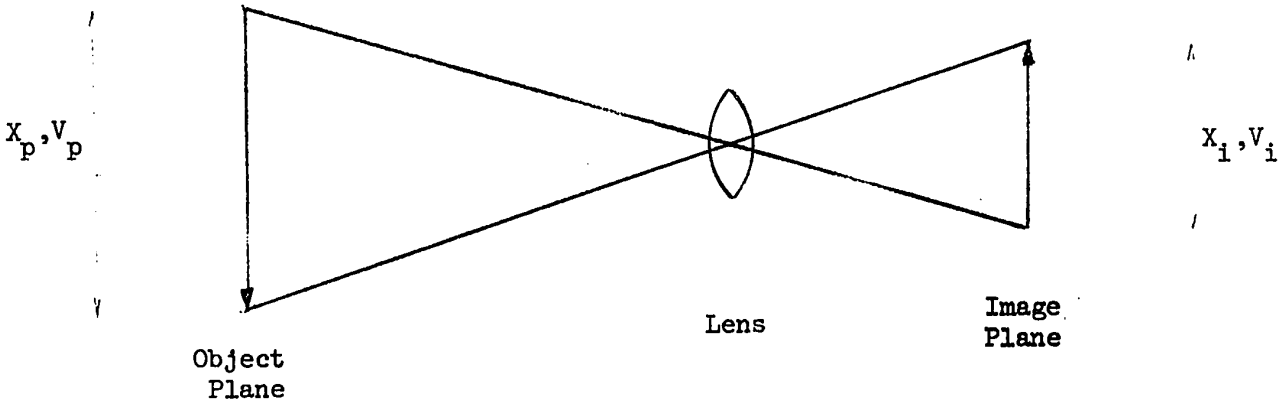

The object-film image magnification is defined as :-

$$M_{of} = X_i/X_p \quad \ldots\ldots\ldots\ldots\ldots\ldots\ldots\ldots\ldots\ldots \quad (1)$$

Let the time taken to traverse the distance 'X_p', by a particle moving at constant velocity, be 't' seconds. This will also be the time for the image to traverse the distance 'X_i'. Therefore:

$$M_{of} = (X_i/t)/(X_p/t) \quad \ldots\ldots\ldots\ldots\ldots\ldots\ldots\ldots \quad (2)$$

$$M_{of} = V_i/V_p \quad \ldots\ldots\ldots\ldots\ldots\ldots\ldots\ldots \quad (3)$$

Thus the image velocity is equal to the product of magnification and object velocity.

Consider now the point image traversing across the film.

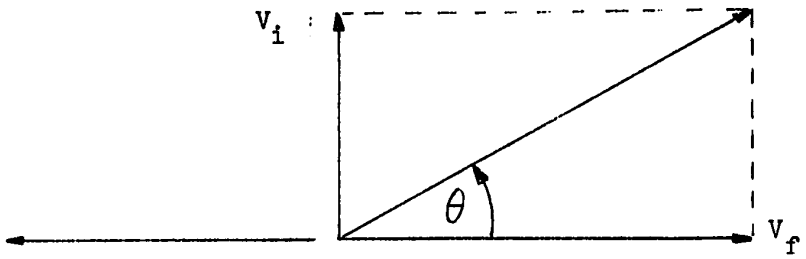

Relative to the film, the image has its own velocity and the negative of the film velocity.

If θ is the angle between the negative of the direction of motion of the film and the resultant streak, then

$$V_i/V_f = \tan(\theta) \quad \ldots\ldots (4)$$

Thus combining equations (3) and (4)

$$V_p = (V_f/M_{of}) \tan(\theta) \quad \ldots\ldots (5)$$

It is recalled that the particle acceleration $\dot{V}_p$ is given by

$$\dot{V}_p \equiv dV_p/dt$$

$$= (dV_p/dX_p)(dX_p/dt)$$

$$= (dV_p/dX_p)V_p$$

$$\dot{V}_p \simeq (\Delta V_p/\Delta X_p)\overline{V}_p \quad \ldots\ldots (6)$$

But the object screen magnification is given by:-

$$M_{os} = X_s/X_p \quad \ldots\ldots (7)$$

$$= \Delta X_s/\Delta X_p \quad \ldots\ldots (8)$$

Thus substituting in Equation 6:

$$\dot{V}_p = [(V_f/M_{of})\overline{\tan(\theta)}][(V_f/M_{of})\Delta\tan(\theta)]/(\Delta X_s/M_{os}) \quad \ldots\ldots (9)$$

or rearranging:

$$\dot{V}_p = (V_f/M_{of})^2(M_{os}/\Delta X_s)[\overline{\tan(\theta)}\Delta\tan(\theta)] \quad \ldots\ldots (9a)$$

In summary, determination of particle velocity requires

knowledge of the film velocity, the object film magnfication and the streak angle. The particle acceleration requires in addition, the object-screen magnification, a screen distance and change of streak angle over that screen distance.

Film Analysis System

Because of the wide distribution of particle velocities and accelerations, it was necessary to take the average of a reasonably large number of readings of streak angle and of change of angle. An automatic analyser was therefore desirable. However, the 16 mm format and the need to look between frames were incompatible with machines which were already available.

A simple system was therefore built (Fig. 13), using a time and motion projector as the basic component. The film advancing claws were retracted so that the film could run freely through the gate. The film take-off and wind-on spools were mounted on special shafts which could be rotated in either direction by a simple pulley-wheel arrangement fixed to a projection table. A similar system was used to adjust the focussing when necessary.

The image from the projector was directed to the underside of a horizontal viewing screen by means of a large front surface mirror.

The most accurate measurements of angle were carried out by means of a drafting machine equipped with a vernier angular scale. The procedure used was as follows:-

A small front surface mirror was placed vertically above the streak image and rotated (about a vertical axis) until the reflected image of the streak provided a smooth continuation of the image in front of the mirror and the unblocked image behind the mirror. In this way, it

FIGURE 13

Film Analysis System

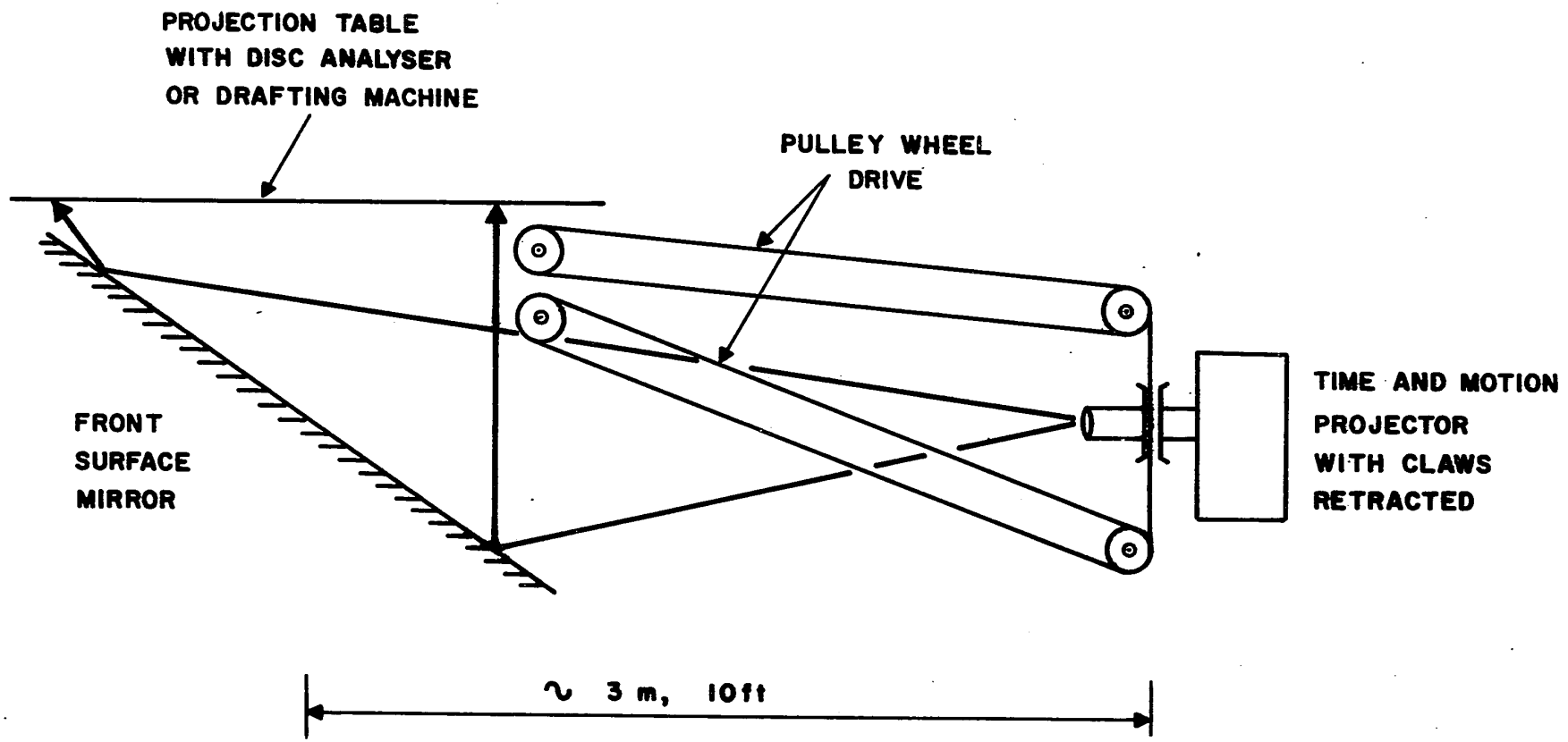
PROJECTION TABLE
WITH DISC ANALYSER
OR DRAFTING MACHINE
PULLEY WHEEL
DRIVE
FRONT
SURFACE
MIRROR
TIME AND MOTION
PROJECTOR
WITH CLAWS
RETRACTED
~ 3 m, 10ft

was found that repeated measurement of the same streak angle gave a standard deviation of less than eight minutes of arc.

For particle acceleration measurements, the streak angle was measured at points one-quarter and three-quarters of the way across the film. At each point, the angle was measured a total of four times, starting with the mirror alternately on either side of its correct position. In this way it was considered that the average reading was reasonably close to the true mean at that point. When any two readings differed by more than twenty minutes of arc, that set of results was discarded and analysis suspended for a short period.

A semi-automatic analyser (Fig. 14), was built and tested and was found to be successful in simple measurement of streak angle. The basis of the device was a rotating plexiglass disc which replaced the regular screen. The disc was rotated until a line marked across the diameter was parallel to the projected streak image. A potentiometer slide-wire wound around one quadrant of the disc was fed from a 200 mV power supply. A voltage tapped off from the wire, was fed to a punched-tape data-logger. Thus on command from the operator, a signal was recorded which was directly proportional to streak angle.

The film-screen magnification required in the data reduction was determined from the ratio of the distance between two marks on the film and the distance between the projected image of the marks on the screen.

Stereo-Streak Device

In the early stages of this work, there was some doubt about the actual distance between the centre of the "cone" of particles

FIGURE 14

Semi-Automatic

Streak Analyser System

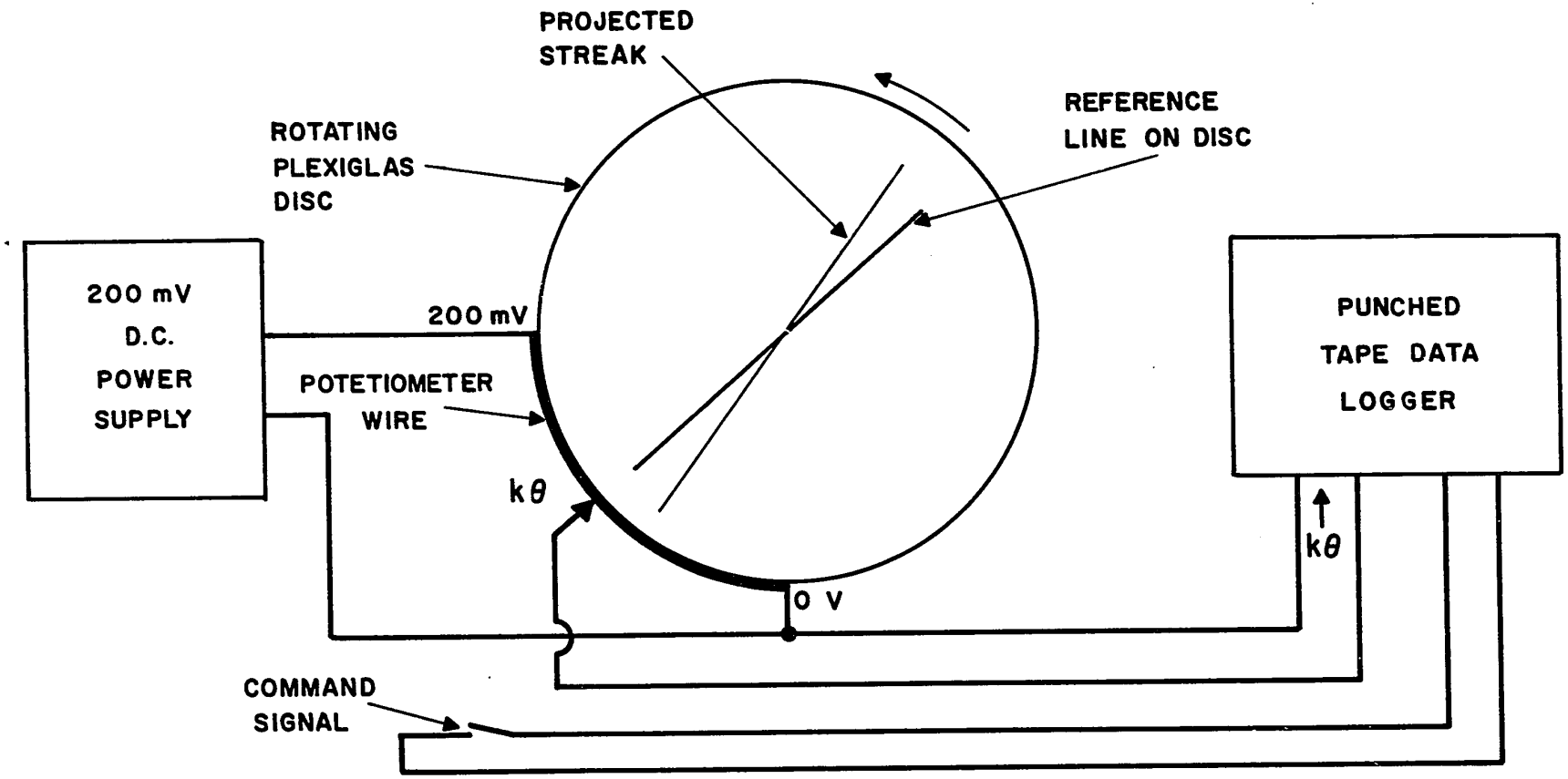
PROJECTED
STREAK
REFERENCE
LINE ON DISC
ROTATING
PLEXIGLAS
DISC
200 mV
D.C.
POWER
SUPPLY
200 mV
POTETIOMETER
WIRE
kθ
0 V
PUNCHED
TAPE DATA
LOGGER
kθ
COMMAND
SIGNAL

emerging from the plasma jet and the film plane. In order to get a positive location of the particles in two dimensions a "stereo-streak" system was devised (Fig. 15), based on the familiar principle of using a beam splitter and two front surface mirrors to combine two views (taken at right angles to each other) into a single image.

In the prototype of the stereo-streak system, the left hand mirror was masked over its top half, and the right hand mirror over its bottom half. As shown in Fig. 16, this allowed a small central overlap of the two images.

During trials of this device, it was found that when either part of the image was out of focus, the other half of the image was absent, because effectively it was not in front of the gate slit. When either half of the streak was in focus, the other half was also seen, but usually not so well in focus. This was attributed to the fact that the optical paths were not exactly equal.

Although the device showed promise, it became redundant due to the depth of field studies mentioned in the next section.

FIGURE 15

General Schematic of Stereo-Streak Device

FIGURE 16

Overlap of Stereo-Streak Images

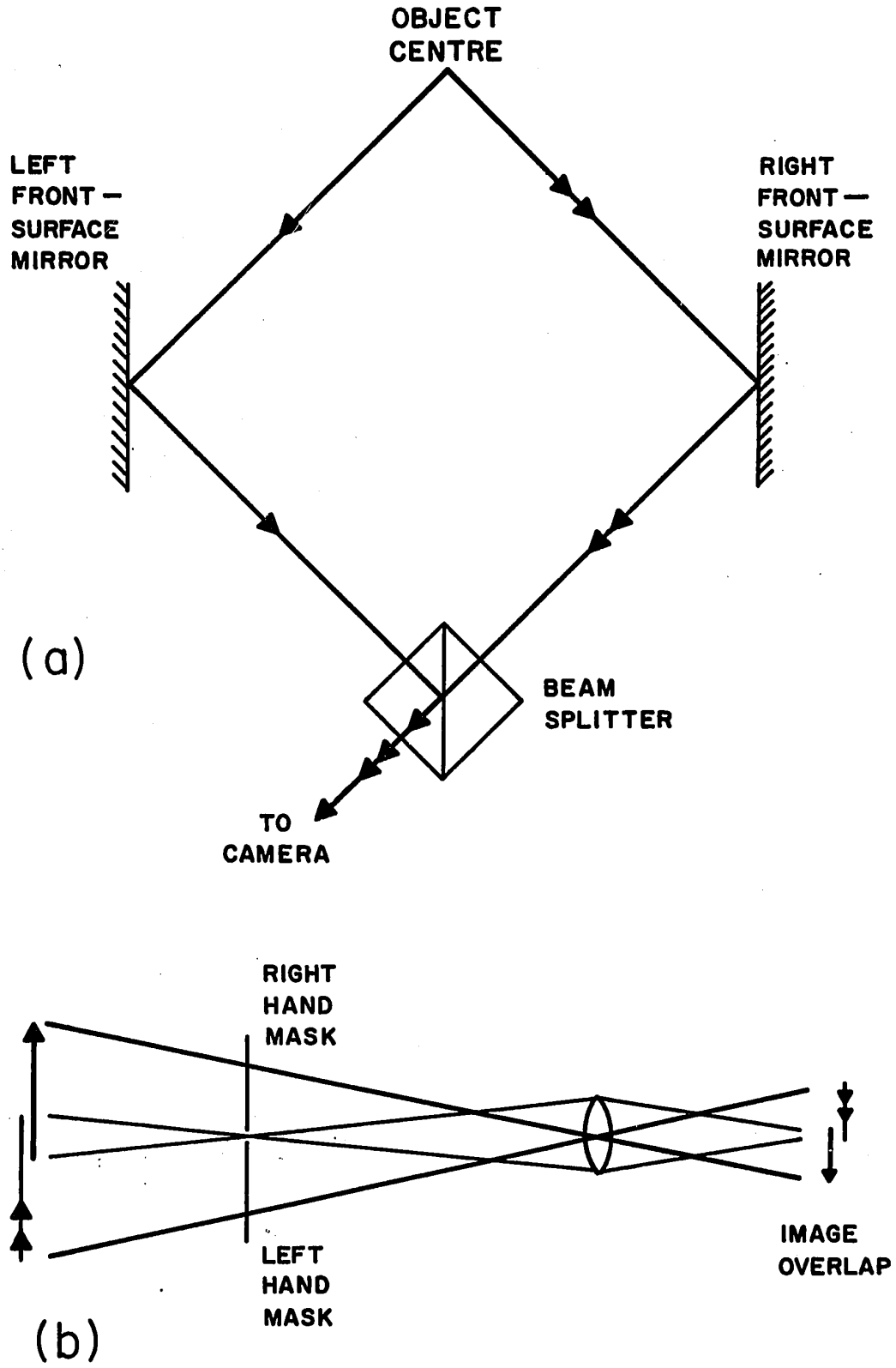
OBJECT
CENTRE
LEFT
FRONT —
SURFACE
MIRROR
RIGHT
FRONT —
SURFACE
MIRROR
(a)
BEAM
SPLITTER
TO
CAMERA
RIGHT
HAND
MASK
LEFT
HAND
MASK
IMAGE
OVERLAP
(b)

SIMULATION STUDIES ON DEPTH OF FIELD

The small size of the particles used in this study, caused considerable focussing difficulties throughout the experimental work. Allowing an overall optical resolution of fifty lines per millimetre in the film plane and a magnification of about 0.2, then the equivalent resolution separation in the object plane would be 100μm, which is the same order of magnitude as the particle diameter.

In order to define the depth of field, the effect of the glass beads was simulated by a disc rotating at 6 000 rpm, having a 50μm hole drilled in its face, while being illuminated from behind by a 650 W tungsten-halide lamp. Using a fixed focus lens setting, the camera was moved in and out of focus in steps of 5 mm (0.2 in), with an exposure of several seconds at each station. Fig. 17, shows the results of these experiments, the projected streak width being plotted against nominal object-film distance. The graph shows that the streak width increased as the deviation from the optimum object-film distance increased. A projected streak width of 3 mm was taken as a reasonable minimum figure, which therefore defined the depth of field as $\pm$ 5 mm.

A further simulation was carried out using the plasma torch particle injection nozzle and glass beads in the range 44-53μm. The nozzle was held vertically downwards and the particles ejected at the same rate as in the formal experiments. Illumination was provided by two 650 W lamps. Careful masking was required to prevent film fogging by scattered light. Again, the camera was traversed through the nominal object film distance. Fig. 18 shows the results plotted in terms of tan(θ) (particle velocity) against distance. It was found that the maximum mean value equivalent to a particle velocity of 10 m/s occurred for an object

FIGURE 17

Definition of Depth

of Field for

Streak Photography

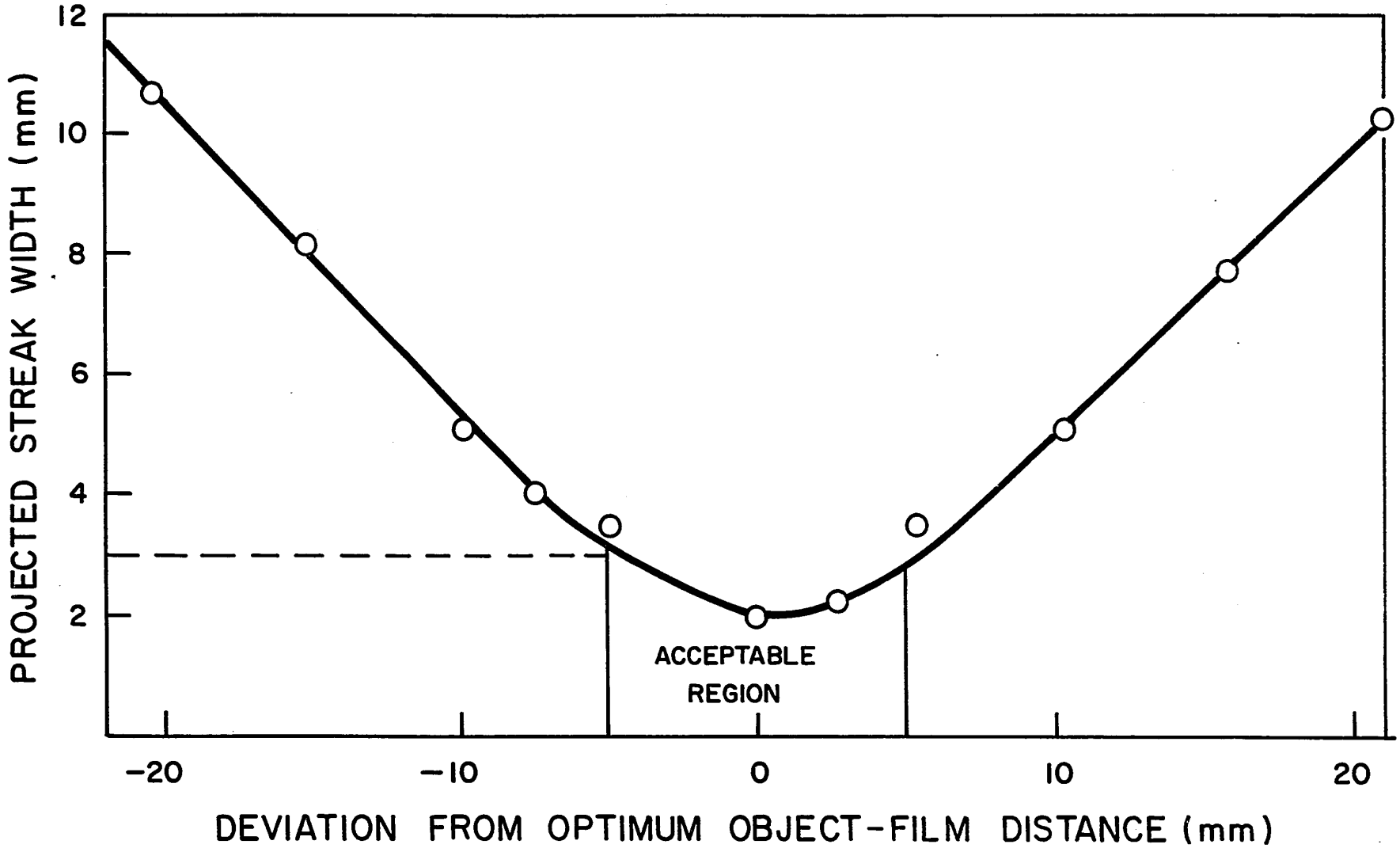
PROJECTED STREAK WIDTH (mm)
12
10
8
6
4
2
ACCEPTABLE
REGION
-20
-10
0
10
20
DEVIATION FROM OPTIMUM OBJECT-FILM DISTANCE (mm)

FIGURE 18

Radial Distribution of Axial Velocity of

Particles Emerging from Plasma Jet

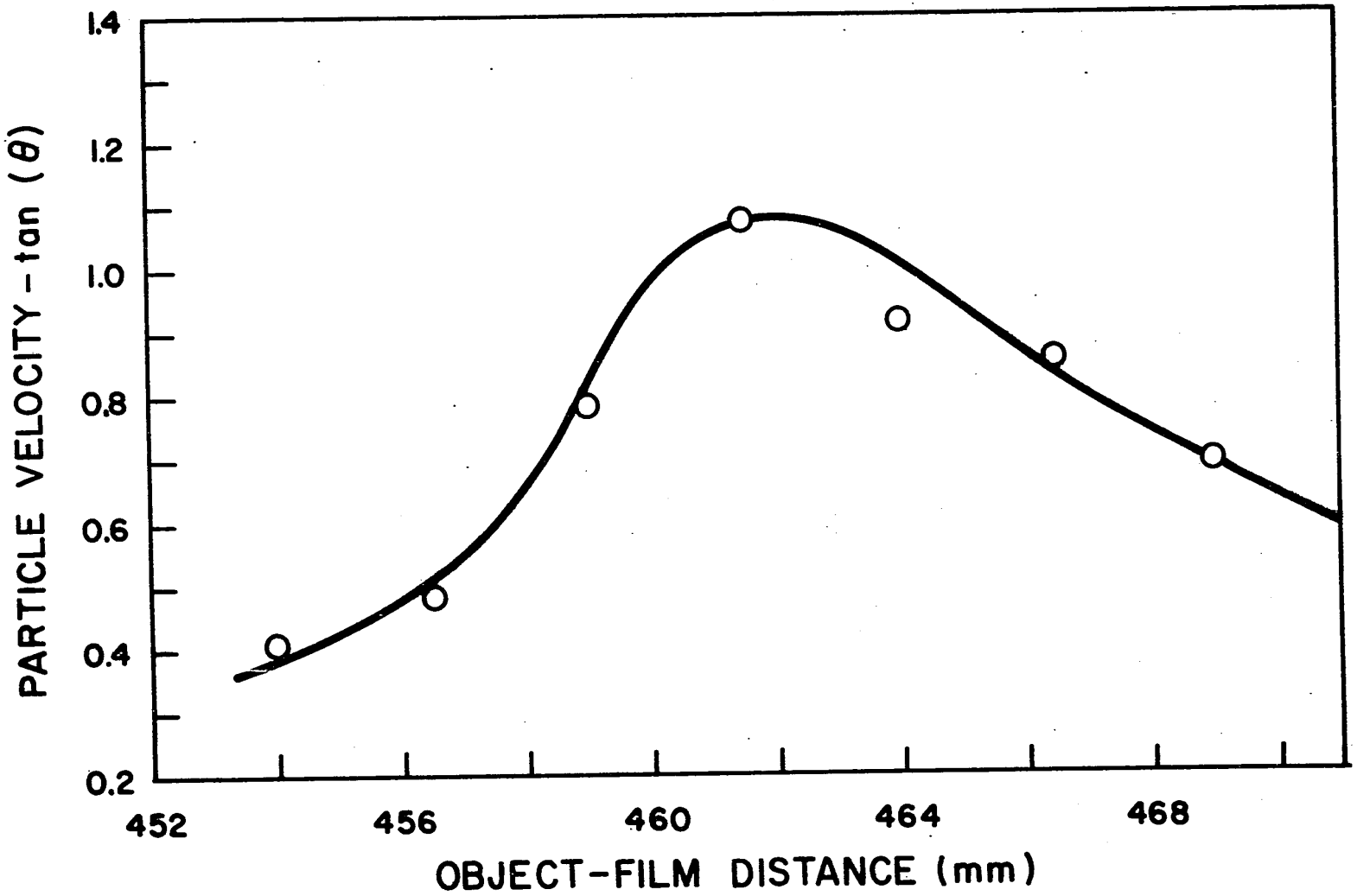
PARTICLE VELOCITY - tan (θ)
1.4
1.2
1.0
0.8
0.6
0.4
0.2
452
456
460
464
468
OBJECT-FILM DISTANCE (mm)

film distance of 462 mm.

Two interesting phenomena were first noted during the course of the simulation experiments using glass beads.

The first point of interest concerned a number of streaks which appeared as a series of dots, rather than as a continuous line. An example is shown in Fig. 19. One explanation of this effect is that surface irregularities of the particles caused the light to be emitted in a preferential direction. Combined with particle rotation, the net result would be seen as periodic flashing. The calculated particle rotation rate was found to be about 3 000 rev/s. This is thought to be a reasonable value, particularly when compared with the results of Nurekenov (5), who obtained rotation rates of about 1 500 rev/s for 100μm coal dust particles in an air cyclone. In both jets and cyclones an intense shear field would be present to cause the particle rotation.

The second phenomenon concerned ghost images. Fig. 20 shows a bright streak extending across the film. (This is a photograph of the real event). Preceding this streak, however, a shorter streak is noticed having the equal, but opposite angle of the full width streak. For this short streak to be a true image, it would be necessary for a particle to move against the jet. The lack of any obvious mechanism for this to happen suggests that the phenomenon was an illusion, rather than a true event. This was proved beyond reasonable doubt by observing a dark background as a piece of white paper was brought close to (but did not enter) the field of view. When the paper was near the edge of the field, a semi-transparent image was seen to approach the edge from the inside of the field. Masking all but the field of view, eliminated this effect completely.

FIGURE 19

Photograph of Actual

Streak

Obtained During Simulation Studies

FIGURE 20

Photograph of Actual

Streak

Obtained During Formal Studies

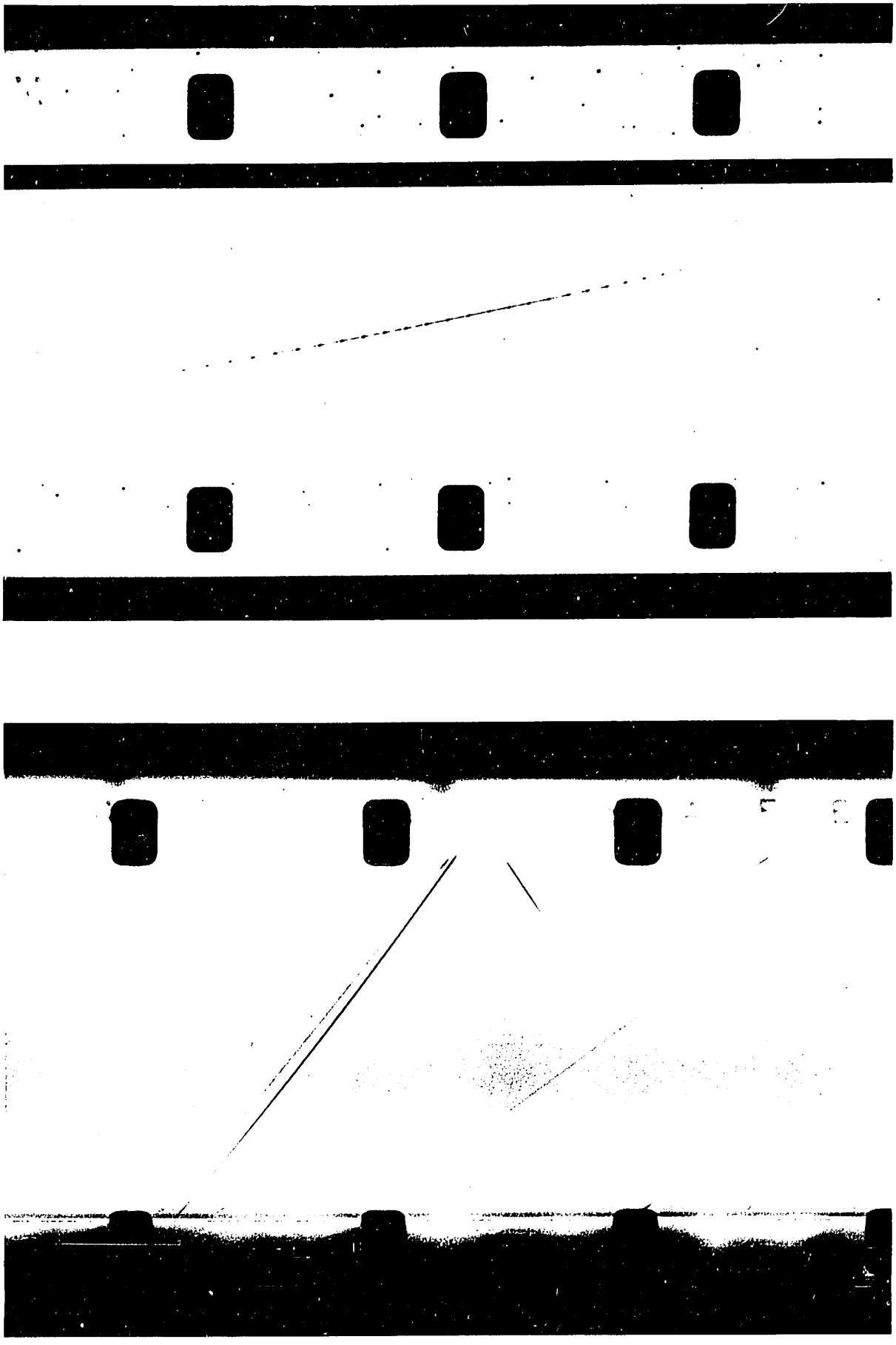

PROCEDURE

The plasma torch was mounted on an inverted tripod with the nozzle pointing vertically downwards (Fig. 21). A cylindrical plug was inserted into the nozzle and a fine steel wire (150μm, 0.006 in diameter) suspended from it. This wire was then used to define the jet axis.

The high-speed camera was mounted on the traversing gear which was fixed to the platform of a standard heavy-duty tripod. The platform had been adjusted to the horizontal plane using a large spirit level. The general arrangement is shown in Fig. 21.

A semi-circular black background was provided behind the plasma torch in order to maximize the contrast with the particles emerging from the flame. The centre panel was of high-quality domestic black velvet with cotton broadcloth on either side. Metal parts intruding into the background were sprayed flat black.

In a typical run, the camera was set at the required distance from the focussing wire and locked in the horizontal direction. The height of the camera was adjusted until the visible flame was just outside the field of view. (In this way, the total distance from the nozzle exit was kept to a minimum.) With the alignment checked to its final position, the camera was loaded with 400 ASA black-and-white reversal film. The focussing wire was then removed and the particle feeder charged with the given size fraction of particles. The plasma torch was then ignited and allowed to come to stable operation. The particle feed was then turned on and the camera started when the feed rate had stabilized. (This was observed by viewing the field below the visible part of the flame, when the particles

FIGURE 21

General Arrangement for Streak Photography

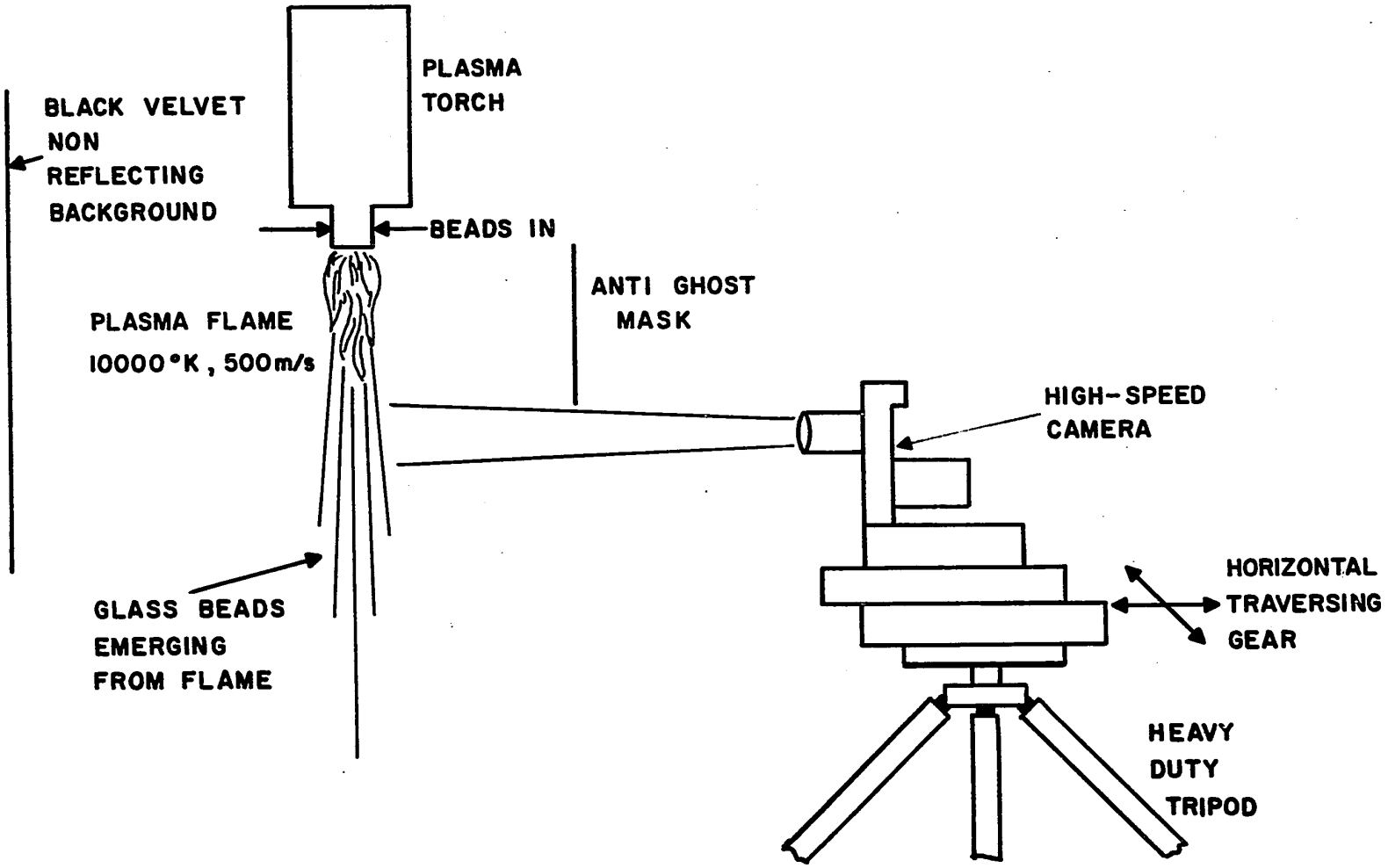
PLASMA
TORCH
BLACK VELVET
NON
REFLECTING
BACKGROUND
BEADS IN
ANTI GHOST
MASK
PLASMA FLAME
10000°K, 500m/s
HIGH-SPEED
CAMERA
GLASS BEADS
EMERGING
FROM FLAME
HORIZONTAL
TRAVERSING
GEAR
HEAVY
DUTY
TRIPOD

in the central region of the jet were seen as red streaks.) The exposed film was removed from the camera and processed in a commercial laboratory under regular conditions.

RESULTS

During the initial recording of the real events, it was found that the number density of streaks on each film was consistently lower than expected. Increasing the object film distance by 5 mm resulted in many more particles being photographed. Careful examination of the particle discharge pattern showed that the particles appeared to exit from the visible flame in two overlapping cones, with about 10-15 mm separation of the cone axes. This could be expected to result from the use of two injection nozzles.

The results of the main experiments are shown in Figs. 22, 23 and 24.

Mean Velocities

In each size range, the mean velocity of one hundred streaks having a projected streak width less than 3 mm was calculated. It is noted in Fig. 22, that the general trend was a decrease in the particle velocity as the particle diameter was increased.

Histograms of Particle Velocities

The four largest particle size ranges showed a distribution of velocities, which could be suitably described by a Gaussian fit. The 30-44μm glass beads showed a skewed distribution. This may have been partially due to imperfect sieving of the particles or possibly to a bias in the analysis due to the resolution problems previously mentioned.

Particle Deceleration

Fig. 24 shows the remarkably high deceleration rates of the particles, which were around 4 000 g. In relation to the size of the

FIGURE 22

Axial Velocity of Particles
at 178 mm from Torch Nozzle Exit
As a Function of Particle Diameter

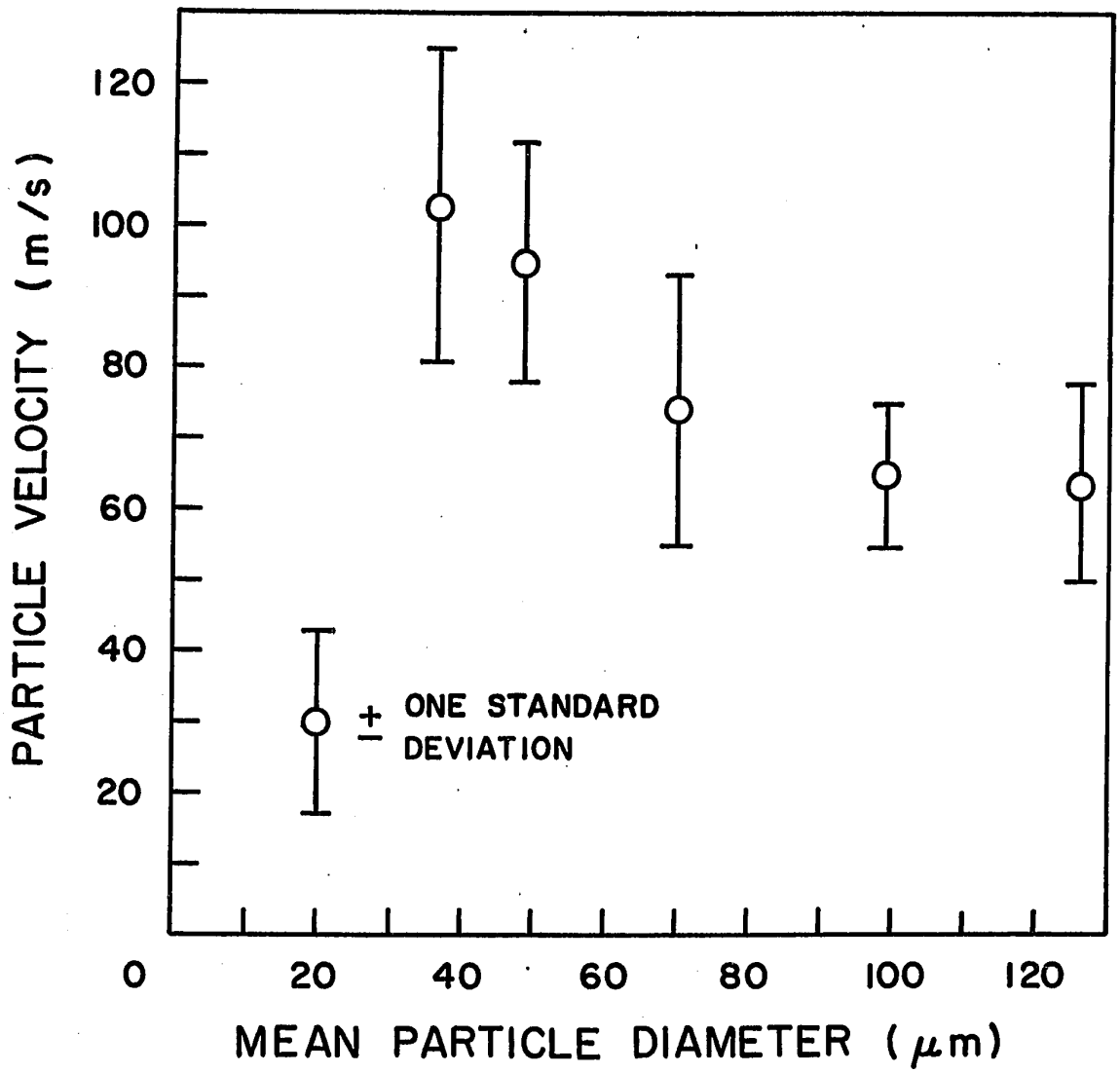
PARTICLE VELOCITY (m/s)
120
100
80
60
40
20
0
20
40
60
80
100
120
MEAN PARTICLE DIAMETER (μm)
± ONE STANDARD DEVIATION

FIGURE 23

Histograms of

Particle Velocities

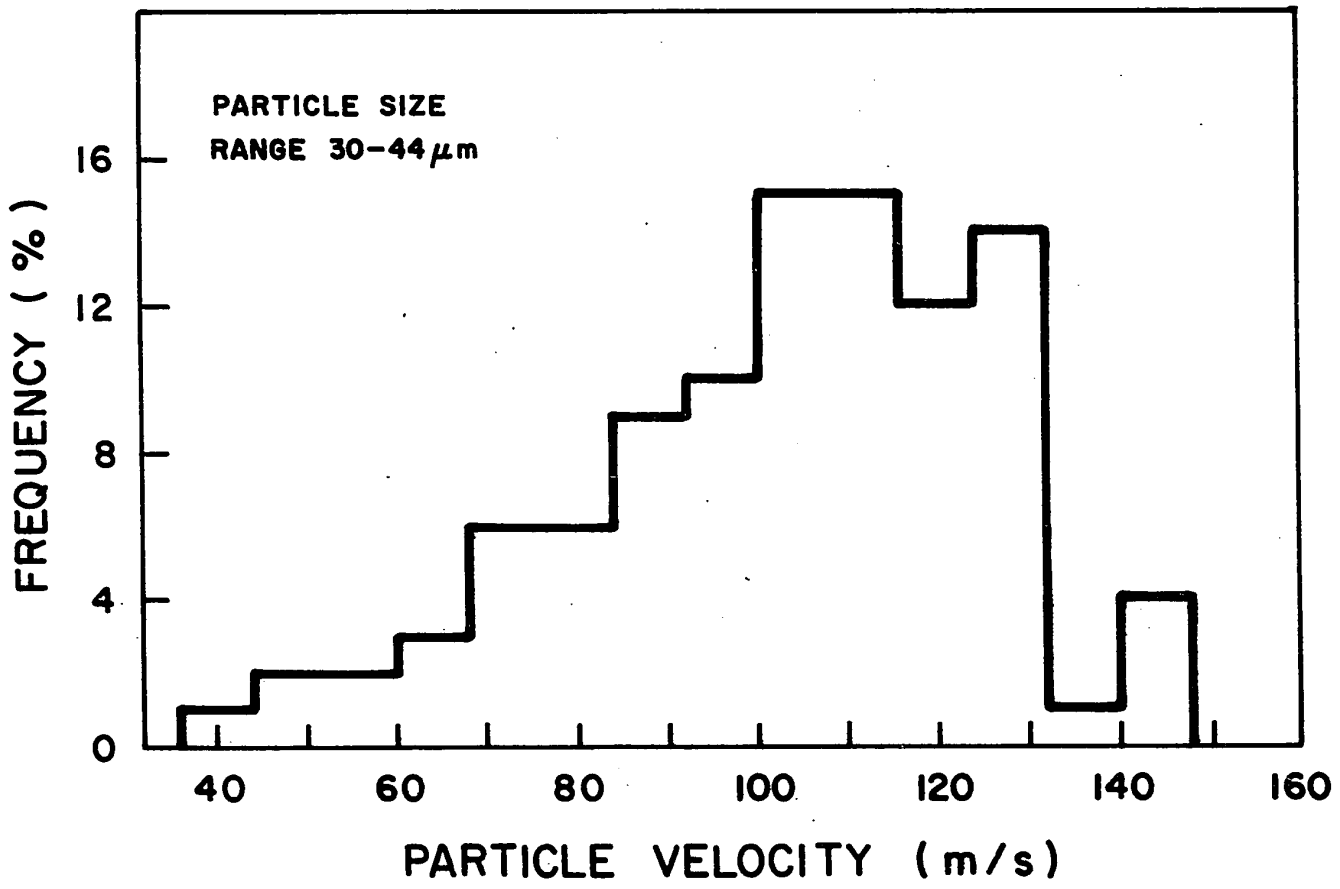
PARTICLE SIZE
RANGE 30-44 μm
FREQUENCY (%)
0
4
8
12
16
40
60
80
100
120
140
160
PARTICLE VELOCITY (m/s)

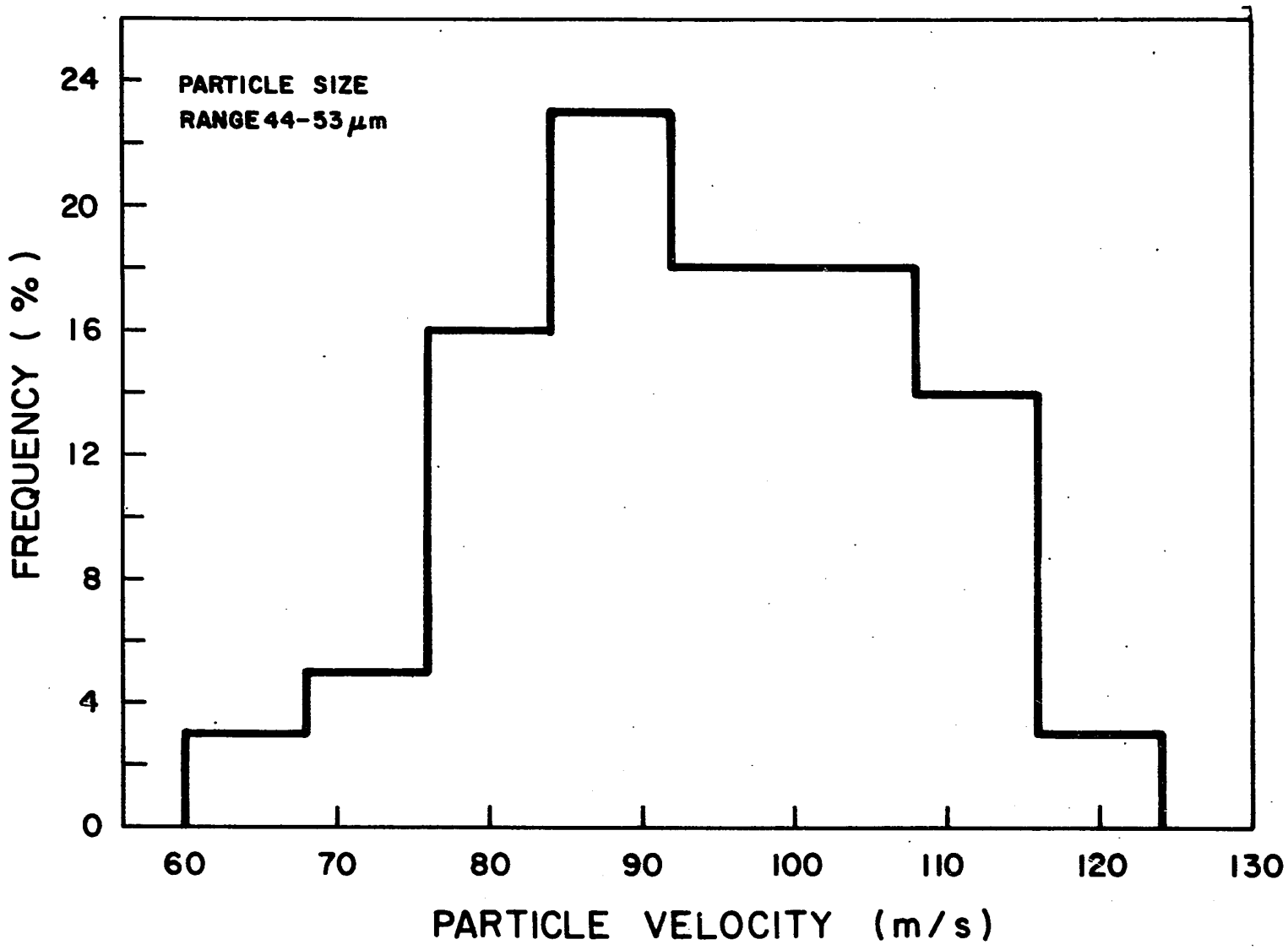
PARTICLE SIZE
RANGE 44-53 μm
FREQUENCY (%)
0
4
8
12
16
20
24
60
70
80
90
100
110
120
130
PARTICLE VELOCITY (m/s)

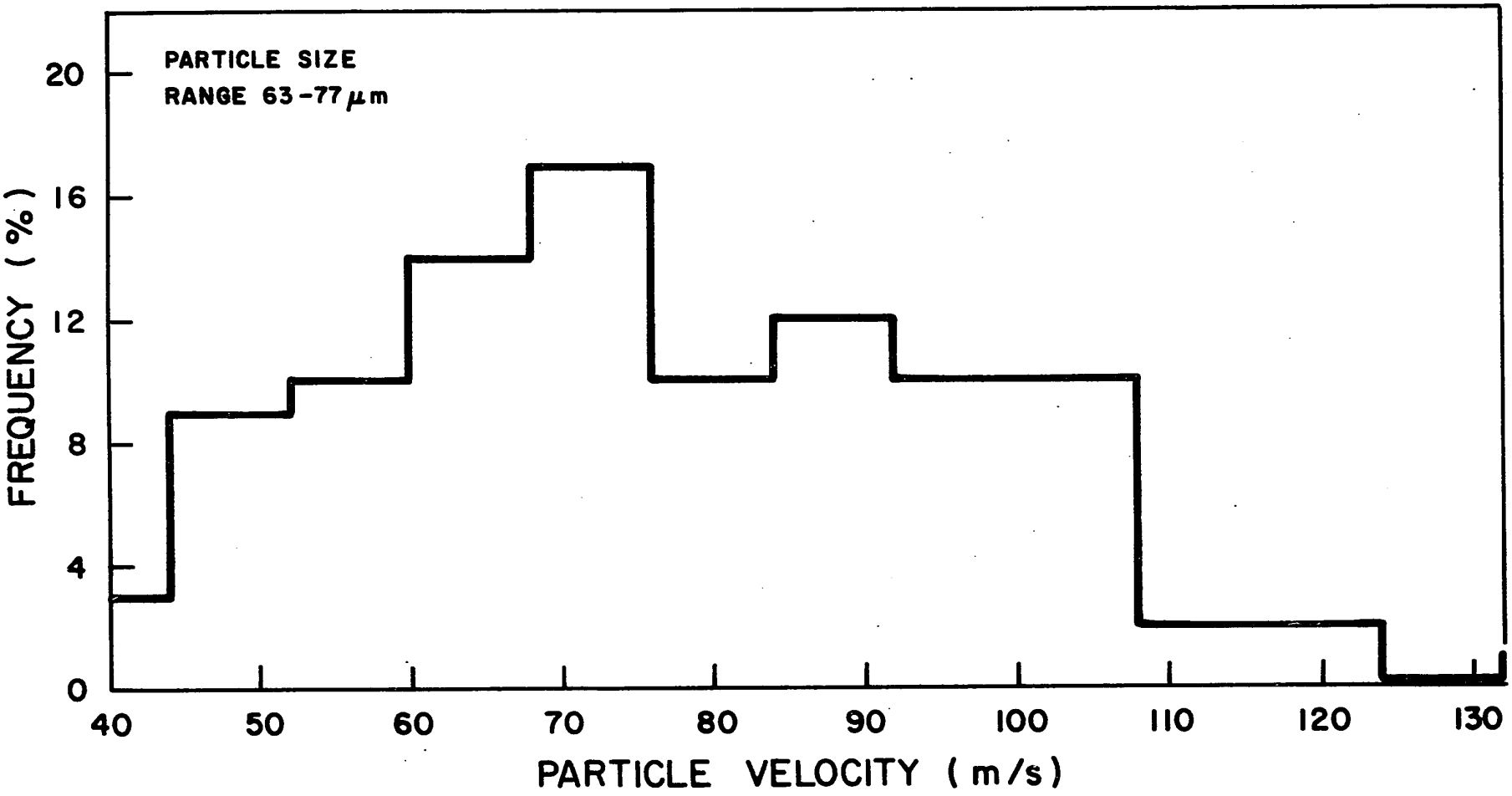
PARTICLE SIZE
RANGE 63-77 μm
FREQUENCY (%)
0
4
8
12
16
20
40
50
60
70
80
90
100
110
120
130
PARTICLE VELOCITY (m/s)

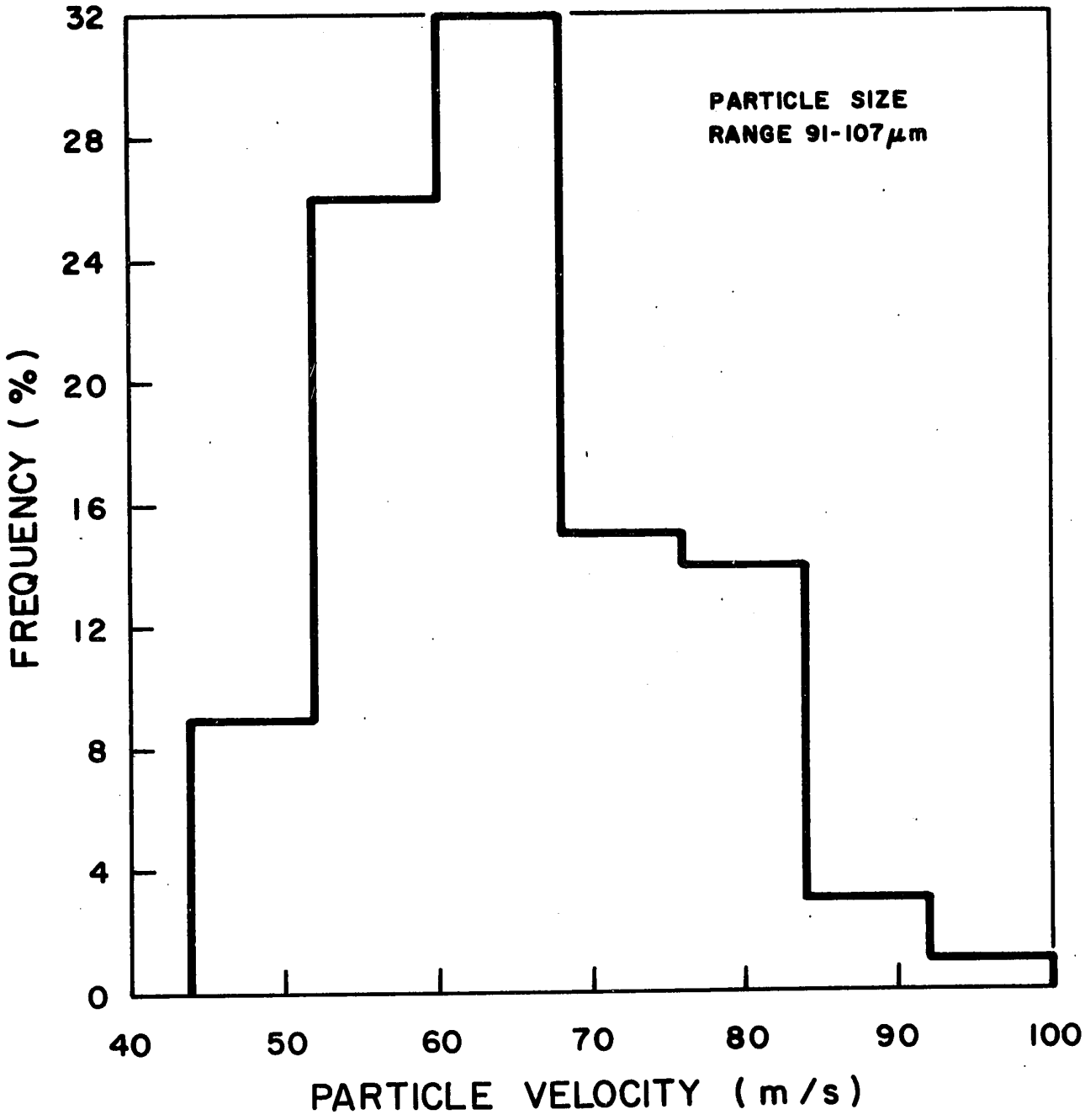
PARTICLE SIZE
RANGE 91-107μm
FREQUENCY (%)
0
4
8
12
16
20
24
28
32
40
50
60
70
80
90
100
PARTICLE VELOCITY (m/s)

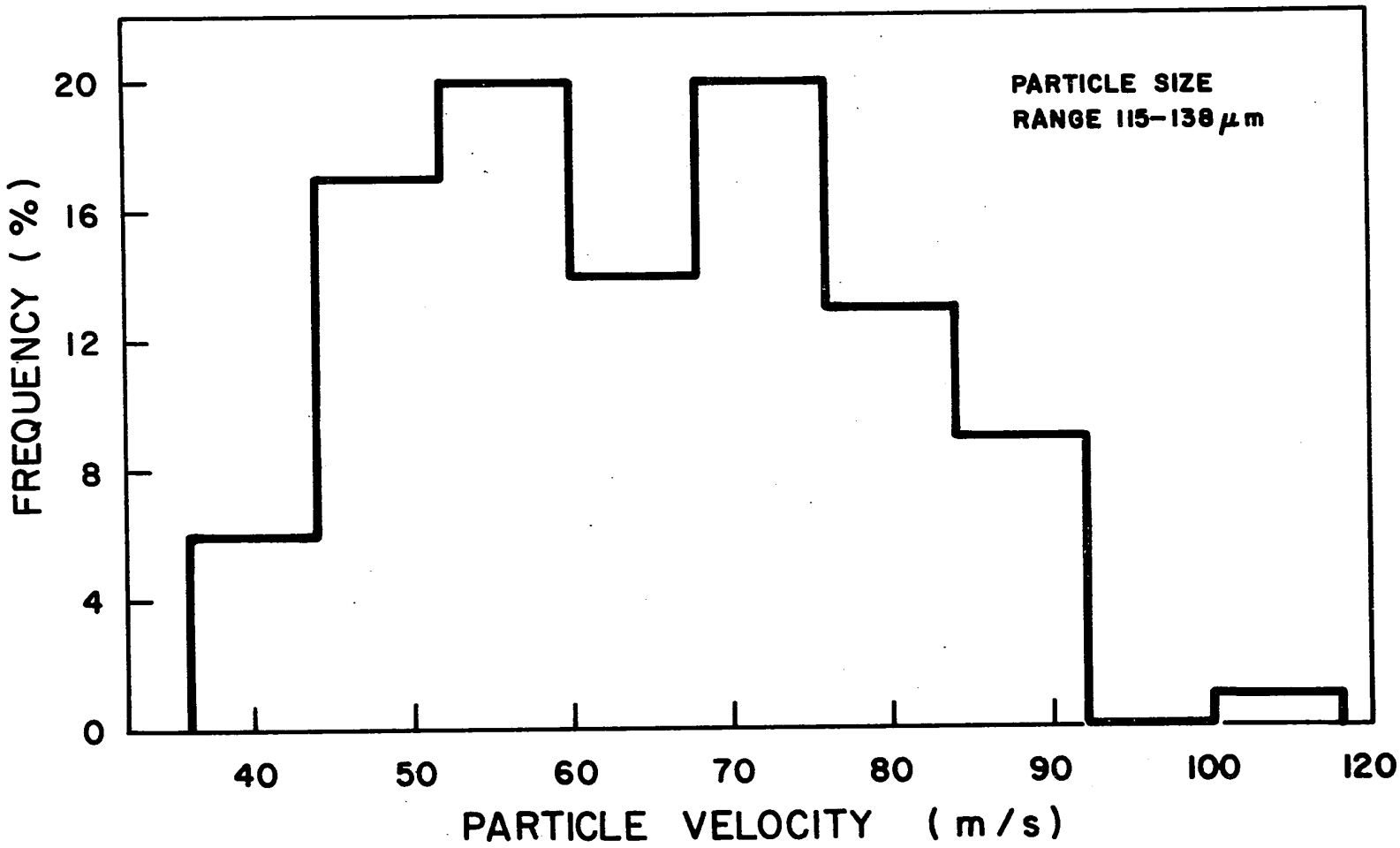
PARTICLE SIZE
RANGE 115–138 μm
FREQUENCY (%)
0
4
8
12
16
20
40
50
60
70
80
90
100
120
PARTICLE VELOCITY (m / s)

FIGURE 24

Variation of Particle Deceleration with Particle Velocity

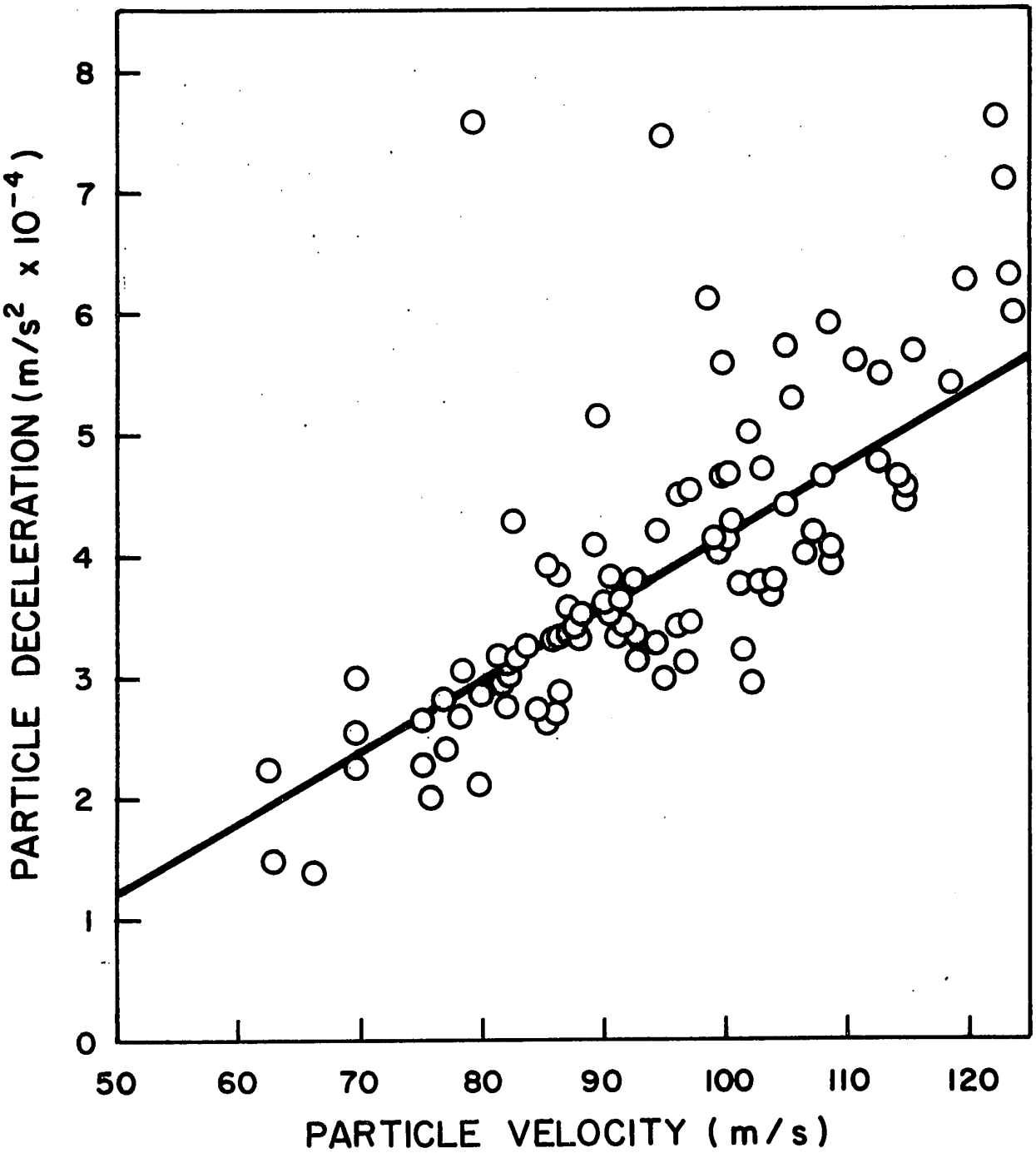
PARTICLE DECELERATION (m/s² x 10⁻⁴)
0
1
2
3
4
5
6
7
8
50
60
70
80
90
100
110
120
PARTICLE VELOCITY (m/s)

particles and their relative velocities, this figure is not at all unusual.

The acceleration modulus N_{AM} is a useful criterion for judging whether (fluid-dynamically) the deceleration is high or low:-

$$N_{AM} = (\dot{V}_p D_p)/(V_R^2) \quad \ldots\ldots (10)$$

$$\simeq 4 \times 10^4 \times 50 \times 10^{-6} \times 10^{-4}$$

$$\simeq 2 \times 10^{-4}$$

As discussed by Wang (6) and Marchildon (7), a value greater than unity is considered high. The results of this work are therefore a case of a low comparative deceleration.

A linear regression analysis of the data in Fig. 24 gave the following result:-

$$-\dot{V}_p = (-1.73 \pm 0.82)(10^4) + (5.85 \pm 0.87)(10^2)V_p \quad \ldots\ldots (11)$$

The correlation coefficient of this fit was 0.65. In other words, 55% of the total variance in the deceleration of the particles was due to random deviations and 45% due to the straight-line fit.

Streak Brightness

The above results could have been summed up as saying "the steeper streaks had a greater curvature". In fact this was one of the first reactions to that particular film. A further impression was that the steeper (faster) streaks were brighter than the slower streaks. This was confirmed in a test in which each streak in a group of one hundred was assigned a brightness value ranging from unity for the dimmest to

five for the brightest. The results of groups 1 and 3 are shown below:-

Brightness Level	Number of Observations	Mean Velocity (m/s)	Standard Deviation (m/s)
1	22	53.6	6.0
3	42	63.5	9.1

The standard "t" test showed that there was a significant difference in the velocities of the two groups at the 99% level. In other words, the faster particles were brighter (and thus hotter).

DISCUSSION OF ERRORS

(i) Film Velocity (V_f)

The film velocity was measured from the distance between timing marks on the film and the time interval between each mark, determined by use of a pulse counter. The error in both cases was estimated to be much less than one percent and was therefore neglected.

(ii) Object Film Magnification

The object film magnification was measured from the actual separation of two marks on the film and their equivalent separation measured against a scale in the object plane. The latter dimension was estimated to have a possible systematic error of about 0.5 mm in 50 mm or one percent. A random error of about the same magnitude was considered due to the effect of a finite depth on the object-lens distance.

(iii) Streak Angle [tan(θ)]

In order to check the reproducibility of angle measurements, ten estimations of the same angle were made, giving a standard deviation of less than eight minutes of arc, which would result in an error of about 0.5%.

(iv) Change of Angle [$\Delta\tan(\theta)$]

Allowing a total error of sixteen minutes of arc for an average change of angle of two degrees, the random error in $\Delta\theta$ [and hence $\Delta \tan(\theta)$] was estimated as 13%.

(v) Object Screen Magnification

Due to the uncertainty in the object size, the error in the object screen magnification was estimated at about 1%.

(vi) Improper Alignment Between Streak and Film

A particle which approached the camera along the axis of the lens would be recorded as having zero velocity in the direction of interest. In the analysis, it was assumed that particles moved parallel to the effective film plane (allowing for the right angle change of direction due to the prism). The possibility of recording only a component of the total particle velocity is considered against the following evidence:-

a) Computer predictions suggested a ratio of particle radial velocity to particle axial velocity of about 3%.

b) Observation of the event through the camera showed the particles moving parallel to the length of the slit.

c) The streak length width ratio was about 20 and only those streaks which traversed the whole film were accepted.

(vii) Film Acceleration

The maximum error introduced by the film acceleration was 0.1%. This error was calculated for the case of maximum film acceleration (i.e. without speed control).

Table I shows a summary of the above information on measurement errors.

TABLE I

Summary of Random and Systematic Errors in Measurement of Particle Velocity and Acceleration

Variable	Random Error %	Systematic Error %
V_f	nil	nil
M_{of}	1	1
$\tan(\theta)$	0.5	3
$\Delta\tan(\theta)$	13	3
M_{os}	1	1
ΔX_s	nil	nil

Using a simplified analysis the maximum expected overall errors would be:-

Velocity

$$V_p = (V_f/M_{of})\tan(\theta)$$

Random Error $= (0 + 1) + (0.5) = \underline{1.5\%}$

Systematic Error $= (0 + 1) + (3) = \underline{4\%}$

Acceleration

$$\dot{V}_p = [(V_f/M_{of})^2(M_{os}/\Delta X_s)][\tan(\theta)\Delta\tan(\theta)]$$

Random Error $= 2(0 + 1) + (1 + 0) + (0.5 + 13) = \underline{16.5\%}$

Systematic Error $= 2(0 + 1) + (1 + 0) + (3 + 3) = \underline{9\%}$

CONCLUSIONS

(i) The working depth of field was $\pm$ 5 mm about the optimum object film distance of 462 mm.

(ii) The glass beads in the jet shear field appeared to be rotating at rates around 3 000 rev/s.

(iii) The injection of particles from two diametrically opposed nozzles into the flame, resulted in two narrow cones of particles, with axial separation of 10-15 mm.

(iv) The mean velocity of particles emerging from the plasma jet decreased from 103 m/s for the 37μm size group to 64 m/s for 127μm size group.

(v) Except for the smallest size range, the distribution of velocities was symmetrical and approximately Gaussian.

(vi) Particle deceleration rates were around 4 000 g but were equivalent to a low acceleration modulus. A least squares linear fit of the deceleration-velocity data was obtained:-

$$-\dot{V}_p = (-1.73 \pm 0.82)(10^4) + (5.85 \pm 0.87)(10^2)V_p \quad \ldots\ldots\ldots (11)$$

($\dot{V}_p$ in metres/second^2, V_p in metres/second)

The correlation coefficient was 0.65.

(vii) Streaks arranged according to levels of their brightness showed statistically different mean velocities (99% level), with the implication that particles with high velocity were hotter than particles with a lower velocity.

(viii) The estimated maximum errors in particle acceleration and velocity were

	Random Error %	Systematic Error %
V_p	1.5	4
$\dot{V}_p$	16.5	9

NOMENCLATURE

D_p	Particle diameter	L
M_{of}	Object-film magnification	-
M_{os}	Object-screen magnification	-
N_{AM}	Acceleration modulus	-
t	Transit time in object plane	T
X_i	Distance in Image Plane	L
X_p	Distance in Object Plane	L
X_s	Distance in Screen Plane	L
V_f	Film velocity	$L\ T^{-1}$
V_i	Particle image velocity	$L\ T^{-1}$
V_p	Actual particle velocity	$L\ T^{-1}$
$\dot{V}_p$	Actual particle acceleration	$L\ T^{-2}$
V_R	Relative velocity	$L\ T^{-1}$
θ	Angle between negative of film velocity and particle image velocity	-

BIBLIOGRAPHY

1. Vursel, F.B., and Polak, L.S., Ind. Eng. Chem. 62, 8 (1970).
2. Dundas, P.H., and Thorpe, M.L., Chem. Eng. Prog. 66, 66 (1970).
3. Humphrey's Corporation (TAFA div) Bow, N.H., Direct Communication (19.VII.71).
4. Lemoine, A., and LeGoff, P., Rev. Gen. Thermique, Jan., 33 (1969); also Lemoine, A., Docteur Ingenieur Thesis, Université de Nancy, France (1969).
5. Hamielec, A.E., Hoffman, T.W., and Ross, L.L., A.I.Ch.E.J. 13, 212 (1967).
6. Nurekenov, E., Problemy Teploenergetiki Prikladnoi Teplofizika VYP-1, 270 (1964).
7. Wang, C.C., M. Eng. Thesis, McGill University, Montreal (1969).
8. Marchildon, K., Ph.D. Thesis, McGill University, Montreal (1965).

PART III

THE MOTION OF

PARTICLES ENTRAINED IN A PLASMA JET

INTRODUCTION

Plasma discharge devices operating at pressures of one atmosphere are now being used on an industrial basis as convenient sources of heat in high temperature reactors. The use of plasmas allows reliable continuous generation of gas temperatures in excess of 10 000°K, with only minor restrictions on the composition of the gas. Industrial exploitation of such high energy levels is now being centered on chemical-metallurgical processes, using multi-particle systems. A specific example of a commerically successful process is the dissociation of zircon sands into zirconia and silica (1). Titanium dioxide has for several years been manufactured by the combustion of titanium tetrachloride in an atmosphere of oxygen heated by a radio-frequency (4 MHz) discharge device (2).

The design of these plasma reactors requires a proper understanding of the transport processes and the reaction kinetics of high temperature multi-particle systems. This section of the thesis is concerned with the study of plasma-particulate momentum transfer, having the overall aim of permitting the prediction of particle residence times. Specifically, this work reports on a comparison between the prediction and experimental measurement of the velocity and deceleration of particles emerging from a plasma flame. The size range of particles used (30-140μm) was chosen to be compatible with commercial practice.

From a fluid-dynamics point of view, a particle entrained in a plasma jet is in an unusual regime:

(i) The particle Reynolds number (0.2 - 20) is between Stokesian (Re < 0.1) and boundary layer (Re > 400) ranges).

(ii) The flow field around the particle is highly non-isothermal with possible temperature ratios as high as 10 between free-stream and particle surface.

(iii) The flow field around the particle departs markedly from its steady-state configuration due to the rapidly changing relative velocity between particle and gas and therefore can cause significant changes in the particle drag coefficient.

(iv) The small diameters of the particles used results in Knudsen numbers which approach the slip and non-continuum ranges.

The basic equation for the drag force on a spherical particle at steady state in an isothermal system may be written:

$$F_D = (-1/2)(C_D)(\rho_g)(\pi D_p^2/4)|V_p - V_g|(V_p - V_g) \quad \ldots\ldots\ldots\ldots\ldots (1)$$

Steady-state isothermal determinations of drag coefficient (C_D) were carried out by Beard and Pruppacher (3) in the range of interest for this study and were confirmed by the numerical computations of Hamielec et al. (4). The results were correlated as follows:-

$$Re < 0.2 \qquad C_D = (24/Re) \quad \ldots\ldots\ldots\ldots\ldots\ldots (2a)$$

$$0.2 \leqslant Re \leqslant 2 \qquad C_D = (24/Re)[1 + 0.1(Re)^{0.99}] \quad \ldots\ldots\ldots (2b)$$

$$2 \leqslant Re \leqslant 21 \qquad C_D = (24/Re)[1 + 0.11(Re)^{0.81}] \quad \ldots\ldots\ldots (2c)$$

$$21 \leqslant Re \leqslant 200 \qquad C_D = (24/Re)[1 + 0.189(Re)^{0.632}] \quad \ldots\ldots\ldots (2d)$$

These results fall a few percent above the standard drag curve (5), but in view of the agreement between computation and experiments, the Beard and Pruppacher results are considered to be the most reliable data available.

Rewriting equation (1) in the form:-

$$F_D = K(\rho_g C_D) \quad \text{.......... (3)}$$

where:-

$$K = (-1/2)(\pi D_p/4)\,|V_p - V_g|\,(V_p - V_g) \quad \text{.......... (4)}$$

it is seen that both the terms inside the bracket of equation (3) are functions of temperature, while K is independent of it. Any discussion of the effect of temperature on particle motion should therefore consider the product of the density and drag coefficient.

Lemoine and LeGoff (6), have stated that the product $(\rho_g C_D)$ is practically independent of temperature and therefore for any given relative velocity, the gas temperature is unimportant in determining particle acceleration. Their statement is valid for different <u>isothermal</u> systems, but reveals nothing of the effect of temperature <u>differences</u> between particle surface and free-stream.

Kassoy <u>et al</u>. (7) carried out numerical computations in the Stokesian regime and obtained a drag coefficient correction factor based on the free-stream properties of the gas. Their results may be approximated by the linear relationship:

$$(C_D)_{ni} = (C_D)_{iso}(1 + 0.55\tau) \quad \text{.......... (5)}$$

where τ is the non-dimensional particle temperature. Thus for τ having a value of unity, equation (3) would become:

$$F_D = (1.55)K[(\rho_g)_\infty(C_D)_\infty] \quad \text{.......... (6)}$$

On the other hand, if the mean-film temperature is used for the

evaluation of ρ_g and C_D, equation (3) can be written:

$$F_D = K[(\rho_g)_{av}(C_D)_{av}] \quad \ldots\ldots\ldots\ldots\ldots\ldots\ldots\ldots\ldots\ldots (7)$$

Equations (6) and (7) would be compatible if the ratio:

$$[(\rho_g)_{av}(C_D)_{av}]/[(\rho_g)_\infty(C_D)_\infty]$$

had the value of 1.55 for $\tau = 1$.

This ratio was evaluated for nitrogen, using a particle temperature of 600°K and a free stream temperature of 300°K. The result of 1.34 showed that there was a significant difference between the Kassoy and the mean film temperature approaches. However, by analogy with the heat transfer where correction factors of the following type are used (8):

$$(Nu)_{ni}/(Nu)_{av} = (\nu_{av}/\nu_\infty)^{0.15} \quad \ldots\ldots\ldots\ldots\ldots\ldots\ldots\ldots\ldots\ldots (8)$$

the following correction was used to match the two approaches:

$$(C_D)_{ni}/(C_D)_{av} = (\nu_{av}/\nu_\infty)^n \quad \ldots\ldots\ldots\ldots\ldots\ldots\ldots\ldots\ldots\ldots (9)$$

$$(C_D)_{ni}/(C_D)_{av} = (1.55/1.34)$$

$$= 1.16$$

$$(\nu_{av}/\nu_\infty) = (238/178)(1152/784)$$

$$= 1.96$$

$$n = \log(1.16)/\log(1.96)$$

$$= \underline{0.21}$$

Calculations performed by Hamielec (9) suggested that only a

small correction to the film temperature drag coefficient would be required at a Reynolds number of about 10. (Hamielec also found that natural convection effects would not be expected to have a significant effect for particles of 50μm diameter.)

A kinematic viscosity ratio correction factor to the mean film temperature drag coefficient would therefore appear to be a reasonable approximation for the effect of the non-isothermal flow-field around a particle at low Reynolds numbers.

In a system where the motion is non-steady (i.e. the relative acceleration is non-zero), the flowfield around a particle must adapt to the changing relative velocity. As in all real systems there is a relaxation time required for this change to take place. Thus any determination of drag coefficient made within this flowfield relaxation time would give a result which would be the sum of a transient and steady-state response. In conventional systems, time scales ($\sim$1 sec) are much longer than relaxation times ($\sim$1 ms) and therefore a transient response is not observed. However, residence times in plasma flames are of the order of one millisecond and the transient response must therefore be taken into account when considering particle motion.

The full equation of motion for creeping flow (low Re) as given by Hinze (10) (and known as the Basset-Boussinesq-Oseen equation) is:

$$(\pi/6)(D_p)^3(\rho_p)(dV_p/dt)$$

$$= -3\pi(\mu_g)(D_p)(V_p - V_g)$$

$$+ (\pi/6)(D_p)^3(\rho_g)(dV_g/dt)$$

$$- (1/2)(\pi/6)(D_p)^3(\rho_g)(dV_p/dt - dV_g/dt)$$

$$- (3/2)(D_p)^2(\pi\mu_g\rho_g)^{1/2}\int_{t_o}^{t}\left[(dV_p/dt' - dV_g/dt')(t - t')^{-1/2}\right]dt'$$

$$+ F_e \qquad \ldots\ldots\ldots\ldots\ldots\ldots\ldots\ldots\ldots\ldots\ldots\ldots\ldots\ldots\ldots\ldots\ldots\ldots\ldots\ldots\ldots\ldots \quad (10)$$

or in a summary form:

$$F_p = F_D + F_{pg} + F_{AM} + F_H + F_e \qquad \ldots\ldots\ldots\ldots\ldots\ldots\ldots\ldots \quad (11)$$

Proceeding from left to right, the terms are:

(i) The particle mass-acceleration product.

(ii) The conventional Stokesian drag.

(iii) The drag due to the pressure gradient.

(iv) The drag due to the so-called added mass.

(v) The Basset history term (effectively the transient response mentioned above).

(vi) External potential forces (gravitational, electric, magnetic, etc.).

In a plasma jet, the gas density is very low compared to the density of the particles and therefore the pressure gradient and added mass terms may be neglected.

Further, the plasma jet is electrically field free and therefore

there should be no electrical forces on the particles even if they had some charge on them. In addition, gravitational effects are of the order of 0.1 percent of the steady-state drag. The equation of motion would therefore reduce to:

$$F_p = F_D + F_H \quad \ldots\ldots\ldots\ldots\ldots\ldots\ldots\ldots\ldots\ldots\ldots\ldots \quad (12)$$

Equation (12) applies for Stokesian motion. On a strict mathematical basis, the equation is only valid for a Reynolds number tending to zero. Odar and Hamilton (11) investigated the motion of a sphere oscillating in oil at Reynolds numbers up to 62. They claimed that their data could be well represented by using a drag force calculated from the standard drag curve, together with added mass and history terms. However coefficients in front of these terms were required. They found that these coefficients appeared to be independent of the Reynolds number but were a function of the reciprocal of the acceleration modulus N_{AM}. An asymtotic value of the history coefficient of 0.48 was suggested for low N_{AM}. From the point of view of the present study, their findings should be viewed with some caution, for the following reasons:

(i) The oil bath used in the experiments was limited in size and in addition the test sphere was supported on probes in line with the direction of motion. Both these effects could have distorted the flowfield to some extent.

(ii) The actual data were reported for a narrow range of N_{AM}, from 0.3 to 3.

(iii) Rimon and Cheng (12) reported a small but definite relation between Reynolds number and calculated relaxation time.

(iv) Interaction between the history and non-isothermal effects in the present study could cause a further possible perturbation of the flowfield.

Turbulence plays a dramatic rôle in particle dynamics by its ability to cause a sharp drop in the particle drag coefficient (13). This phenomenon occurs as a result of the transition of the laminar boundary layer around a sphere to a turbulent boundary layer. However, in a plasma-particulate system, the small particle diameters ($\sim$50μm) and the high kinematic viscosities result in low Reynolds numbers ($Re < 20$), even though the relative velocities are high ($\sim$100 m/s). As a result, the defects in the flowfield due to viscosity extend far beyond "a thin layer close to the surface of the particle". It is therefore improper to talk of the existence of a Prandtl-type boundary layer at low Reynolds numbers. Therefore if a boundary layer does not exist under the conditions of interest, there is no meaning in the expression "boundary layer transition".

As a result of the difficulty of applying experimental techniques, very little of a quantitative nature is known about the turbulence characteristics of a plasma jet. Langmuir probe correlation studies have been made at low gas pressures ($\sim$10 mmHg) where the indicated turbulence intensity was about 25% (14). It was also shown that the maximum turbulence intensity was not at the centreline, but typically at about eight diameters off the axis. This is in contrast to free isothermal jets (for example reference 15). At normal ambient pressures the high gas temperature of a plasma would necessitate a large diameter water-cooled Langmuir probe. This could affect the validity of the results,

both by distorting the flowfield and also by changing the "plasma-sheath" around the Langmuir probe.

One potentially useful technique which could possibly be applied to plasma-jet turbulence is laser anemometry (29), but at the present time, this technique is still in the development stage.

In the absence of information to the contrary, it may be assumed that the Eulerian scale of turbulence in a plasma jet is of the same order of magnitude as the diameter of the anode-nozzle. In the present case, using a 10 mm diameter nozzle and 50μm particles, the ratio of turbulence scale to particle diameter would be 200. Because the scale of turbulence would be so much larger than the particles, it is suggested that if a particle is engulfed by an eddy, it would "react" as if there had simply been a change in the free stream velocity. Studies of the motion of particles in pipe flow (10, 16, 17, 18, 19) have generally assumed the Stokesian particle drag coefficient ($C_D = 24/Re$) to be unchanged by the effect of turbulence. Kuchanov and Levich (20) suggested that the maximum particle-fluid interaction would occur when the Stokesian relaxation time $[(2\rho_p + \rho_g)(D_p)^2/(36\mu)]$ was equal to the Kolmogorov time scale $[(\nu/\varepsilon)^{1/2}]$. One essential difference between the above studies (10, 16, 17, 18, 19) and the present work is that while the mean velocity of the particles in pipe flow would be equal to that of the fluid, the mean relative velocity between particle and fluid in a plasma jet would generally be of the order of 100 m/s. For such a case, Mujumdar (21) has suggested that the transit time $(D_p/|V_p - V_g|)$ could be an important parameter.

Non-continuum effects were studied by Zarin (22). Increases in drag coefficient in the slip flow regime ($0.01 < Kn < 0.1$) varied between three and eight percent for Reynolds numbers of 100 and 4 000 respectively. For the present work therefore, these effects may be ignored.

EXPERIMENTAL

EQUIPMENT

The equipment used in this study has been described in detail in the earlier sections of this thesis. The main items of equipment were:-

a) A 40kW D.C. plasma-torch

b) A calorimetric probe

c) A High-Speed Ciné-Camera operating in streak mode

EXPERIMENTAL PROCEDURE

The details of the procedure are given in the first two experimental sections of the thesis. In brief, the following work was carried out:

a) The torch was operated at one set condition throughout the experiments.

b) Axial profiles of temperature and velocity of the argon plasma and concentration of entrained air were determined by use of the calorimetric probe. (During these measurements, no particles were fed into the torch, but the carrier gas was maintained at an equivalent flowrate.) Radial profiles of temperature and velocity were obtained by thermocouple and uncooled Pitot-tube at a distance of 178 mm from the nozzle exit.

c) In turn, five separate fractions of glass beads (in the overall size range 30-140μm) were injected into the plasma jet and their mean exit velocities determined by use of the ciné camera. In addition the deceleration of the 44-53μm group was also determined.

EXPERIMENTAL RESULTS

The basic results were presented in Part I and Part II of the experimental section of the thesis as listed below:

Temperature radial profile, Pt. I, Fig. 16, p. 106

Velocity radial profile Pt. I, Fig. 17, p.107

Axial profiles of temperature velocity and concentration,

Pt. I, Fig. 14, p. 104

Mean particle axial velocity versus particle diameter,

Pt. II, Fig. 22, p. 144

also this section, Fig. 2.

Particle deceleration versus particle velocity, Part II, Fig. 24, p. 150

The mean particle velocity decreased from 103 m/s for the 37μm group to 64 m/s for the 127μm group. The average ratio of standard deviation to the mean of the particle velocity was about 21%. For the 48.5μm group, the mean particle velocity was 95 m/s. The least squares linear regression analysis of the deceleration data was:

$$- dV_p/dt = (-1.73 \pm 0.82)(10^4) + (5.85 \pm 0.87)(10^2)(V_p) \quad .... (13)$$

The particle deceleration corresponding to the mean velocity was 3 900 g.

As shown in appendix B, the experimental drag coefficient was calculated from the equation:

$$(C_D)_{Exp} = (-4/3)(dV_p/dt)(\rho_p/\rho_g)(D_p)/[|V_p - V_g|(V_p - V_g)] \quad ..... (14)$$

Because no method was found suitable for measurement, the particle temperature was assumed in turn to be 1 600, 1 900, 2 200 and 2 500°K.

The expected non-isothermal drag coefficient was calculated for

the equivalent mean film temperature, using the Beard and Pruppacher data (3) and three kinematic viscosity ratio exponents (0.0, 0.15, 0.5):

$$(C_D)_{ni} = (C_D)_{B+p}(\nu_{av}/\nu_\infty)^n \quad \ldots\ldots\ldots\ldots\ldots\ldots\ldots \quad (15)$$

The "Excess Drag" was then calculated from the defining equation:

$$(C_D)_{xs} = [(C_D)_{Exp}/(C_D)_{ni} - 1](100) \quad \ldots\ldots\ldots\ldots\ldots\ldots \quad (16)$$

The results are summarised in Table 1 on the following page.

Allowing that the true kinematic viscosity ratio exponent was between 0.0 and 0.15 and that the true particle temperature was between its boiling point (2 500°K) and the temperature at which it would glow red-hot (1 600°K according to manufacturers), then it is seen that the measured excess drag was somewhere between 26 and 46% or a nominal average of 35%.

SIMULATION

Previous attempts at simulating the motion of particles in plasma flames used rather gross simplifications to obtain residence times. These simplifications included Stokesian motion, isothermal and relaxed flowfield (i.e. no history), and spherical geometry (when the actual feed was irregular in shape).

In the simulation discussed here, the above factors were taken into account and corrections incorporated into a general computer program (listed at the end of the thesis in Appendix C). This program used a Kutta-Merson predictor-corrector process to integrate the equation of motion:

TABLE 1 - EXCESS DRAG

Percentage increase of drag coefficient
above the expected value

n \ T_p °K	1600	1900	2200	2500
0	42	43	43	44
0.15	32	29	26	23
0.5	10	1	-7	-14

T_p - particle temperature

n - kinematic viscosity ratio exponent

$$(dV_p/dt) = (-3/4)(\rho_g/\rho_p)[(C_D)_{ni}/D_p]|V_p - V_g|(V_p - V_g)$$

$$-[(9/\rho_p)(1/\pi)^{1/2}] \ldots$$

$$\ldots \int_a^b \left[(\mu_{av}\rho_{av})^{1/2}(1/D_p)(dV_p/dt' - dV_g/dt')(t - t')^{-1/2}\right]dt' \quad \ldots (17)$$

The first term on the right represented the Beard and Pruppacher drag term corrected for a non-isothermal flowfield, while the Basset history term was modified to include the $(\mu_{av}\rho_{av})^{1/2}(1/D_p)$ term under the integration sign.

The distributions of temperature, velocity and concentration of the plasma jet were modelled in the axial direction using the data obtained from the calorimetric probe measurements. While carrying out computations with varying particle diameters, a simple radial profile model was used with the particle radial injection velocity fixed at 10 m/s. (This velocity had been previously determined during actual injection nozzle studies "in the cold"). For distances greater than 10 mm beyond the nozzle exit the radial profiles were assumed flat. At the nozzle, the profiles of temperature and velocity were assumed parabolic. While testing the effect of a varying radial injection velocity, a more realistic Gaussian radial profile model was used. Half radii of temperature and velocity were obtained by interpolation between the data of Carleton (23) (working close to the nozzle exit of his torch) and the data obtained at a distance of 178 mm from the nozzle exit of the torch used in the present work. According to Kleinstein (24), the axial profiles of temperature and concentration in a plasma jet should be almost similar. For simplicity, it was therefore assumed that the half radii of temperature and concentration were equal.

Because of the need to calculate mean film temperatures, the particle surface temperature was required. This was calculated using the Ranz-Marshall correlation (25) corrected for non-isothermal effects (8), ionisation effects (26) and recombination effects (27). The latter correction was necessary due to the entrainment of considerable quantities of air by the hot argon jet. At each position of the particle along its trajectory the magnitude and direction of the relative velocity vector was calculated, followed by the Reynolds number and hence the drag coefficient.

The radial acceleration was taken as the component of the steady-state drag in that direction, without any history effect. This was justified by preliminary calculations which showed that the history term was generated by the gas deceleration and not the particle acceleration. Since radial velocities in a jet are low, it would be expected that radial history could be ignored.

The axial acceleration of the particle was calculated as the sum of the axial component of the steady-state drag and an axial history term evaluated by the method of Odar (28):

$$\int_a^b \left[(\mu_{av}\rho_{av})^{1/2}(1/D_p)(dV_p/dt' - dV_g/dt')(t - t')^{-1/2}\right] dt'$$

$$\simeq \overline{(\mu_{av}\rho_{av})^{1/2}}\,\overline{(1/D_p)}\,\overline{(dV_p/dt' - dV_g/dt')}\int_a^b (t - t')^{1/2} dt'$$

$$\simeq \overline{(\mu_{av}\rho_{av})^{1/2}}\,\overline{(1/D_p)}\,\overline{(dV_p/dt' - dV_g/dt)}\left(-2\left[t - t'\right]_a^b\right) \qquad \text{..... (18)}$$

A set of computations was carried out as above for the mean particle diameter of each of the size ranges used. In addition, a set of computations was made, with the history term neglected.

A third set of results was generated for the 48.5μm group, for varying particle inlet velocity.

RESULTS OF COMPUTATIONS

The computation results are summarised in Figures 1, 2, 3, 4 and 5. Figure 1 shows typical predictions of particle axial velocity against axial displacement, for 50 and 100μm particles, with and without the history term included. The points of interest are:

(i) Without history the particles accelerated to a maximum velocity where the particle velocity equalled the gas velocity. The particles then decelerated against the braking effect of the gas.

(ii) With history, the maximum particle velocity occurred prior to the reversal of direction of the relative velocity.

Figure 2 shows the exit axial particle velocities against particle diameter. It is noted that the experimental measurements (also shown) were sandwiched between the predictions with and without history. As the particle diameter was increased, there would appear to have been some trend of the experimental results toward the predictions without history.

Figure 3 shows computations of particle residence time for an axial distance of 178 mm (with and without history) for varying particle diameters of 178 mm. The trend was from a time of about 1 ms for 30μm particles to about 4 ms for 140μm particles. The effect of history was to increase particle residence times by about 10% for 30μm particles and by about 30% for 140μm particles.

Figure 4 shows the computed history effect as a fraction of the axial drag, ranging from about 25% for 30μm particles to 95% for 140μm particles.

FIGURE 1

Predicted Axial Velocity

Versus

Axial Displacement

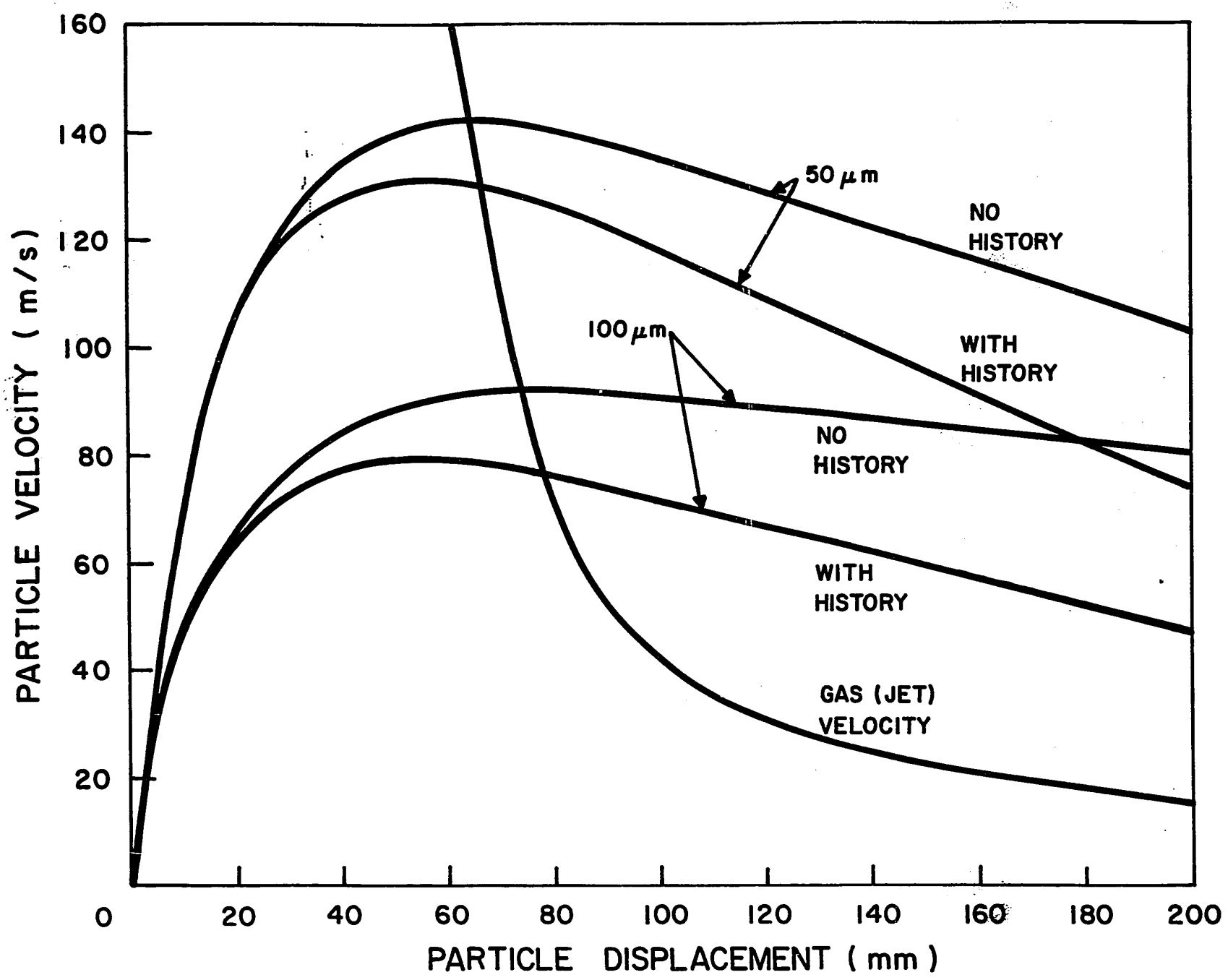
160
140
120
100
80
60
40
20
0
20
40
60
80
100
120
140
160
180
200
PARTICLE VELOCITY (m/s)
PARTICLE DISPLACEMENT (mm)
50 μm
NO HISTORY
WITH HISTORY
100 μm
NO HISTORY
WITH HISTORY
GAS (JET) VELOCITY

FIGURE 2

Measured and Predicted Axial Particle Velocity

Versus Particle Diameter

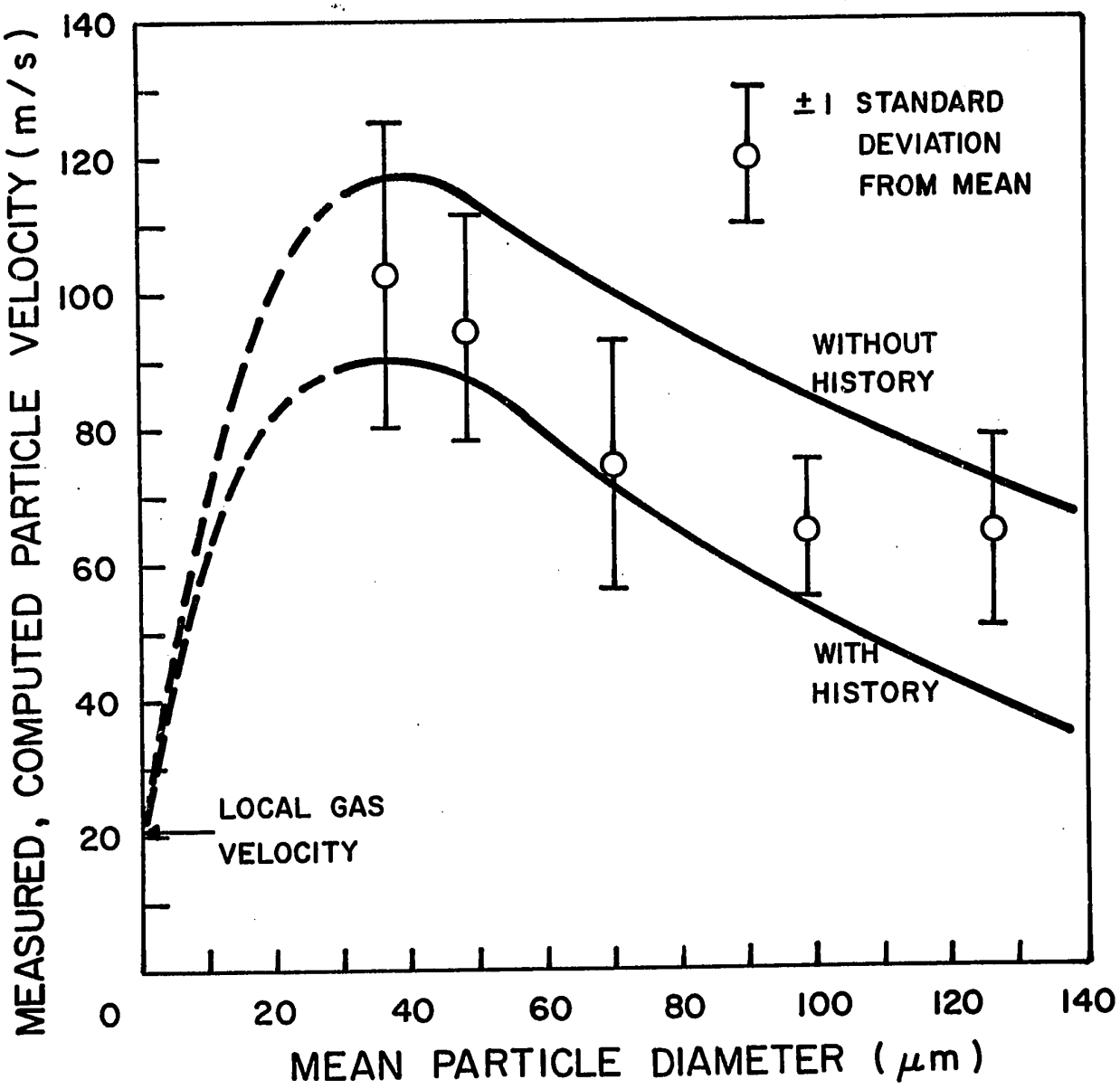
MEASURED, COMPUTED PARTICLE VELOCITY (m/s)
140
120
100
80
60
40
20
0
20
40
60
80
100
120
140
MEAN PARTICLE DIAMETER (μm)
±1 STANDARD DEVIATION FROM MEAN
WITHOUT HISTORY
WITH HISTORY
LOCAL GAS VELOCITY

FIGURE 3

Computed

Particle Residence Time

Versus

Particle Diameter

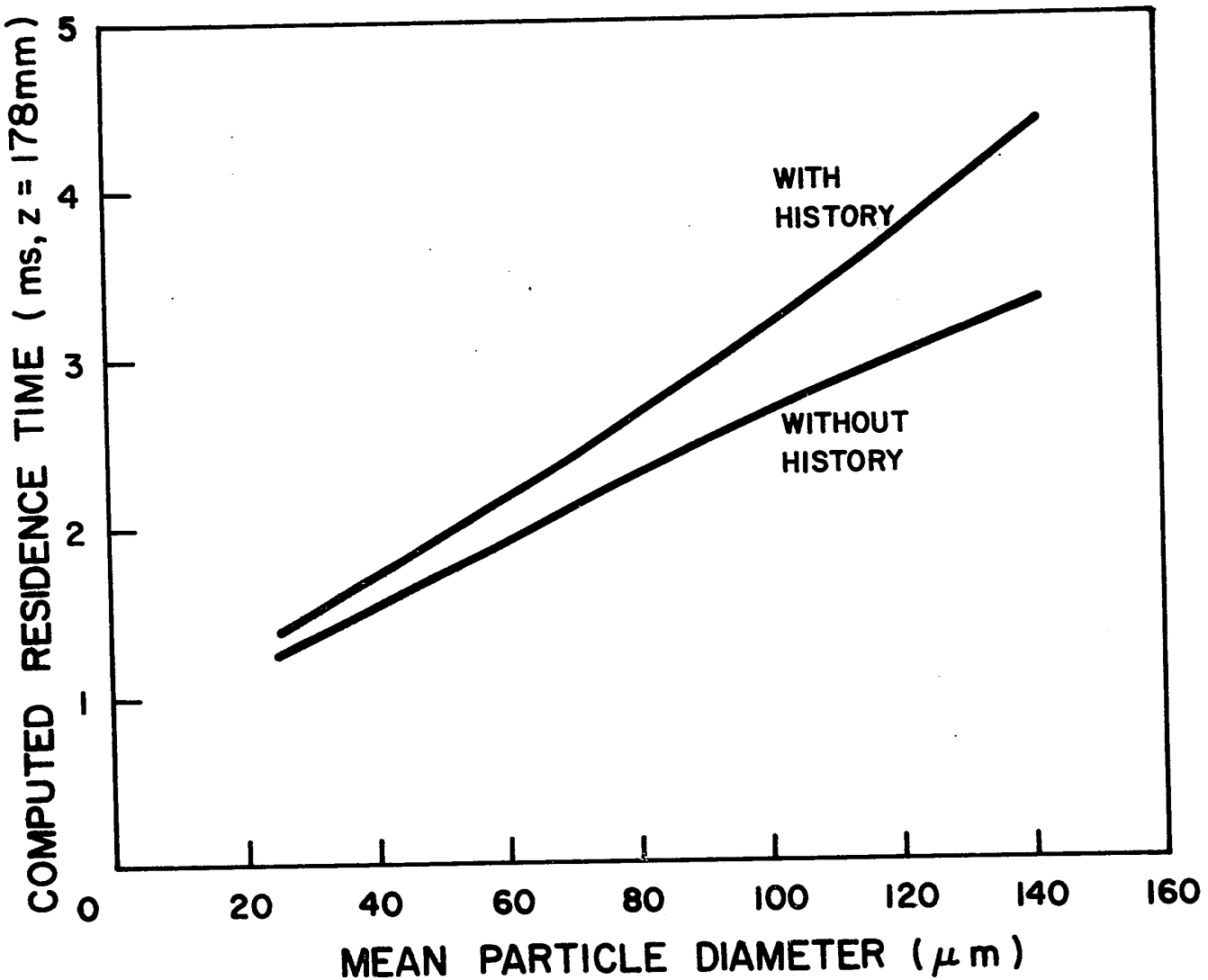
COMPUTED RESIDENCE TIME (ms, z = 178mm)
0
1
2
3
4
5
20
40
60
80
100
120
140
160
MEAN PARTICLE DIAMETER (μm)
WITH HISTORY
WITHOUT HISTORY

FIGURE 4

Computed

Basset History Effect

as a

Fraction of Axial Drag

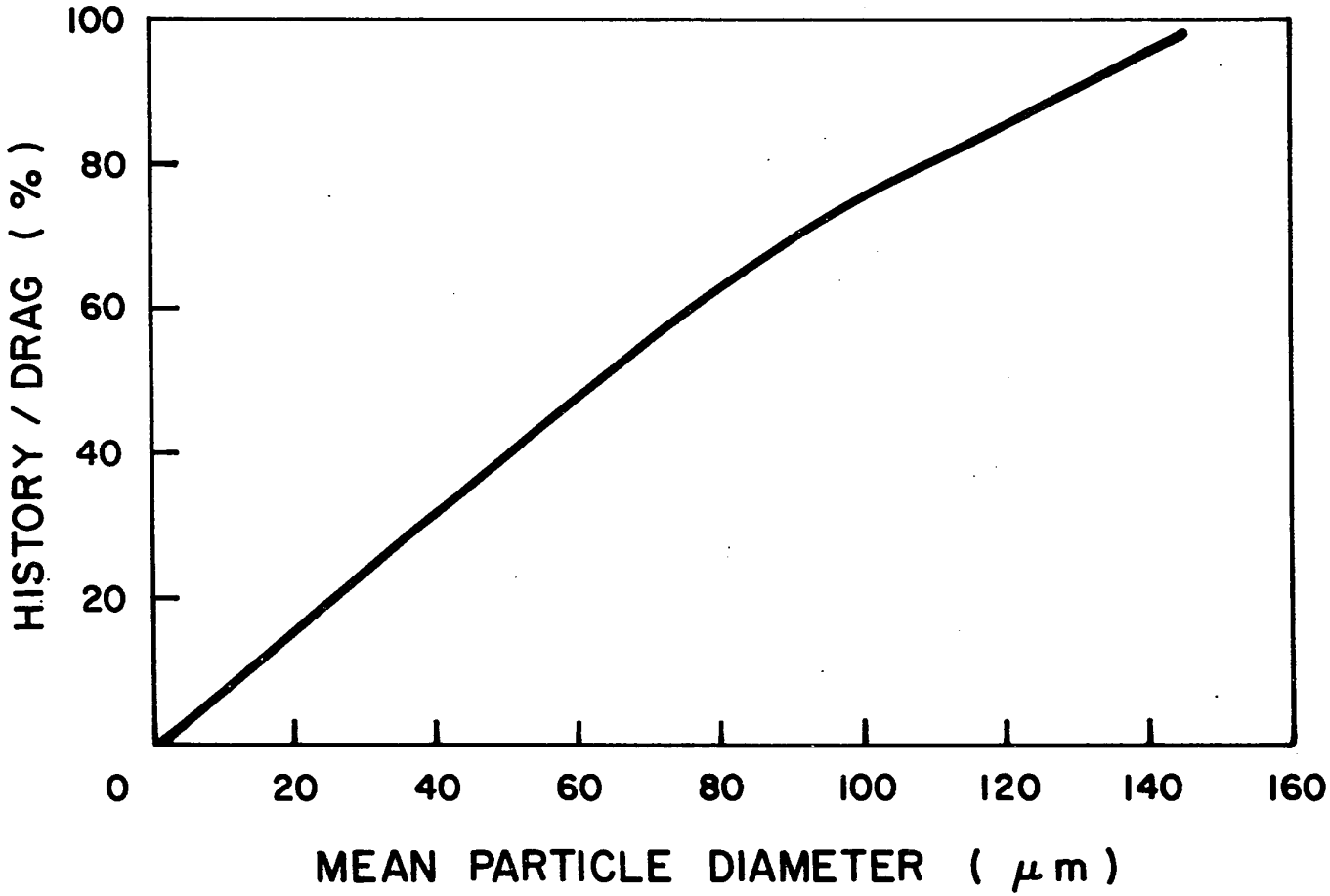
100
80
60
40
20
HISTORY / DRAG (%)
0
20
40
60
80
100
120
140
160
MEAN PARTICLE DIAMETER (μm)

FIGURE 5

Effect of Variation of

Particle Radial Injection Velocity

on

Radial Displacement

Axial Velocity

Residence Time

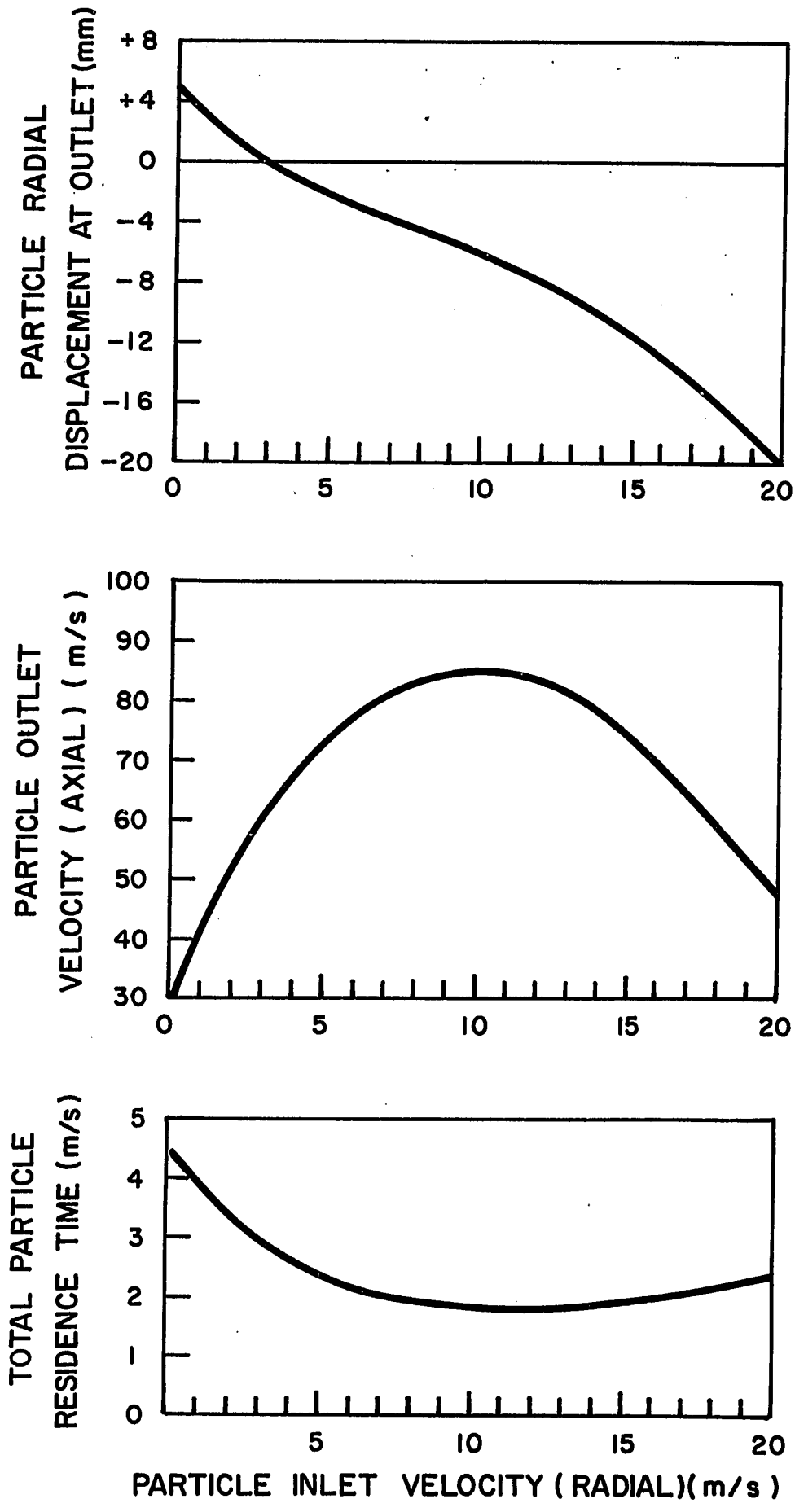
PARTICLE RADIAL DISPLACEMENT AT OUTLET (mm)
+8
+4
0
-4
-8
-12
-16
-20
0
5
10
15
20
PARTICLE OUTLET VELOCITY (AXIAL) (m/s)
100
90
80
70
60
50
40
30
0
5
10
15
20
TOTAL PARTICLE RESIDENCE TIME (m/s)
5
4
3
2
1
0
5
10
15
20
PARTICLE INLET VELOCITY (RADIAL)(m/s)

Figure 5 shows the effect of a varying particle radial injection velocity on the computed radial displacement, axial velocity and residence time for particles having a diameter of 48.5μm. The results showed a maximum predicted particle exit velocity of about 85 m/s, with an almost symmetrical fall-off on either side of the inlet velocity of 10 m/s. The minimum computed residence time was about 2 ms for an equivalent radial displacement of 6 mm. (The result of using a more realistic radial profile model of the plasma jet was to reduce the predicted history effect by about 4%, with negligible change in particle exit velocity.)

A special run of the program was made to test the effect of the particles being non-isothermal. For the largest group, the particle surface temperature was assumed to be at its boiling point (2 500°K) during the heating stage and at the temperature of the gas during its cooling stage. No significant difference was found in the predicted particle velocity or acceleration compared to the earlier predictions.

During all the above computations, particle evaporation was predicted to be negligible. The effect of evaporation for the smallest particle diameters of interest, was only at the level of the fifth significant figure.

DISCUSSION

1. Origins of the Distributions of Particle Velocities

The standard deviation of the measured velocities of the five size groups of particles varied from 15% to 25% of the mean velocity, with an average deviation of 21%. The possible origins of these rather wide distributions are discussed below:

i) Measurement errors could have caused a maximum random uncertainity of about 1.5% in the measured particle velocity. (This was discussed in detail in Part II of the experimental section of this thesis.)

ii) Each group of particles had a size range (±10%) given by the "fourth root of two" standard sieve sizes. From the computer predictions (Fig. 2), it is possible to convert the particle diameter range into a (predicted) velocity range. The error suggested by this method ranged from zero percent at $D_p \sim 36\mu m$ to 15% at $D_p \sim 60\mu m$. Thus it can be seen that the range of particle diameters could have contributed significantly to the distribution of particle velocities.

iii) It is unrealistic to assume that all particles would enter the plasma jet from the injection nozzle at exactly the same velocity. Allowing a more than generous variation in this injection velocity between 5 m/s to 15 m/s, the variation in the exit velocity would be about 8% for the 44-53μm group (Fig. 5).

iv) (In the discussion which follows, "turbulence" includes the perturbations of the jet flowfield resulting from the periodic fluctuation of the arc discharge - see Pt. I). As considered in the Introduction, turbulence can have an important randomizing effect

when dealing with the motion of small particles. The so-called "transit time" (21), given by $[D_p/|V_p - V_g|]$, is a measure of the time taken for an element of fluid to travel from the front to the rear of the particle. In the case of the present work, this time is of the order:

$$(50 \times 10^{-6})/(100)$$

$$= 0.5\mu s \quad \ldots\ldots\ldots \text{(for the smallest particles)}$$

and

$$(150 \times 10^{-6})/(50)$$

$$= 3\mu s \quad \ldots\ldots\ldots \text{(for the largest particles)}$$

Since this transit time is so very much shorter than the period of turbulent fluctuations (100μs - 1 ms), it is reasonable to suggest that the gas velocity and temperature to which a particle is subjected in the plasma flame, are not the time averages, but the instantaneous values of these quantities. (In contrast to the present study, the transit time in the experiments reported by Torobin and Gauvin (13) would have been of the order of one millisecond or comparable to the period of turbulent fluctuations). As a result of being subjected to the instantaneous values of gas temperature and velocity, one particle injected into the plasma flame would be subject to (say) a "fast and hot" pocket of gas, while another particle would be subject to a "slow and cold" pocket of gas. In order to assess the effect of a random component of gas velocity on

the particle velocity, a simplified computer simulation was carried out. It was assumed that the particle experienced a local gas velocity, everywhere along its trajectory, which was only 90% of the measured gas velocity at the particular axial displacement. The predicted particle velocity at the flame exit was found to be reduced from 88.5 m/s to 79.5 m/s, (i.e. about 10%). This calculation also had the merit of providing an estimate of the possible effect of an error in the gas velocity, resulting from using the large calorimetric (Pitot) probe.

In summary therefore, the major causes of particle velocity distribution were probably:

the range of particle diameters in each size group;

the variation in the particle radial injection velocity;

the randomizing effect of the turbulent jet fluctuations.

2. Effect of the Basset History Term on the Drag Coefficient

a) Measurement Errors

In Part II of this thesis, it was noted that a random error of about 16.5% could occur in the measurement of the particle deceleration. Since the particle deceleration versus particle velocity data were fitted by a least squares linear regression analysis (correlation coefficient 0.65), it may be suggested that the error in the mean deceleration(calculated from the regression analysis) would not be more than a few percent from the true mean deceleration.

While the random measurement error would in itself explain a large part of the scatter in the deceleration-velocity plot, it would also mask any true variation of particle deceleration at a fixed relative velocity. Potential sources of such variation would be the range of particle diameters

(± 10%), small variations in particle density and also possible differences in particle temperature. (The variation in particle temperature could result from the temperature fluctuations of the gas and different particles travelling through different temperature zones of the plasma.)

Simultaneous systematic errors of ± 4% and ± 9% in the particle velocity and deceleration were also considered possible. To make this point clear, a "true" particle velocity of 104% would be equivalent to a "true" particle deceleration of 109%. Rewriting equation 14

$$C_D = k_D(dV_p/dt)/\left[|V_p - V_g|(V_p - V_g)\right] \quad \ldots\ldots\ldots\ldots\ldots\ldots (19)$$

A simple evaluation of the error in the drag coefficient for a particle velocity of 100 m/s and a gas velocity of 20 m/s, would give the ratio of the true to estimated drag coefficient as:

$$(C_D'/C_D) = [109/(104-20)^2]/[100/(100-20)^2] \quad *$$

$$= \underline{0.99}$$

Thus the measured drag coefficient would be underestimated by one percent. The error in the Reynolds number would be given by:

$$(Re'/Re) = (104-20)/(100-20) \quad *$$

$$= \underline{1.05}$$

Assuming for simplicity, that the motion was near Stokesian, the error in the expected drag coefficient would be:

$$(C_D'/C_D) = 1/1.05 \quad *$$

$$= \underline{0.95}$$

* Note

Primed quantities refer to "true" values, unprimed quantities refer to the measured values.

Thus the error in the excess drag would be:

$$\left[(0.99/0.95) - 1\right](100) = 4\%.$$

It was also noted in Pt. II of this thesis that the radial displacement of particles could be as much as 5 mm from the axis. This was confirmed by the computer predictions, which indicated a possible radial displacement of particles of about 6 mm. The error in the relative velocity due to the Gaussian distribution would be about one percent as seen below:

$$(V_p - V_g)'/(V_p - V_g) = \left[(100 - 0.95 \times 20)/(100 - 20) - 1\right](100)$$

$$= \left[(81/80) - 1\right](100)$$

$$= \underline{1.25\%}$$

Thus in summary, the systematic and random errors of measurement would lead to errors of a few percent in the estimation of the excess drag. Compared to the question of the effects of particle temperature and kinematic viscosity ratio exponent, these systematic and random error effects are not considered to be of major importance.

b) Comparison of Measured Excess Drag and the Computed History Effect

The predicted history effect for the 44-53μm group of particles varied between 28% and 36%, depending on the radial injection velocity and the simulation of the radial profile. The lower value was considered to be the more reasonable value. These predictions should be compared with the experimental excess drag (25% - 43%). In view of the experimental difficulties and the uncertainties in the simulation, the agreement between

prediction and measurement is considered most remarkable. The use of the Basset history term would therefore appear justified in calculations of unsteady-state motion where the particle Reynolds number changes rapidly with time. However, it cannot be said whether or not the present results are in agreement with Odar's data where he used a coefficient of 0.48 (28) in the evaluation of the effect of history. While it would be desirable to carry out a more-ideal experiment of non-steady motion of particles in plasma flames, the required precision of both computation and experiments would be less than practical.

Comparing the present predictions of the particle velocities both with and without the Basset history term (Fig. 2) it may be seen that the use of Odar's coefficient would have resulted in a line approximately half way between the two earlier predictions. This Odar line would then have been a reasonable fit to the measured particle velocity.

CONCLUSIONS

(i) The measured velocities of groups of particles emerging from a plasma jet were in good agreement with computer predictions, taking into account the non-isothermal non-relaxed nature of the flowfield.

(ii) Significant increases in the instantaneous drag on particles in a non-steady system such as a plasma jet were predicted, ranging from about 20% for 30μm particles to 100% for 150μm particles.

(iii) Experimental determination of the excess drag of 44-53μm particles emerging from a plasma jet were in agreement with the above predictions.

NOMENCLATURE

C_D	Drag coefficient
$(C_D)_A$	Drag coefficient evaluated at mean film temperature
$(C_D)_{B+p}$	Beard and Pruppacher drag coefficient
$(C_D)_{Exp}$	Experimental drag coefficient
$(C_D)_{iso}$	Isothermal drag coefficient
$(C_D)_{ni}$	Non-isothermal drag coefficient
$(C_D)_{xs}$	Excess in experimental drag coefficient-equation 17
D_p	Particle diameter
F_{AM}	Force due to added mass
F_E	Force due to potential field
F_H	Force due to Basset History term
F_p	Total force on particle
F_{pg}	Force due to pressure gradient
k	Defined in equation 4
k_D	Defined in equation 21
Kn	Knudsen number
k_T	Defined in equation 9
Nu	Nusselt number
$(Nu)_{ni}$	Non-isothermal Nusselt number
$(Nu)_{av}$	Nusselt number evaluated at mean film temperature

NOMENCLATURE (cont'd)

N_{AM}	Acceleration modulus $\lvert dV/dt - dV_g/dt \rvert (D_p)/(V_p - V_g)^2$
Re	Reynolds number (evaluated at mean film temperature)
T	Temperature
T_p	Particle temperature
T_∞	Bulk gas temperature
t	Real time
t'	Convolution time (for history integral)
V_g	Gas velocity
V_p	Particle velocity
ε	Local rate of energy dissipation per unit mass
μ_g	Viscosity of gas
$(\mu_g)_{av}$, μ_{av}	Viscosity of gas evaluated at mean film temperature
ν	Kinematic viscosity of fluid
ν_{av}	Kinematic viscosity evaluated at mean film temperature
ν_∞	Kinematic viscosity evaluated at bulk gas temperature
ρ_g	Gas density
$(\rho_g)_{av}$	Gas density evaluated at mean film temperature
$(\rho_g)_\infty$	Gas density evaluated at bulk gas temperature
τ	Temperature ratio $(T_p - T_\infty)/(T_\infty)$

BIBLIOGRAPHY

1 Humphrey's Corp., Bow, N.H., U.S.A. Private Communication (19.VII.71).

2 Dundas, P.H., and Thorpe, M.L., Chem. Eng. Prog. 66, 66 (1970).

3 Beard, K.V., and Pruppacher, H.R., J. The Atmos. Sci. 26, 1066 (1969).

4 Hamielec, A.E., Hoffman, T.W., and Ross, L.L., A.I.Ch.E.J. 13, 212 (1967).

5 Lapple, C.E., and Shepherd, C.B., Ind. Eng. Chem. 32, 605 (1940).

6 Lemoine, A., and LeGoff, P., Chimie et Industrie 102, 1304 (1969).

7 Kassoy, D.R., Adamson, T.C., and Messiter, A.E., Physics of Fluids 9, 671 (1966).

8 Ahmed, A.M., Mech. Eng. Res. Labs., T.N. 67-5, McGill Univ., Montreal (1967).

9 Hamielec, A.E., McMaster Univ., Hamilton. Private Communication (June 1971).

10 Hinze, J.O., "Turbulence", McGraw Hill (1959).

11 Odar, F., and Hamilton, W.S., J. Fluid Mech. 18, 302 (1964).

12 Rimon, Y., and Cheng, S.I., Physics of Fluids 19, 949 (1969).

13 Torobin, L.B., and Gauvin, W.H., Can. J. Chem. Eng. 37, 129 (1959);
" " " " " Can. J. Chem. Eng. 37, 167 (1959).

14 Johnston, T.W., Richards, C., Ghosh, A.K., Carswell, A.I., and Graf, K. Symposium on Turbulence of Fluids and Plasmas, Polytechnic Institute of Brooklyn, P. 65 (1968).

15 Abramovich, G.N. "The Theory of Turbulent Jets", M.I.T. Press (1963).

16 Soo, S.L., Ihrig, H.K., El Kouh, A.F., Trans A.S.M.E., J. Basic Eng. 609 (1960).

17 Shirazi, M.A., Chao, B.T., and Jones, B.G., "On the Motion of Small Particles in a Turbulent Fluid Field", Nuclear Engineering Laboratories Report, Univ. of Illinois at Urbana, Illinois.

18 Jones, B.G., Chao, B.T., Shirazi, M.A., "An Experimental Study of the Motion of Small Particles in a Turbulent Fluid Field". Nuclear Eng. Lab Report, Univ. of Illinois at Urbana, Illinois.

19 Goldschmidt, V.W., Householder, M.K., Ahmadi, G., and Chuang, S.C. International Symposium on Two-Phase Systems, Haifa, Israel, August-September 1971.

20 Kuchanov, S., and Levich, V., Soviet Physics, Doklady 12, 549 (1967).

21 Mujumdar, A.S., McGill University, Montreal. Private communication, June (1971).

22 Zarin, N., NASA CR-1585 (1970).

23 Carleton, F.E., Ph.D. Thesis, Univ. of Michigan (1970).

24 Kleinstein, G., J. Spacecraft 1, 403 (1964).

25 Ranz, W.E., and Marshall, W.R., Chem. Eng. Prog. 48, 141 (1952); 48, 173 (1952).

26 Petrie, T.W., Ph.D. Thesis, Univ. of Minnesota (1969).

27 Chluldzinski, G.R., Ph.D. thesis, Univ. of Michigan (1964).

28 Odar, F., U.S. Army, CRREL-RR-190 (1966).

29 Fridman, J.D., Huffaker, R.M., and Kinnard, R.F., Laser Focus, Nov. (1968).

SUMMARY OF EXPERIMENTAL WORK

The frequency of oscillation of the cathode-anode voltage-drop of a d.c. plasma torch operating on nitrogen, was studied by means of a pulse counter. The frequency range was found to be 5 to 15 kHz, increasing with plasma gas flowrate and power input. The calculated nominal nozzle velocity was found to agree with the generally expected values.

The same plasma torch, but with different anode and cathode, was operated on argon at an arc current of 650 A, and an arc voltage of 30V. The axial profiles of temperature, velocity and of concentration of entrained air, were determined by means of a calorimetric probe. The maximum temperature was found to be 11 600°K at a distance of 25 mm from the torch nozzle exit, with a corresponding gas velocity of 410 m/s. The calorimetric temperature agreed with published spectroscopic temperature data. It was found that the axial temperature and velocity profiles were identical, with 90% decay occurring within a distance of 10 nozzle diameters. Radial profiles of temperature and velocity of the jet were determined by a bare-junction thermocouple and uncooled Pitot tube at a distance of 178 mm from the nozzle exit. The distributions were close to Gaussian, with a ratio of velocity half-width to temperature half-width of 0.68.

Close-sized glass microspheres in the overall range 30-140μm were injected radially into the flame just above the torch nozzle exit. The particles were observed emerging from the flame parallel to the torch axis, with no apparent deviation from rectilinear motion. The mean velocity

of each group of particles was determined by high-speed ciné-streak photography. The mean velocities decreased from 103 m/s for the 37μm size group to 64 m/s for the 127μm size group. The deceleration of particles in the 44-54μm group was also determined by the ciné-streak technique. The data were fitted by a least squares linear regression analysis:

$$- dV_p/dt = (-1.73 \pm 0.82)(10^4) + (5.85 \pm 0.87)(10^2)(V_p)$$

with a correlation coefficient of 0.65. The maximum observed deceleration was 8 000 g.

Drag coefficients calculated from the experimental data showed an excess of about 30% over the most reliable estimate of steady-state drag coefficients.

A computer program was written to simulate the motion of the microspheres in the plasma jet. As a result of the non-steady relative motion between particles and gas, it was found that the Basset history term of the full equation of motion could build up to a magnitude comparable to the conventional drag term. The predicted value of the Basset history term was found to be in accord with the experimental measurements of the excess drag. Predicted particle residence times were around 4μs.

The experimental values of the particle axial velocity were bounded by an upper limit given by predictions <u>without</u> the history term and a lower limit given by predictions <u>including</u> the history term. The average standard deviation in the particle velocities (21%) did not allow preference for either set of predictions.

CONTRIBUTION TO KNOWLEDGE

The present study of the motion of particles entrained in a plasma jet indicates that:

(i) The residence times of particles, of about 100μm diameter, in a plasma flame may be predicted by conventional approaches, with a probable accuracy of about 20%.

(ii) As a result of the non-steady relative motion in a plasma-particulate system, the instantaneous particle drag coefficient can show marked deviation from the standard curve. The magnitude of this deviation may be calculated using the Basset history term of the full equation of motion.

RECOMMENDATIONS FOR FUTURE WORK

It is suggested that the development of Langmuir-probe and laser-anemometer techniques would be a useful contribution to the study of velocity and turbulence in the plasma jet.

An assessment should be made of the practicality of using high-speed infra-red film for the determination of particle temperature.

The stereo-streak device should be developed as a method for determining the radial distribution of particle number density. (This information would be of interest in the modelling of a plasma reactor.)

The motion of particles in isothermal jets should be studied by experiment and computation. The value of the history effect, under such conditions, should be compared with the values obtained using the plasma jet.

APPENDIX A

SAMPLE CALCULATION OF GAS TEMPERATURE BY CALORIMETRIC PROBE

BASIC INFORMATION

Concentration of gas sample	55% air 45% argon
Pressure upstream of critical orifice	623 mm Hg
Calorimeter water flowrate	14.0 cm^3/s
Calorimetric temperature rise	66.4μV
Mean jacket temperature rise	241.2μV
Mean strut-calorimeter temperature difference	56μV

CALCULATIONS

Mean Specific Heats of gas

(300°K) $\overline{C_p} = 0.25 \times 0.55 + 0.124 \times 0.45$

$= 0.137 + 0.056$

$= \underline{0.193 \text{ cal gm}^{-1} \text{°K}^{-1}}$

(300°K - 1 200°K) $\overline{C_p} = 0.266 \times 0.55 + 0.124 \times 0.45$

$= 0.146 + 0.056$

$= \underline{0.202 \text{ cal gm}^{-1} \text{°K}^{-1}}$

(300°K) $\overline{C_v} = 0.178 \times 0.55 + 0.074 \times 0.45$

$= \underline{0.131 \text{ cal gm}^{-1} \text{°K}^{-1}}$

$\overline{C_p}/\overline{C_v} = 0.193/0.131$

$= \underline{1.48}$

Choked Orifice Correction Factor

[Shapiro, A.H., Compressible Fluid Flow", Vol. 1, p. 85 (1953)]

$$\Gamma_M = 1.48\left[2/(1 + 1.48)\right]^{\left[(1.48 + 1)/(1.48 - 1)\right]}$$

$$= 1.48(0.806)^{5.12}$$

$$= 1.48 \times 0.333$$

$$= 0.490$$

$$\dot{M}_g/\dot{M}_A = \left[(0.490 \times 34.0)/(0.467 \times 29)\right]^{1/2}$$

$$= \underline{1.11}$$

Gas Mass Flowrate

From calibration graph

Gas flowrate as air ..... = 0.0554 gm/s

Gas flowrate as argon-air mixture = 0.0554 x (orifice correction factor)

= 0.0554 x 1.11

= 0.0614 gm/s

True Calorimeter Water Temperature Rise

Strut calorimeter correction = 20.4μV

Mean jacket calorimeter ΔT = 251-66.4

= 184.8μV

Jacket calorimeter correction = (4.7 x 8.0)/14.0

= 2.7μV

Total correction ..... = 20.4 + 27

= 23.1μV

Corrected Calorimeter Output

= 66.4 - 23.1

= 43.3μV

= 43.3/40.1

= 1.08°K

Corrected Heat Flux to Calorimeter Water

= 1.08 x 14 ..... (temperature rise-x-mass flowrate)

= 15.2 cal/s

Enthalpy Changes of Gas

= 15.2/0.0614 ..... (corrected heat flux) /(gas mass flowrate)

= 250 cal/gm

Temperature Change of Gas

= 250/0.202 ..... $(\Delta h_g / \overline{C_p})$

= 1220°K

Inlet Gas Temperature

= 1220 + 300

= 1520°K

APPENDIX B

SAMPLE CALCULATION OF EXCESS DRAG

BASIC INFORMATION

Gas temperature	900°K
Gas Concentration of Argon	8%
Particle Temperature (Assumed)	1 600°K
Particle Density (Measured)	2.36
Mean Particle Diameter	48.5μm
Mean Velocity of Particles	95 m/s
Mean Velocity of Gas	20.6 m/s

Particle Deceleration

$$dV_p/dt = -1.73 \times 10^4 + 5.85 \times 10^2(V_p) \quad (m/s^2)$$

Viscosities ($gm\ cm^{-1}sec^{-1}$)(10^6)

T_g °K	Argon	Nitrogen	Oxygen
900	501	371	441
1250	631	460	548

Densities ($gm\ cm^{-3}$)(10^6)

T_g °K	Argon	Nitrogen	Oxygen
900	505	353	405
1250	381	266	301

CALCULATIONS

Mean Viscosity of Gas at 900°K

$$= (501 \times 0.08 + 371 \times 0.92 \times 0.79 + 441 \times 0.92 \times 0.21)(10^{-6})$$

$$= \underline{395 \times 10^{-6}\ gm\ cm^{-1}sec^{-1}}$$

Mean Viscosity of Gas at 1250°K

$$= (631 \times 0.08 + 460 \times 0.92 \times 0.79 + 545 \times 0.92 \times 0.21)(10^{-6})$$

$$= \underline{491 \times 10^{-6}\ gm\ cm^{-1}sec^{-1}}$$

Mean Densities

Basis of calculation is one gram-mole of the gas.

Total Mass of Gas

$= 40 \times 0.08 + 28 \times 0.92 \times 0.79 + 32 \times 0.92 \times 0.21$

$= 3.2 + 20.4 + 6.2$ gm

$= \underline{29.7 \text{ gm}}$

Total Volume of Gas at 900°K

$= 3.2 \times 10^6/505 + 20.4 \times 10^6/353 + 6.2 \times 10^6/405$

$= (0.63 + 5.76 + 1.53)(10^4)$

$= \underline{7.93 \times 10^4 \text{ cm}^3}$

Mean Gas Density at 900°K

$= 29.7/(7.93 \times 10^4)$

$= \underline{3.75 \times 10^{-4} \text{ gm cm}^{-3}}$

Total Volume of Gas at 1250°K

$= 3.2 \times 10^6/381 + 20.4 \times 10^6/266 + 6.2 \times 10^6/301$

$= (0.84 + 7.65 + 2.06)(10^4)$

$= \underline{1.05 \times 10^5 \text{ cm}^3}$

Mean Gas Density at 1250°K

$= 29.7/1.05 \times 10^5$

$= \underline{2.82 \times 10^{-4} \text{ gm cm}^{-3}}$

Reynolds Number (at Mean Film Temperature)

$Re = (D_p)|V_p - V_g|(\rho_g)/\mu_g$

$= (48.5 \times 10^{-4})(95.0 - 20.6)(2.82 \times 10^{-4})/(4.91 \times 10^{-4})$

$= \underline{20.7}$

Particle Deceleration

$$dV_p/dt = -1.73 \times 10^4 + 5.85 \times 10^2(V_p)$$

$$= -1.73 \times 10^4 + 5.85 \times 10^2(95)$$

$$= \underline{3.83 \times 10^4 \text{ m/s}^2} \qquad (3.91 \times 10^3 \text{ g.})$$

Experimental Drag Coefficient

$$(C_D)_{Exp} = (-4/3)(dV_p/dt)(\rho_p/\rho_g)(D_p)/[|V_p - V_g|(V_p - V_g)]$$

$$= (4/3)(3.83 \times 10^4)(2.36 \times 10^4/2.82)(48.5 \times 10^{-4})/(95 - 20.6)^2$$

$$= \underline{3.75}$$

Beard and Pruppacher Drag Coefficient

$$(C_D)_{B+p} = (24/Re)[1 + 0.11(Re^{0.81})]$$

$$= \underline{2.64}$$

Excess Drag ("Isothermal")

$$(C_D)_{xs} = [(C_D)_{Exp}/(C_D)_{B+p} - 1](100)$$

$$= [(3.75/2.64) - 1] \times 100$$

$$= \underline{42\%}$$

Ahmed-Type Non-Isothermal Correction Factor

$$(\nu_{av}/\nu_\infty)^{0.15} = [(491/282)/(395/375)]^{0.15}$$

$$= \underline{1.08}$$

Excess Drag ("Non-Isothermal")

$$(C_D)_{xs} = [(C_D)_{Exp}/(C_D)_{ni} - 1](100)$$

$$= [3.75/(2.64 \times 1.08) - 1](100)$$

$$= \underline{32\%}$$

APPENDIX C

COMPUTER PROGRAM

i Program Listing

ii List and Explanation of Subroutines

iii Abbreviated Nomenclature

```
FORTRAN IV G LEVEL  19                    MAIN                    DATE = 71161          15/1

0001                  COMMON/MKN/VARG(29),VNIT(29),VOXY(29)
0002                  COMMON/PART/RP,RHOP
0003                  COMMON/DEP/Y(10)
0004                  COMMON/PROBE/CAR,TG,VG,AG
0005                  COMMON/AREAT/TEMP(29)
0006                  COMMON/AREAD/RHOAR(29),RHON(29),RHOO(29),RHOX(29)
0007                  COMMON/AREAV/VISAR(29),VISN(29),VISO(29),VISX(29)
0008                  COMMON/AREAC/CONAR(29),CONN(29),CONO(29),CONX(29)
0009                  COMMON/A1/CP
0010                  COMMON/GAS/KQ
0011                  COMMON/AREATP/TPET(20)
0012                  COMMON/PETFAC/PF(20)
0013                  COMMON/VAPN/TBOIL,VLAMDA
0014                  COMMON/BASSET/K1,HTERM,X1(1000),ARMURO(1000)
0015                  DO 997 I = 1,13
0016                  READ(5,97)TPET(I),PF(I)
0017              997 WRITE(6,87)TPET(I),PF(I)
0018               87 FORMAT(/T10,2E15.3)
0019               97 FORMAT(2F20.4)
0020               88 FORMAT(/T10,4E15.3)
0021               98 FORMAT(4F20.4)
0022                  DO 99 I=1,29
0023                  READ(5,98)TEMP(I),RHOAR(I),VISAR(I),CONAR(I)
0024               99 WRITE(6,88)TEMP(I),RHOAR(I),VISAR(I),CONAR(I)
0025                  DO 96 I=1,29
0026                  READ(5,98)TEMP(I),RHON(I),VISN(I),CONN(I)
0027               96 WRITE(6,88)TEMP(I),RHON(I),VISN(I),CONN(I)
0028                  DO 95 I=1,29
0029                  READ(5,98)TEMP(I),RHOO(I),VISO(I),CONO(I)
0030               95 WRITE(6,88)TEMP(I),RHOO(I),VISO(I),CONO(I)
0031               94 FORMAT(2F20.4)
0032                  DO 77 I=1,29
0033                  READ (5,98) TEMP(I),VARG(I),VNIT(I),VOXY(I)
0034              77  WRITE (6,88)TEMP(I),VARG(I),VNIT(I),VOXY(I)
0035                  READ(5,94)RP,RHOP
0036                  WRITE(6,84)RP,RHOP
0037               84 FORMAT(/T10,2E15.3)
0038                  TBOIL = 2500.
0039                  VLAMDA = 3300.
0040                  T = 0.0
0041                  DELT = 0.01
0042                  DT = 0.000010
0043                  DTMIN = 0.000000001
0044                  ACCP = 0.01
0045                  N = 6
0046                  READ(5,92)Y(1),Y(2),Y(3)
0047                  WRITE(6,82)Y(1),Y(2),Y(3)
0048               82 FORMAT(/T10,3E15.3)
0049               92 FORMAT(3F15.5)
0050                  Y(4) = 0.5
0051                  Y(5) = -1000.0
0052                  Y(6) = RP
0053                  WRITE(6,91)
0054               91 FORMAT('1',/T10,'AXIALTEMPERATUE AND VELOCITY TRAJECTORY
```

```
FORTRAN IV G LEVEL  19                    MAIN                    DATE = 71161          15/1

                  1',/T10,'USING RANZ-MARSHALL HEAT TRANSFER CORRELATION',

                                                                                        '///)
0055                   WRITE(6,191)
0056              191  FORMAT(///T13,'TIME',T28,'AXIAL',T43,'AXIAL',
                     1T58,'RADIAL',T73,'RADIAL',T88,'PARTICLE',T103,'GAS',
                     1T118,'PARTICLE',/T28,'DISTANCE',T43,'VELOCITY',T58,'DISTANCE',
                     1T73,'VELOCITY',T88,'TEMP',T103,'TEMP',T118,'RADIUS',
                     1/T13,'SECS',T28,'CMS',T43,'CMS/SEC',T58,'CMS',T73,'CMS/SEC',
                     1T88,'DEG-K',T103,'DEG-K',T118,'CMS'///)
0057                   CALL MERSON(T,DELT,DT,DTMIN,ACCP,N,&101,&102)
0058              101  WRITE(6,191)
0059                   WRITE(6,89)
0060               89  FORMAT(///T10,'INTEGATION COMPLETED SUCCESSFULLY')
0061                   GO TO 887
0062              102  WRITE(6,888)
0063              888  FORMAT(///T10,'MERSON STOPPED',/T10,'STEP LENGTH TOO SMALL')
0064              887  CONTINUE
0065                   STOP
0066                   END

 *OPTIONS IN EFFECT*   ID,EBCDIC,SOURCE,NOLIST,NODECK,LOAD,NOMAP
 *OPTIONS IN EFFECT*   NAME = MAIN      , LINECNT =       56
 *STATISTICS*     SOURCE STATEMENTS =       66,PROGRAM SIZE =     2262
 *STATISTICS*   NO DIAGNOSTICS GENERATED
```

```
EVEL  19                    MERSON              DATE = 71161          15/16/1

      SUBROUTINE MERSON(X,DELX,DX,DXMIN,TOLKM,N,*,*)
C     INTEGRATES FROM X TO (X+DELX)
C     DX IS ESTIMATE FOR INTEGRATION STEP NECESSARY
C     DXMIN IS MINIMUM STEP LENGTH TO BE PERMITTED
C     TOLKM IS REQUIRED ACCURACY
C     N IS NUMBER OF DEPENDENT VARIABLES
C     CONTROL TRANSFERRED TO FIRST LABEL IF INTEGRATION FALLS:X AND Y(I)
C    1THEN CONTAIN NEW VALUES
C     CONTROL TRANSFERRED TO SECOND LABEL IF INTEGRATION FAILS: X AND
C    2Y(I) THEN CONTAIN MOST RECENT CORRECT VALUES
C     IN EITHER CASE, DX CONTAINS CURRENT STEP LENGTH
      DIMENSION Y(10),YOLD(10),FK(5,10),DY(10)
      COMMON/FF/AHMED2
      COMMON/BASSET/K1,HTERM,X1(1000),ARMURO(1000)
      COMMON/PROBE/CAR,TG,VG,AG
      COMMON /DEP/Y/GRAD/DY
      COMMON/PETFAC/PF(20)
      COMMON/AREATP/TPET(20)
      COMMON/VAPN/TBOIL,VLAMDA
      COMMON/REYNOD/VR,RHOMIX,VISCAV,RENO,RKNUD
      COMMON/HTRANS/QCPZ,CHPZ,CHP,CH
      COMMON/IONREC/CHLUDZ,CONCN,PETRIE
      COMMON/MKN/VARG(29),VNIT(29),VOXY(29)
      TOLA=5.*TOLKM
      TOLB=TOLA/32.
      FINTS=DELX/DX+0.5
      INTS=IFIX(FINTS)
      IF(INTS.LT.1)INTS=1
      DX=DELX/INTS
      FMULT=DX/3.
      K1 = 1
      X1(1) = X
      GO TO 4
C     ERROR CHECK
    1 IF(ERR.GT.TOLA) GO TO 20
      IF(ERR.LT.TOLB) GO TO 21
C     INTEGRATION SATISFACTORY: CALCULATE NEW POINTS
    3 DO 2 I=1,N
    2 Y(I)=YOLD(I)+0.5*FK(1,I)+2.0*FK(4,I)+0.5*FK(5,I)
      WRITE(6,99)X,Y(1),Y(2),Y(4),Y(5),Y(3),TG,Y(6)
      HDRAG = HTERM/DY(2)
      WRITE(6,98)K1,X1(K1),ARMURO(K1),HTERM,DY(2),HDRAG,RENO,RKNUD
   98 FORMAT(/T2 ,'K1,X1RELACC,HIS,ACCY,HIS/ACCY,RE,KN,',I4,7E12.3)
   99 FORMAT(/T9,7E15.3,1E15.7)
      WRITE(6,97)DY(6)
   97 FORMAT(/T10,'DY(6)',1E12.3)
      IF(Y(1).GT.20.0) RETURN 1
      IF(INTS.EQ.1) RETURN 1
    6 INTS=INTS-1
      PRESERVE CURRENT VALUES
    4 XOLD=X
      DO 5 I=1,N
    5 YOLD(I)=Y(I)
      IHALF=0
```

```
FORTRAN IV G LEVEL  19                MERSON              DATE = 71161          15/16/1

0042                    GO TO 9
                  C     ERROR EXCESSIVE: HALVE STEP
0043               20   DX=0.5*DX
0044                    K1 = K1 -3
0045                    IF(DX.LT.DXMIN) GO TO 19
0046                    INTS=INTS+INTS
0047                    IHALF=1
0048                    GO TO 8
                  C     STEP LENGTH TOO SMALL: INTEGRATION FAILS
0049               19   X=XOLD
0050                    DO 23 I=1,N
0051               23   Y(I)=YOLD(I)
0052                    RETURN 2
                  C     ERROR SMALL: STEP LENGTH MAY BE INCREASED IF POSSIBLE
                  C     CHECK IF STEP PREVIOUSLY HALVED (PREVENTS CYCLING)
0053               21   IF(IHALF.EQ.1) GO TO 3
                  C     CHECK IF INTS EVEN
0054                    IDUBLE=INTS/2
0055                    IF((IDUBLE*2).EQ.INTS) GO TO 22
                  C     NOT POSSIBLE: INTS ODD
0056                    GO TO 3
                  C     DOUBLE STEP LENGTH
0057               22   INTS=IDUBLE
0058                    DX=2.*DX
0059                    K1 = K1 -3
                  C     GO BACK TO LAST POINT, AND INTEGRATE WITH NEW DX
0060                8   FMULT=DX/3.
0061                    DO 7 I=1,N
0062                7   Y(I)=YOLD(I)
0063                    X=XOLD
                  C     MAIN INTEGRATION PROCESS STARTS HERE ****
                  C     ADVANCE X BY DX
0064                9   CALL DERIVS
0065                    DO 18 IS=1,5
0066                    GO TO (31,30,32,33,30),IS
0067               31   X=X+FMULT
0068                    GO TO 30
0069               32   X=X+0.5*FMULT
0070                    GO TO 30
0071               33   X=XOLD+DX
                  C     UPDATE Y(I)
0072               30   DO 10 I=1,N
0073                    FK(IS,I)=FMULT*DY(I)
0074                    GO TO (11,12,13,14,10),IS
                  C     PREDICTOR AT (X+DX/3.)
0075               11   Y(I)=YOLD(I)+FK(1,I)
0076                    GO TO 10
                  C     CORRECTOR FOR (X+DX/3.)
0077               12   Y(I)=YOLD(I)+0.5*(FK(1,I)+FK(2,I))
0078                    GO TO 10
                  C     ADVANCE TO (X+DX/2.)
0079               13   Y(I)=YOLD(I)+0.375*FK(1,I)+1.125*FK(3,I)
0080                    GO TO 10
                  C     ADVANCE TO (X+DX)
```

```
FORTRAN IV G LEVEL  19                    MERSON              DATE = 71161          15/16/

0081            14 Y(I)=YOLD(I)+1.5*FK(1,I)-4.5*FK(3,I)+6.0*FK(4,I)
0082            10 CONTINUE
0083               IF(IS.EQ.5) GO TO 16
                C     EVALUATE DERIVATIVES
0084               GO TO (42,41,43,44,41),IS
0085            42 K1 = K1 + 1
0086               X1(K1) = X1(K1 -1)+ FMULT
0087               GO TO 41
0088            43 K1 = K1 + 1
0089               X1(K1) = X1(K1-1) + 0.5*FMULT
0090               GO TO 41
0091            44 K1 = K1 +1
0092               X1(K1) = X1(K1-1) + 1.5*FMULT
0093            41 CONTINUE
0094               CALL DERIVS
0095               GO TO 18
                C     ON LAST INTEGRATION, EVALUATE ERROR
0096            16 ERR=0.0
0097               DO 17 I=1,N
0098               EI=ABS(FK(1,I)-4.5*FK(3,I)+4.0*FK(4,I)-0.5*FK(5,I))
0099               IF(ERR.LT.EI) ERR=EI
0100            17 CONTINUE
0101            18 CONTINUE
0102               GO TO 1
0103               END

 *OPTIONS IN EFFECT*   ID,EBCDIC,SOURCE,NOLIST,NODECK,LOAD,NOMAP
 *OPTIONS IN EFFECT*   NAME = MERSON   , LINECNT =       56
 *STATISTICS*     SOURCE STATEMENTS =       103,PROGRAM SIZE =      2958
 *STATISTICS*   NO DIAGNOSTICS GENERATED
```

FRAN IV G LEVEL 19 DERIVS DATE = 71161 15/16/14

```
01                SUBROUTINE DERIVS
02                COMMON/FF/AHMED2
03                COMMON/GRAD/DY(10)
04                COMMON/PART/RP,RHOP
05                COMMON/DEP/Y(10)
06                COMMON/BASSET/K1,HTERM,X1(1000),ARMURO(1000)
07                COMMON/PROBE/CAR,TG,VG,AG
08                COMMON/AREAT/TEMP(29)
09                COMMON/AREAD/RHOAR(29),RHON(29),RHOO(29),RHOX(29)
10                COMMON/AREAV/VISAR(29),VISN(29),VISO(29),VISX(29)
11                COMMON/AREAC/CONAR(29),CONN(29),CONO(29),CONX(29)
12                COMMON/A1/CP
13                COMMON/GAS/KQ
14                COMMON/PETFAC/PF(20)
15                COMMON/AREATP/TPET(20)
16                COMMON/VAPN/TBOIL,VLAMDA
17                COMMON/MKN/VARG(29),VNIT(29),VOXY(29)
18                COMMON/REYNOD/VR,RHOMIX,VISCAV,RENO,RKNUD
19                COMMON/HTRANS/QCPZ,CHPZ,CHP,CH
20                COMMON/IONREC/CHLUDZ,CONCN,PETRIE
21                DY(1) = Y(2)
22                DY(4) = Y(5)
23                CALL PROFYL
24                IF(Y(1).GT.1.0) GO TO 55
25                IF(Y(4).GT.0.5) GO TO 55
26                RADFAK = 1.0 -(Y(4)/0.5)*(Y(4)/0.5)
27                AXFAK = 1.0 - (1.0 - RADFAK)*Y(1)*Y(1)
28                VG = VG*RADFAK/AXFAK
29                TG = (TG - 300.)*RADFAK/AXFAK + 300.
30             55 CONTINUE
31                TREF = (TG + Y(3))/2.
32                VRY = Y(2) - VG
33                VRX = Y(5)
34                VR = SQRT(VRY**2 + VRX**2)
35                ABSVR = ABS(VRY/VRX)
36                BETA = ATAN(ABSVR)
37                DO 41 KQ = 1,3
38                CALL LAGINT(TREF,RHOGAS)
39                CALL VISCTY(TREF,VISGAS)
40                CALL CONDY(TREF,CONGAS)
41                GO TO (31,32,33,34),KQ
42             31 VISCAR = VISGAS
43                CONAR1 = CONGAS
44                RHOAR1 = RHOGAS
45                GO TO 41
46             32 VISCN = VISGAS
47                CONN1 = CONGAS
48                RHON1 = RHOGAS
49                GO TO 41
50             33 VISCO = VISGAS
51                CONO1 = CONGAS
52                RHOO1 = RHOGAS
53                GO TO 41
54             34 VISCX = VISGAS
```

```
RAN IV G LEVEL  19                    DERIVS                  DATE = 71161            15/16/14

                CONX1 = CONGAS
                RHOX1 = RHOGAS
             41 CONTINUE
                CAR = CAR/100.
                VISCAV = VISCAR*CAR + VISCN*(1.-CAR)*0.79 + VISCO*(1.-CAR)*0.21
                WAR = 40.*CAR
                WN = 28.*(1.-CAR)*0.79
                WO = 32.*(1.0-CAR)*0.21
                RHOMIX = (WAR + WN + WO)/(WAR/RHOAR1+ WN/RHON1 + WO/RHOO1)
                CONAV = CONAR1*CAR + CONN1*(1.-CAR)*0.79 + CONO1*(1.-CAR)*0.21
                DO 441 KQ = 1,3
                CALL LAGINT(TG  ,RHOGAS)
                CALL VISCTY(TG  ,VISGAS)
                GO TO (331,332,333,334),KQ
            331 VISCAR = VISGAS
                RHOAR1 = RHOGAS
                GO TO 441
            332 VISCN = VISGAS
                RHON1 = RHOGAS
                GO TO 441
            333 VISCO = VISGAS
                RHOO1 = RHOGAS
                GO TO 441
            334 VISCX = VISGAS
                RHOX1 = RHOGAS
            441 CONTINUE
                VISBLK = VISCAR*CAR + VISCN*(1.-CAR)*0.79 + VISCO*(1.-CAR)*0.21
                WAR = 40.*CAR
                WN = 28.*(1.-CAR)*0.79
                WO = 32.*(1.0-CAR)*0.21
                RHOBLK = (WAR + WN + WO)/(WAR/RHOAR1+ WN/RHON1 + WO/RHOO1)
                AHMED = VISCAV/RHOMIX/(VISBLK/RHOBLK)
        C       REYNOLDS NUMBER
                RENO = 2.*Y(6)*ABS(VR)*RHOMIX/VISCAV
                CALL VSOUND(TREF,CAR,CSMIX)
                RMACH = VR/CSMIX/100.
                IF(RENO.GT.1.0) GO TO 666
                RKNUD = RMACH/RENO
                GO TO 667
            666 RKNUD = RMACH/SQRT(RENO)
            667 CONTINUE
        C       DRAG COEFFICIENTS
                IF(RENO.GT.0.2) GO TO 222
                CD = 24./RENO
                GO TO 100
            222 IF(RENO.GT.2.0) GO TO 3
                COR = 1. + 0.10*RENO**0.99
                CD = 24.*COR/RENO
                GO TO 100
              3 IF(RENO.GT.21.) GO TO 4
                COR = 1.+ 0.11*RENO**0.81
                CD = 24.*COR/RENO
                GO TO 100
              4 COR = 1. + 0.189*RENO**0.632
```

```
RAN IV G LEVEL  19                    DERIVS                  DATE = 71161            15/16/14

7                 CD = 24.*COR/RENO
8               100 CONTINUE
              C      CALCULATE ACCELERATION
9               103 GRAV = 981.
0                   IF(ABS(AHMED-1.).LT.0.01) GO TO 800
1                   AHMED2 = AHMED**0.15
2                   GO TO 801
3               800 AHMED2 = AHMED
4               801 CONTINUE
5                   DRAG =  3.*RHOMIX*CD/(8.*RHOP*Y(6))*ABS(VR)*VR*AHMED2
6                   SIGNX = VRX/ABS(VRX)
7                   IF(ABS(VRY).LT.0.1) GO TO 77
8                   SIGNY = VRY/ABS(VRY)
9                   GO TO 78
0                77 SIGNY = 1.0
1                78 CONTINUE
2                   DRAGX =-DRAG*COS(BETA)*SIGNX
3                   DRAGY =-DRAG*SIN(BETA)*SIGNY
4                   IF(K1.NE.1) GO TO 202
5                   DY(2) = GRAV + DRAGY
6                   ARMURO(1) = (DY(2) - AG)*SQRT(VISCAV*RHOMIX)/Y(6)
7                   GO TO 201
8               202 ARMURO(K1) = ARMURO(K1-1)
9               200 CALL HISTRY
0                   DY(2) = GRAV + DRAGY + HTERM
1                   ARC = DY(2)-AG
2                   ARCMR = ARC*SQRT(VISCAV*RHOMIX)/Y(6)
3                   ARATIO = ARCMR/ARMURO(K1)
4                   IF(ABS(ARATIO-1.).LT.0.05) GO TO 201
5                   ARMURO(K1) = ARCMR
6                   GO TO 200
7               201 CONTINUE
8                   DY(5) = DRAGX
              C     HEAT TRANSFER COEFFICIENTS
              C USING RANZ MARSHALL AND MEAN FILM PROPERTIES
9                   CH = (2.+0.515*SQRT(RENO) )*CONAV/(2.*Y(6))*AHMED2
0                   CALL CORION(TG,PETRIE)
1                   CHP = CH*PETRIE
2                   IF(TG.LT.7000.) GO TO 777
3                   CONCN = 7.300E17
4                   GO TO 778
5               777 CONCN = 10.0**(15.54  +(TG-4000.)/3000.*2.32)
6               778 CONTINUE
7                   CHLUDZ = 1.0 + 75./87.*(CONCN/7.300E17)*((1.0 - CAR)/0.1)
8                   CHPZ = CHP*CHLUDZ
9                   QCPZ = CHPZ*4.0*3.142*Y(6)*Y(6)*(TG-Y(3))
0                   IF(Y(3).GT.TBOIL) GO TO 101
1               104 CALL SPHEAT(Y(3),CP)
2                   DY(3) = QCPZ*3./(4.0*3.142*Y(6)*Y(6)*Y(6)*RHOP*CP)
3                   DY(6) = 0.0
4                   GO TO 102
5               101 IF(Y(3).GT.TG) GO TO 104
6                   VAPOR = QCPZ/LAMDA
7                   DY(6) =-VAPOR/(4.*3.142*Y(6)*Y(6)*RHOP)
```

```
RAN IV G LEVEL  19                    DERIVS                  DATE = 71161            15/16/14

3                   DY(3) = 0.0
9                 102 CONTINUE
)                   RETURN
l                   END

PTIONS IN EFFECT*   ID,EBCDIC,SOURCE,NOLIST,NODECK,LOAD,NOMAP
PTIONS IN EFFECT*   NAME = DERIVS   , LINECNT =        56
TATISTICS*     SOURCE STATEMENTS =       161,PROGRAM SIZE =      3664
TATISTICS*   NO DIAGNOSTICS GENERATED
```

```
'RAN IV G LEVEL  19                    HISTRY                  DATE = 71161            15/16/14

)1                  SUBROUTINE HISTRY
)2                  COMMON/DEP/Y(10)
)3                  COMMON/BASSET/K1,HTERM,X1(1000),ARMURO(1000)
)4                  COMMON/PART/RP,RHOP
)5                  HIS = 0.0
)6                  DO 1 I=2,K1
)7                  H = (ARMURO(I) + ARMURO(I-1))/2.*(-2.)*
                   1(SQRT(X1(K1) -X1(I)) -SQRT(X1(K1) -X1(I-1)))
)8                1 HIS = HIS + H
)9                  HTERM =-HIS*9./(2.*SQRT(3.142)*RHOP)
 0                  RETURN
 1                  END

IPTIONS IN EFFECT*   ID,EBCDIC,SOURCE,NOLIST,NODECK,LOAD,NOMAP
IPTIONS IN EFFECT*   NAME = HISTRY   , LINECNT =        56
TATISTICS*     SOURCE STATEMENTS =        11,PROGRAM SIZE =       552
TATISTICS*   NO DIAGNOSTICS GENERATED
```

```
ORTRAN IV G LEVEL  19                    PROFYL                DATE = 71161          15/16/

0001                  SUBROUTINE PROFYL
0002                  COMMON/GAS/KQ
0003                  COMMON/PROBE/CAR,TG,VG,AG
0004                  COMMON/DEP/Y(10)
0005                  IF(Y(1).GT.2.54) GO TO 1
0006                  Z = Y(1)/2.54
0007                  CAR = 100. -3.0*Z
0008                  TG = 13000. - 1400.*Z
0009                  VG = 46000. - 4800.*Z
0010                  AG = VG*(-4800.)
0011                  GO TO 10
0012                1 IF(Y(1).GT.5.08) GO TO 2
0013                  Z = (Y(1) - 2.54)/2.54
0014                  CAR = 97.0 - 16.0*Z
0015                  TG = 11600. - 5200.*Z
0016                  VG = 41200. - 17400.*Z
0017                  AG = VG*(-17400.)
0018                  GO TO 10
0019                2 IF(Y(1).GT.7.62) GO TO 3
0020                  Z = (Y(1) - 5.08)/2.54
0021                  CAR = 81.0 - 62.0*Z
0022                  TG = 6400. - 5000.*Z
0023                  VG = 23800. - 18600.*Z
0024                  AG = VG*(-18600.)
0025                  GO TO 10
0026                3 IF(Y(1).GT.20.32) GO TO 4
0027                  Z = (Y(1) -7.62)/12.70
0028                  CAR = 19.0 - 14.0*Z
0029                  TG = 1400. - 800.*Z
0030                  VG = 5200. -3700.*Z
0031                  AG = VG*(-3700.)
0032                  GO TO 10
0033                4 CAR = 0.00
0034                  TG = 600.
0035                  VG = 1500.
0036                  AG = 0.0
0037               10 CONTINUE
0038                  RETURN
0039                  END

*OPTIONS IN EFFECT*   ID,EBCDIC,SOURCE,NOLIST,NODECK,LOAD,NOMAP
*OPTIONS IN EFFECT*   NAME = PROFYL   , LINECNT =      56
*STATISTICS*     SOURCE STATEMENTS =      39,PROGRAM SIZE =     914
*STATISTICS*   NO DIAGNOSTICS GENERATED
```

```
ORTRAN IV G LEVEL  19                    LAGINT                DATE = 71161          15/16/1
0001                  SUBROUTINE LAGINT(TF,RHOGAS)
                C      LAGRANGE INTERPOLATION METHOD
                C      USING NEAREST FOUR POINTS
                C      TO POINT OF INTEREST
0002                  COMMON/GAS/KQ
0003                  COMMON/AREAD/RHOAR(29),RHON(29),RHOO(29),RHOX(29)
0004                  COMMON/AREAT/TEMP(29)
0005                  DIMENSION Y(29),Y2(4),T2(4)
0006                  GO TO(31,32,33,34),KQ
0007               31 DO 4 I=1,29
0008                4 Y(I)=RHOAR(I)
0009                  GO TO 1
0010               32 DO 5 I=1,29
0011                5 Y(I)=RHON(I)
0012                  GO TO 1
0013               33 DO 6 I=1,29
0014                6 Y(I)=RHOO(I)
0015                  GO TO 1
0016               34 DO 77 I=1,29
0017               77 Y(I)=RHOX(I)
0018                1 CONTINUE
0019                  DO 3 I=1,29
0020                  IF (TF.LT.TEMP(I)) GO TO 2
0021                3 CONTINUE
0022                2 CONTINUE
                C NOW WE HAVE THE VALUE OF I
                C TEST IF IN FIRST OR LAST BOX
00                    IF(I.GT.2) GO TO 7
0024                  DO 8 I=1,4
0025                  Y2(I)=Y(I)
0026                8 T2(I)=TEMP(I)
0027                  GO TO 100
0028                7 IF(I.EQ.29)GO TO 9
0029                  DO 10 J=1,4
0030                  Y2(J)=Y(I-3+J)
0031               10 T2(J)=TEMP(I-3+J)
0032                  GO TO 100
0033                9 DO 11 J=1,4
0034                  Y2(J)=Y(25+J)
0035               11 T2(J)=TEMP(25+J)
0036              100 C = 0.0
0037                  DO 52 I =1,4
0038                  ZXI = T2(I)
0039                  P=1.
0040                  DO 40 J=1,4
0041                  IF(I-J)35,40,35
0042               35 ZXJ = T2(J)
0043                  A=(TF-ZXJ)/(ZXI-ZXJ)
0044                  P=P*A
0045               40 CONTINUE
0046                  B = P*Y2(I)
0047                  C=C+B
00                 52 CONTINUE
00                    RHOGAS=C

0050                  RETURN
0051                  END
```

```
ORTRAN IV G LEVEL  19                    VISCTY              DATE = 71161          15/16/14

0001                  SUBROUTINE VISCTY(TF,VISGAS)
0002                  COMMON/GAS/KQ
0003                  COMMON/AREAV/VISAR(29),VISN(29),VISO(29),VISX(29)
0004                  COMMON/AREAT/TEMP(29)
0005                  DIMENSION Y(29)
0006                  GO TO (31,32,33,34),KQ
0007                31 DO 4  I=1,29
0008                 4 Y(I) = VISAR(I)
0009                   GO TO 1
0010                32 DO 5  I=1,29
0011                 5 Y(I) = VISN(I)
0012                   GO TO 1
0013                33 DO 6  I =1,29
0014                 6 Y(I) = VISO(I)
0015                   GO TO 1
0016                34 DO 7  I =1,29
0017                 7 Y(I) = VISX(I)
0018                 1 DO 11  I= 1,29
0019                   IF(TF.LT.TEMP(I))GO TO 2
0020                11 CONTINUE
0021                 2 CONTINUE
0022                   SLOPE = (Y(I)-Y(I-1))/(TEMP(I)-TEMP(I-1))
0023                   VISGAS = Y(I-1)+SLOPE*(TF-TEMP(I-1))
0024                   RETURN
0025                   END

 *OPTIONS IN EFFECT*   ID,EBCDIC,SOURCE,NOLIST,NODECK,LOAD,NOMAP
 *OPTIONS IN EFFECT*   NAME = VISCTY   , LINECNT =        56
 *STATISTICS*     SOURCE STATEMENTS =        25,PROGRAM SIZE =       922
 *STATISTICS*   NO DIAGNOSTICS GENERATED
```

```
FORTRAN IV G LEVEL  19                  CONDY                  DATE = 71161          15/16/

0001                  SUBROUTINE CONDY(TF,CONGAS)
0002                  COMMON/GAS/KQ
0003                  COMMON/AREAC/CONAR(29),CONN(29),CONO(29),CONX(29)
0004                  COMMON/AREAT/TEMP(29)
0005                  DIMENSION Y(29)
0006                  GO TO (31,32,33,34),KQ
0007                31 DO 4 I=1,29
0008                 4 Y(I) = CONAR(I)
0009                   GO TO 1
0010                32 DO 5 I =1,29
0011                 5 Y(I) = CONN(I)
0012                   GO TO 1
0013                33 DO 6 I=1,29
0014                 6 Y(I) = CONO(I)
0015                   GO TO 1
0016                34 DO 7 I=1,29
0017                 7 Y(I) = CONX(I)
0018                 1 CONTINUE
0019                   DO 11 I =1,29
0020                   IF(TF.LT.TEMP(I)) GO TO 2
0021                11 CONTINUE
0022                 2 CONTINUE
0023                   SLOPE = (Y(I) -Y(I-1))/(TEMP(I) - TEMP(I-1))
0024                   CONGAS = Y(I-1) + SLOPE*(TF -TEMP(I-1))
0025                   RETURN
0026                   END

 OPTIONS IN EFFECT*   ID,EBCDIC,SOURCE,NOLIST,NODECK,LOAD,NOMAP
 *OPTIONS IN EFFECT*   NAME = CONDY    , LINECNT =        56
 *STATISTICS*     SOURCE STATEMENTS =        26,PROGRAM SIZE =       922
 *STATISTICS*   NO DIAGNOSTICS GENERATED
```

```
FORTRAN IV G LEVEL  19                  SPHEAT                 DATE = 71161          15/16/

0001                  SUBROUTINE SPHEAT(TP,CP)
0002                  CP = 0.20 + 0.06*(TP - 273.)/427.
0003                  RETURN
0004                  END

 *OPTIONS IN EFFECT*   ID,EBCDIC,SOURCE,NOLIST,NODECK,LOAD,NOMAP
 *OPTIONS IN EFFECT*   NAME = SPHEAT   , LINECNT =        56
 *STATISTICS*     SOURCE STATEMENTS =         4,PROGRAM SIZE =       334
 *STATISTICS*   NO DIAGNOSTICS GENERATED
```

```
FORTRAN IV G LEVEL  19                  LININT              DATE = 71161          15/1

0001                  SUBROUTINE LININT(X,Y,N,XIN,YOUT)
                C
                C     GENERAL LINEAR  INTERPOLATION SCHEME USING AN ARRAY OF X'S & Y'S
                C     EACH HAVING N ELEMENTS
                C     INPUT KNOWN X AND OUTPUT CALCULATED Y
                C
0002                  DIMENSION X(110),Y(110)
0003                  DO 1 I=1,N
0004                  L=I
0005                  IF(XIN.LT.X(I))GO TO 2
0006            1     CONTINUE
0007            2     CONTINUE
0008                  SLOPE=(Y(L)-Y(L-1))/(X(L)-X(L-1))
0009                  YOUT=Y(L-1)+SLOPE*(XIN-X(L-1))
0010                  RETURN
0011                  END
```

```
FORTRAN IV G LEVEL  19                  VSOUND              DATE = 71161          15/1

0001                  SUBROUTINE VSOUND (TREF,CAR,CSMIX)
0002                  COMMON/AREAT/TEMP(29)
0003                  COMMON/MKN/VARG(29),VNIT(29),VOXY(29)
0004                  CALL LININT (TEMP,VARG,29,TREF,CSAR)
0005                  CALL LININT (TEMP,VNIT,29,TREF,CSN2)
0006                  CALL LININT (TEMP,VOXY,29,TREF,CSO2)
0007                  CSMIX=CSAR*CAR+CSN2*(1.-CAR)*0.79+CSO2*(1.-CAR)*0.21
0008                  RETURN
0009                  END
```

```
FORTRAN IV G LEVEL  19                  CORION              DATE = 71161          15/1

0001                  SUBROUTINE CORION(TF,PETRIE)
0002                  COMMON/PETFAC/PF(20)
0003                  COMMON/AREATP/TPET(20)
0004                  IF(TF.LT.7000.) GO TO 3
0005                  IF(TF.GT.13000.) GO TO 4
0006                  DO 11   I= 1,13
0007                  IF(TF.LT.TPET(I)) GO TO 2
0008               11 CONTINUE
0009                2 CONTINUE
0010                  SLOPE = (PF(I)-PF(I-1))/(TPET(I)-TPET(I-1))
0011                  PETRIE = PF(I-1) + SLOPE*(TF- TPET(I-1))
0012                  GO TO 5
0013                3 PETRIE = 1.0
0014                  GO TO 5
0015                4 PETRIE = 3.2
0016                5 CONTINUE
0017                  RETURN
0018                  END
```

NOTES ON COMPUTER PROGRAM

Subroutines

MERSON	-	basic integration process
DERIVS	-	calculates first and second derivatives of particle displacement, in both axial and radial directions and either rate of change of particle diameter or temperature
HISTRY	-	evaluates the Basset history term
PROFYL	-	evaluates axial concentration, temperature, velocity and acceleration of gas
LAGINT	-	evaluates density of gas by Lagrangian interpolation
VISCTY	-	evaluates viscosity of gas by linear interpolation
CONDY	-	evaluates conductivity of gas by linear interpolation
SPHEAT	-	evaluates specific heat of glass
VSOUND	-	evaluates velocity of sound of gas
LININT	-	general linear interpolation scheme

NOMENCLATURE

ACCP	Accuracy parameter
AHMED	Kinematic viscosity ratio (ν_{av}/ν_{∞})
AG	Gas acceleration
ARMURO	$(dV_p/dt - dV_g/dt)[(\rho_g)_{av}(\mu_g)_{av}]^{1/2}(2/D_p)$
BETA	Angle between the relative velocity vector and radial direction
CD	Drag coefficient
CH	Heat transfer coefficient
CHP	Heat transfer coefficient corrected for ionisation
CHPZ	Heat transfer coefficient corrected for ionisation and recombination
HTERM	Particle acceleration due to Basset history term
K1	Counter on number of integration steps taken
N	Number of variables
QCPZ	Heat flux, corrected for large temperature differences, ionisation and recombination
RENO	Reynolds number
RHOBLK	Gas density evaluated at free stream temperature
RHOGAS	Gas density
RHOMIX	Gas density evaluated at mean film temperature
RKNUD	Knudsen number
RMACH	Mach number
TBOIL	Boiling point of glass
TREF	Mean film temperature

NOMENCLATURE (cont'd)

X1	Integration time array
Y(1)	Particle axial displacement
Y(2)	Particle axial velocity
Y(3)	Particle temperature
Y(4)	Particle radial displacement
Y(5)	Particle radial velocity
Y(6)	Particle radius

APPENDIX D

PROPERTIES OF GASES AT ELEVATED TEMPERATURES

GASES

Argon

Nitrogen

Oxygen

Helium (Included for reference only, but not used in the present work)

PROPERTIES

Density

Conductivity

Enthalpy

Viscosity

PROPERTIES OF ARGON AS A FUNCTION OF TEMPERATURE

ARGON

TEMP DEG-K	DENS G-CC X 1 000	CONDUCTY CALS/(CM SEC DEG-K) X1 000 000	ENTHPY CALS/GM	VISCTY G/(CM-SEC) X 1 000 000
300.	1.6328	41.9	37.2	229.
400.	1.2566	52.5	49.6	283.
500.	0.9734	63.1	62.0	337.
600.	0.7700	70.9	74.4	378.
700.	0.6330	78.7	86.8	419.
800.	0.5490	86.4	99.2	460.
900.	0.5047	94.2	111.6	501.
1000.	0.4867	102.0	124.0	542.
1100.	0.4360	108.0	136.4	578.
1200.	0.3963	114.0	148.8	613.
1300.	0.3657	120.0	161.2	649.
1400.	0.3422	126.0	173.6	684.
1500.	0.3240	132.0	186.0	720.
1600.	0.3028	138.6	198.4	753.
1700.	0.2846	145.2	210.8	787.
1800.	0.2687	151.8	223.2	820.
1900.	0.2550	158.4	235.6	854.
2000.	0.2430	165.0	248.0	887.
2100.	0.2312	171.2	260.4	920.
2200.	0.2206	177.4	272.8	953.

ARGON

TEMP DEG-K	DENS G-CC X 1 000	CONDUCTY CALS/(CM SEC DEG-K) X1 000 000	ENTHPY CALS/GM	VISCTY G/(CM-SEC) X 1 000 000
2300.	0.2111	183.6	285.2	986.
2400.	0.2024	189.8	297.6	1019.
2500.	0.1945	196.0	310.0	1052.
2600.	0.1869	202.0	322.4	1084.
2700.	0.1800	208.0	334.8	1115.
2800.	0.1735	214.0	347.2	1147.
2900.	0.1675	220.0	359.6	1178.
3000.	0.1620	226.0	372.0	1210.
3100.	0.1567	232.0	384.4	1242.
3200.	0.1518	238.0	396.8	1275.
3300.	0.1472	244.0	409.2	1307.
3400.	0.1429	250.0	421.6	1340.
3500.	0.1388	256.0	434.0	1372.
3600.	0.1349	261.8	446.4	1404.
3700.	0.1313	267.6	458.8	1436.
3800.	0.1278	273.4	471.2	1469.
3900.	0.1246	279.2	483.6	1501.
4000.	0.1215	285.0	496.0	1533.
4100.	0.1185	290.6	508.4	1563.
4200.	0.1157	296.2	520.8	1593.

ARGON

TEMP DEG-K	DENS G-CC X 1 000	CONDUCTY CALS/(CM SEC DEG-K) X1 000 000	ENTHPY CALS/GM	VISCTY G/(CM-SEC) X 1 000 000
4300.	0.1130	301.8	533.2	1623.
4400.	0.1104	307.4	545.6	1653.
4500.	0.1080	313.0	558.0	1683.
4600.	0.1056	318.6	570.7	1712.
4700.	0.1034	324.2	583.3	1742.
4800.	0.1012	329.8	596.0	1771.
4900.	0.0992	335.4	608.6	1801.
5000.	0.0972	341.0	621.3	1830.
5100.	0.0953	346.2	634.0	1858.
5200.	0.0935	351.4	646.6	1887.
5300.	0.0918	356.6	659.3	1915.
5400.	0.0901	361.8	671.9	1944.
5500.	0.0885	367.0	684.6	1972.
5600.	0.0869	372.4	697.1	2001.
5700.	0.0854	377.8	709.5	2029.
5800.	0.0839	383.2	722.0	2058.
5900.	0.0825	388.6	734.4	2086.
6000.	0.0811	394.0	746.9	2115.
6100.	0.0798	399.2	759.3	2141.
6200.	0.0785	404.4	771.7	2167.

ARGON

TEMP DEG-K	DENS G-CC X 1 000	CONDUCTY CALS/(CM SEC DEG-K) X1 000 000	ENTHPY CALS/GM	VISCTY G/(CM-SEC) X 1 000 000
6300.	0.0772	409.6	784.1	2193.
6400.	0.0760	414.8	796.5	2219.
6500.	0.0749	420.0	808.9	2245.
6600.	0.0737	424.8	821.6	2272.
6700.	0.0726	429.6	834.3	2299.
6800.	0.0716	434.4	846.9	2326.
6900.	0.0705	439.2	859.6	2353.
7000.	0.0695	444.0	872.3	2380.
7100.	0.0685	448.8	885.6	2406.
7200.	0.0675	453.6	898.9	2432.
7300.	0.0666	458.4	912.3	2458.
7400.	0.0657	463.2	925.6	2484.
7500.	0.0648	468.0	938.9	2510.
7600.	0.0639	472.4	953.1	2536.
7700.	0.0631	476.8	967.3	2562.
7800.	0.0623	481.2	981.6	2588.
7900.	0.0615	485.6	995.8	2614.
8000.	0.0607	490.0	1010.0	2640.
8100.	0.0600	494.6	1026.2	2662.
8200.	0.0592	499.2	1042.4	2684.

ARGON

TEMP DEG-K	DENS G-CC X 1 000	CONDUCTY CALS/(CM SEC DEG-K) X1 000 000	ENTHPY CALS/GM	VISCTY G/(CM-SEC) X 1 000 000
8300.	0.0585	503.8	1058.6	2706.
8400.	0.0578	508.4	1074.8	2728.
8500.	0.0571	513.0	1091.0	2750.
8600.	0.0564	517.4	1110.0	2774.
8700.	0.0557	521.8	1129.0	2798.
8800.	0.0550	526.2	1148.0	2822.
8900.	0.0544	530.6	1167.0	2846.
9000.	0.0537	535.0	1186.0	2870.
9100.	0.0531	539.2	1210.2	2892.
9200.	0.0525	543.4	1234.4	2914.
9300.	0.0518	547.6	1258.6	2936.
9400.	0.0512	551.8	1282.8	2958.
9500.	0.0506	556.0	1307.0	2980.
9600.	0.0500	560.4	1338.2	3004.
9700.	0.0494	564.8	1369.4	3028.
9800.	0.0488	569.2	1400.6	3052.
9900.	0.0483	573.6	1431.8	3076.
10000.	0.0477	578.0	1463.0	3100.
10100.	0.0471	582.4	1504.8	3124.
10200.	0.0465	586.8	1546.6	3148.

ARGON

TEMP DEG-K	DENS G-CC X 1 000	CONDUCTY CALS/(CM SEC DEG-K) X1 000 000	ENTHPY CALS/GM	VISCTY G/(CM-SEC) X 1 000 000
10300.	0.0460	591.2	1588.4	3172.
10400.	0.0454	595.6	1630.2	3196.
10500.	0.0448	600.0	1672.0	3220.
10600.	0.0443	604.4	1728.6	3242.
10700.	0.0437	608.8	1785.2	3264.
10800.	0.0431	613.2	1841.8	3286.
10900.	0.0425	617.6	1898.4	3308.
11000.	0.0420	622.0	1955.0	3330.
11100.	0.0414	626.2	2029.4	3352.
11200.	0.0408	630.4	2103.8	3374.
11300.	0.0403	634.6	2178.2	3396.
11400.	0.0397	638.8	2252.6	3418.
11500.	0.0391	643.0	2327.0	3440.
11600.	0.0386	647.2	2426.6	3462.
11700.	0.0380	651.4	2526.2	3484.
11800.	0.0374	655.6	2625.8	3506.
11900.	0.0368	659.8	2725.4	3528.
12000.	0.0362	664.0	2825.0	3550.
12100.	0.0356	668.8	2950.2	3570.
12200.	0.0351	673.6	3075.4	3590.

ARGON

TEMP DEG-K	DENS G-CC X 1 000	CONDUCTY CALS/(CM SEC DEG-K) X1 000 000	ENTHPY CALS/GM	VISCTY G/(CM-SEC) X 1 000 000
12300.	0.0345	678.4	3200.6	3610.
12400.	0.0339	683.2	3325.8	3630.
12500.	0.0333	688.0	3451.0	3650.
12600.	0.0327	691.2	3610.2	3672.
12700.	0.0321	694.4	3769.4	3694.
12800.	0.0315	697.6	3928.6	3716.
12900.	0.0310	700.8	4087.8	3738.
13000.	0.0304	704.0	4247.0	3760.
13100.	0.0298	712.0	4432.2	3782.
13200.	0.0292	720.0	4617.4	3804.

PROPERTIES OF NITROGEN AS A FUNCTION OF TEMPERATURE

NITROGEN

TEMP DEG-K	DENS G-CC X 1 000	CONDUCTY CALS/(CM SEC DEG-K) X1 000 000	ENTHPY CALS/GM	VISCTY G/(CM-SEC) X 1 000 000
300.	1.1525	62.0	75.4	178.
400.	0.8841	78.4	112.6	218.
500.	0.6826	94.9	149.7	257.
600.	0.5384	106.8	176.3	286.
700.	0.4419	118.6	202.9	314.
800.	0.3833	130.5	229.4	343.
900.	0.3530	142.3	256.0	371.
1000.	0.3413	154.2	282.6	400.
1100.	0.3054	167.8	311.4	424.
1200.	0.2771	181.3	340.3	448.
1300.	0.2550	194.9	369.1	472.
1400.	0.2378	208.4	398.0	496.
1500.	0.2240	222.0	426.8	520.
1600.	0.2074	233.6	458.4	542.
1700.	0.1928	245.2	490.1	564.
1800.	0.1800	256.8	521.7	587.
1900.	0.1687	268.4	553.4	609.
2000.	0.1590	280.0	585.0	631.
2100.	0.1506	291.0	605.0	655.
2200.	0.1433	302.0	625.0	679.

NITROGEN

TEMP DEG-K	DENS G-CC X 1 000	CONDUCTY CALS/(CM SEC DEG-K) X1 000 000	ENTHPY CALS/GM	VISCTY G/(CM-SEC) X 1 000 000
2300.	0.1371	313.0	645.0	702.
2400.	0.1317	324.0	665.0	726.
2500.	0.1270	335.0	685.0	750.
2600.	0.1229	346.2	708.0	771.
2700.	0.1192	357.4	731.0	791.
2800.	0.1157	368.6	754.0	812.
2900.	0.1124	379.8	777.0	832.
3000.	0.1090	391.0	800.0	853.
3100.	0.1045	402.2	828.0	876.
3200.	0.0999	413.4	856.0	900.
3300.	0.0952	424.6	884.0	923.
3400.	0.0906	435.8	912.0	947.
3500.	0.0860	447.0	940.0	970.
3600.	0.0817	457.2	970.0	990.
3700.	0.0776	467.4	1000.0	1010.
3800.	0.0737	477.6	1030.0	1030.
3900.	0.0700	487.8	1060.0	1050.
4000.	0.0667	498.0	1090.0	1070.
4100.	0.0640	507.8	1128.0	1092.
4200.	0.0616	517.6	1166.0	1114.

NITROGEN

TEMP DEG-K	DENS G-CC X 1 000	CONDUCTY CALS/(CM SEC DEG-K) X1 000 000	ENTHPY CALS/GM	VISCTY G/(CM-SEC) X 1 000 000
4300.	0.0595	527.4	1204.0	1136.
4400.	0.0577	537.2	1242.0	1158.
4500.	0.0560	547.0	1280.0	1180.
4600.	0.0546	557.4	1324.0	1200.
4700.	0.0533	567.8	1368.0	1220.
4800.	0.0520	578.2	1412.0	1240.
4900.	0.0507	588.6	1456.0	1260.
5000.	0.0494	599.0	1500.0	1280.
5100.	0.0476	610.8	1608.0	1302.
5200.	0.0458	622.6	1716.0	1324.
5300.	0.0439	634.4	1824.0	1346.
5400.	0.0419	646.2	1932.0	1368.
5500.	0.0400	658.0	2040.0	1390.
5600.	0.0381	670.4	2154.0	1412.
5700.	0.0362	682.8	2268.0	1434.
5800.	0.0345	695.2	2382.0	1456.
5900.	0.0328	707.6	2496.0	1478.
6000.	0.0312	720.0	2610.0	1500.
6100.	0.0299	742.0	2778.0	1538.
6200.	0.0288	764.0	2946.0	1576.

NITROGEN

TEMP DEG-K	DENS G-CC X 1 000	CONDUCTY CALS/(CM SEC DEG-K) X1 000 000	ENTHPY CALS/GM	VISCTY G/(CM-SEC) X 1 000 000
6300.	0.0278	786.0	3114.0	1614.
6400.	0.0268	808.0	3282.0	1652.
6500.	0.0260	830.0	3450.0	1690.
6600.	0.0252	853.6	3770.0	1724.
6700.	0.0245	877.2	4090.0	1758.
6800.	0.0239	900.8	4410.0	1792.
6900.	0.0233	924.4	4730.0	1826.
7000.	0.0228	948.0	5050.0	1860.
7100.	0.0224	966.4	5684.0	1898.
7200.	0.0221	984.8	6318.0	1936.
7300.	0.0218	1003.2	6952.0	1974.
7400.	0.0215	1021.6	7586.0	2012.
7500.	0.0213	1040.0	8220.0	2050.
7600.	0.0210	1064.0	8456.0	2082.
7700.	0.0208	1088.0	8692.0	2114.
7800.	0.0205	1112.0	8928.0	2146.
7900.	0.0203	1136.0	9164.0	2178.
8000.	0.0201	1160.0	9400.0	2210.
8100.	0.0199	1174.0	9660.0	2264.
8200.	0.0198	1188.0	9920.0	2318.

NITROGEN

TEMP DEG-K	DENS G-CC X 1 000	CONDUCTY CALS/(CM SEC DEG-K) X1 000 000	ENTHPY CALS/GM	VISCTY G/(CM-SEC) X 1 000 000
8300.	0.0196	1202.0	10180.0	2372.
8400.	0.0195	1216.0	10440.0	2426.
8500.	0.0193	1230.0	10700.0	2480.
8600.	0.0191	1244.0	10940.0	2488.
8700.	0.0188	1258.0	11180.0	2496.
8800.	0.0185	1272.0	11420.0	2504.
8900.	0.0183	1286.0	11660.0	2512.
9000.	0.0180	1300.0	11900.0	2520.
9100.	0.0178	1320.0	12060.0	2546.
9200.	0.0175	1340.0	12220.0	2572.
9300.	0.0173	1360.0	12380.0	2598.
9400.	0.0170	1380.0	12540.0	2624.
9500.	0.0168	1400.0	12700.0	2650.
9600.	0.0165	1412.0	12860.0	2668.
9700.	0.0162	1424.0	13020.0	2686.
9800.	0.0159	1436.0	13180.0	2704.
9900.	0.0156	1448.0	13340.0	2722.
10000.	0.0154	1460.0	13500.0	2740.
10100.	0.0153	1471.0	13700.0	2772.
10200.	0.0151	1482.0	13900.0	2804.

NITROGEN

TEMP DEG-K	DENS G-CC X 1 000	CONDUCTY CALS/(CM SEC DEG-K) X1 000 000	ENTHPY CALS/GM	VISCTY G/(CM-SEC) X 1 000 000
10300.	0.0150	1493.0	14100.0	2836.
10400.	0.0149	1504.0	14300.0	2868.
10500.	0.0148	1515.0	14500.0	2900.
10600.	0.0146	1527.0	14720.0	2912.
10700.	0.0144	1539.0	14940.0	2924.
10800.	0.0143	1551.0	15160.0	2936.
10900.	0.0141	1563.0	15380.0	2948.
11000.	0.0139	1575.0	15600.0	2960.
11100.	0.0137	1586.0	15840.0	2988.
11200.	0.0136	1597.0	16080.0	3016.
11300.	0.0134	1608.0	16320.0	3044.
11400.	0.0133	1619.0	16560.0	3072.
11500.	0.0132	1630.0	16800.0	3100.
11600.	0.0132	1641.0	17080.0	3114.
11700.	0.0131	1652.0	17360.0	3128.
11800.	0.0131	1663.0	17640.0	3142.
11900.	0.0130	1674.0	17920.0	3156.
12000.	0.0129	1685.0	18200.0	3170.
12100.	0.0127	1696.6	18480.0	3196.
12200.	0.0124	1708.2	18760.0	3222.

NITROGEN

TEMP DEG-K	DENS G-CC X 1 000	CONDUCTY CALS/(CM SEC DEG-K) X1 000 000	ENTHPY CALS/GM	VISCTY G/(CM-SEC) X 1 000 000
12300.	0.0121	1719.8	19040.0	3248.
12400.	0.0118	1731.4	19320.0	3274.
12500.	0.0115	1743.0	19600.0	3300.
12600.	0.0112	1754.4	20160.0	3314.
12700.	0.0109	1765.8	20720.0	3328.
12800.	0.0106	1777.2	21280.0	3342.
12900.	0.0103	1788.6	21840.0	3356.
13000.	0.0100	1800.0	22400.0	3370.
13100.	0.0096	1810.0	23020.0	3396.
13200.	0.0092	1820.0	23640.0	3422.

PROPERTIES OF OXYGEN AS A FUNCTION OF TEMPERATURE

OXYGEN

TEMP DEG-K	DENS G-CC X 1 000	CONDUCTY CALS/(CM SEC DEG-K) X1 000 000	ENTHPY CALS/GM	VISCTY G/(CM-SEC) X 1 000 000
300.	1.3078	64.0	65.2	206.
400.	1.0066	81.9	87.3	253.
500.	0.7800	99.7	109.4	299.
600.	0.6173	116.5	133.0	335.
700.	0.5077	133.2	156.5	370.
800.	0.4405	149.9	180.1	406.
900.	0.4048	166.6	203.6	441.
1000.	0.3899	183.3	227.2	477.
1100.	0.3476	195.2	253.9	505.
1200.	0.3139	207.2	280.5	533.
1300.	0.2873	219.1	307.2	562.
1400.	0.2665	231.1	333.8	590.
1500.	0.2500	243.0	360.5	618.
1600.	0.2321	253.4	387.2	641.
1700.	0.2166	263.8	414.0	664.
1800.	0.2034	274.2	440.7	686.
1900.	0.1920	284.6	467.5	709.
2000.	0.1820	295.0	494.2	732.
2100.	0.1724	305.0	521.5	753.
2200.	0.1638	315.0	548.9	774.

OXYGEN

TEMP DEG-K	DENS G-CC X 1 000	CONDUCTY CALS/(CM SEC DEG-K) X1 000 000	ENTHPY CALS/GM	VISCTY G/(CM-SEC) X 1 000 000
2300.	0.1559	325.0	576.2	795.
2400.	0.1487	335.0	603.6	816.
2500.	0.1420	345.0	630.9	837.
2600.	0.1353	358.8	658.7	861.
2700.	0.1289	372.6	686.5	885.
2800.	0.1225	386.4	714.4	908.
2900.	0.1163	400.2	742.2	932.
3000.	0.1100	414.0	770.0	956.
3100.	0.1030	428.4	868.0	989.
3200.	0.0960	442.8	966.0	1022.
3300.	0.0889	457.2	1064.0	1054.
3400.	0.0819	471.6	1162.0	1087.
3500.	0.0750	486.0	1260.0	1120.
3600.	0.0673	514.8	1542.0	1180.
3700.	0.0600	543.6	1824.0	1240.
3800.	0.0535	572.4	2106.0	1300.
3900.	0.0481	601.2	2388.0	1360.
4000.	0.0440	630.0	2670.0	1420.
4100.	0.0451	614.8	3036.0	1386.
4200.	0.0473	599.6	3402.0	1352.

OXYGEN

TEMP DEG-K	DENS G-CC X 1 000	CONDUCTY CALS/(CM SEC DEG-K) X1 000 000	ENTHPY CALS/GM	VISCTY G/(CM-SEC) X 1 000 000
4300.	0.0500	584.4	3768.0	1318.
4400.	0.0528	569.2	4134.0	1284.
4500.	0.0550	554.0	4500.0	1250.
4600.	0.0526	587.4	4620.0	1310.
4700.	0.0494	620.8	4740.0	1370.
4800.	0.0457	654.2	4860.0	1430.
4900.	0.0418	687.6	4980.0	1490.
5000.	0.0381	721.0	5100.0	1550.
5100.	0.0364	732.3	5140.0	1574.
5200.	0.0352	743.6	5180.0	1598.
5300.	0.0342	755.0	5220.0	1622.
5400.	0.0335	766.3	5260.0	1646.
5500.	0.0330	777.6	5300.0	1670.
5600.	0.0324	788.1	5344.0	1692.
5700.	0.0318	798.6	5388.0	1714.
5800.	0.0313	809.0	5432.0	1736.
5900.	0.0308	819.5	5476.0	1758.
6000.	0.0303	830.0	5520.0	1780.
6100.	0.0296	840.8	5564.0	1804.
6200.	0.0289	851.6	5608.0	1828.

OXYGEN

TEMP DEG-K	DENS G-CC X 1 000	CONDUCTY CALS/(CM SEC DEG-K) X1 000 000	ENTHPY CALS/GM	VISCTY G/(CM-SEC) X 1 000 000
6300.	0.0283	862.4	5652.0	1852.
6400.	0.0276	873.2	5696.0	1876.
6500.	0.0270	884.0	5740.0	1900.
6600.	0.0266	894.8	5788.0	1922.
6700.	0.0262	905.6	5836.0	1944.
6800.	0.0259	916.4	5884.0	1966.
6900.	0.0255	927.2	5932.0	1988.
7000.	0.0252	938.0	5980.0	2010.
7100.	0.0247	948.4	6028.0	2032.
7200.	0.0243	958.8	6076.0	2054.
7300.	0.0238	969.2	6124.0	2076.
7400.	0.0234	979.6	6172.0	2098.
7500.	0.0230	990.0	6220.0	2120.
7600.	0.0227	1000.0	6272.0	2144.
7700.	0.0225	1010.0	6324.0	2168.
7800.	0.0223	1020.0	6376.0	2192.
7900.	0.0221	1030.0	6428.0	2216.
8000.	0.0219	1040.0	6480.0	2240.
8100.	0.0216	1050.0	6534.0	2262.
8200.	0.0214	1060.0	6588.0	2284.

OXYGEN

TEMP DEG-K	DENS G-CC X 1 000	CONDUCTY CALS/(CM SEC DEG-K) X1 000 000	ENTHPY CALS/GM	VISCTY G/(CM-SEC) X 1 000 000
8300.	0.0211	1070.0	6642.0	2306.
8400.	0.0208	1080.0	6696.0	2328.
8500.	0.0205	1090.0	6750.0	2350.
8600.	0.0202	1102.0	6804.0	2372.
8700.	0.0199	1114.0	6858.0	2394.
8800.	0.0196	1126.0	6912.0	2416.
8900.	0.0194	1138.0	6966.0	2438.
9000.	0.0191	1150.0	7020.0	2460.
9100.	0.0188	1158.0	7078.0	2480.
9200.	0.0186	1166.0	7136.0	2500.
9300.	0.0184	1174.0	7194.0	2520.
9400.	0.0182	1182.0	7252.0	2540.
9500.	0.0180	1190.0	7310.0	2560.
9600.	0.0179	1200.0	7368.0	2582.
9700.	0.0177	1210.0	7426.0	2604.
9800.	0.0176	1220.0	7484.0	2626.
9900.	0.0175	1230.0	7542.0	2648.
10000.	0.0174	1240.0	7600.0	2670.
10100.	0.0173	1250.0	7714.0	2672.
10200.	0.0171	1260.0	7828.0	2674.

OXYGEN

TEMP DEG-K	DENS G-CC X 1 000	CONDUCTY CALS/(CM SEC DEG-K) X1 000 000	ENTHPY CALS/GM	VISCTY G/(CM-SEC) X 1 000 000
10300.	0.0169	1270.0	7942.0	2676.
10400.	0.0168	1280.0	8056.0	2678.
10500.	0.0166	1290.0	8170.0	2680.
10600.	0.0164	1300.0	8298.0	2720.
10700.	0.0163	1310.0	8426.0	2760.
10800.	0.0161	1320.0	8554.0	2800.
10900.	0.0159	1330.0	8682.0	2840.
11000.	0.0157	1340.0	8810.0	2880.
11100.	0.0155	1350.0	8948.0	2900.
11200.	0.0152	1360.0	9086.0	2920.
11300.	0.0150	1370.0	9224.0	2940.
11400.	0.0148	1380.0	9362.0	2960.
11500.	0.0145	1390.0	9500.0	2980.
11600.	0.0142	1398.0	9646.0	3002.
11700.	0.0139	1406.0	9792.0	3024.
11800.	0.0137	1414.0	9938.0	3046.
11900.	0.0134	1422.0	10084.0	3068.
12000.	0.0132	1430.0	10230.0	3090.
12100.	0.0130	1440.0	10404.0	3110.
12200.	0.0129	1450.0	10578.0	3130.

OXYGEN

TEMP DEG-K	DENS G-CC X 1 000	CONDUCTY CALS/(CM SEC DEG-K) X1 000 000	ENTHPY CALS/GM	VISCTY G/(CM-SEC) X 1 000 000
12300.	0.0128	1460.0	10752.0	3150.
12400.	0.0127	1470.0	10926.0	3170.
12500.	0.0126	1480.0	11100.0	3190.
12600.	0.0125	1490.0	11420.0	3210.
12700.	0.0124	1500.0	11740.0	3230.
12800.	0.0122	1510.0	12060.0	3250.
12900.	0.0121	1520.0	12380.0	3270.
13000.	0.0120	1530.0	12700.0	3290.
13100.	0.0119	1540.0	13080.0	3310.
13200.	0.0118	1550.0	13460.0	3330.

PROPERTIES OF HELIUM AS A FUNCTION OF TEMPERATURE

HELIUM

TEMP DEG-K	DENS G-CC X 1 000	CONDUCTY CALS/(CM SEC DEG-K) X1 000 000	ENTHPY CALS/GM	VISCTY G/(CM-SEC) X 1 000 000
300.	0.1636	357.1	375.0	199.
400.	0.1259	420.7	500.0	239.
500.	0.0975	484.4	625.0	279.
600.	0.0771	549.1	750.0	310.
700.	0.0633	613.8	875.0	341.
800.	0.0549	678.6	1000.0	372.
900.	0.0504	743.3	1125.0	403.
1000.	0.0485	808.0	1250.0	434.
1100.	0.0435	864.4	1375.0	464.
1200.	0.0395	920.8	1500.0	494.
1300.	0.0364	977.2	1625.0	524.
1400.	0.0341	1033.6	1750.0	554.
1500.	0.0323	1090.0	1875.0	584.
1600.	0.0301	1154.0	1996.6	619.
1700.	0.0283	1218.0	2118.3	654.
1800.	0.0267	1282.0	2239.9	689.
1900.	0.0253	1346.0	2361.6	724.
2000.	0.0241	1410.0	2483.2	759.
2100.	0.0230	1468.0	2607.4	790.
2200.	0.0219	1526.0	2731.5	821.

HELIUM

TEMP DEG-K	DENS G-CC X 1 000	CONDUCTY CALS/(CM SEC DEG-K) X1 000 000	ENTHPY CALS/GM	VISCTY G/(CM-SEC) X 1 000 000
2300.	0.0210	1584.0	2855.7	853.
2400.	0.0201	1642.0	2979.8	884.
2500.	0.0194	1700.0	3104.0	915.
2600.	0.0186	1758.0	3228.2	946.
2700.	0.0178	1816.0	3352.3	977.
2800.	0.0171	1874.0	3476.5	1008.
2900.	0.0165	1932.0	3600.6	1039.
3000.	0.0159	1990.0	3724.8	1070.
3100.	0.0154	2042.0	3848.9	1098.
3200.	0.0149	2094.0	3973.1	1126.
3300.	0.0144	2146.0	4097.2	1154.
3400.	0.0139	2198.0	4221.4	1182.
3500.	0.0135	2250.0	4345.5	1210.
3600.	0.0132	2306.0	4469.7	1231.
3700.	0.0129	2362.0	4593.8	1252.
3800.	0.0125	2418.0	4718.0	1274.
3900.	0.0123	2474.0	4842.1	1295.
4000.	0.0120	2530.0	4966.3	1316.
4100.	0.0117	2582.0	5090.5	1353.
4200.	0.0114	2634.0	5214.6	1390.

HELIUM

TEMP DEG-K	DENS G-CC X 1 000	CONDUCTY CALS/(CM SEC DEG-K) X1 000 000	ENTHPY CALS/GM	VISCTY G/(CM-SEC) X 1 000 000
4300.	0.0111	2686.0	5338.8	1426.
4400.	0.0108	2738.0	5462.9	1463.
4500.	0.0106	2790.0	5587.1	1500.
4600.	0.0103	2838.0	5711.3	1526.
4700.	0.0101	2886.0	5835.5	1552.
4800.	0.0099	2934.0	5959.6	1578.
4900.	0.0097	2982.0	6083.8	1604.
5000.	0.0095	3030.0	6208.0	1630.
5100.	0.0093	3082.0	6332.2	1658.
5200.	0.0091	3134.0	6456.3	1686.
5300.	0.0089	3186.0	6580.5	1714.
5400.	0.0087	3238.0	6704.6	1742.
5500.	0.0084	3290.0	6828.8	1770.
5600.	0.0083	3340.0	6953.0	1796.
5700.	0.0081	3390.0	7077.2	1822.
5800.	0.0079	3440.0	7201.3	1848.
5900.	0.0078	3490.0	7325.5	1874.
6000.	0.0076	3540.0	7449.7	1900.
6100.	0.0075	3592.0	7573.8	1928.
6200.	0.0074	3644.0	7698.0	1956.

HELIUM

TEMP DEG-K	DENS G-CC X 1 000	CONDUCTY CALS/(CM SEC DEG-K) X1 000 000	ENTHPY CALS/GM	VISCTY G/(CM-SEC) X 1 000 000
6300.	0.0072	3696.0	7822.1	1984.
6400.	0.0071	3748.0	7946.3	2012.
6500.	0.0070	3800.0	8070.4	2040.
6600.	0.0069	3848.0	8194.5	2066.
6700.	0.0068	3896.0	8318.7	2092.
6800.	0.0067	3944.0	8442.8	2118.
6900.	0.0066	3992.0	8567.0	2144.
7000.	0.0065	4040.0	8691.1	2170.
7100.	0.0064	4084.0	8815.3	2194.
7200.	0.0063	4128.0	8939.4	2218.
7300.	0.0061	4172.0	9063.6	2242.
7400.	0.0060	4216.0	9187.7	2266.
7500.	0.0059	4260.0	9311.9	2290.
7600.	0.0059	4308.0	9436.1	2316.
7700.	0.0058	4356.0	9560.3	2342.
7800.	0.0057	4404.0	9684.4	2368.
7900.	0.0057	4452.0	9808.6	2394.
8000.	0.0056	4500.0	9932.8	2420.
8100.	0.0056	4550.0	10057.1	2446.
8200.	0.0056	4600.0	10181.4	2472.

HELIUM

TEMP DEG-K	DENS G-CC X 1 000	CONDUCTY CALS/(CM SEC DEG-K) X1 000 000	ENTHPY CALS/GM	VISCTY G/(CM-SEC) X 1 000 000
8300.	0.0055	4650.0	10305.8	2498.
8400.	0.0055	4700.0	10430.1	2524.
8500.	0.0055	4750.0	10554.4	2550.
8600.	0.0055	4794.0	10678.8	2574.
8700.	0.0054	4838.0	10803.1	2598.
8800.	0.0054	4882.0	10927.5	2622.
8900.	0.0054	4926.0	11051.8	2646.
9000.	0.0054	4970.0	11176.2	2670.
9100.	0.0053	5018.0	11301.0	2696.
9200.	0.0053	5066.0	11425.8	2722.
9300.	0.0053	5114.0	11550.7	2748.
9400.	0.0052	5162.0	11675.5	2774.
9500.	0.0052	5210.0	11800.3	2800.
9600.	0.0052	5254.0	11925.1	2824.
9700.	0.0052	5298.0	12049.9	2848.
9800.	0.0051	5342.0	12174.8	2872.
9900.	0.0051	5386.0	12299.6	2896.
10000.	0.0051	5430.0	12424.4	2920.
10100.	0.0050	5476.0	12596.6	2944.
10200.	0.0050	5522.0	12768.7	2968.

HELIUM

TEMP. DEG-K	DENS G-CC X 1000	CONDUCTY CALS/(CM SEC DEG-K) X1000000	ENTHPY CALS/GM	VISCTY G/(CM-SEC) X 1000000
10300.	0.0050	5568.0	12940.9	2992.
10400.	0.0049	5614.0	13113.0	3016.
10500.	0.0049	5660.0	13285.2	3040.
10600.	0.0049	5706.0	13457.4	3064.
10700.	0.0048	5752.0	13629.5	3088.
10800.	0.0048	5798.0	13801.7	3112.
10900.	0.0048	5844.0	13973.8	3136.
11000.	0.0047	5890.0	14146.0	3160.
11100.	0.0047	5935.0	14318.1	3184.
11200.	0.0047	5980.0	14490.3	3208.
11300.	0.0046	6025.0	14662.4	3232.
11400.	0.0046	6070.0	14834.6	3256.
11500.	0.0046	6115.0	15006.7	3280.
11600.	0.0045	6160.0	15178.9	3304.
11700.	0.0045	6205.0	15351.0	3328.
11800.	0.0044	6250.0	15523.2	3352.
11900.	0.0044	6295.0	15695.3	3376.
12000.	0.0044	6340.0	15867.5	3400.
12100.	0.0043	6384.0	16039.8	3424.
12200.	0.0043	6428.0	16212.1	3448.

HELIUM

TEMP DEG-K	DENS G-CC X 1 000	CONDUCTY CALS/(CM SEC DEG-K) X1 000 000	ENTHPY CALS/GM	VISCTY G/(CM-SEC) X 1 000 000
12300.	0.0043	6472.0	16384.4	3472.
12400.	0.0042	6516.0	16556.7	3496.
12500.	0.0042	6560.0	16729.0	3520.
12600.	0.0042	6604.0	16901.0	3544.
12700.	0.0041	6648.0	17073.0	3568.
12800.	0.0041	6692.0	17245.0	3592.
12900.	0.0041	6736.0	17417.0	3616.
13000.	0.0040	6780.0	17589.0	3640.
13100.	0.0040	6823.0	17761.2	3663.
13200.	0.0040	6866.0	17933.3	3686.

BIBLIOGRAPHY

1. Drellishak, K.S., Knopp, C.P., and Cambel, A.B., A.E.D.C., TDR-63-146 (1963).

2. Drellishak, K.S., A.E.D.C., TDR-64-22 (1964).

3. Yung, K., Weissman, S., and Mason, E.A., Physics of Fluids 5, 672 (1962).

4. Amdur, I., and Mason, E.A., Physics of Fluids 1, 370 (1958).

5. Dawe, R.A., and Smith, E.B., Science Journal 166, 679 (1969).